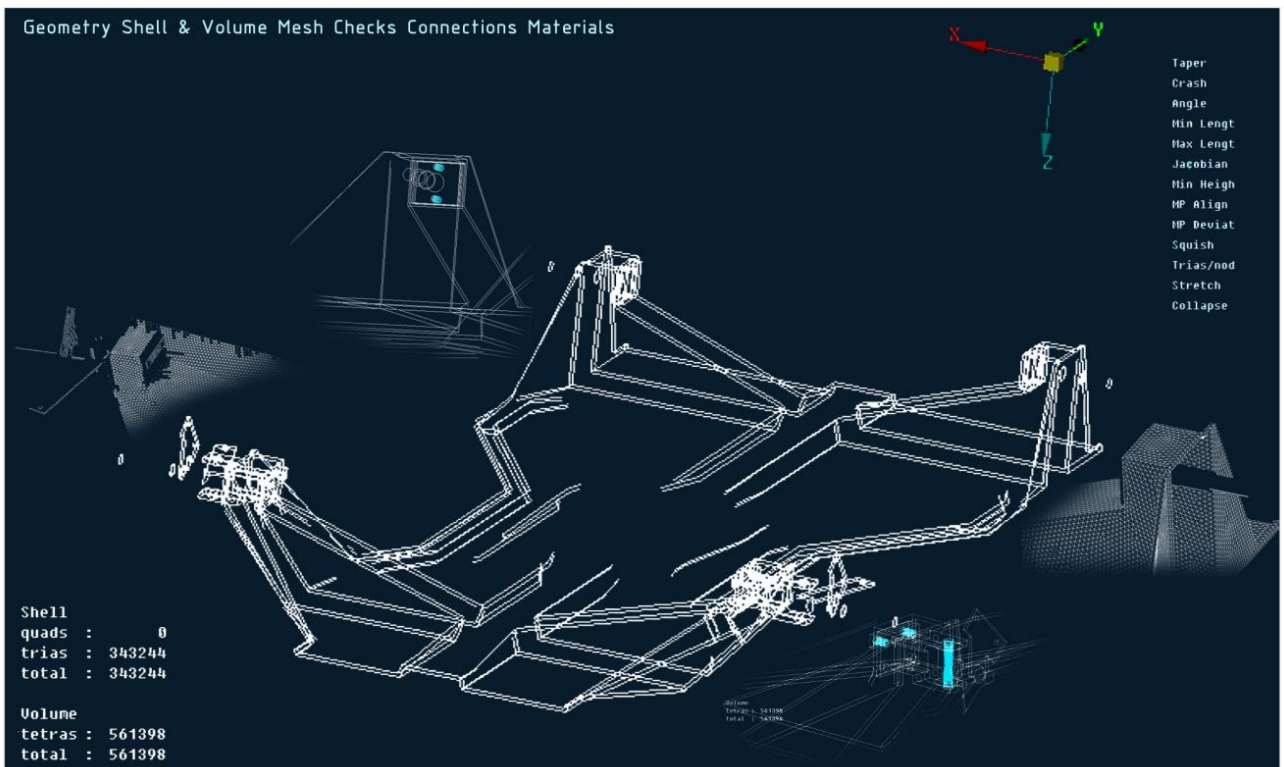




Technical University of Crete
School of Production Engineering and Management

“Design of an efficient and lightweight chassis, suitable for an Electric car”

Diploma Thesis



Evangelos Ch. Tsirogiannis

Supervised by: Georgios E. Stavroulakis, Professor

Chania, GREECE, January 2015

"I believe that we start to see our true personalities when we go through the most difficult moments. This is when we get stronger."

~Ayrton Senna~

Formula 1 world champion

To my family, friends and Papapostolis Fafoutis

ACKNOWLEDGEMENTS

First of all, I would like to thank my professor Mr. Georgios Stavroulakis who was confident in me and supported me in all the stages of my thesis. I also thank him for his guidance and dedication to our project.

I would also like to thank the members of the research team Tucer and especially Tucer's supervisor Professor Mr. Nikolaos Tsourveloudis for entrusting me with the project, as well as the opportunity that he presented to me to accomplish my goals through the team Tucer for two years in a row, as a mechanical engineer as well as a driver.

Furthermore, I am grateful to the company BETA CAE systems S.A. for the sponsorship of ANSA and μ ETA softwares, and for the technical assistance they provided us regarding this software. I particularly want to thank Mr. Christos Tassios, Mr Ioannis Asaniotis, Mr. Apostolos Mitroglou, Mr. Athanasios Papadopoulos and Mr. Ioannis Nerantzis for the wonderful cooperation and for the great service that they provided to me.

Additionally, I would like to mention the laboratory CAD of TUC and particularly the supervisor teacher of the laboratory Mr. Nikolaos Mpilalis, who provided appropriate literature for design issues. I would also like to thank laboratory staff Mr. Pavlos Koulouridakis and Mr. Ioannis Katsigiannis for the immediate assistance in design issues.

I am also grateful to Mr. Alexandros Gotsis for his knowledge and guidance in terms of composite materials. Mr. Konstantinos Providakis and Mrs. Maria Stavroulaki assisted me, to a great extent, in the research of material strength and statics respectively.

I would also like to express my gratitude to Mr. Stamatis Angelinas and Mr. Ioannis K. Nikolos for the literature that he suggested to me regarding the domain of chassis design.

Moreover, many thanks to the mathematician and member of the Greek Mathematical Society, Pagonis Theodoros. He provided me with countless suggestions and constructive criticism, which in many ways, helped me to overcome issues related with mathematics.

Last but not least, my friends and my colleagues Marina Kalantzi, Konstantinos Georgoulas, Georgios Koumartzakis, Nikolaos Kafritsas, Ioannis Tzortzis, Dimitrios Komnos, Georgios Kalogiannidis, Konstantinos Papakipis, Giorgos Lilis and Nikolaos Ververis for their immediate assistance, when it was necessary.

ABSTRACT

The design of an urban car's chassis for the "Shell Eco Marathon" competition takes into account many performance parameters referring to the usage and the type of the vehicle and a variety of different constraints such as the overall weight, strength, stiffness and cost. In order to meet these demands, the chassis must be easily manufacturable and affordable. Towards this direction, a new design approach of a lightweight carbon fiber monocoque chassis, for an electric urban car, is proposed, which conforms to structural, aesthetic, and ergonomic requirements.

Initially, a new chassis design of an environmentally friendly, urban vehicle is presented, and based on that, a lighter and stronger innovative design approach is suggested. For the development of this innovative approach and during the conceptual design phase, the parametric design method was chosen, in order for the design to be modified easily. Additionally, the chassis high efficiency was obtained by following appropriate steps, rules and techniques which conform to the vehicle structural and dynamical constraints. These methods combined with the choice of carbon fiber, as a construction material, achieved the minimization of the overall chassis mass, maximizing strength performance. The mechanical properties of a composite material such as the carbon fiber were also calculated during the design process.

Furthermore, for academic and research purposes, a model that automatically calculates the total loads that are applied on a vehicle's chassis, was created. The equations that were used to implement this model are derived from the theory of Vehicle Dynamics and are explained thoroughly. In order to validate the derived model, data such as track width, wheelbase, center of gravity, mass, et cetera were used as inputs. At the same time, a worst case stress scenario was chosen and the model's output was evaluated for the new, as well as the previous chassis design. The first step of a finite element analysis (FEA) method was performed by the pre-processor ANSA, a software of BETA CAE Systems, in order to evaluate the resistance of these two chassis designs, under this extreme stress scenario and to simulate them with the ANSYS solver. However, the ANSYS simulation was outside of the scope of this thesis. Finally, the manufacturing methods which are utilized to construct the carbon fiber monocoque chassis, are also explained.

Contents

ACKNOWLEDGEMENTS	VII
ABSTRACT	IX
1. INTRODUCTION	25
1.1 Shell Eco Marathon: The Challenge.....	25
1.2 Awards.....	25
1.3 Statement of work.....	26
1.4 Design approach.....	26
2 SELECTION OF VEHICLE TYPE AND CONCEPT	29
2.1 An overview of the different vehicle structure types	29
2.2 Modern structure types	37
2.2.1 Subframes.....	53
2.3 Chassis materials	54
2.4 Chassis joining	61
2.5 Chassis improvements.....	68
3 CONCEPTUAL DESIGN STAGE	73
3.1 Strength and stiffness requirements.....	73
3.1.1 Strength requirements	73
3.1.2 Stiffness requirements	73
3.2 Introduction to the simple structural surfaces (SSS) method	74
3.2.1 Definition of a simple structural surface (SSS)	74
3.2.2 Structural subassemblies that can be represented by a simple structural surface (SSS)	75
3.2.3 Example of integral car body with typical SSS idealizations.....	76
3.3 Free body diagrams for the SSSs	78
3.3.1 The standard sedan	78
3.3.2 Open (convertible/cabriolet) variants.....	89
4 CAD / COMPUTER-AIDED DESIGN	97
4.1 Parametric design.....	97
4.2 Eco Racer chassis 2014	100
4.2.1 Chassis design.....	100
4.2.2 Design of the parts around the chassis	103

4.3	New chassis design	106
4.3.1	Ergonomics.....	106
4.3.2	New chassis' design stages	110
4.3.3	Design of the parts around the new chassis.....	114
5	MECHANICAL PROPERTIES OF CHOSEN MATERIALS.....	119
5.1	Mechanical properties of previous chassis.....	119
5.1.1	Mechanical properties of the parts around the previous chassis.....	120
5.2	Mechanical properties of new chassis.....	120
5.2.1	Material choice	120
5.2.2	Designing with composites	121
5.2.3	Mechanical properties of the parts around the new chassis.....	136
6	MASS AND CENTER OF GRAVITY CALCULATION	137
6.1	Previous chassis	137
6.1.1	Mass definition.....	137
6.1.2	Center of gravity determination	137
6.2	New chassis.....	139
6.2.1	Mass definition.....	139
6.2.2	Center of gravity determination	140
7	CHASSIS CHARACTERISTICS.....	141
7.1	Previous chassis	141
7.2	New chassis.....	141
8	VEHICLE DYNAMICS	143
8.1	Introduction to vehicle dynamics	143
8.1.1	Vehicle fixed coordinate system	143
8.1.2	Earth fixed coordinate system	144
8.1.3	Euler angles.....	145
8.2	Deformation modes.....	146
8.2.1	Longitudinal torsion	146
8.2.2	Vertical bending	146
8.2.3	Lateral bending	147
8.2.4	Horizontal lozenging	147
8.3	Dynamic axle loads.....	147
8.3.1	Static loads.....	149
8.3.2	Weight transfer from acceleration	149

8.4	Braking performance.....	150
8.4.1	Calculation of the torque generated by the rotor.....	152
8.4.2	Weight transfer from deceleration	159
8.5	Cornering performance	165
8.5.1	Low-speed turning.....	166
8.5.2	Roll moment distribution	167
8.6	Aerodynamic performance.....	169
8.7	Ride performance	172
9	DETERMINE THE WORST CASE STRESS SCENARIO	175
9.1	Lateral worst case stress scenario.....	175
9.2	Longitudinal worst case stress scenario	180
9.3	Combination of cornering and braking worst case stress scenario	181
10	CHASSIS LOAD CALCULATOR (CLC) MODEL.....	183
10.1	The dynamics of the Eco Racer chassis 2014	183
10.1.1	Vertical dynamics – static load	184
10.1.2	Lateral dynamics – cornering performance	185
10.1.3	Longitudinal dynamics – braking performance	187
10.1.4	Combination load case	191
10.2	Monocoque chassis dynamics	195
10.2.1	Vertical dynamics – static load	195
10.2.2	Lateral dynamics – cornering performance	196
10.2.3	Longitudinal dynamics – braking performance	196
10.2.4	Combination load case	198
11	CAE / COMPUTER-AIDED ENGINEERING	201
11.1	FEA / Finite element analysis.....	202
11.2	Theories of failure	205
11.3	Modelling (Pre-processing)	207
11.3.1	Carbon fiber monocoque chassis	208
11.3.2	Aluminium space frame chassis	240
12	FINAL DECISION	265
13	MANUFACTURING PROCESS.....	267
13.1	Composite materials.....	267
13.1.1	Composite resins (matrices)	267
13.1.2	Gel coat.....	268

13.1.3	PVA.....	269
13.2	Composite molding processes	269
13.2.1	Hand lay-Up.....	269
13.2.2	Vacuum bagging.....	270
13.2.3	Vacuum assisted resin infusion (V.A.R.I).....	270
13.3	Carbon fiber molding	271
13.4	Developing parts to be molded	272
14	FUTURE PROPOSALS	275
	Citations and Bibliography	280

List of Figures

Figure 2-1 Open section ladder frame chassis of the 1920s (courtesy of Vauxhall Archive Centre) [2]	30
Figure 2-2 Grillage frame [2]	30
Figure 2-3 Chassis structural analysis diagram (Donkin 1925) [2].....	31
Figure 2-4 Car Body Manufacture in the 1920s (courtesy of Vauxhall Archive Centre) [2]	32
Figure 2-5 Springs in parallel [2].....	32
Figure 2-6 Construction details of a timber framed “fabric body” [2].....	33
Figure 2-7 Laterally positioned pair of body mountings [2].....	34
Figure 2-8 Body and body mounts in series in torsion [2]	34
Figure 2-9 Cruciform braced chassis frame (Booth 1938 by permission Council of I.Mech.E.) [2] 35	
Figure 2-10 Free body diagrams of cruciform brace members [2]	35
Figure 2-11 Multiple attachments of body to frame [2]	36
Figure 2-12 Twin tube frame of Auto Union racing car (1934–1937) (courtesy of Deutsches Museum, Munchen) [2].....	37
Figure 2-13 Box which is not triangulated [4]	38
Figure 2-14 Triangulated Box [4]	38
Figure 2-15 Space frame chassis [2]	38
Figure 2-16 Maserati “Birdcage” chassis [2].....	39
Figure 2-17 Gordon Keeble space frame chassis [2]	40
Figure 2-18 Sheet steel backbone chassis (courtesy Lotus Cars Ltd) [2].....	40
Figure 2-19 Backbone chassis views.....	41
Figure 2-20 Lotus Elan chassis	41
Figure 2-21 Tatra used a backbone chassis on large military trucks.....	42
Figure 2-22 VW Beetle floorpan	43
Figure 2-23 Lotus Elise Chassis	43
Figure 2-24 Lotus Elise tub chassis design made from glued-together aluminium sheet [5]	44
Figure 2-25 Pannels closing the sides of the box [4]	44
Figure 2-26 Monocoque chassis.....	45
Figure 2-27 Mass-production monocoque chassis.....	45
Figure 2-28 Carbon fiber monocoque chassis of McLaren F1 sport car [5]	47
Figure 2-29 Ferrari F50 Engine [5]	48
Figure 2-30 Enzo Ferrari Chassis.....	48
Figure 2-31 Porsche Carrera GT Chassis.....	49
Figure 2-32 Lamborghini Aventador LP 700-4 Chassis	49
Figure 2-33 KTM XBOW Chassis	50
Figure 2-34 Bugatti Veyron Chassis	50
Figure 2-35 Koenigsegg Chassis.....	51
Figure 2-36 Modular Toolkits in the Volkswagen Group [6]	52
Figure 2-37 The MQB Platform [6]	53
Figure 2-38 Front subframe.....	53
Figure 2-39 Rear subframe	54
Figure 2-40 Steel Material	55
Figure 2-41 Steel chassis structure.....	56
Figure 2-42 Aluminium Material	56

Figure 2-43 Aluminium chassis structure.....	57
Figure 2-44 Titanium Material	57
Figure 2-45 Magnesium Material.....	58
Figure 2-46 Porche’s Magnesium wheel.....	59
Figure 2-47 Fiberglass Material.....	59
Figure 2-48 Carbon Fibre Material.....	60
Figure 2-49 Carbon fibre chassis structure (KTM XBOW)	61
Figure 2-50 Seam Welding 1	61
Figure 2-51 Seam welding 2	62
Figure 2-52 Seam welding 3	63
Figure 2-53 Seam welding 4.....	63
Figure 2-54 Spot welding 1	63
Figure 2-55 Spot welding 2	64
Figure 2-56 Spot welding 3	65
Figure 2-57 Spot welding 4.....	65
Figure 2-58 Stitch welding	65
Figure 2-59 Bolts	66
Figure 2-60 Rivets.....	66
Figure 2-61 Rivets.....	67
Figure 2-62 Bonded joints.....	67
Figure 2-63 Bonded joints in industry.....	68
Figure 2-64 Material choice	69
Figure 2-65 Bracing	69
Figure 2-66 Tubular Bracing.....	70
Figure 2-67 Rollcage.....	70
Figure 2-68 Roll cage for racing use.....	71
Figure 2-69 Welding Improvements	71
Figure 2-70 A – quad box to rail support, B – tunnel strap, C – floor to roof pole, D – rear shocks to rear floor support, E – front shock to radiator support [8]	72
Figure 3-1 The concepts of stiffness and strength [2]	73
Figure 3-2 Definition of a simple structural surface [2]	75
Figure 3-3 Examples of structures that are simple structural surfaces [2].....	76
Figure 3-4 Saloon (sedan) car structure [2]	76
Figure 3-5 SSS half-model of sedan (saloon) structure [2]	77
Figure 3-6 Baseline model – bending loads [2].....	79
Figure 3-7 Baseline model – bending case, end and edge loads [2].....	80
Figure 3-8 Vehicle in pure torsion [2]	82
Figure 3-9 Frontal structure [2].....	83
Figure 3-10 Forces on dash panel [2].....	84
Figure 3-11 Parcel shelf [2]	85
Figure 3-12 Edge forces in the standard sedan in the torsion load case [2].....	85
Figure 3-13 Rear seat aperture with diagonal braces (courtesy Vauxhall Heritage Archive [2])....	87
Figure 3-14 Sideframe [2]	88
Figure 3-15 Components of forces Q_3 and Q_4 [2]	88
Figure 3-16 Simple structural surfaces model of open vehicle [2]	90
Figure 3-17 Simplified bending load case for open vehicle [2].....	91

Figure 3-18 Sidewall shear force and bending moment diagrams for simplified bending load case [2]	92
Figure 3-19 Edge loads in torsion load case on open vehicle [2]	92
Figure 3-20 Open vehicle sidewall in torsion load case [2]	93
Figure 3-21 Chevrolet corvette structure (courtesy of General Motors Corporation) [2]	94
Figure 3-22 City car cabriolet conversion (courtesy Honda UK Ltd and Automotive Engineering magazine) [2]	95
Figure 3-23 Longitudinally and laterally orientated torsion box [2]	96
Figure 3-24 Example of open vehicle with torsion box on dash region [2]	96
Figure 4-1 Parametric design decision-making processes [11]	98
Figure 4-2 "Explicit design" [12]	99
Figure 4-3 Parametrically generated model [12]	99
Figure 4-4 ER14 design (View 1)	100
Figure 4-5 ER14 design (View 2)	101
Figure 4-6 ER14 design (View 3)	101
Figure 4-7 ER14 design (View 4)	102
Figure 4-8 ER14 design (View 5)	102
Figure 4-9 ER14 during manufacturing	103
Figure 4-10 Front spindle base	104
Figure 4-11 Front spindle	104
Figure 4-12 Rear semi-axle kit	105
Figure 4-13 Body panel (View 1) [12]	105
Figure 4-14 Body panel (View 2) [12]	106
Figure 4-15 95th percentile male driver template [15]	107
Figure 4-16 95th percentile male sketch on our new chassis design	108
Figure 4-17 Major Ergonomic Rules in our new chassis design	109
Figure 4-18 New Chassis First Design Stage	110
Figure 4-19 New Chassis Second Design Stage	111
Figure 4-20 New Chassis design (View 1)	112
Figure 4-21 New Chassis design (View 2)	112
Figure 4-22 New Chassis design (View 3)	113
Figure 4-23 New Chassis design (View 4)	113
Figure 4-24 New Chassis design (View 5)	114
Figure 4-25 New Chassis design (View 6)	114
Figure 4-26 Front spindle base	115
Figure 4-27 Front spindle	115
Figure 4-28 Rear semi-axle kit	116
Figure 4-29 Roll Bar	116
Figure 4-30 Body Panel (View 1) [12]	117
Figure 4-31 Body Panel (View 2) [12]	118
Figure 5-1 6082-T6 aluminium hollow sections	119
Figure 5-2 Data for some engineering materials in the form of areas on a map of Young's modulus E against density ρ [19]	121
Figure 5-3 Relationships between classes of engineering materials, showing the evolution of composites [23]	122

Figure 5-4 Unidirectional fiber composites	123
Figure 5-5 Simplified parallel model of unidirectional composite [23]	123
Figure 5-6 Confirmation of the rule-of-mixtures relationship for the Young moduli, E_c , of unidirectional composites consisting of tungsten wires in Al-4%Cu alloy and glass rods in epoxy resin [23]	124
Figure 5-7 Simple series model of a composite [23].....	125
Figure 5-8 Definition of a shear relative to the x_1x_2 Cartesian axes [23].....	126
Figure 5-9 Variation of the compression moduli of polyester-matrix composites with volume fraction of four species of reinforcing fibers [23]	127
Figure 5-10 Definition of elastic constants for an anisotropic thin composite lamina [23]	128
Figure 5-11 A simple unidirectional composite lamina under tensile load [23].....	129
Figure 5-12 Kies's model (1962) for strain magnification during transverse loading of a unidirectional composite [23].....	129
Figure 5-13 Schematic illustration of compression failure modes in unidirectional composites [23]	130
Figure 5-14 Schematic illustration of interlaminar shear failure in a unidirectional laminate [23]	131
Figure 5-15 Dependence of Young's modulus, $E(\theta)$ and the shear modulus, $G(\theta)$, on the angle, θ , between the fibers and the stress axis for a carbon-fiber composite and a silica/epoxy composite [23]	132
Figure 5-16 Multi-ply laminates [24]	132
Figure 5-17 The effect of cross-laminating on Young's modulus and the shear modulus of a T300/5208 carbon-fiber/epoxy composite [23]	133
Figure 5-18 Effect of randomising the fiber orientations on the stiffnesses of CFRP and CRP laminates [23]	134
Figure 5-19 Values of the Krenchel efficiency factor for various fiber groupings [23].....	135
Figure 6-1 Previous chassis's mass.....	137
Figure 6-2 Center of gravity determination of ER14.....	137
Figure 6-3 Center of Gravity of ER14	138
Figure 6-4 Center of Gravity of ER14	138
Figure 6-5 Mass definition of the new chassis.....	140
Figure 6-6 New chassis' mass.....	140
Figure 7-1 The previous chassis design to be tested	141
Figure 7-2 The suggested chassis design to be tested	142
Figure 8-1 SAE Vehicle Axis System [2]	144
Figure 8-2 Vehicle in an Earth Fixed Coordinate System [2].....	145
Figure 8-3 Euler angles [44]	145
Figure 8-4 Longitudinal Torsion [7].....	146
Figure 8-5 Vertical Bending [7]	146
Figure 8-6 Lateral Bending [7].....	147
Figure 8-7 Horizontal Lozenging [7]	147
Figure 8-8 Arbitrary forces acting on a vehicle [35].....	148
Figure 8-9 Braking Performance [44].....	150
Figure 8-10 Typical Modern Automotive Brake System [47].....	151
Figure 8-11 Energy Conversion [49].....	152

Figure 8-12 Front and end view of the rotor [47]	153
Figure 8-13 Brake force generated by the rotor [49]	153
Figure 8-14 The Brake Pedal [49]	154
Figure 8-15 Optimal pedal force gain properties [35]	155
Figure 8-16 Brake pads [47].....	157
Figure 8-17 The rotor [47]	158
Figure 8-18 Basic Brake Operation [47].....	163
Figure 8-19 Brake Balance [49].....	163
Figure 8-20 Low-speed turning vehicle [51]	166
Figure 8-21 Cornering of a bicycle model [35]	167
Figure 8-22 Simple vehicle roll moment [43]	167
Figure 8-23 Force of a simple vehicle in cornering [35]	168
Figure 8-24 Aerodynamic forces and moments acting on a car [35]	170
Figure 8-25 The ride dynamic system [35]	172
Figure 8-26 Example of fatigue loading event [2].	173
Figure 8-27 Example of proving ground event [2].....	173
Figure 8-28 Vertical symmetric (“bending”) load case (courtesy of MIRA UK) [2].	174
Figure 8-29 Vertical asymmetric (“pure torsion”) load case (courtesy of National Motor Museum, Beaulieu) [2].	174
Figure 9-1 Shell Eco Marathon’s track in Rotterdam, Netherlands. [55]	176
Figure 9-2 Racing line	177
Figure 9-3 Apex. [4]	178
Figure 9-4 The motion of the car follows a parabola	178
Figure 9-5 Geometry of a turning vehicle. [35]	179
Figure 9-6 Deceleration because of stationary preceding vehicle	181
Figure 10-1 Static load distribution on front and rear axle [28].....	183
Figure 10-2 Weight transfer during the roll(left corner). [4].....	186
Figure 10-3 Weight transfer during the pitch (decceleration). [4].....	190
Figure 10-4 Combination load case (Rear view).....	194
Figure 10-5 Combination load case (Front view)	194
Figure 10-6 Combination load case (Side view)	195
Figure 11-1 Common element types used for meshing. [30].....	203
Figure 11-2 Common Element Types Used in ANSYS Workbench Simulation [60].....	204
Figure 11-3 Maximum Normal Stress Theory.....	205
Figure 11-4 Maximum Shear Stress Theory	206
Figure 11-5 Von Mises effective stress.....	207
Figure 11-6 Ansa in CAE process flow [61]	208
Figure 11-7 Carbon Fiber Monocoque Chassis’ Parts (View 1)	209
Figure 11-8 Carbon Fiber Monocoque Chassis’ Parts (View 2)	209
Figure 11-9 Face Problem (View 1)	210
Figure 11-10 Face Problem (View 2)	210
Figure 11-11 Redesign the monocoque to encounter the face problem (View 1)	211
Figure 11-12 Redesign the monocoque to encounter the face problem (View 2)	211
Figure 11-13 Geometry check	212
Figure 11-14 Geometry Check on the Monocoque Chassis	212

Figure 11-15 Triple Cons on the Monocoque (View 1)	213
Figure 11-16 Triple Cons on the Monocoque (View 2)	213
Figure 11-17 Geometry on the Monocoque Fixed (View 1)	214
Figure 11-18 Geometry on the Monocoque Fixed (View 2)	214
Figure 11-19 Penetration-Intersections check.....	215
Figure 11-20 Intersections Check on the Monocoque.....	215
Figure 11-21 Intersections on the Monocoque Fixed.....	216
Figure 11-22 Materials definition	216
Figure 11-23 Material Definition on the Monocoque Chassis.....	217
Figure 11-24 Properties definition.....	218
Figure 11-25 Shell Mesh on the Monocoque Chassis.....	219
Figure 11-26 Volume Mesh on the Monocoque Chassis (View 1).....	220
Figure 11-27 Volume Mesh on the Monocoque Chassis (View 2).....	220
Figure 11-28 Volume Mesh on the Monocoque Chassis (View 3).....	221
Figure 11-29 Volume Mesh on the Monocoque Chassis (View 4).....	221
Figure 11-30 Volume Mesh on the Monocoque Chassis (View 5).....	222
Figure 11-31 Volume Mesh on the Monocoque Chassis (View 6).....	222
Figure 11-32 Volume Mesh on the Monocoque Chassis (View 7).....	223
Figure 11-33 Volume Mesh on the Monocoque Chassis (View 8).....	223
Figure 11-34 Volume Mesh on the Monocoque Chassis (View 9).....	224
Figure 11-35 Volume Mesh on the Monocoque Chassis (View 10).....	224
Figure 11-36 Volume Mesh on the Monocoque Chassis (View 11).....	225
Figure 11-37 Volume Mesh on the Monocoque Chassis (View 12).....	225
Figure 11-38 Volume Mesh on the Monocoque Chassis (View 13).....	226
Figure 11-39 Volume Mesh on the Monocoque Chassis (View 14).....	226
Figure 11-40 Negative volume check.....	227
Figure 11-41 Penetration-Intersections check.....	227
Figure 11-42 Duplicate elements check.....	227
Figure 11-43 Undefined check.....	228
Figure 11-44 Bolt connections on the monocoque Chassis (View 1).....	228
Figure 11-45 Bolt connections on the monocoque Chassis (View 2).....	229
Figure 11-46 Bolt connections on the monocoque Chassis (View 3).....	229
Figure 11-47 Bolt connections on the monocoque Chassis (View 4).....	229
Figure 11-48 Contact Flanges on the Monocoque Chassis (View 1).....	230
Figure 11-49 Contact Flanges on the Monocoque Chassis (View 2).....	230
Figure 11-50 Contact Flanges on the Monocoque Chassis (View 3).....	231
Figure 11-51 Loading Constraints on the Monocoque Chassis.....	232
Figure 11-52 Permanent Static Loads on the Monocoque Chassis	233
Figure 11-53 Driver's Pressure on the Monocoque Chassis (View 1).....	234
Figure 11-54 Driver's Pressure on the Monocoque Chassis (View 2).....	234
Figure 11-55 Driver's Pressure on the Monocoque Chassis (View 3).....	235
Figure 11-56 Front Axle Loads on the Monocoque Chassis (View 1).....	236
Figure 11-57 Front Axle Loads on the Monocoque Chassis (View 2).....	236
Figure 11-58 Front Axle Loads on the Monocoque Chassis (View 3).....	237
Figure 11-59 Front Axle Loads on the Monocoque Chassis (View 4).....	238

Figure 11-60 Front Axle Loads on the Monocoque Chassis (View 5)	238
Figure 11-61 Gravity Acceleration on the Monocoque Chassis (View 1)	239
Figure 11-62 Gravity Acceleration on the Monocoque Chassis (View 2)	239
Figure 11-63 Aluminium Space Frame's Parts (View 1)	240
Figure 11-64 Aluminium Space Frame's Parts (View 2)	241
Figure 11-65 Aluminium Space Frame's Parts (View 3)	241
Figure 11-66 Geometry check	242
Figure 11-67 Geometry Check on the Aluminium Space Frame	242
Figure 11-68 Triple Cons on the Aluminium Space Frame (View 1)	243
Figure 11-69 Triple Cons on the Aluminium Space Frame (View 2)	243
Figure 11-70 Triple Cons on the Aluminium Space Frame (View 3)	244
Figure 11-71 Triple Cons on the Aluminium Space Frame (View 4)	244
Figure 11-72 Penetration-Intersections check	245
Figure 11-73 Intersections Check on the Aluminium Space Frame	245
Figure 11-74 Geometry & Intersections on the Aluminium Space Frame fixed	246
Figure 11-75 Materials definition	246
Figure 11-76 Materials Definition on the Aluminium Space Frame	247
Figure 11-77 Properties definition	248
Figure 11-78 Shell Mesh on the Aluminium Space Frame (View 1)	249
Figure 11-79 Shell Mesh on the Aluminium Space Frame (View 2)	250
Figure 11-80 Volume Mesh on the Aluminium Space Frame (View 1)	250
Figure 11-81 Volume Mesh on the Aluminium Space Frame (View 2)	251
Figure 11-82 Volume Mesh on the Aluminium Space Frame (View 3)	251
Figure 11-83 Volume Mesh on the Aluminium Space Frame (View 4)	252
Figure 11-84 Volume Mesh on the Aluminium Space Frame (View 5)	252
Figure 11-85 Volume Mesh on the Aluminium Space Frame (View 6)	253
Figure 11-86 Negative volume check	253
Figure 11-87 Penetrations-Intersections check.....	254
Figure 11-88 Duplicate elements check	254
Figure 11-89 Undefined check.....	254
Figure 11-90 Bolt connections on the Aluminium Space Frame (View 1)	255
Figure 11-91 Bolt connections on the Aluminium Space Frame (View 2)	255
Figure 11-92 Bolt connections on the Aluminium Space Frame (View 3)	256
Figure 11-93 Contact Flanges on the Aluminium Space Frame (View 1)	256
Figure 11-94 Contact Flanges on the Aluminium Space Frame (View 2)	257
Figure 11-95 Contact Flanges on the Aluminium Space Frame (View 3)	258
Figure 11-96 Loading Constraints on the Aluminium Space Frame (View 1)	259
Figure 11-97 Loading Constraints on the Aluminium Space Frame (View 2)	259
Figure 11-98 Front Axle Loads on the Aluminium Space Frame (View 1)	260
Figure 11-99 Permanent Static Loads on the Aluminium Space Frame (View 1)	261
Figure 11-100 Permanent Static Loads on the Aluminium Space Frame (View 2)	261
Figure 11-101 Driver's Pressure on the Aluminium Space Frame (View 1)	262
Figure 11-102 Driver's Pressure on the Aluminium Space Frame (View 2)	263
Figure 11-103 Gravity Acceleration on the Aluminium Space Frame (View 1)	263
Figure 11-104 Gravity Acceleration on the Aluminium Space Frame (View 2)	264

Figure 11-105 Gravity Acceleration on the Aluminium Space Frame (View 3)	264
Figure 13-1 Hand Lay-Up.....	270
Figure 13-2 Vacuum Bagging	270
Figure 13-3 Vacuum Assisted Resin Infusion	271
Figure 13-4 The undrafted rib (A) scrapes all the way out, while the drafted rib (B) pops out unblemished. [69]	272
Figure 13-5 Draft angle (View 1)	272
Figure 13-6 Draft angle (View 2)	273
Figure 13-7 Draft angle (View 3)	273
Figure 13-8 Draft angle(View 4)	273
Figure 13-9 Draft angle (View 5)	273
Figure 14-1 ER14 at the European Shell Eco Marathon 2014, in Rotterdam, the Netherlands. [70]	277
Figure 14-2 Training from Marc Gene, Driver of Formula1 Scuderia-Ferrari, with the Shell Eco Marathon Technology Manager and Student Liaison, Norman Koch, at the European Shell Eco Marathon 2013, in Rotterdam, the Netherlands. [70]	277
Figure 14-3 Shell Student Energy Challenge Award and People's Choice Award, at the European Shell Eco Marathon 2013, in Rotterdam, the Netherlands. [71]	278
Figure 14-4 Training by David Salters, Head of Engine Development for Scuderia-Ferrari, during our visit to the Ferrari factory in Maranello, Italy, May 2013. [71]	278

List of Tables

Table 2-1 Lotus Elise characteristics [5]	44
Table 2-2 Carbon-fiber panels vs carbon-fiber monocoque chassis [5]	47
Table 3-1 The moments of most of the forces about G [2]	88
Table 3-2 The moments of Q3 and Q5 forces [2]	89
Table 3-3 The edge forces in the end structures [2]	91
Table 3-4 The equilibrium equations (Torsion load case) [2]	93
Table 5-1 Mechanical and physical properties of AISI 9000 Series Steel [18]	120
Table 5-2 Properties of unidirectional CFRP	136
Table 5-3 Properties of multi-ply laminates	136
Table 6-1 The different centers of gravity of the vehicle's parts are added up and form the main center of gravity	139
Table 6-2 Previous vehicle's center of gravity	139
Table 6-3 New vehicle's center of gravity	140
Table 7-1 Previous chassis characteristics	141
Table 7-2 New chassis characteristics	141
Table 8-1 Air resistance coefficients of different vehicles types	171
Table 10-1 Static load distribution on front and rear axle	184
Table 10-2 Static load distribution on left and right wheels	184
Table 10-3 Vertical dynamics - Static load	184
Table 10-4 The data used for the calculation of lateral dynamics	185
Table 10-5 Cornering force	185
Table 10-6 Load transfer from cornering	185
Table 10-7 Mass distribution on front and rear axle during cornering	186
Table 10-8 New center of gravity during cornering	186
Table 10-9 Mass distribution on left and right wheels	187
Table 10-10 The data used for the calculation of longitudinal dynamics	187
Table 10-11 Brake system dimensions	188
Table 10-12 Dynamic characteristics of the vehicle	188
Table 10-13 Force on balance bar by the driver	188
Table 10-14 Braking force calculation	189
Table 10-15 Deceleration and stopping distance	189
Table 10-16 Load transfer from braking	190
Table 10-17 Mass distribution on left and right wheels during braking	190
Table 10-18 New center of gravity during braking and cornering coexistence	191
Table 10-19 Mass distribution on front and rear axles	191
Table 10-20 The cornering force on each wheel	191
Table 10-21 Combination load case	192
Table 10-22 Total dynamic loads on each wheel (z axis)	192
Table 10-23 Cornering forces and moments from contact patch to the center of axle	192
Table 10-24 Braking forces	193
Table 10-25 Vertical distances	193
Table 10-26 Braking forces and moments from disc effective radius to the axle	193
Table 10-27 Vertical dynamics - Static load	195
Table 10-28 Cornering force	196

Table 10-29 Load transfer from cornering.....	196
Table 10-30 New center of gravity during cornering.....	196
Table 10-31 Mass distribution on left and right wheels	196
Table 10-32 Load transfer from braking	197
Table 10-33 New center of gravity during braking and cornering.....	197
Table 10-34 Mass distribution on front and rear axles.....	197
Table 10-35 The cornering force on each wheel	197
Table 10-36 Combination load case.....	198
Table 10-37 Total dynamic loads on each wheel (z axis)	198
Table 10-38 Cornering forces and moments from contact patch to the center of axle.....	198
Table 10-39 Braking forces.....	199
Table 10-40 Vertical distances	199
Table 10-41 Braking forces and moments from disc effective radius to the axle	199
Table 11-1 Pressure applied from the driver's body weight.....	233
Table 11-2 Pressure applied from the driver's body weight.....	262
Table 12-1 Chassis comparison	265

1. INTRODUCTION

1.1 Shell Eco Marathon: The Challenge

TUCER (Technical University of Crete Eco Racing) team has developed zero emission urban vehicles since 2007. The first vehicle was built in 2008, and until 2014 two more one-seated urban concept vehicles followed. The team consists of teachers, employees, undergraduate and graduate students who have a passion for applied engineering - mechanical engineering and motor sport. The team structure follows the standard of professional groups of the area with specialized subgroups in every subset of the vehicle. All members of the team work and participate voluntarily. At the same time, vehicles and innovations are developed solely inside the collaborating laboratories. TUCER (Technical University of Crete Eco Racing), is a research group that studies, designs, develops and manufactures prototypes of low-power city vehicles. The team is mainly supported by the Machine Tools Laboratory and the Intelligent Systems and Robotics Laboratory in the Department of Production Engineering and Management in the Technical University of Crete. The main aim of the group is to develop a prototype vehicle, which is used as a development platform for the research of technologies related to: non-conventional fuels, optimal power management, road safety, environmentally friendly design, new materials and autonomous navigation. Thus, the team investigates and develops advanced technology vehicles entirely in the workshops of TUC.

1.2 Awards

The first big success took place in May 2010 in Germany, the Circuit of EUROSPEEDWAY-Lausitz. At Shell Eco-marathon the team won the first prize in vehicle safety, ADAC Safety Award (among 224 institutions) succeeding consumption performance: 373 km per litre of petrol, taking part in the "high" category of urban vehicles with ER10, a prototype electric vehicle, equipped with hydrogen fuel cells. This category of vehicles was created in 2003 in order to reach conventional cars of everyday use. The next competition in which the team TUCER participated was held on 26-28 May 2011, which was also at the Circuit of EUROSPEEDWAY in Germany. Introducing an improved vehicle, ER11, managed to impress and won the first prize in vehicle safety, for the second consecutive year, the ADAC Safety Award (among 212 institutions). Meanwhile, the 430 km per litre of petrol brought the vehicle to 8th place in its class. The team participated for the fifth time in the international competition of fuel economy, Shell Eco Marathon 2012, which was held on 14-19 May in Rotterdam, the Netherlands. The group presented an entirely new vehicle (ER12) with reduced weight and aerodynamic rate, winning the fourth place in its category, which was the best ranking received by a Greek team in the competition. In the 2013 contest held in Rotterdam in the Netherlands for second year in a row, the improved vehicle ER13 managed to reach the fourth place in its category by achieving the best performance of the team in consumption so far, with 600 km per litre of petrol.

At the same time, the team won the Shell Student Energy Challenge Award, from 183 groups who were invited to present a study on the future energy prospects of the planet in 2050. However, apart from the judges, the team won the confidence of the public and the People's Choice Award. Moreover, the ability given to us to drive one of the three Formula1 simulators of Scuderia-Ferrari has been a great honor. This invaluable experience has been realized in the presence of the Shell Eco Marathon Technology Manager and Student Liaison, Norman Koch and the Formula 1 driver of Scuderia-Ferrari, Marc Gene, who gave to us additional information related to an efficient driving race. Another honor was the invitation of the TUCER group from Scuderia-Ferrari to its factory in Maranello, Italy, where we observed (παρακολούθησαμε) the production process as well as were introduced to their new technologies by the Head of Engine Development, Dave Salters. Now the TUC Eco Racing has won four trophies in six years and continues to confirm that it is among the best teams in Europe. The participation of the group is under the auspices of the TUC and remains.

1.3 Statement of work

The main goal of this thesis is to find a strategy plan for the efficiency of a vehicle structure. Efficiency for a vehicle structure means high strength in bending and torsional loads, with low mass. Lower mass results in lower vehicle consumption, that is essential for better results. To achieve this, a new chassis design is proposed that is lighter and stronger than the previous one [1].

Until now, the team has been working on the chassis using aluminium. Additional material is required to meet stiffness and strength demands which partly cancel the advantage of the lightweight chassis. The necessary addition of material increases the vehicle mass. Therefore, another material is needed that offers mass reduction, superb specific stiffness and strength characteristics, as well as great design freedom.

Furthermore, so far the chassis had been space frame. That means, first of all, that this kind of chassis is difficult to be manufactured because it is made out of many parts that are assembled together. Also, there is not enough space on this kind of chassis. This results in creating extra bases on which more engineering and electrical parts can be placed, that add additional weight to the chassis. Finally, there are more efficient and more innovative types of vehicle chassis that can be used for our purpose rather than space frame. So, a new approach is proposed, a monocoque chassis design. This type of design should be lighter, stiffer and stronger than the space frame, as well as easier to manufacture and more spacious.

1.4 Design approach

To achieve a high quality design the following approach is used:

- the design specifications should compromise with the team's targets.
- the loads that act on the axles are analyzed and calculated.

- the structural possibilities and limitations regarding the available materials are investigated.
- the structural engineering aspects regarding a lightweight though stiff and strong and easy to manufacture design are presented.
- Ergonomic and safety issues are evaluated.
- All these factors are then combined in the final design and modelled using FEA techniques.

2 SELECTION OF VEHICLE TYPE AND CONCEPT

The following must be considered for a good vehicle chassis:

- a) The appropriate chassis type for the required application.
- b) The correct layout of structural elements to ensure satisfactory load paths, without discontinuities, through the vehicle structure.
- c) Choosing suitable size of panels, sections and joints of chassis.

When chassis is designed taking into consideration the load paths, this will make vehicle's foundation achieve torsion, that is, a stiffness which will make the vehicle more efficient. Below are estimates regarding the loads between the structural components of the chassis. This is done using the Simple Structural Surface (SSS) method to achieve an accurate conceptual design. However, structural components, which make up the load paths, need to be re-sized for effective results. Furthermore, we can detect stiffness of chassis by applying the Finite Element Analysis (FEA) method [2].

2.1 An overview of the different vehicle structure types

Below is a summary of the evolution of the different vehicle structures which have been used over the years for passenger cars, highlighting the engineering factors.

The underfloor chassis frame

The body of the vehicle and the chassis was first manufactured separately. This enabled:

- The chassis to function as a separate unit and all the mechanical parts assembled on it.
- Flexibility in manufacturing
- A variety of body styles could be matched to the chassis.

The semi-elliptic spring could easily be fitted on this type of chassis frame, which was a widespread manufacturing process in the 1920's, and was preferred due to the fact that motor vehicle industry manufactured the chassis and the body separately [2].

The underfloor chassis frame, which was regarded as the structure of the car, consisted of a more or less flat "ladder frame". This incorporated two open section (usually pressed C-section) sideframes running the full length of the vehicle, connected together by open section cross-members running laterally and riveted to the side frames at 90 degrees joints. Such a frame belongs to a class of structures called "grillages" [2].

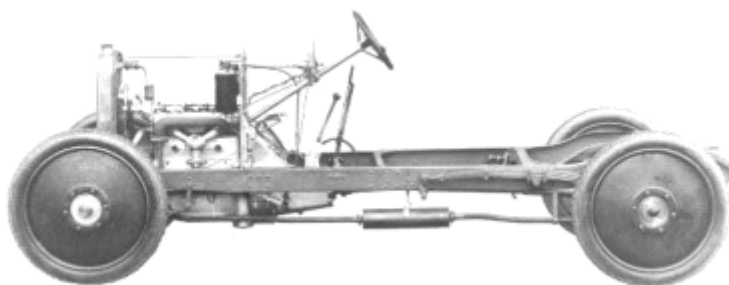


Figure 2-1 Open section ladder frame chassis of the 1920s (courtesy of Vauxhall Archive Centre) [2]

A grillage is a flat (“planar”) structure subjected to loads normal to its plane. The active internal loads in an individual member of such a frame are:

- (a) Bending about the in-plane lateral axis of the member.
- (b) Torsion about the longitudinal axis of the member in the plane of the frame.
- (c) Shear force in a direction normal to the plane of the frame.

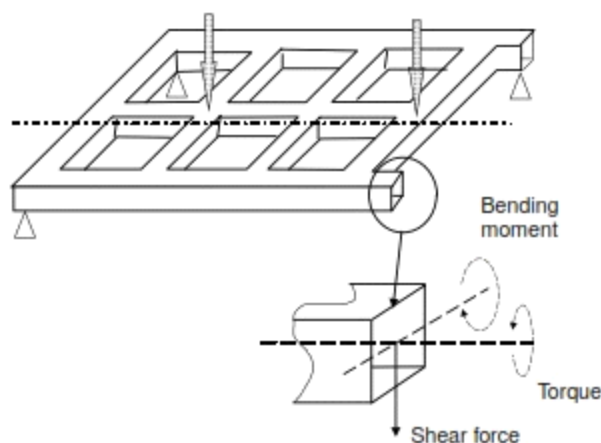


Figure 2-2 Grillage frame [2]

Open section members as well as the riveted T-joints which were used (1920s-1930s) on chassis frames, resulted in the chassis having low torsion stiffness. Texts from the 1920s show that considerable design attention was paid only to the bending behaviour of the structure, mainly from the strength point of view. Donkin’s diagram shows the shear force and bending moment for the chassis frame, which is brought about by the static weight of the chassis and the components assembled on the chassis. This diagram is compared with the distribution of bending strength in the chassis side members. One notices that torsion was not taken into account at this stage of design. However, torsion stiffness is a criterion characteristic of how competent the vehicle structure. In other words, when we have good torsional design we obtain a high level of vehicle handling, lower vehicle vibrations and there is great compatibility of chassis and body.

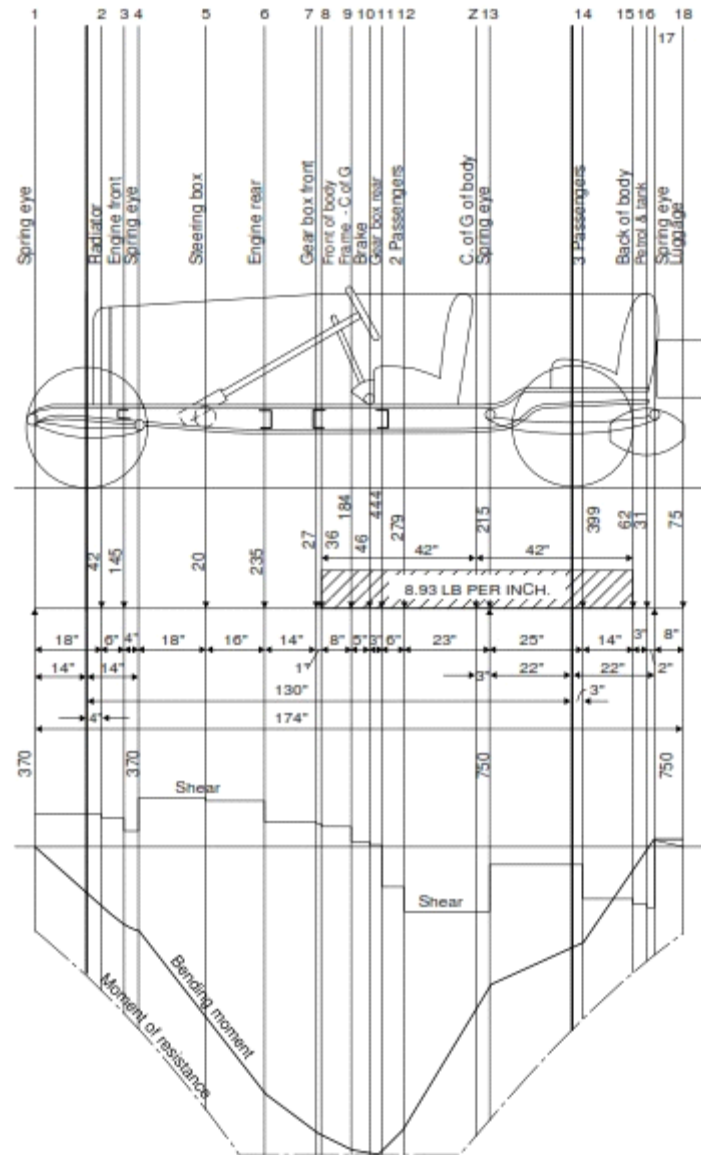


Figure 2-3 Chassis structural analysis diagram (Donkin 1925) [2]

Passenger car bodies (in 1920's) were very flexible because they were not designed to carry road loads and in particular torsion loads. And as a result, there was all sorts of problems such as "rattling", "squeaking" and cracks being formed between the chassis and the body, due to carrying structural loads. It was the body-on-chassis design which cause the aforementioned problems.



Figure 2-4 Car Body Manufacture in the 1920s (courtesy of Vauxhall Archive Centre) [2]

The diagram below shows two springs in parallel where the load is shared between the springs in proportion to their relative stiffnesses. If we consider that the body and chassis are connected only at their ends, we have the following results:

$$T_{\text{TOTAL}} = T_{\text{BODY}} + T_{\text{CHASSIS}}$$

$$K_{\text{TOTAL}} = K_{\text{BODY}} + K_{\text{CHASSIS}}$$

$$T_{\text{BODY}}/T_{\text{CHASSIS}} = K_{\text{BODY}}/K_{\text{CHASSIS}}$$

- where T = torque and K = torsional stiffness.

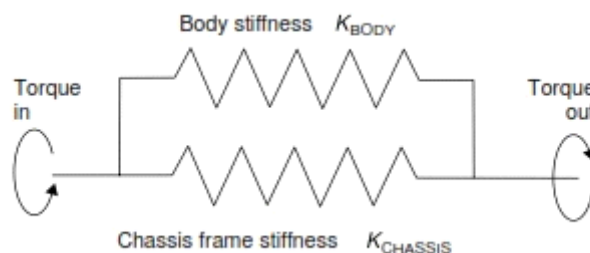


Figure 2-5 Springs in parallel [2]

From the diagram we conclude that, when the body is flexible and the chassis frame is rigid, the torsion load passes through the latter, and vice versa.

Over the years, we notice a change in construction of the vehicle, where bodies are manufactured to be more flexible in regards to torsion, because flexible metal joints are

used between the timber body parts and also flexible materials are used on the outer skin of the body.

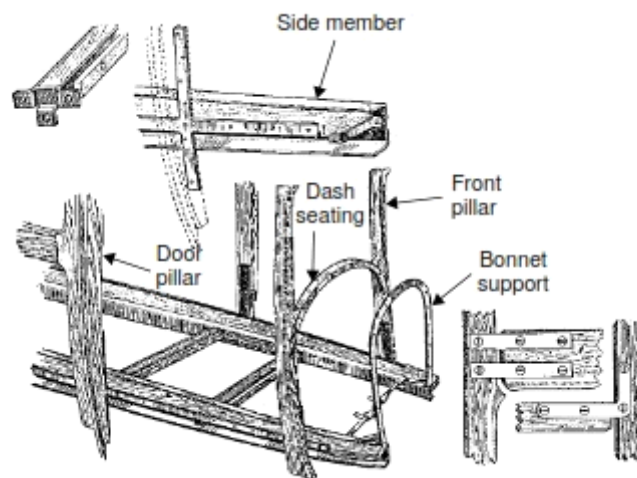


Figure 2-6 Construction details of a timber framed “fabric body” [2]

We observe that with closed shell structures, we have a greater effectiveness in torsion, because the outer skin is subjected locally to shear. Low torsion stiffness results when flexible materials are used to form the outer skin of the body, for example fabric. The “Weymann fabric saloon” body is a typical example of this. Another design approach was when very thin aluminium cladding with deliberate structural discontinuities at key points was used to decrease the accumulation of stresses in the car body. This design approach was not suitable for mass production.

Therefore, we observe that the pressed steel car body replaced the former technology, in the 1930s. Steel sheets comprised the body which were welded together and as a result greater stiffness in torsion was achieved. Yet, we still have the separate “body-on-chassis” technology as well as the fact that the parts of the chassis are made of open sections.

As regards the “springs in parallel” analogy, we now have a greater proportion of the load being taken through the body, because of an increase in stiffness. However, the different degrees of stiffness between the body and the chassis causes problems such as rattling, or damage to body mounts. In order to overcome these problems a number of approaches were devised, some of which are explained below [2]:

(a) Flexible mountings are placed laterally among the body and the chassis and work as torsion springs (1930s). The torsional stiffness K_{MOUNT} of the pair of mounts is:

$$K_{\text{MOUNT}} = K_{\text{LIN}} B^2 / 2$$

- where K_{LIN} is the linear stiffness of the individual elastomer body mounts
- where B is the body width

As a result, the two pairs of springs are placed in series with the body. Regarding the latter, the overall stiffness is lower than that of the individual elements in series.

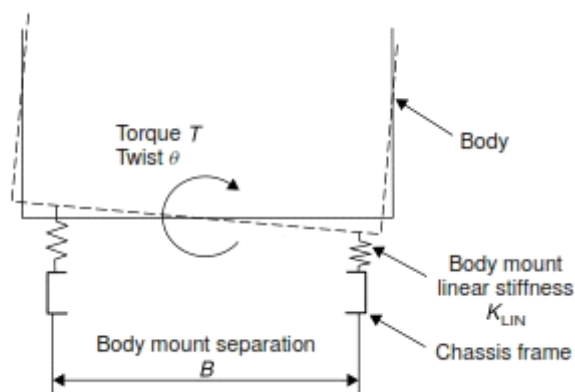


Figure 2-7 Laterally positioned pair of body mountings [2]

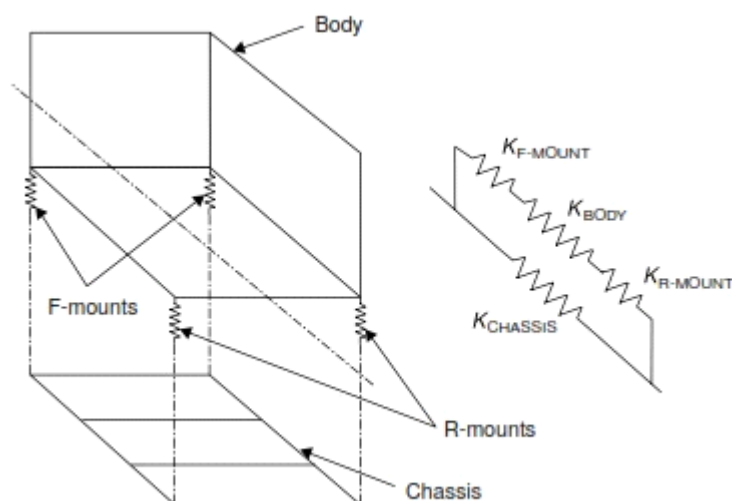


Figure 2-8 Body and body mounts in series in torsion [2]

Therefore, the overall flexibility is the sum of the individual flexibilities:

$$1/K_{\text{TOTAL}} = 1/K_{\text{F-MOUNT}} + 1/K_{\text{BODY}} + 1/K_{\text{R-MOUNT}}$$

- where K = torsion stiffness and $1/K$ = torsional flexibility.

When the flexible mountings were placed laterally among the body and the chassis, many attempts to minimize the torsion load percentage, that was carried by the body happened so that the maximization of the overall stiffness could be achieved.

(b) The goal of the approach (a) was the improvement of the chassis frame stiffness, so that it would be capable of handling more load. Nonetheless, the utilization of open section parts in addition to riveted chassis technology was still the only tendency.

Cruciform brace which consists of open section parts was commonly used in order to increase the torsion stiffness. This brace was included in the chassis frame and was well connected, in shear, to the side members of the chassis.

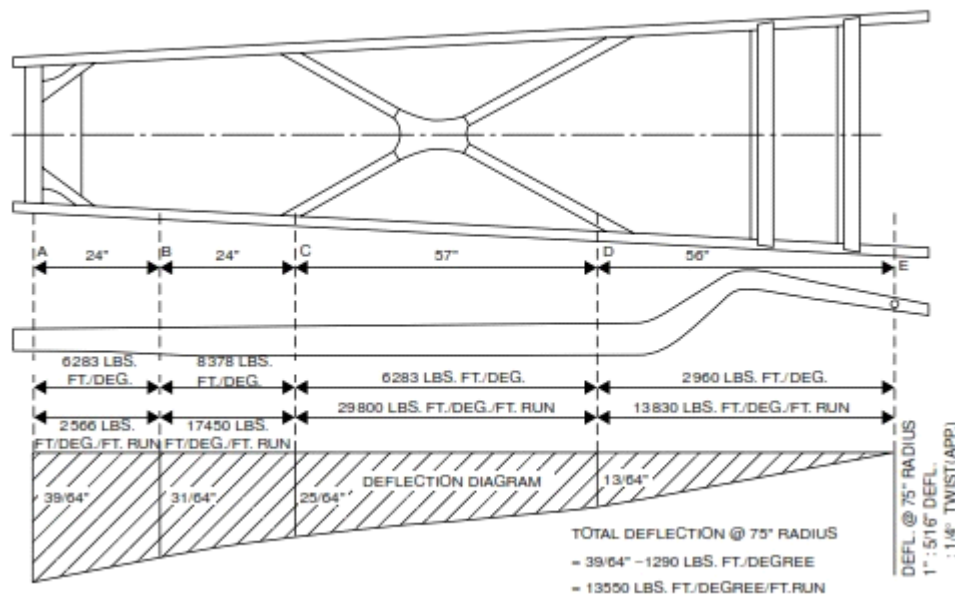


Figure 2-9 Cruciform braced chassis frame (Booth 1938 by permission Council of I.Mech.E.) [2]

Figure 2-10 shows the operation of a cruciform brace when it is subjected to torsion. On the left-hand side, the input torque causes a pair of equal and opposite forces that are reacted with a pair of equal and opposite forces on the right.

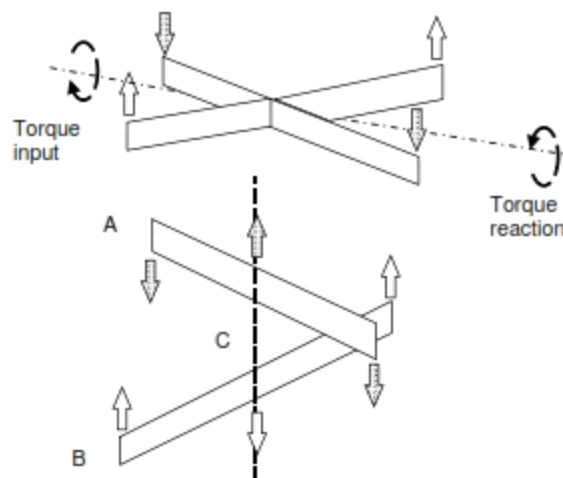


Figure 2-10 Free body diagrams of cruciform brace members [2]

Moreover, the components of a cruciform brace and the loads that are acted on each component, in a torsion load case, are showed in the above body diagrams. In the first

component, A, vertical loads are applied downward at its edges and are reacted with an upward force F at point C. This force is reacted with an equal and opposite force F' at point C on component B. Thus, in the second component, B, vertical loads are applied upward at its edges and are reacted with the force F' .

The use of open sections was apprehended due to the sole application of bending and shear forces towards the individual components A, B.

According to Booth's paper, in 1938, the torsion stiffness of the vehicles with cruciform brace chassis were calculated among 1000 and 1750 Nm/deg. The greatest cruciform brace chassis (with open sections) was probably the Lagonda's V12 chassis, with 2000 Nm/deg. torsion stiffness (Bastow 1945 and 1978). In that period, the improvement of the torsion stiffness was still essential.

d) The utilization of closed cross-members was an additional method of increasing torsion stiffness of the chassis. Closed section components have proven to be of greater stiffness in torsion than the open section ones. However, the overall stiffness was still not of great importance compared with today's.

(e) By the mid-1930s it was realized that the steel body was much stiffer than the chassis in both bending and torsion. Greater "integration" of the body with the chassis frame was also used in some designs. A body attached to the chassis frame by a large number of screws, thus using some of the high torsion stiffness of the body. This approach led eventually to the modern "integral body".

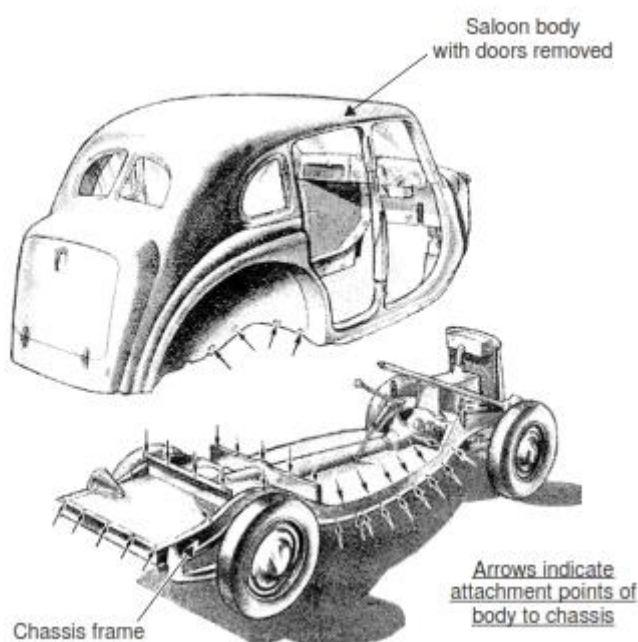


Figure 2-11 Multiple attachments of body to frame [2]

(f) The ultimate version of the underfloor chassis frame using small section members is the "twin tube" or "multi tube" frame. This is still essentially a ladder type grillage frame, with side members connected by lateral cross-members. However, now both the

side members and the crossmembers consist of closed section tubes. The advantage of this arrangement is that typically, for members of similar cross sectional dimensions, a member with a closed section will be thousands of times stiffer in torsion than an equivalent open section member. Also adjacent members are usually welded together in this construction method, and such joints are much stiffer than riveted connections. The overall torsion stiffness of the chassis assembly improves accordingly.

This type of structure was used in specialist racing vehicles between the late 1930s and the 1950s. For example, the Auto Union racing car (1934–1937) shown in Figure 2-12 used this system, as did many sports racing cars in the 1950s, such as Ferrari and Lister Jaguar. Examples of these may be seen in “Costin and Phipps” book (1961).

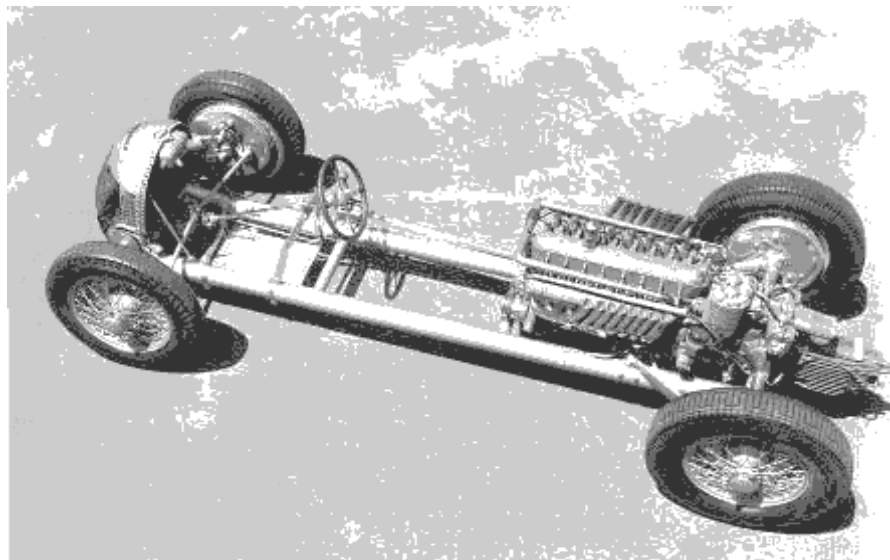


Figure 2-12 Twin tube frame of Auto Union racing car (1934–1937) (courtesy of Deutsches Museum, Munchen) [2]

Separate ladder frames, with either open or closed section members, are still used widely on certain types of passenger car such as “sport utility vehicles” (SUVs) and they are almost universal on commercial heavy goods vehicles.

2.2 Modern structure types

Studying the evolution of vehicle structures helps to understand some weaknesses in these structures. Turning now to the modern structure types, we will examine some chassis types so as to select the appropriate type of our chassis, as well as its appropriate design [3].

Space-Frame Chassis

The diagram below shows a box, with a top, bottom and two sides, but the box is missing the front and back. The box when pushed collapses easily because there is no support in the front or back [4].

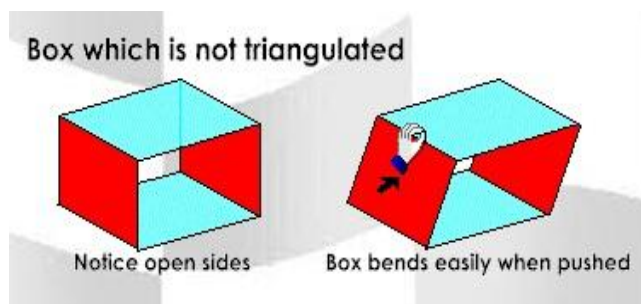


Figure 2-13 Box which is not triangulated [4]

Cars need to be supported in order to operate properly, and so we triangulate the box by bracing it diagonally. This effectively adds the front and back which were missing, only instead of using panels, we use tubes to form the brace. See below:

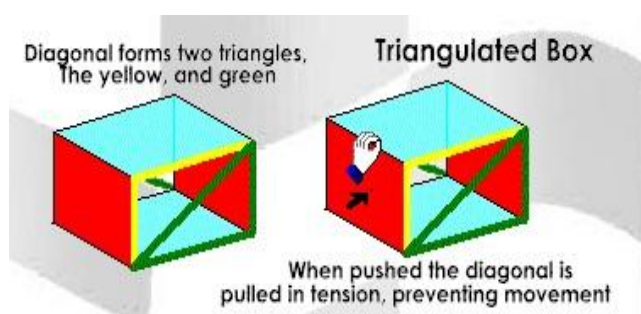


Figure 2-14 Triangulated Box [4]

The triangulated box above imparts strength by stressing the green diagonal in tension. Tension is the force trying to pull at both ends of the diagonal. Another force is called compression. Compression tries to push at both ends of the diagonal (Shown above in the horizontal yellow tube). In a given size and diameter tube or diagonal, compression will always cause the tube to buckle long before the same force would cause the tube to pull apart in tension.

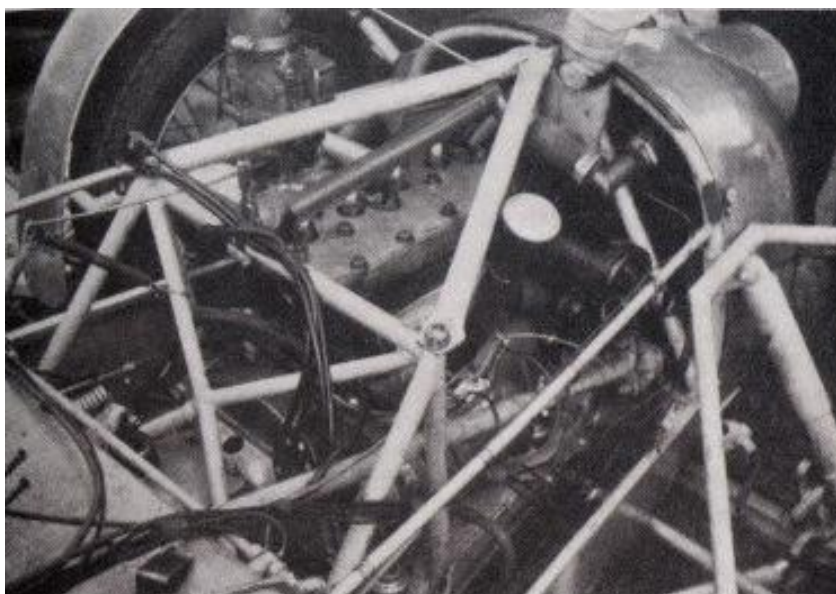


Figure 2-15 Space frame chassis [2]

As we mentioned above, the problem with a ladder-frame chassis is that, although strong, it is not very stiff. The suspension and steering systems on cars are designed on the basis that they are mounted to a solid object, so having a chassis that "squirms" under load prevents the suspension from being effective. Obviously, this is a major issue when we are designing a vehicle, and so it is here that we shall look. If one were to try and make a ladder-frame chassis stiffer, the natural starting point would be to add bracing to prevent twist. The picture 2-15 above shows bracing struts on a chassis built by Lotus founder Colin Chapman, based on the ladder-frame from an Austin 7, which stiffen up the structure significantly.

Once the idea of bracing a chassis against twisting is introduced, the next logical progression is to consider the following fact; If the bracing is preventing the chassis twisting, the question we pose is: do the main chassis members have to also resist twisting, or can all those forces be left to the bracing components? Working on this principal, it should be possible to build a chassis where every single member has a bracing attachment, and has no twisting forces acting on it, just compression and tension. It is this principle that applies to spaceframes, removing bending forces acting on chassis members to allow one to make them smaller, thinner and lighter at the same time as building a stiffer overall structure.



Figure 2-16 Maserati "Birdcage" chassis [2]

The picture 2-16 shows a Maserati "Birdcage" chassis, which is just about the perfect example of this design philosophy. We notice how thin the tubes are, because each one has only tension and compression loads, and therefore they will not bend. The principle which applies here is that each member is only loaded in the direction which it's strongest.

Obviously, not every gap between tubes can be braced (there needs to be enough room for the driver to sit in the car etc), thus in reality the chassis members must re-

tain some resistance to bending. However, this structure is much stiffer than a ladder-frame chassis at a far lower weight. One major disadvantage is, due to many tubes used for the design, there is little space available, which is not good for carrying loads. Also, the design relies on even distribution of loading, so it is not suited to carrying a couple of tons on the back of a truck, for instance.

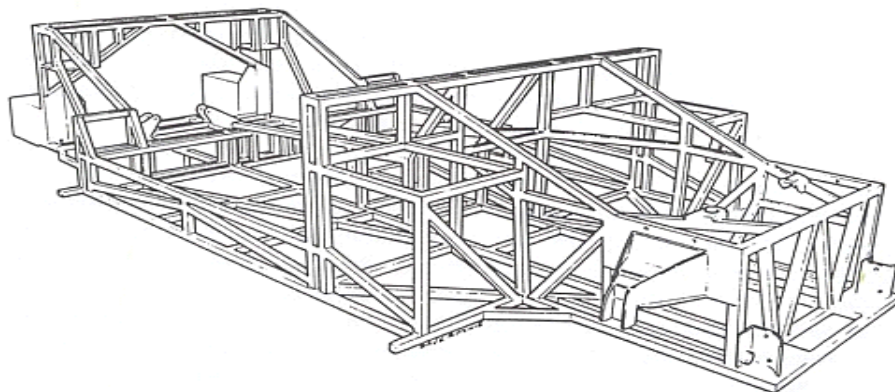


Figure 2-17 Gordon Keeble space frame chassis [2]

A secondary problem is that a spaceframe is complex to build. Even leaving aside the difficulty of ensuring that all required bracing has been designed in, the trouble is to weld all the sections together accurately. Even for a relatively simple space frame, such as the Gordon Keeble chassis pictured above (Figure 2-17), this is a hugely labour-intensive exercise, far more so than any ladder-frame design. An advantage is that the materials and principles used are simple and as a result a very stiff, light structure can be assembled without any special techniques. It is for this reason that, although now overshadowed in terms of ultimate performance by other designs, the space-frame chassis remains a very popular way of building high-performance vehicles where speed of production, interior space, and ultimate stiffness and weight-reduction can be sacrificed in exchange for being able to use relatively basic materials and techniques. Most kit cars, as well as many racing vehicles, use space-frame construction.

Backbone Chassis

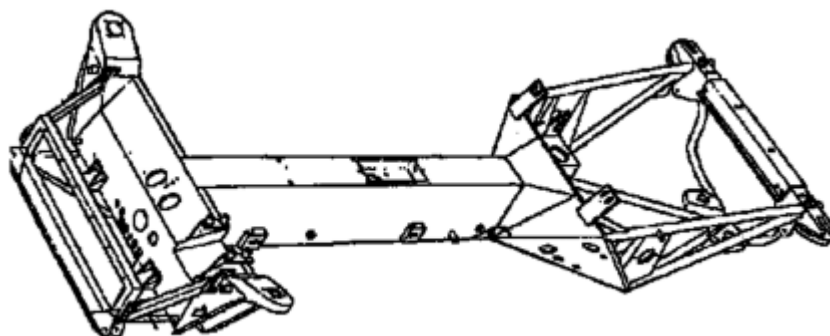


Figure 2-18 Sheet steel backbone chassis (courtesy Lotus Cars Ltd) [2]

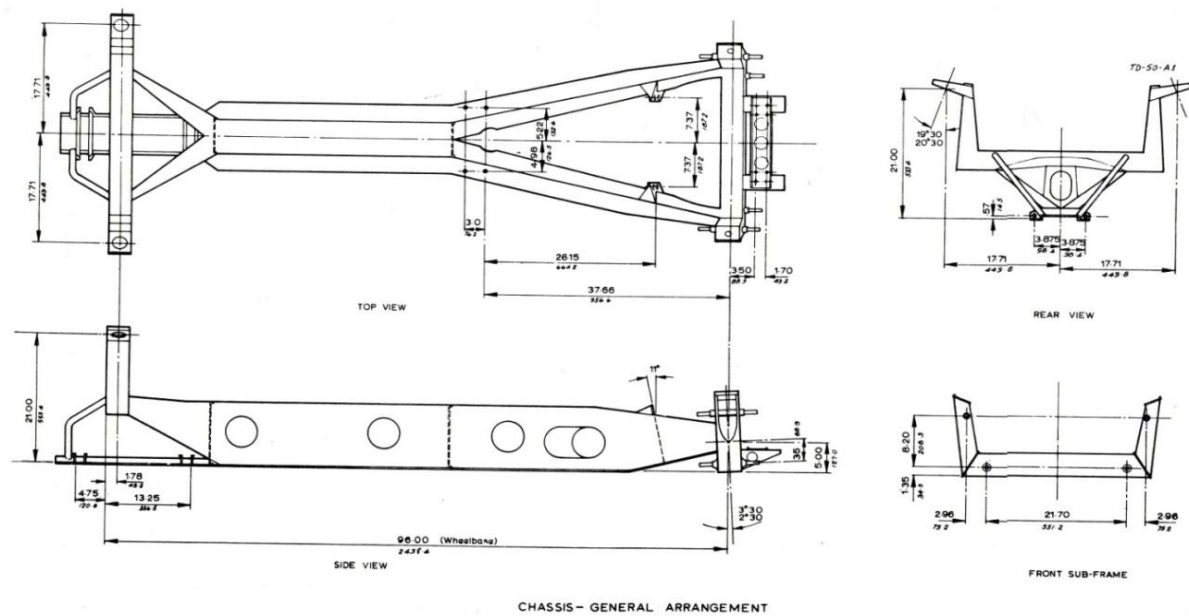


Figure 2-19 Backbone chassis views



Figure 2-20 Lotus Elan chassis

A space-frame chassis works by distributing the loadings on it across the whole structure. However, as mentioned, having to make room in the middle for the driver reduces the possibility of running bracing struts across, and so reduces the possible stiffness of the structure. If the passenger were hung on the outside area of the chassis, one would have no issues with being able to fit the bracing in place. Although this would necessitate moving the chassis rails closer together to fit between the seats, the loss of stiffness this would cause can be compensated for by the fact that one can now add almost unlimited bracing to this central area. Rather than using several tubes, the easiest way to accomplish this would be to use a panel across the surface of the frame - effectively making a single, giant square-section down the centre of the chassis. And if this is done, one might as well just do away with all the tubing and make the central section into a square-section made from folded and welded sheet metal. On the chassis for the original Lotus Elan, in the previous photo, we can see that this has been taken to the logical conclusion, with most of the structure made from folded sheets.



Figure 2-21 Tatra used a backbone chassis on large military trucks

A backbone chassis like this can actually be slightly stiffer than a space frame of the same weight. However, because the chassis has to fit within the confines of the centre of the body, it can only be made so stiff. As such, it tends to lend itself better to small or medium sized vehicles, as large, powerful cars do not necessarily have enough of a proportional increase in the room available for the central backbone to allow it to be scaled up to cope with the increased loads. This is not so much of an issue for extremely large vehicles, though, and Czechoslovakian manufacturer Tatra has successfully used a backbone chassis on large military trucks, although in this case the chassis structure is tubular rather than square. Although Colin Chapman is often credited with inventing the backbone design, it's actually Tatra who first developed it.

It must be noted that with the backbone chassis, the structural component of the car in the centre allows the outer body panels to be made from very light material such as composites or aluminium. While this is good for weight-reduction, it also means that a backbone chassis car is not necessarily the place for a passenger to be in the event of a side impact, as there is not much protection there. The DeLorean was designed using a backbone chassis (with the help of Lotus), and was designed from the outset to be an extremely safe car, with good side-impact protection. The reason being is that the DeLorean was part backbone chassis, and part monocoque. In fact, this is true for most backbone-chassis vehicle designs.

Floorpans & Tubs



Figure 2-22 VW Beetle floorpan

Having established the use of folded sheet metal for chassis components, we can turn to designing a "chassis" from sheet metal. The most difficult way of doing this would be to take many individual pieces of metal, fold them into tubes and weld them together. The easier way would be to press two large sheets of metal with many ribs, and then press them together so that the ribs form tubes between the two sheets. This is a similar structure to a ladder-frame chassis. In the picture 2-22 is a VW Beetle floorpan, we can see how the pressed steel forms a backbone-like structure along the length of the car. The Citroen 2CV also used a floorpan. This process allows for many of the advantages of a ladder-frame chassis (such as the adaptability for various body designs) without the time and labour penalties for manufacturing such a structure from carefully-aligned individual components.



Figure 2-23 Lotus Elise Chassis



Figure 2-24 Lotus Elise tub chassis design made from glued-together aluminium sheet [5]

An improvement on the floorpan idea is building a tub out of sheet metal or composites, so that the "walls" of the tub help add stiffness. The Lotus Elise chassis is a very good example of a tub design, made from glued-together aluminium sheet. This provides the car with a very stiff structure onto which the other components can be mounted - one of the reasons why the Elise is proclaimed by many to be the best-handling production car ever built [5].

Table 2-1 Lotus Elise characteristics [5]

Lotus Elise	
Weight of chassis	65 kg
Torsional stiffness	11,000 Nm/degree
Thickness of extrusion	1.5 mm

Monocoque Chassis

In contrast to Spaceframes, the monocoque chassis uses panels, just like the sides of the box pictured above (Figure 2-14). Instead of small tubes forming the shape of a box, an entire panel provides the strength for a given side (Figure 2-25).

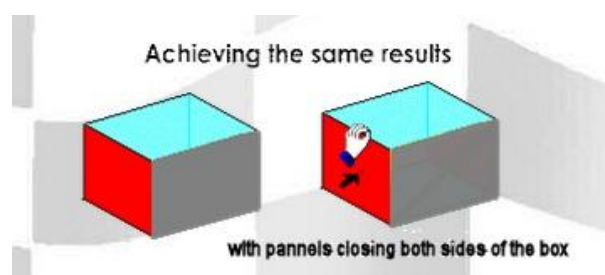


Figure 2-25 Pannels closing the sides of the box [4]

The designs we have examined so far are where a chassis takes all the structural loading, and the body panels sit on the outside. The problem with this is that no matter how light the chassis is, when putting the body panels in place, weight will be added. There are two solutions to this problem. First, one could fit only the bare minimum of panels required to cover the chassis, made from the thinnest, lightest material such as sheet aluminium, similar to the Lotus Seven, which is little more than a thinly-skinned chassis.

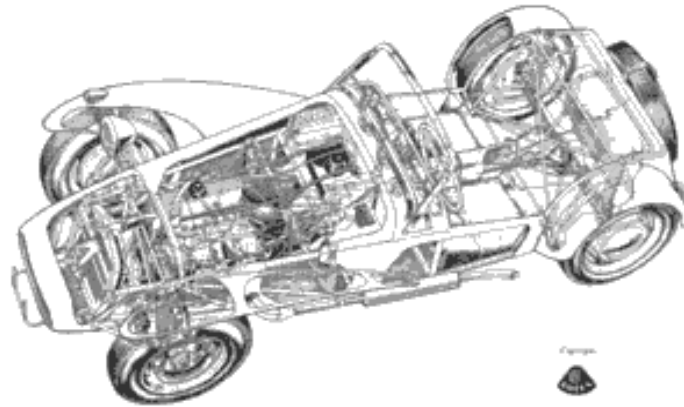


Figure 2-26 Monocoque chassis

As previously mentioned, shaped sheet metal can be used to make chassis sections and body panels. Thus, one could also use the body panels themselves as chassis members, thereby eliminating any unnecessary body weight. This is known as a monocoque or a single shell. This approach has the panels of a structure give it its outer appearance and provides structural strength, which we see in aircraft designs, and known as a “stressed skin” construction. It is the progression of the use of pressed panels, but rather than just construct what is known as ‘sandwich tubes’ for the floor, this is also done for the side panels. The floorpan is similar to a ladder-frame, which consists of pressed sheets, however, the monocoque resembles the construction of a space frame since one can press more complicated shapes and as a result bracing members can be placed in more places, which means a stiffer structure is built with more space inside.



Figure 2-27 Mass-production monocoque chassis

Monocoque is the most popular method used in manufacturing vehicles as regards mass-production because it allows for a light, stiff structure with open-plan inside, plus the fact that it is easier to assemble in a factory, and particularly easy for computerized-robotized factories. Despite not having the same strength as a heavy ladder-frame chas-

sis, the monocoque remains the most preferred option when taking cost and the efficiency of production into account.

The thinner material used in monocoque design makes the vehicle easier to buckle, but because of this, we have the improved safety of what is called 'crumple zones', which allow the impact of a crash to be distributed to a number of panels crumpling them in the process. As a consequence of this process, the length of time it takes the vehicle to halt is prolonged which protects the passengers in the car as it reduces the accelerative forces on them. This system can be applied to the ends of chassis rails; however, the degree of protection is much less with the separate chassis arrangement, as was used in the past. One drawback to this is that on impact, the bodyshell is completely damaged and thus must be thrown away, yet it is quite a minor point as there are no fatalities because of this. These crumple zones can act in any direction which allows the designer to apply them to side impacts as well. In fact, the designer has many choices regarding which direction he/she wants the component to be stiff and which to be crumpled.

Carbon-fiber monocoque chassis

Carbon fiber is used in racing cars as well as spacecrafts and airplanes due to its great rigidity-to-weight ratio. We notice that FIA allows group B racing category cars to use any technology as long as 200 road cars or more are also manufactured. For this reason, we have the carbon-fiber body panels in the Ferrari 288GTO and Porsche 959.

Monocoque skins incorporate composite materials in their structure, this means there is more strength, stiffness and flexibility which can be controlled in different fiber directions. Direction of the fibres is carefully designed, and layers of materials used in the skin are placed on top of others to produce different mechanical properties in different directions as well as keeping weight at an optimum level. In addition to this, composite materials are ideal for the many parts of the vehicle.

Due to the great number and types of functional demands for the monocoque as well as the multiple plies necessary for the carbon (or other composite laminate) a complex loading situation is created which means detailed analysis and calculations need to be taken into account. Finite element analysis (FEA) programs are used today as this provides information regarding modeling multiple materials, simulating short duration impact dynamics, and complex contact conditions as well as multiple components. Such software programs allow engineers to choose the best locations for attachment points and the direction of the fibers.

Using a carbon/epoxy monocoque benefits designers as it allows for integration, freedom to customize the laminate at the attachment points and overcoming unnecessary stresses or delamination (that is when it splits into thin layers).

Carbon-Fiber Panels VS Carbon-Fiber Monocoque Chassis

The Porsche 959 used carbon-fiber in body panels, and if one were to compare it with the McLaren F1's carbon-fiber monocoque, without hesitation, we could state that the latter is by far superior as it supports the engine / drivetrain and suspensions, and also serves as a very rigid survival cell.

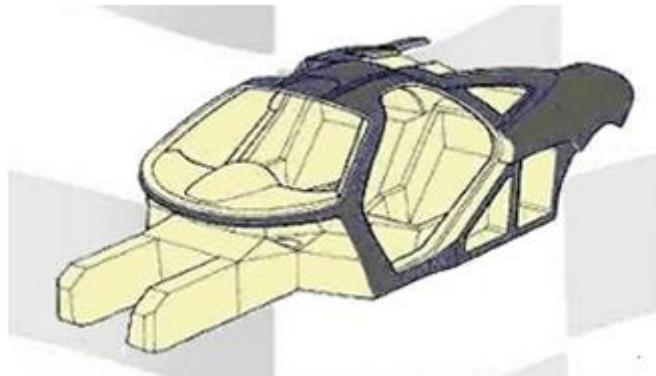


Figure 2-28 Carbon fiber monocoque chassis of McLaren F1 sport car [5]

The Porsche 959, Ferrari 288GTO, Ferrari F40 and even lately, the Porsche 911 GT1 are examples of supercars that use carbon-fiber in body panels, but because body panels do not contribute to mechanical strength, using carbon fiber over aluminium does not save weight. The stress member is still the chassis most often found in a much heavier and weaker steel tubular frame.

Table 2-2 Carbon-fiber panels vs carbon-fiber monocoque chassis [5]

Car	Body	Chassis
Ferrari 288GTO (1985)	carbon fiber panels	steel tubular space frame
Porsche 959 (1987)	carbon fiber panels	steel monocoque
Ferrari F40 (1988)	carbon fiber panels + doors	steel tubular space frame
McLaren F1 (1993)	carbon fiber panels	carbon fiber monocoque
Ferrari F50 (1996)	carbon fiber panels + doors	carbon fiber monocoque
Lamborghini Diablo SV (1998)	mostly aluminium panels, with carbon fiber bonnet + engine lid	steel tubular space frame
Lamborghini Diablo GT (1999)	mostly carbon fiber panels + aluminium doors	steel tubular space frame

The carbon-fiber monocoque chassis first appeared in 1981 with McLaren's MP4/1 Formula One racing car, designed by John Barnard. This chassis is far more superior to any other designed, as it offers superior rigidity yet optimizes weight. Later followed the Bugatti EB110SS (not to be confused with the Bugatti EB110GT) and the Ferrari F50.

Unlike the McLaren F1, the Ferrari F50's rear suspensions are directly bonded to the engine and gearbox assembly which means the engine becomes the stressed member supporting the load from the rear axle. The whole engine, gearbox, and rear suspensions structure is then bonded into the carbon fiber chassis through light alloy. The first to be constructed in this way as regards road cars.

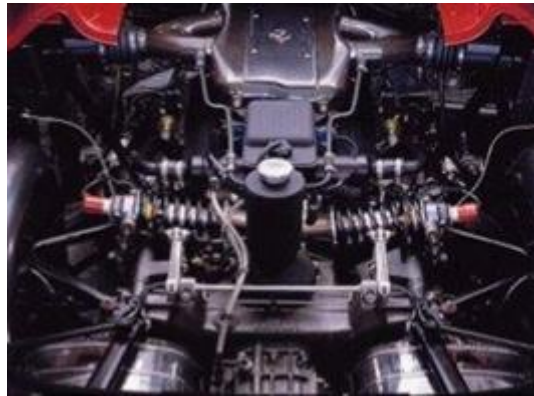


Figure 2-29 Ferrari F50 Engine [5]

In the following pictures we can see some carbon-fiber monocoque chassis:



Figure 2-30 Enzo Ferrari Chassis



Figure 2-31 Porsche Carrera GT Chassis

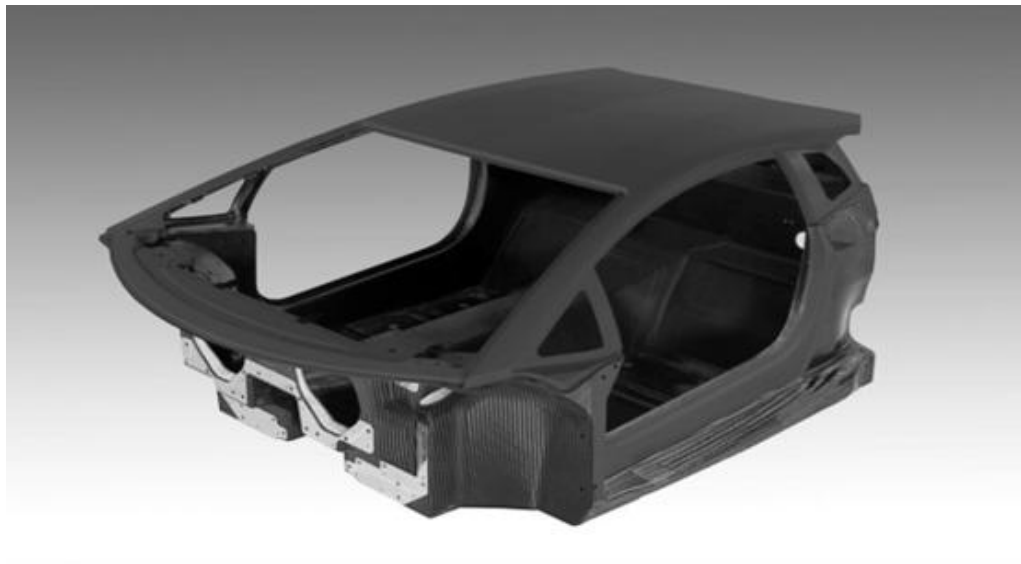


Figure 2-32 Lamborghini Aventador LP 700-4 Chassis

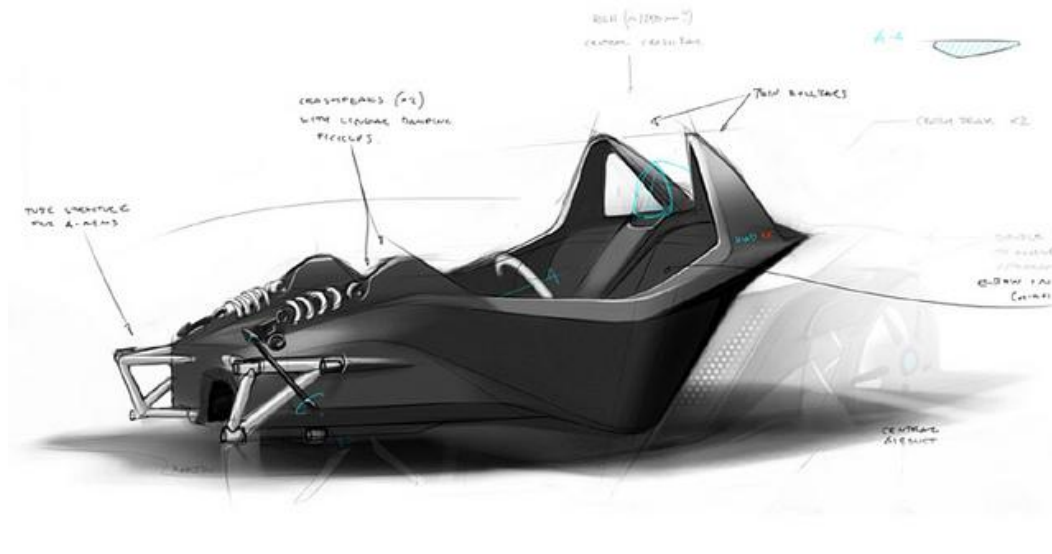


Figure 2-33 KTM XBOW Chassis



Figure 2-34 Bugatti Veyron Chassis



Figure 2-35 Koenigsegg Chassis

Modular Transverse Toolkit Strategy (MQB)

Significantly reducing the fuel consumption of the vehicles, producing them at globally competitive costs and simultaneously increasing profitability and productivity – these are the Volkswagen Group’s goals for its modular toolkits. They represent the further development of their platform and modular strategy, which has its origins in the mid-1990s. The latest member of our toolkit family is the Modular Transverse Toolkit (MQB). The basic principle is simple: build an architecture that’s flexible enough to accommodate anything, from a supermini like the Polo to a seven-seat SUV like the one VW will introduce in the U.S. market in 2015. This is more than just the chassis, though, as it concerns a common component strategy far beyond anything ever implemented until now [6] [7]. The MQB system will allow them, to reduce vehicle weight and fuel consumption and to offer new technologies. The toolkits also make it possible for them to produce different models in different quantities and even from different brands at one plant, in the same facility. Furthermore, it allows VW to create more cars that are more tailored for specific markets at a lower cost [5].

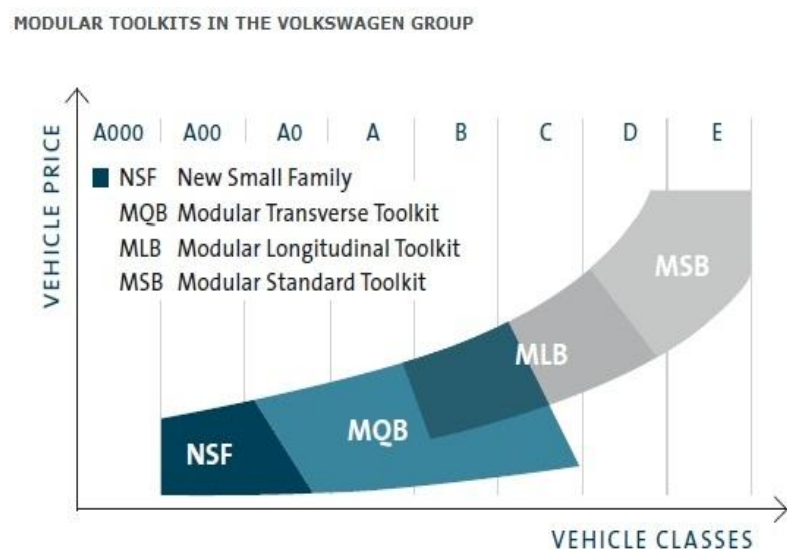


Figure 2-36 Modular Toolkits in the Volkswagen Group [6]

Almost every vehicle from the VW Group that is transverse-front-engined and bigger than a VW Up will eventually be based on the MQB parts matrix. It lays down a series of hard points for a huge range of cars and powertrains. These hard points determine the common design of production line. But they also allow systems (for example entertainment systems or aircon or axles) of differing sizes and complexities to be fitted, provided their mounts link with the hard points. All the electric systems are also designed to pair up with the MQB's unified electrical architecture.

Well, the MQB has created an extremely flexible vehicle architecture that permits dimensions determined by the concept such as the wheelbase, track width, wheel size and seat position to be harmonized Group-wide and deployed variably, because the platform can be shrunk and stretched depending on the car. Other dimensions, for example the distance between the pedals and the middle of the front wheels, are always the same and guarantee a uniform system in the front of the car.



Figure 2-37 The MQB Platform [6]

Take that fundamental concept, stretch it across many different vehicle types, sizes and brands, then build them by the millions, and you begin to sense the enormity of Volkswagen's rapidly evolving "mega-platform" strategy and its potential impact on competitors around the globe. The new platform features a far greater degree of plug-and-play modularity, flexibility and parts commonality than at Toyota, General Motors Co, Ford and other competitors.

2.2.1 Subframes



Figure 2-38 Front subframe

It is common for most cars to have all the main components mounted onto the chassis. There are however cases where a subframe is used, (a separate mini chassis) where certain parts of the vehicle are carried (engine and drive train or the rear suspension), and which is then attached to the main chassis or the body. One example is the mini where

we find a front subframe carrying the engine, gearbox and front suspension while a rear subframe carries the rear suspension. This is type of design is mainly to be found with a monocoque design.

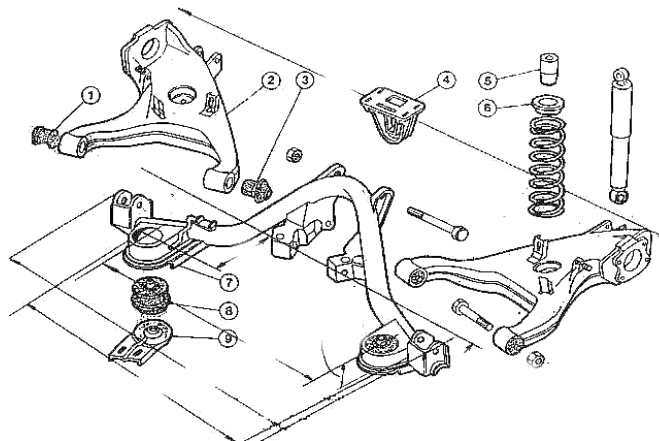


Figure 2-39 Rear subframe

One of the benefits of a subframe is that it enables the manufacturer to assemble the parts together before assembling the entire vehicle as well as it being adaptable (like a ladder-frame chassis), that is, one sub-frame assembly can be combined with a number of different bodyshells. Furthermore, many of the stiffness benefits of a space-frame or backbone chassis can be achieved, (such as the suspension mountings) without forgoing the benefits of using a monocoque bodyshell to build the vehicle's main structure. We notice that the earliest monocoque designs lacked this degree of stiffness. Therefore, having a rigid traditional chassis will, for example give belt-and-braces reassurance for suspension mounting points. Whereas in more modern designs, one achieves tight, accurate tolerances on the sub assembly and accuracy of the alignment of the major structure, which are less critical to correct suspension alignment, for example.

2.3 Chassis materials

Steel, (in its various forms), has been the most commonly used material for the manufacture of vehicle chassis, but over the years there have been other materials used also, which are presented below:

Steel

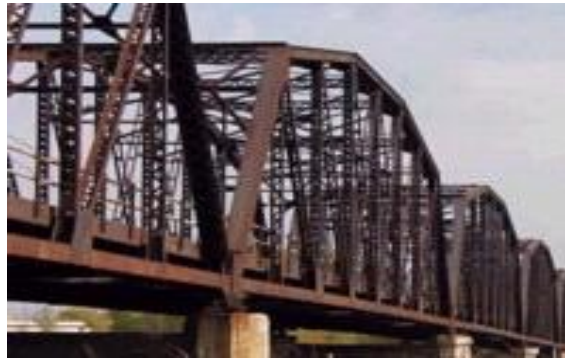


Figure 2-40 Steel Material

Steel, as a material, is the most accessible, the most available, easy to manufacture and economically viable. This metal is ideal for vehicle chassis manufacturing on a commercial scale as well as the fact that the physical properties of steel provide a great many benefits. For example, steel as a material enables a stiff structured chassis to be constructed on which other components can work efficiently. This metal rates highly on yield strength (this means its likelihood of bending under load), and ultimate strength. Another advantage is that steel has a high resistance of fatigue failure (that is where a material fails due to repeated loading and unloading, even though the loads involved may be far below the ultimate strength of the material), which means if the chassis flexes under a load, it will not cause critical failure. Another advantage, which may be overlooked, as it does not concern the majority of car owners, is that when in other remote areas of the world, on an expedition, for example in a jeep, one will always find a worker who can work with steel, as it is the oldest and most common material.

The greatest drawback regarding steel is its density (mass of material for a given volume) which causes it to be very heavy. This has become a problem since making a vehicle lighter is of great importance nowadays as this saves on fuel consumption. Added to this, the safety equipment which is installed also leads to the vehicle becoming heavier.

Another slight drawback is the corrosion of steel over time and when exposed to the elements. This means that damage will occur only if the bare metal is exposed. However, in most cases, corrosion can be prevented by applying a layer of protection onto the vehicle.

Therefore when weighing up the advantages and disadvantages of this material, one concludes that there are far more advantages, and as a result one can predict that steel will be the most preferable material in years to come.



Figure 2-41 Steel chassis structure

Aluminium



Figure 2-42 Aluminium Material

Aluminium, compared with steel, is much lighter due to its smaller density (35% that of steel). Yet, when it is used as a structural material it is an alloy, that means that other metals are added such as magnesium, zinc or others, to create the end metal. The reason being is that aluminium on its own has a very low yield strength for a vehicle chassis.

Aluminium as an alloy has less stiffness (compared to steel which is three times stiffer), but at the same time, aluminium alloy is a material which can save on weight. This is why manufacturers are looking to find a way to overcome the stiffness drawback that it presents, and simultaneously take advantage of its lightness.

One example to illustrate the above situation regarding the use of aluminium is with the round tube. A round tube is a component of a chassis, and the loads which act on this tube act on its centreline. The metal wall of this tube are a certain distance away from the centreline, and has a leverage against these loads. This means that the larger the

diameter of the tube, the more leverage the material has to act against the load. Thus, the lower weight of the aluminium allows one to build a large-diameter aluminium chassis tube which will save on weight if we compare it to a regular-diameter steel one, and at the same time it will maintain the required stiffness. Alternatively, one can thicken the wall of the tubes. However, if we were to compare a steel tube and an aluminium alloy of the same thickness, the latter would have much less stiffness.

Yet, it is essential that the aluminium structure be stiff due to the fact that this material has a significantly lower fatigue tolerance when compared with steel. Therefore, to eliminate fatigue, aluminium structures are constructed much stiffer than steel ones. If one is to compare the difference in weight between the same design in aluminium and in steel, we note that this does not come near to the 65% density difference, despite the fact that weight is saved. As regards corrosion, aluminium alloy is better, as it is less likely to be corroded because the material itself forms an outer oxide layer that prevents it from corroding more.

Although aluminium is more expensive and more difficult to work with, it is still popular in chassis designs.



Figure 2-43 Aluminium chassis structure

Titanium



Figure 2-44 Titanium Material

Titanium is viewed as the “supreme” material. Its density is about half of steel’s density, and over half of steel’s stiffness value. As concerns ultimate strength and yield strength, we see that steel and titanium are very similar.

Therefore the methods used to build with titanium mirror those of aluminium, that is, tubes should be larger in diameter than steel ones, so as to compensate for the lower stiffness in titanium. One need to clarify at this point that titanium needs to be an alloy as well. However, when titanium is compared to aluminium, it is not as weak as straight aluminium.

Titanium is resistant to corrosion and fatigue failure, yet its cost is very high, which makes it a less desirable option when manufacturing a common road vehicle.

Magnesium



Figure 2-45 Magnesium Material

Magnesium is the lightest of all the metals used in a vehicle chassis, and has a density of a quarter of steel’s. Its strength and rigidity is less than aluminium, but with good design, a light and stiff structure can be built from it.

One disadvantage is that it is a metal which reacts easily, so there is a danger of it igniting under extreme cases. Even though the material used in vehicles is very thick, which means there no risk of this occurring, there needs to be much care taken during the manufacturing process, especially when there is filing from machining operations, and other similar processes.

Magnesium is mainly used to make shapes for the mounting of brackets or braces. Some manufacturers are also attempting to apply magnesium sheets and extruded sections in other possible areas of the vehicle. One of the positive aspects of this metal is that it is easily recycled, which suits the times we live in where recycling has become a top priority in manufacturing of many products, vehicles included. We observe that this metal has been used in the manufacture of wheels, where they are made to have high-

strength and low-weight. Although most alloy wheels are made from aluminium alloys, there is also the competition-spec equipment (mostly those used by rally drivers) which is made from magnesium alloy. However the magnesium wheel costs almost five times more than an aluminium one, and thus road vehicles are not fitted with them due to their high price.



Figure 2-46 Porche's Magnesium wheel

Fibreglass

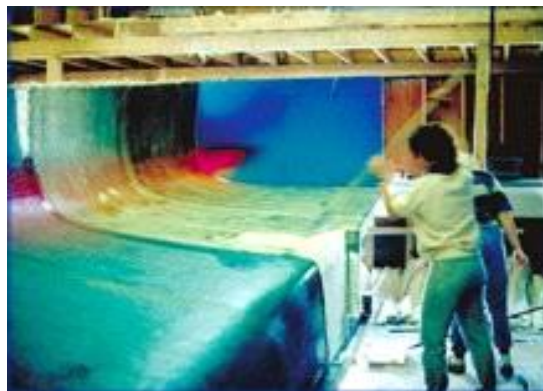


Figure 2-47 Fiberglass Material

Fibre glass is what is known as a Glass Fibre Reinforced Plastic (GFRP or GRP), where strands of glass are added to a plastic mixture making this material an option for structural components in cars. Granted that it is incomparable to the stiffness obtained by using steel, nor does it match the strength of steel, it can, however, be moulded into almost any shape or form. For example a bodyshell can be created by one piece using this

material. This means there are no seams and thus no weak points. The material allows for variable thickness in places but which are all in the one piece; very thick near high-load areas such as suspension mountings, and very thin in unstressed panels.

The drawbacks to this material is that it is time-consuming to make, and that it is subject to being chemical reactions such as creep. Also, certain paints cannot be applied directly onto fiberglass making it more limited as a material. Another disadvantage is that at very high temperatures, it softens which may cause damage. For example if it were set on fire, or if the exhaust manifold happened to be very near the panels it would be affected.

Fibreglass has been used mainly in sports cars which are not constructed as a sole chassis but with a separate chassis or subframe. If the bodyshell is made from fiberglass, there will still be metal inserts to spread the load at the mounting points.

Carbon Fibre



Figure 2-48 Carbon Fibre Material

Carbon Fibre Reinforced Plastic (CFRP/CRP) is a similar notion to fiberglass where carbon strands are added to reinforce the medium.

Carbon fibre's density is similar to that of fiberglass, but what is worth noting is that it has the strength of aluminium alloy and the stiffness of steel. The reason being is that carbon fibre uses a woven mat of fibres, and the in order to achieve the optimum strength and stiffness, one must maintain the correct alignment of this weave. In other words this material cannot be compression moulded, but instead it must be laid up in layers, which requires specialized skill coupled with the fact that it is time consuming. As a result the cost increases greatly.

Thus, due to the high cost of the material, a manufacturer of road vehicles will not choose this for the entire vehicle, but it will be used in certain areas of the vehicle such as the roof or bonnet (flat panels) as one can save on weight here. It is in F1 cars that

one will come across carbon fibre tub chassis because these vehicles require maximum stiffness and strength coupled with minimum weight, not to mention that one has the luxury of being able to afford them.



Figure 2-49 Carbon fibre chassis structure (KTM X-BOW)

2.4 Chassis joining

Chassis joining is inevitable, regardless of the material one is going to use or the design on which the vehicle is going to be based.

Seam Welding



Figure 2-50 Seam Welding 1

Welding is a process where we join two metal pieces by melting them into each other at the points where they meet. This can be done through gas welding (the heat is generated by burning gas), which uses acetylene along with pure oxygen creating a flame which melts the metal. One may also use other gases in the welding process when the metal's melting point is below 1500 degrees Celsius (which is that of steel). Another way to produce heat when welding is through electrical resistance. Furthermore a stronger joint can be created by dipping a rod of fillet metal coated in flux into the weld, which

will also prevent oxygen appearing in the molten metal, and thus weakening the structure.



Figure 2-51 Seam welding 2

As concerns electrical welding, the fillet is used as a conductor and the electrical current passes through the metal, producing heat. The different types of welding are:

- Arc welding, which is a process where a welding rod is used, and the rod needs to be replaced as it is consumed in the process. The rod can contain flux to prevent oxygen from getting into weld by leaving a slag on the surface of the weld which is later hammered away.
- Metal Inert Gas (MIG) welding. Here, there is a reel of wire instead of a rod, which passes through a flexible tube and then a hand-held gun as the trigger of gun is pulled while simultaneously inert gas (non-reactive) flows into the weld, and covers this area thereby preventing oxygen from entering. MIG welding offers the advantage that it can be robotized and ideal for production-line work.
- Tungsten Inert gas (TIG) is similar to MIG. The only difference is that a tungsten tip is used rather than the reel of wire, and is not consumed while welding. Also, an additional rod may be used to add any additional material. TIG welding is also very efficient and can be used in robotized manufacturing also.
- Seam welding produces a long line of weld to join together the parts. Usually it is the entire surface of where the components meet, thus creating a very strong join. However, there is the danger of distortion depending on the amount of heat and the type of metal involved. Another drawback is that it is time-consuming.

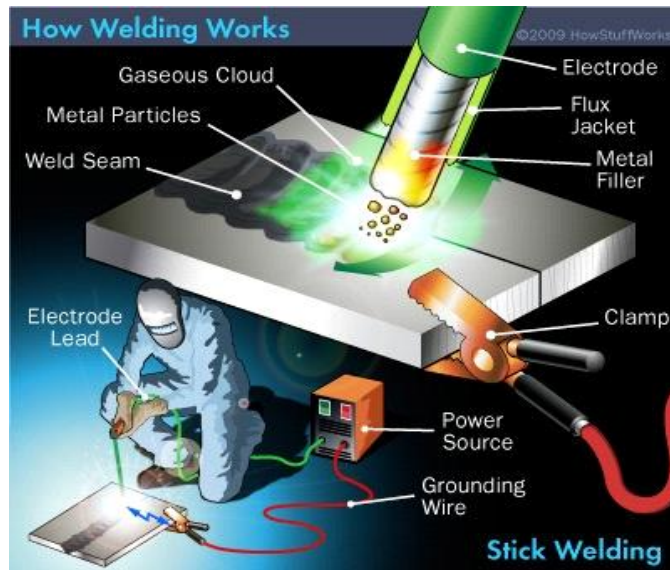


Figure 2-52 Seam welding 3



Figure 2-53 Seam welding 4

Spot Welding



Figure 2-54 Spot welding 1

Spot welding involves electrical welding, which is used to fasten two sheets together. The sheets are clamped together by two rods and the electric current is sent through the join so as to stick them together. This method seems to be efficient and popular as concerns production-line manufacturing especially with monocoque bodyshells. Another advantage is that, compared to traditional welding, it is less likely to distort because the surrounding panel is heated. The drawbacks here are that it is not as strong as seam welding, because less area is welded and the fact that load forces are not equally distributed across the joint.



Figure 2-55 Spot welding 2

Another way to make a spot weld is by creating a small hole in one panel, and then welding through to the other panel. This is mainly the case when working with replacement panels so that the joints appear to be the same as the original. This technique is known as “plug” welding because the welding fills up the hole with “a plug of weld”, rather than using spot welding.

Once again the limitation here is that this welding technique is used only with sheet materials, and cannot be used to join tubes. Furthermore, spot welding does not seal joints, which means when considering chassis panels this must be taken into account. An example of this is when the Mini was first manufactured, it let in water because the overlapping panels trapped the rainwater. It was because on the prototype Mini, the seam-welded joints did not allow one to see that an overlapping joint could possibly hold in the water, and this got past the spot welds on the production line. After this, the design of the panels was changed to overlap the other way.

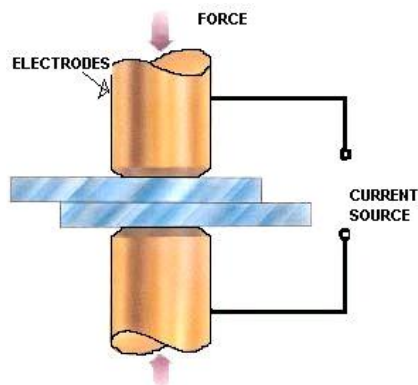


Figure 2-56 Spot welding 3



Figure 2-57 Spot welding 4

Stitch Welding



Figure 2-58 Stitch welding

There is very little difference between stitch welding and seam welding. In the stitch welding, however short welds are made along the joint rather than a continuous line, which lessens distortion since less heat is applied to the material. Stitch welding is not so common with chassis manufacture, except in cases where it needs galvanizing (a chemical process that dips the parts in a hot bath to cover them in a coating) to stop corrosion. It is preferable as it leaves a gap enabling gases to escape whereas seam welds may trap the air between the components which causes them to expand with the heat and thus lead to cracking the weld.

Bolts & Threaded Fasteners



Figure 2-59 Bolts

The positive aspect of bolts and threaded fasteners (nuts and screws) is the fact that they are removable and do not destroy the material. This means they can be reassembled without needing to use any new material, or the components can be loosened and realigned or replaced. Nevertheless, the negative points to this is that fasteners will loosen over time due to the car's vibration, and the joint will not be as stiff as one that has been welded together. Furthermore, the load at the joints will pass through the fasteners which means it may not be evenly distributed. It is more common to use threaded fasteners to attach the parts to the chassis, rather than construct the chassis itself. There are cases where parts need to be varied for a different model of vehicle or where an area of the chassis needs to become removable then it is bolted, for example the bracing strut that blocks the access for engine removal is one such case.

Rivets



Figure 2-60 Rivets

Rivets work in the same way as a bolt does but the process is different. With rivets, rather than tightening the fastener down as happens with bolts, the ends of a short rod that run through the hole are crushed thus clamping and joining the pieces together. Rivets were originally used for the construction of bridges and ships, and were forced into shape after being heated up and softened. The method is secure and still used, but it requires a lot of time. With vehicles, the more common rivet is known as the 'pop rivet'. It is a hollow tube with a flange on it, and a pin running from the end without the

flange which protrudes approximately 5cm out at the other end. The hollow tube is thrust through a hole of the components so that joining occurs, and finally the pin is pulled which crushes the tube back against the flange and sandwiches the join in between, and the final stage is where the pin is snapped off. This method can be robotized, thus making it much less time-consuming and efficient.

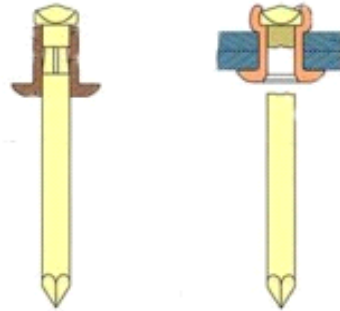


Figure 2-61 Rivets

Rivets are faster in the assembly process compared to threaded fasteners, and less likely to loosen under the vibration. However, they cannot be reused, as once they have been loosened they are destroyed. In car design, it is more effective to load them in shear, that is across the rivet, rather than in tension which is along the length of the rivet. Rivets are not used as much in major structural joining, but more so in additional brackets and panels. This type of join is commonly seen in kit cars or aircrafts which use it to hold the outer panelling together. In vehicle production, we notice that it is least favored, and even when it has been used in a vehicle before, today spot welding will replace it.

Bonded Joints



Figure 2-62 Bonded joints

The use of adhesives is another method to bond joints. The most common are epoxy with a hardener being used to create a chemical reaction (known as accelerant), other methods are to heat the glue in an oven. This method allows the load at the joint to be spread across the mating surface equally and evenly and thus preventing a “hot spot”. As a result the manufacturer need not use the thicker panels but is free to use thinner and lighter ones. Glue is also a good choice as the vehicle is not subjected to heat which affects and may distort metal, as happens with welding.



Figure 2-63 Bonded joints in industry

Adhesives are very strong, and especially those used for industry, being long-lasting and guaranteed. However, the surface needs to be carefully prepared to ensure maximum strength and durability when joining the surfaces with adhesives. Another advantage, especially in contemporary society is that adhesives can be broken down again if the appropriate degree of heat is applied to them, thus the different parts and materials can be separated if necessary and recycled. A bonded joint is used with all composite structure vehicles such as F1 cars and supercars. There are also the aluminium-framed vehicles where this method is applied, for example we not it in the Lotus Elise. Along with binding, there is the additional security of fasteners (rivets) which are used to hold the joints in place for the required time, rather than having to mount it on a jig.

2.5 Chassis improvements

Chassis design and manufacture need to fulfill certain standards which allow them to be produced and put on the road at an affordable price. Certain adjustments and improvements will be made to vehicles that will be used for heavy duty or for different types of racing.

Material Choice



Figure 2-64 Material choice

When improving on a design, one takes into account the most appropriate materials required for the purpose of the vehicle. Steel is accessible in different grades, thus rebuilding a chassis using a higher grade will reinforce it and render it stronger. For example, in drag racing, the vehicle needs to have its chassis built from a minimum grade of metal so that it is qualified to run in the race. Tubing is also an area which can be improved upon. For example, the most cost-effective way to make tubing is to use a flat sheet of metal, roll it into the shape and weld it at the seam (this is known as an electrical resistance welded or ERW). The seam, in this case, becomes a weak point, and so pressing out a tube in one piece where there is no seam is of a higher quality, especially in space frame chassis used for a special purpose, and when building additional components, such as, roll cages. One need to remember that completely different materials cannot be added or replaced unless one redesigns the structure for it to be suitable to the different properties, for example, a steel chassis which is rebuilt to the same specifications from an aluminium one will be much lighter, but prone to flexing.

Bracing

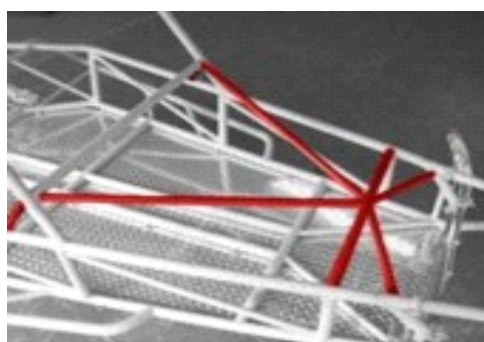


Figure 2-65 Bracing

Bracing can be added to stiffen the chassis and reinforce mounting points. One example is the sports version of Ford Escort, where bodyshells of different versions were used

compared to the regular versions, by adding small reinforcement panels at critical points, and as a result, the shell became stiffer and stronger.

Another form of bracing is known as triangular, which is used across the areas of the chassis left open to allow for other components, such as, engine bays and others. One also sees in monocoque body shells, where they have been modified, a brace running along the tops of the suspension mounts to stop it from flexing.



Figure 2-66 Tubular Bracing

Bracing depends on the chassis design, and its purpose so if the chassis is designed as a family car or a sports car, will depend on what is done. When adding extra bracing, this also adds to the cost as well as reducing the vehicle's practicality. Extra bracing, thus means that it will not usually be included on a production model. Also during the design of extra bracing, we note that it should run between points that are already load-bearing and use plates to spread the loads required.

Rollcages



Figure 2-67 Rollcage

Roll cages or roll-over protection devices, are a space frame designed to protect the chassis in the case of a major accident. It is a retro-fitted to an existing chassis for extra reinforcement. This varies from a bent tube positioned behind the driver's seat to other points on the car.

These roll cages provide stiffening which are linked up to suspension mounting points. We note that rollcages fitted to a rally car or touring car provide sufficient reinforcement and will make the monocoque almost obsolete.



Figure 2-68 Roll cage for racing use

In racing, professionally built cages must meet a set of regulations. It is most common that a cage be made from seamless tubing with specific thickness and grade of metal. The protection and safety that a roll cage provides has been proven many a time with a great deal of examples.

Welding Improvements



Figure 2-69 Welding Improvements

BodysHELLS are mainly manufactured by spot welding the panels together, but in order to increase stiffness stitch or seam welding is used instead, and care must be taken due to the great amount and degree of heat required to weld. Suspension mounting points and the engine bay are areas of the vehicle which require additional welding, and because it is time consuming and laborious, one opts for a full roll cage to be fitted, where this can be done.

Other Improvements

Factor A is a quad box to rail reinforcement, Factor B is a tunnel strap, Factor C is a floor to roof pole, Factor D is an inverted V support between the rear shock towers and the rear floor, and Factor E is a front shock to radiator support [8].



Figure 2-70 A – quad box to rail support, B – tunnel strap, C – floor to roof pole, D – rear shocks to rear floor support, E – front shock to radiator support [8]

3 CONCEPTUAL DESIGN STAGE

The great demands which appear in the competitive market presuppose that design should have dynamic and compatible procedures. Due to the fact that time is limited, one can not rely on the feedback one receives after a car is designed so as to redesign it and produce a better one. Taking this factor into account, many designers now use the CAE method stage in conjunction with the Simple Structural Surfaces (SSS) method to determine the structural concepts in all cases [2].

Once the kind of load is defined, (that is shear or bending and so on), then one can move ahead with designing the indispensable characteristics of structure to constituent. One need not know the accuracy of the loads.

3.1 Strength and stiffness requirements

The main aim of the structure is not only to preserve the form of the vehicle but also to support all the different loads existing on it. It is necessary for a designer to achieve adequate strength and stiffness on a vehicle structure with as little mass as possible [2].

3.1.1 Strength requirements

Strength can be defined as: the maximum force that the structure can support. This means that all parts of the vehicle must operate fully and normally regardless of the load which is applied to it. When there is sudden overloading due to extreme load cases or when there is material fatigue, this may result in loss of function. The overstressing of vehicle parts beyond their elastic limit will eventually lead to their failure. Varying load cases cause different local loads. However, the structure should have enough strength for each load case.

3.1.2 Stiffness requirements

The stiffness K of the structure relates the deflection Δ produced when load P is applied, i.e. $P = K \Delta$. It applies only to structures in the elastic range and is the slope of the load vs deflection graph.

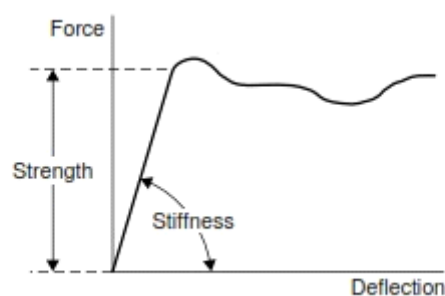


Figure 3-1 The concepts of stiffness and strength [2]

The stiffness of the chassis can affect the handling, the vibrational behavior and in general, the whole behaviour of the car. Thus, the stiffness of the chassis shows its effect

tiveness. There are several load cases that are used to understand the effectiveness of the vehicle structure and each of them cause different deformation modes. These deformations are large only if the structure is low in stiffness, something inefficient as far as the function of the structure. The two most common load cases are:

1. Bending stiffness K_b , which relates the symmetrical vertical deflection of a point near the centre of the wheelbase to multiples of the total static loads on the vehicle. A simplified version of this is to relate the deflection to a single, symmetrically applied load near the centre of the wheelbase.
2. Torsion stiffness K_t , relates the torsional deflection θ of the structure to an applied pure torque T about the longitudinal axis of the vehicle. The vehicle is subjected to the “pure torsion load case” (where the torque is applied as equal and opposite couples acting on suspension mounting points at the front and rear), and the twist θ is measured between the front and rear suspension mountings. Twist at intermediate points along the wheelbase is sometimes also measured in order to highlight regions of the structure needing stiffening. What should be pointed out is that an appropriate torsion stiffness is a very difficult characteristic to be achieved by the designer.

3.2 Introduction to the simple structural surfaces (SSS) method

Undoubtedly, during the conceptual design stage, the usage of the simple structural surfaces is of crucial importance. The SSS method is a method that was created in order to model the function of a vehicle structure. There is the assumption that the structure consists of plane surfaces (with no curvature), so that this method can be applied.

Each plane surface must be maintained in equilibrium by a series of forces. This method helps the engineer to understand the type of the loads that are applied to each of the parts of the structure (bending loads, shear loads, tension loads, compression loads and so on). The aforementioned loads are created by the weight of parts attached to them. Hence, the adjacent parts have equal and opposite forces acting on them. It also helps realize that there is continuity for load paths, through the structure, and that the overall equilibrium of the structure is achieved. In this way, the sufficiency of the structure can be defined [2].

3.2.1 Definition of a simple structural surface (SSS)

Figure 3-2 shows a plane structural element or subassembly. It can be approximated to be rigid in its plane. The length (a) and height (b) are large in comparison to the thickness (t). Considering sections in the x - y plane and y - z plane, the second moments of area are:

$$I_x = at^3/12$$

$$I_y = tb^3/12$$

$$I_z = bt^3/12$$

The thickness (t) is small. Hence, for the second moments of area:

$$I_y \gg I_x$$

$$I_y \gg I_z$$

The SSS has little (or no) resistance for moments about the x and z axis. Additionally, normal loads in y axis result in flexing of the SSS by bending about the z or x axis. However, it has resistance for bending moments about the y axis as well as for direct loads (F_x , F_z) acting in its plane.

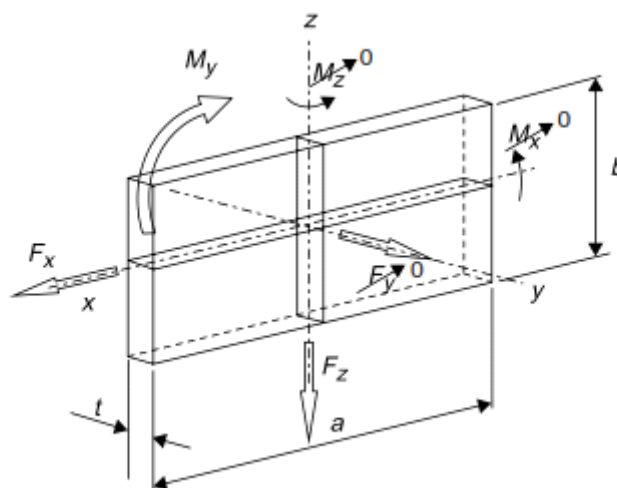


Figure 3-2 Definition of a simple structural surface [2]

3.2.2 Structural subassemblies that can be represented by a simple structural surface (SSS)

Figure 3-3 shows some simple structural surfaces, with good rigidity, carrying shear loads as indicated by the edge loads Q_1 and Q_2 [2].

- The basic panel will have limited capacity if its thickness is small due to the tendency to buckle.
- Stiffening the basic panel by swaging can increase the load capacity.
- A reinforced hole can increase the load capacity.
- The pin-jointed framework will also provide suitable structural properties for the loads Q_1 and Q_2 .
- A ring frame such as the windscreen frame has sufficient corner joint stiffness and sidebeam stiffness which will provide a satisfactory SSS.

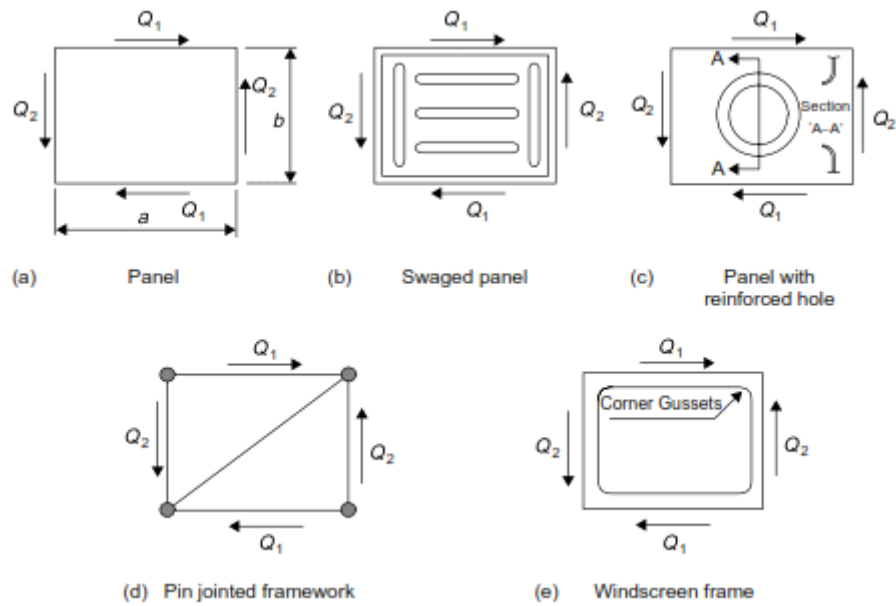


Figure 3-3 Examples of structures that are simple structural surfaces [2]

3.2.3 Example of integral car body with typical SSS idealizations

The right side of a sedan car body is observed in Figure 3-4, in which the use of the SSS method is very helpful.



Figure 3-4 Saloon (sedan) car structure [2]

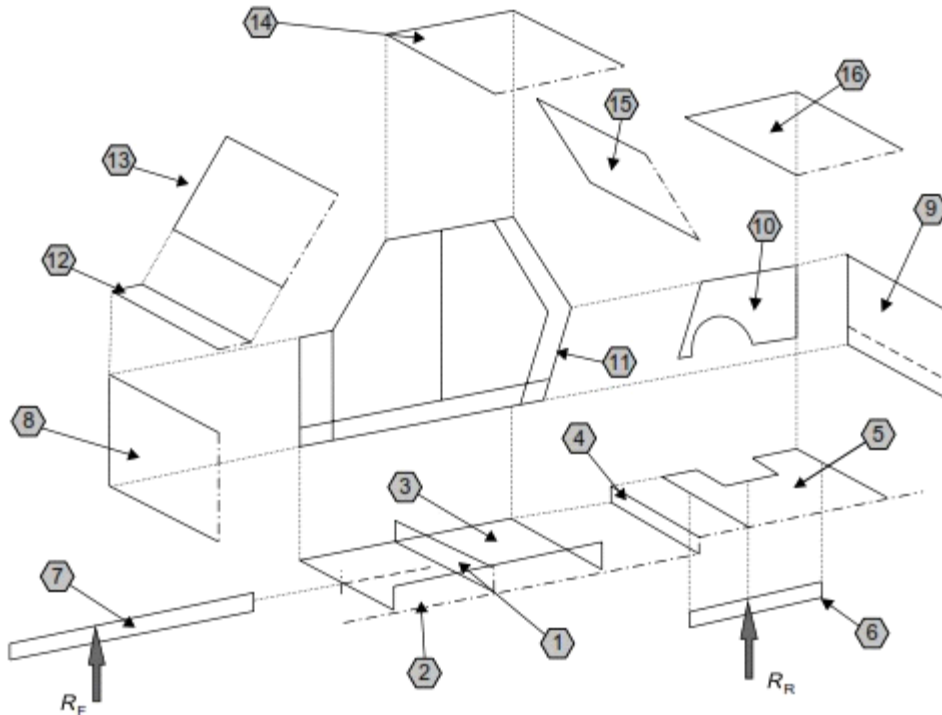


Figure 3-5 SSS half-model of sedan (saloon) structure [2]

- Surface (1): represents the floor cross-beam under the front seats. It carries the seat loads and it also supports the engine rail at the front end of the engine.
- Surface (2): represents the central longitudinal tunnel and carries the seat loads together with the floor cross-beam under the front seats.
- Surface (3): represents the floor panel itself. It will not carry vertical loads but is essential for carrying shear in the torsion load condition.
- Surface (4): represents the cross-beam under the rear seats. It provides a similar function to the floor cross-beam under the front seats.
- Surface (5): represents the luggage compartment floor.
- Surface (6): represents the longitudinal that carries both the luggage loads and the reaction R_R from the rear suspension. Usually the luggage compartment floor is at a higher level than the central floor panel and this is faithfully represented in the SSS model.
- Surface (7): represents the engine rail at the front end of the engine that carries the engine/transmission loads and the reaction R_F from the front suspension.
- Surface (8): represents the dash panel that supports the engine rail at the front end of the engine together with the floor cross-beam under the front seats. The dash panel will be required to carry loads across to the sideframe near to the "A"-pillar. It will also form part of the torsion box for the torsion load case.
- Surface (9): represents the rear panel that is required react to the load from the longitudinal (6) and to carry the loads out to the rear quarter panel.
- Surface (10): represents the rear quarter panel. It is attached to the main side-frame.

- Surface (11): represents the main sideframe. Note, surfaces (10) and (11) could be regarded as one component.
- The upper structure, consisting of upper dash or cowl plenum (12), the windscreen frame (13), the roof (14), the backlight frame (15) and the boot or trunk top frame (16), all form part of the torsion box in a similar way to the box van.

An important design feature of this model is the detail of surfaces (9) and (16), the rear panel and the top frame of the boot. The torsional stiffness of the body can be severely reduced if these structures are not designed with sufficient care. Care is required to ensure adequate shear stiffness is obtained by raising the level of the boot “lift over” or by increasing the width of the sides. However, this needs to be balanced with consideration for a low “lift-over” and wide opening dimension for the customer.

3.3 Free body diagrams for the SSSs

The free body diagrams are first presented. Then, the equilibrium equations for each SSSs, for both a standard sedan and for an open (convertible/cabriolet) car.

3.3.1 The standard sedan

This structure consists of surfaces, such as roof, floor, windscreen, sideframes, front and rear bulkheads. Not only the bending but also the torsion load case is applied to this structure and the load paths that are produced from each load case are analyzed.

3.3.1.1 Bending load case scenario

Figure 3-6 shows the bending load case for a sedan car structure. The loads that cause this bending load case scenario are:

- a) the power-train load, F_{pt} .
- b) the front seats with passengers load, F_{pf} .
- c) the rear seats with passengers load, F_{pr} .
- d) the luggage load, F_t .

These loads are produced by the weights of the parts multiplied by a load factor and are applied in the simple structural surfaces. Then, the bending and shear loads that act on each part are calculated and assuming these, the stress levels that can resist the structure are defined [2].

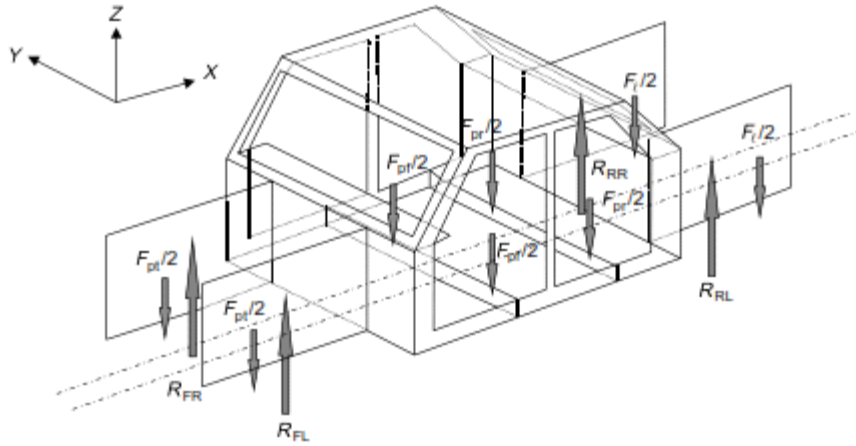


Figure 3-6 Baseline model – bending loads [2]

Developing the model it can be seen that we require edge loads and end loads to ensure all SSSs are in equilibrium. These edge/end loads are indicated by the forces P_1 to P_{13} . When beginning the bending analysis it is essential to start at the central floor area. In this simple model it is assumed that the passenger loads are carried by the two transverse floor beams SSS (1) and (2). These floor beams are supported at each end by the sideframe forces P_1 and P_2 . Note that there is an equal but opposite force acting on the sideframe. Consider now the inner front wings SSS (3) and (4), the loads acting on these are the loads from the power train $P_t/2$ and from the front suspension R_{FL} . The applied loads $F_{pt}/2$ and R_{FL} are held in equilibrium by the end loads P_4 and P_5 and by the edge (shear) load P_3 . The shear load P_3 reacts into the dash panel while the end load P_4 reacts into the front parcel shelf (6), and P_5 into the floor panel (11). These forces can be obtained by the equations of statics, i.e. resolving forces and taking moments. When building the SSS model representing the vehicle it must always be remembered that the forces must act in the plane of an SSS. Failure to provide sufficient SSSs to satisfy this requirement soon reveals a weakness or unsatisfactory load path in the structure. Note, the horizontal SSS (6) is necessary in order to carry force P_4 .

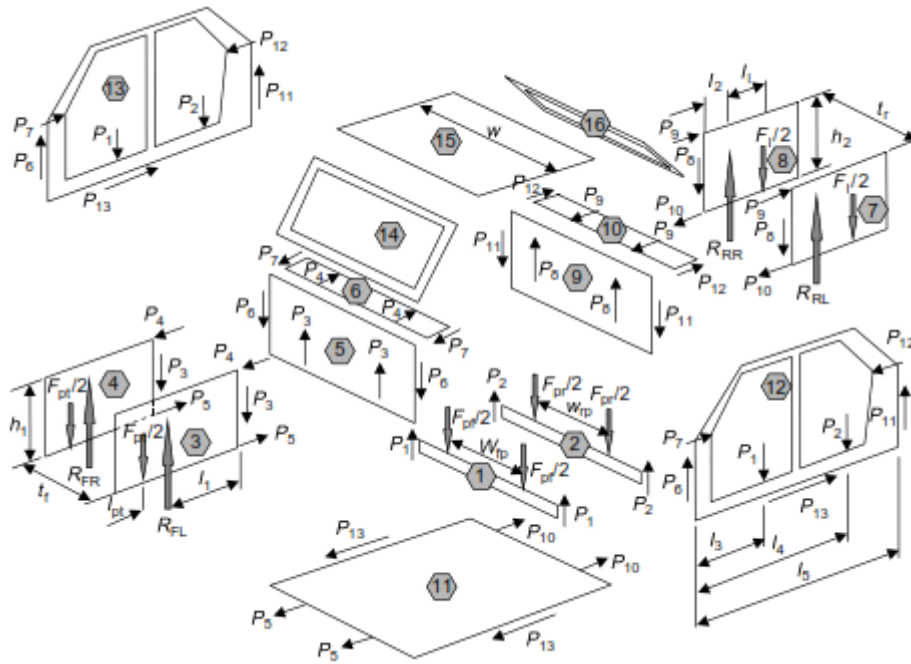


Figure 3-7 Baseline model – bending case, end and edge loads [2]

It should be noted that there are forces with appropriate magnitude (equal and opposite forces) so as the equilibrium for each component to be achieved. According to the Jason C. Brown, A. John Robertson, Stan T. Serpento formula:

Transverse floor beam (front) (1)

Resolving forces vertically and by symmetry (loads are assumed to be applied symmetrically about the vehicle longitudinal centreline):

$$P_1 = F_{ptf}/2 \quad (3.1)$$

Transverse floor beam (rear) (2)

Resolving forces vertically and by symmetry:

$$P_2 = F_{prt}/2 \quad (3.2)$$

Left and right front inner wing panel (3) and (4)

Resolving forces vertically for the left-hand panel:

$$P_3 = R_{FL} - F_{ptf}/2 \quad (3.3)$$

A similar equation is obtained for the right-hand panel. Taking moments about the rear lower corner:

$$P_4 = \{R_{FL}l_1 - F_{ptf}(l_1 + l_{pt})/2\}/h_1 \quad (3.4)$$

Resolving forces horizontally:

$$P_5 = P_4 \quad (3.5)$$

Dash panel (5)

Equal and opposite reaction forces P_3 to those on the wing panels act on this SSS. Resolving forces vertically and by symmetry:

$$P_6 = P_3 \quad (3.6)$$

Front parcel shelf (6)

Equal and opposite reaction forces P_4 to those on the inner wing panels act on this SSS. Resolving forces horizontally and by symmetry:

$$P_7 = P_4 \quad (3.7)$$

Rear quarter panels (7) and (8)

Resolving vertically for the left-hand panel:

$$P_8 = R_{RL} - F_\ell/2 \quad (3.8)$$

Taking moments about the front lower corner:

$$P_9 = \{R_{RL}l_2 - F_\ell(l_1 + l_2)/2\}h \quad (3.9)$$

Resolving forces horizontally:

$$P_{10} = P_9 \quad (3.10)$$

Similar equations apply for the right-hand panel.

Panel behind the rear seats (9)

Resolving forces vertically and by symmetry:

$$P_{11} = P_8 \quad (3.11)$$

Rear parcel shelf (10)

Resolving forces horizontally and by symmetry:

$$P_{12} = P_9 \quad (3.12)$$

Floor panel (11)

Reaction forces P_5 from the inner front wing panels and forces P_{10} from the rear quarter panel are applied to this SSS. These will not necessarily be equal so additional forces P_{13} are required acting at the sides which react on the sideframes. It will be assumed these forces act in the direction although when numerically evaluated, these may be negative (i.e. in the opposite directions). Resolving forces horizontally:

$$2P_{13} = 2(P_{10} - P_5) \quad (3.13)$$

Left-hand and right-hand sideframes (12) and (13)

Both sideframes are loaded identically. Examining the forces acting on the sideframes shows that these have already been obtained from equations (3.1), (3.2), (3.6), (3.7), (3.11), (3.12) and (3.13). However, it is necessary to check that equilibrium conditions are satisfied by applying the equations of statics. Experience has shown that it is essen-

tial to make this equilibrium check as errors do occur with the use of the many equations. Resolving forces vertically:

$$P_6 - P_1 - P_2 + P_{11} = 0$$

Resolving forces horizontally:

$$P_7 + P_{13} - P_{12} = 0$$

Moments may be taken about any point but in order to reduce the algebra it is better to take moments about a point where two forces act. For example, take moments about the lower corner of the windscreen pillar where P_6 and P_7 act. This simplifies the equation by eliminating two terms. Moments about the lower corner of the windscreen:

$$P_1 l_3 + P_2 l_4 - P_{11} l_5 - P_{12} (h_2 - h_1) = 0$$

In practice some rounding errors due to difficulties in defining the exact positions of each force may occur. It should now be noted that windscreen frame (14), roof panel (15), and back-light (16) SSSs are not subject to any load for this bending case.

3.3.1.2 The pure torsion load case scenario

Whilst driving, we subject the car to pure torsion, when it is momentarily exposed to equal and opposite loads, both at the front (R_{FT}) and the rear axle (R_{RT}). The consequences of that, would be the wheels on each side (along with the suspension), to act differently from one another. The pure torsion scenario could happen if the car hit a bump on the road and only its torsion loads were considered.

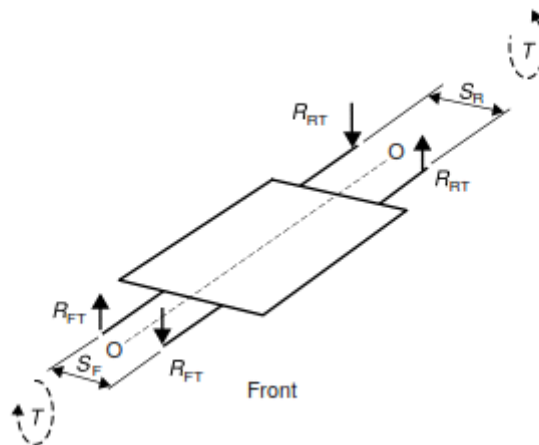


Figure 3-8 Vehicle in pure torsion [2]

The pure torsion load case subjects the individual SSS to edge forces. The forces of the pure torsion load case, differ from the ones of the bending case. The torsion stiffness of a car proves its competitiveness against less stiff cars. As far as torsion is concerned, the solutions to achieve a mass efficient integral sedan structure are [2]:

- 1) The passenger compartment is made of a closed system of SSS, in shear.
- 2) The wheel loads that are being transferred to the torsion box must comply with the continuity of the load paths at the dash.

The torque T is applied about axis O-O as couple $R_{FT} S_F$ at the front suspension. This must be balanced by an equal and opposite couple $R_{RT} S_R$ due to the reaction forces R_{RT} at the rear suspension:

$$T = R_{FT} S_F = R_{RT} S_R$$

Hence

$$R_{FT} = T/S_F \quad R_{RT} = R_{FT} S_F/S_R = T/S_R$$

According to the Jason C. Brown, A. John Robertson, Stan T. Serpento formula:

End structures

(a) Front and rear inner fenders

On the right-hand fender, the suspension load acts upward. This is reacted by an equal downward force on the panel where it is joined to the bulkhead. For moment equilibrium, the couple caused by the offset L_1 of forces R_{FT} is balanced by complementary shear forces P_{FT} at top and bottom of the panel:

$$R_{FT} L_1 = P_{FT} h_1 \quad \text{thus} \quad P_{FT} = R_{FT} L_1 / h_1 = T L_1 / (S_F h_1)$$

Forces P_{FT} are reacted by equal forces, fed into the top and bottom flanges as shear flows. These will in turn be reacted by axial forces P_{FT} in the flanges, where the flanges meet the passenger compartment. The upper flange is of thin sheet material, so that the reaction P_{FT} will be concentrated at the junction between the web and the flange so that the latter can be treated as a “boom”. The lower flange is usually the “engine mounting rail” consisting of a substantial box member. This may also be treated as a boom here. The left-hand fender will behave similarly, but with the forces in opposite directions.

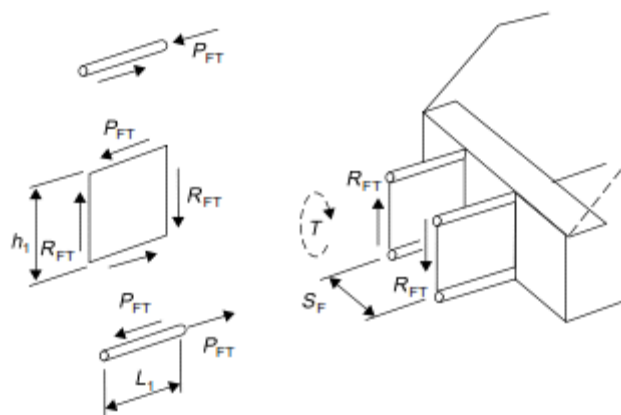


Figure 3-9 Frontal structure [2]

In the standard sedan, the rear inner fenders will behave in an identical way to the front ones, with the forces in the appropriate directions. The vertical shear force on the rear fender is R_{RT} and the reaction forces in the top and bottom flanges P_{RT} are:

$$P_{RT} = R_{RT}L_2/h_2 = TL_2/(S_Rh_2)$$

- where L_2 = loaded length and h_2 = height of rear inner fender.

(b) Dash

Torque T is applied to the engine bulkhead by the reactions R_{FT} from the fender webs acting at a separation S_F giving a couple $P_{FT}S_F = T$.

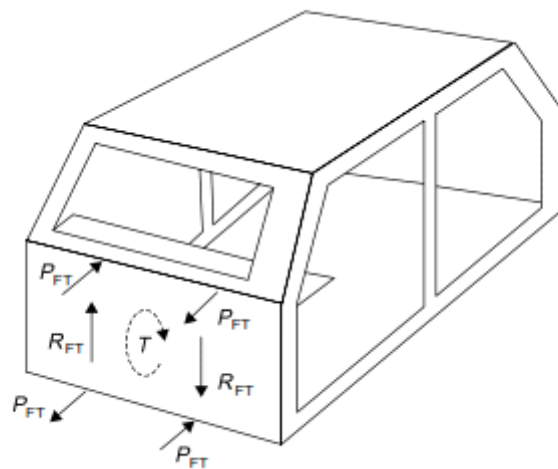


Figure 3-10 Forces on dash panel [2]

The reactions P_{FT} to the fender upper flange forces are carried by the parcel shelf which must be stiff in the appropriate direction. The reactions to the engine rail forces P_{FT} pass to the floor as in-plane forces in the directions shown in Figure 3-12. The rear fender forces are reacted in an identical way. Owing to the directions of the suspension forces in the torsion case, forces P_{RT} apply a couple to the parcel shelves of $P_{RT}S_R$. This is also the case for the floor.

(c) Parcel shelf/upper dash

The parcel shelf acts as a beam, carrying the couple $P_{FT}S_F$ out to the sideframe at the mid A-pillars. The end forces Q_{X1} form a couple to balance this couple, thus:

$$Q_{X1}B = P_{FT}S_F \quad \text{giving} \quad Q_{X1} = P_{FT}S_F/B$$

The shear forces in the parcel shelf (acting in a horizontal plane) and the bending moments (acting about a vertical axis). By similar reasoning the rear parcel shelf reaction forces Q_{X2} are:

$$Q_{X2} = P_{RT}S_R/B$$

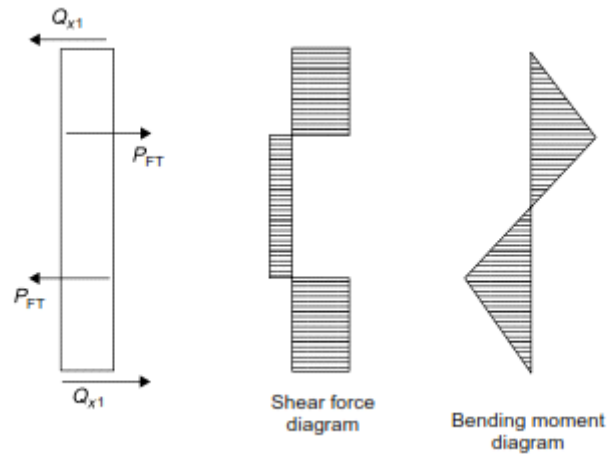


Figure 3-11 Parcel shelf [2]

Passenger compartment

(a) Engine bulkhead

The shear forces R_{FT} from the fender webs are reacted on the engine bulkhead. This creates a couple $T = R_{FT}S_F$. This couple is reacted by shear forces Q_1 and Q_2 acting on the edges of the bulkhead, forming couples Q_1h_1 and Q_2B .

For lateral force equilibrium: $Q_1 \text{ TOP} = Q_1 \text{ BOTTOM} = Q_1$

For vertical force equilibrium: $Q_2 \text{ LEFT} = Q_2 \text{ RIGHT} = Q_2$

For moment equilibrium: $T = Q_1h_1 + Q_2B$

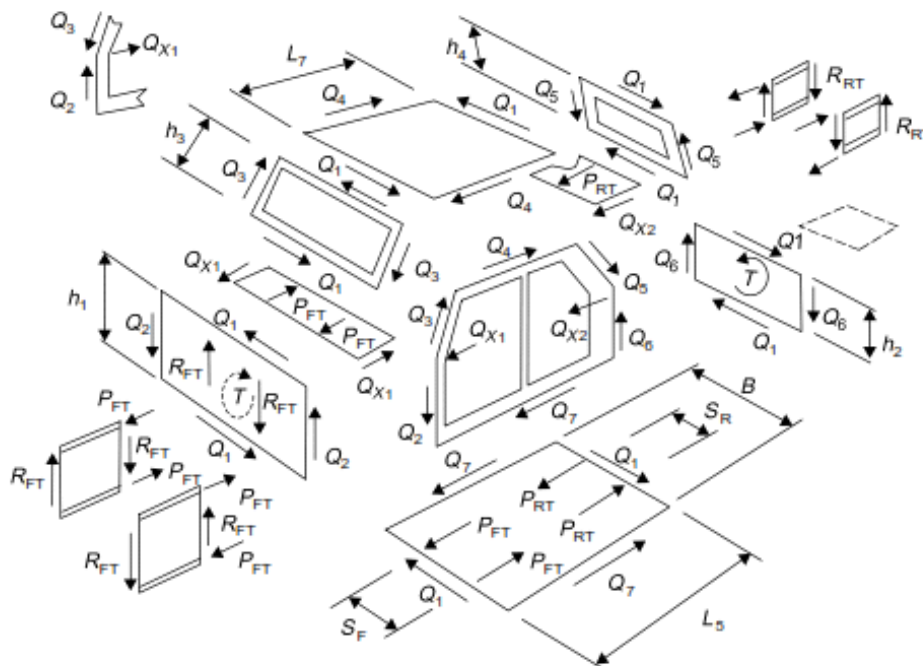


Figure 3-12 Edge forces in the standard sedan in the torsion load case [2]

(b) Front windshield

Shear force Q_1 from the top of the engine bulkhead is reacted by an equal force on the bottom of the windshield frame. For horizontal force equilibrium, this will be balanced by an equal force Q_1 on the top edge of the frame. These forces Q_1 form a couple Q_1h_3 which must be balanced by a couple Q_3B from complementary shear forces Q_3 on the sides of the frame.

$$Q_1h_3 - Q_3B = 0$$

This frame achieves its shear stiffness from the local in-plane bending stiffness (i.e. about an axis normal to the plane of the windshield frame). It is thus working as a “ring beam”.

(c) Roof

Shear force Q_1 is fed to the front of the roof from the top of the windshield frame. This will be balanced by edge force Q_1 at the rear. These forces form a couple Q_1L_7 which must be balanced by a complementary couple Q_4B from the edge forces Q_4 on the roof sides. Thus, for moment equilibrium:

$$Q_1L_7 - Q_4B = 0$$

(d) Backlight (rear window) frame

Force Q_1 from the rear of the roof is reacted by an equal and opposite force on the top of the rear window frame and this, in turn, is balanced by a force Q_1 on the bottom of the window frame. The couple Q_1h_4 from these forces is balanced by the complementary couple Q_5B from edge forces Q_5 on the sides of the backlight frame.

$$\text{For moment equilibrium: } Q_1h_4 - Q_5B = 0$$

(e) Rear seat bulkhead

Shear force Q_1 is passed from the backlight frame to the top of the rear bulkhead. The top and bottom edge forces Q_1 on the rear bulkhead and forces Q_6 on its sides form couples which are balanced by the couple $T = R_{RT}S_R$ applied by the rear fender webs to this panel.

$$\text{Thus for moment equilibrium: } T = Q_1h_2 + Q_6B$$

As before Q_{1TOP} and $Q_{1BOTTOM}$ are equal and opposite, as are Q_{2LEFT} and Q_{2RIGHT} . Because of the externally applied torque T , the edge forces Q_1 , Q_6 do not form opposing couples (although overall the panel must be in moment equilibrium). As on all such surfaces with additional external forces or moments, force Q_1 is the net force on the top of this panel. The rear seat bulkhead is sometimes a continuous panel, or it may consist of a truss structure, formed by punching triangular holes leaving diagonal members forming a “triangulated truss” SSS.

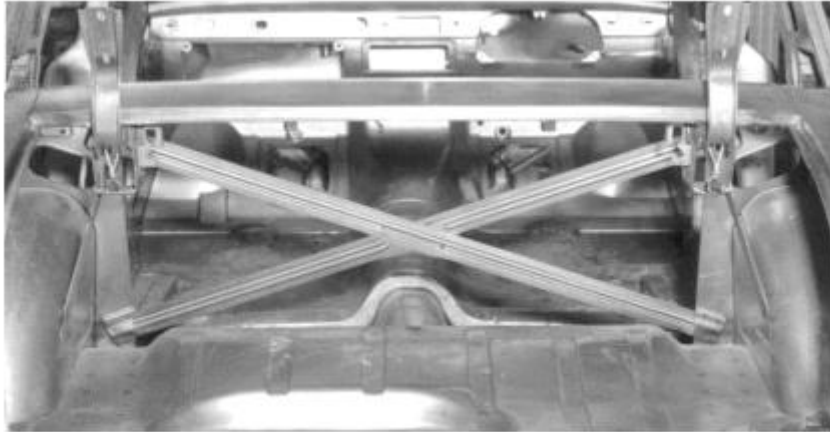


Figure 3-13 Rear seat aperture with diagonal braces (courtesy Vauxhall Heritage Archive [2])

(f) Floor

This receives equal and opposite edge forces Q_1 from the front and rear bulkheads and Q_7 at the sides, from the sideframes. The forces Q_1 and Q_7 are oriented so as to form complementary couples Q_1L_5 and Q_7B , except that now additional forces P_{FT} and P_{RT} from the lower longitudinals of the front and rear fenders cause additional couples $P_{FT}S_F$ and $P_{RT}S_R$. All the pairs of forces Q_1, Q_7, P_{FT}, P_{RT} balance out for force equilibrium.

$$\text{For moment equilibrium: } Q_1L_5 - Q_7B = P_{FT}S_F + P_{RT}S_R$$

Often, the engine rails run for some distance under the floor, and this gives a good connection path (in shear) for force P_{FT} between the engine rail and the floor.

(g) Sideframes

The edges of the sideframe react edge forces $Q_2Q_3Q_4Q_5Q_6Q_7$ from the surfaces attached to it, and Q_{x1} and Q_{x2} from the front and rear parcel shelves. The sideframes on opposite sides of the vehicle experience identical edge loads, but in opposite directions. Force and moment equilibrium will be obeyed. Clearly, the sideframes are crucial in “gathering” the edge forces from the other surfaces. For moment equilibrium, take moments about an arbitrary point G distance X behind the lower A-pillar centreline and Z above the rocker centreline. If r_2 to r_7 are the moment arms of forces Q_2 to Q_7 about point G, then:

$$\begin{aligned} -r_2Q_2 + r_3Q_3 + r_4Q_4 + r_5Q_5 - r_6Q_6 + r_7Q_7 \\ = Q_{x1}(h_1 - Z) + Q_{x2}(h_2 - Z) \dots \end{aligned}$$

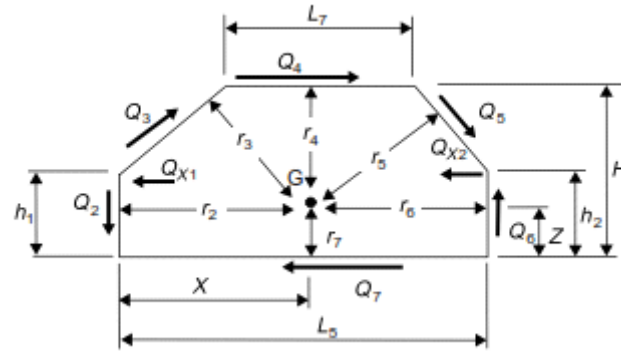


Figure 3-14 Sideframe [2]

The moments of most of the forces about G are shown in Table 3-1 (taking clockwise moments as positive). The forces Q_3 and Q_5 act on the upper A- and C-pillars, which are at angles θ_A and θ_C from the vertical. These forces can be resolved into vertical and horizontal components. Noting that the line of action of Q_5 passes through the C-pillar waist joint (point E) and that of Q_3 passes through the A-pillar waist joint (point B), then the moments of these forces are given in Table 3-2.

Table 3-1 The moments of most of the forces about G [2]

Edge force	Moment about G	Moment arm about G
Lower A-pillar	$-Q_2X$	$r_2 = X$
Header (roof rail)	$Q_4(H - Z)$	$r_4 = H - Z$
Lower C-pillar	$-Q_6(L_5 - X)$	$r_6 = L_5 - X$
Rocker	Q_7Z	$r_7 = Z$
Parcel shelf reactions		
Front	$-Q_{x1}(h_1 - Z)$	$h_1 - Z$
Rear	$-Q_{x2}(h_2 - Z)$	$h_2 - Z$

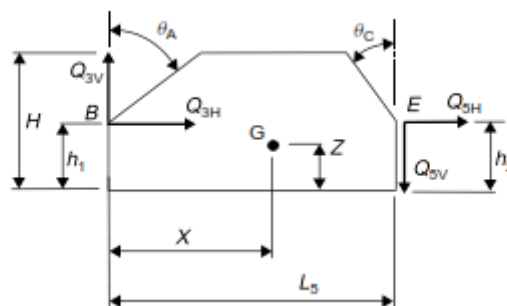


Figure 3-15 Components of forces Q_3 and Q_4 [2]

Table 3-2 The moments of Q3 and Q5 forces [2]

<i>Force</i>	<i>Component</i>	<i>Moment about G</i>	<i>Moment arm about G</i>
Q_{3H}	$Q_3 \sin(\theta_A)$	$(h_1 - Z)Q_3 \sin(\theta_A)$	$r_{3H} = (h_1 - Z)$
Q_{3V}	$Q_3 \cos(\theta_A)$	$(X)Q_3 \cos(\theta_A)$	$r_{3V} = (X)$
Q_{5H}	$Q_5 \sin(\theta_C)$	$(h_2 - Z)Q_5 \sin(\theta_C)$	$r_{5H} = (h_2 - Z)$
Q_{5V}	$Q_5 \cos(\theta_C)$	$(L_5 - X)Q_5 \cos(\theta_C)$	$r_{5V} = (L_5 - X)$

<i>Force</i>	<i>Moment about G</i>	<i>Moment arm about G</i>
Q_3	$Q_3\{(h_1 - Z) \sin(\theta_A) + X \cos(\theta_A)\}$	$r_3 = (h_1 - Z) \sin(\theta_A) + X \cos(\theta_A)$
Q_5	$Q_5\{(h_2 - Z) \sin(\theta_C) + (L_5 - X) \cos(\theta_C)\}$	$r_5 = (h_2 - Z) \sin(\theta_C) + (L_5 - X) \cos(\theta_C)$

For sideframe equilibrium, all moments acting about G will sum to zero ($\Sigma M = 0$):

$$\begin{aligned}
 & - Q_2 X + Q_3\{(h_1 - Z) \sin(\theta_A) + X \cos(\theta_A)\} + Q_4(H - Z) + \dots \\
 & \dots Q_5\{(h_2 - Z) \sin(\theta_C) + (L_5 - X) \cos(\theta_C)\} - Q_6(L_5 - X) + \dots \\
 & \dots Q_7 Z - Q_{x1}(h_1 - Z) - Q_{x2}(h_2 - Z) = 0
 \end{aligned}$$

3.3.2 Open (convertible/cabriolet) variants

Convertibles/cabriolets or “open vehicles” are vehicles without a roof. Due to the lack of a roof this type of vehicle appears to have a disadvantage concerning the load paths, because it is not a “closed box” as opposed to the sedan. Added measures must take place in order to make sure that the "open vehicle" structure can resist the stresses. Hence, this structure usually is of a greater mass than the sedan vehicle [2].

Tucer’s chassis is separated from its body panel, therefore, it “behaves” similarly to the open convertible/cabriolet plan, because the roof plays no structural part in both of them. Accordingly, during the conceptual design stage of chassis, there needs to be great emphasis on the open convertible/cabriolet variants. We also need to take into account the disadvantages that the open convertible/cabriolet has in comparison with the standard sedan and find solutions considering these disadvantages.

Additionally, during the conceptual design stage, we must illustrate the load paths of an open vehicle to understand how it “behaves”, when external forces are applied to it. Extra solutions for further improvement of an open vehicle structure are proposed.

3.3.2.1 Illustration of load paths in open vehicle

Figure 3-16 demonstrates the load paths in an open car. The front and the rear end structures of an open car behave the same way a standard sedan would. Deep inner fenders front and rear are supported in shear by the compartment bulkhead while the

top and bottom flange (or “boom”) forces are carried by parcel shelves and floor, respectively. Inspection of the connection of the parcel shelf to the A-pillar reveals the absence of the upper sideframe to act as an open truss. The lower A-pillar (shown in Figure 3-16) carries all the parcel shelf reaction, and hence needs to be stiff in bending and shear. “Fill-in” shear panels A and C with appropriate flanges carry the shear and bending down from the parcel shelves to the compartment sidewall (or rocker panel). This is necessary for both torsion and bending load cases. The lower sidewall works alone in bending, and so must also be stiff, but it tends to be less stiff than the sideframe on a sedan car because it is less deep.

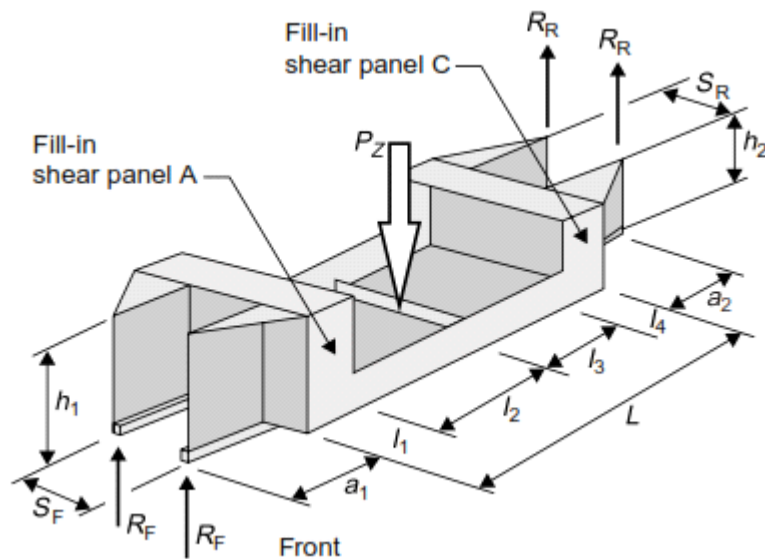


Figure 3-16 Simple structural surfaces model of open vehicle [2]

3.3.2.2 Bending load case scenario

Figure 3-17 shows the bending load case scenario for an open vehicle. In this scenario, a vertical load P_z is applied to the cross-member of the structure (the loads on each side are equal and their magnitudes are $P_z/2$). The load paths that are produced from this load case are presented below.

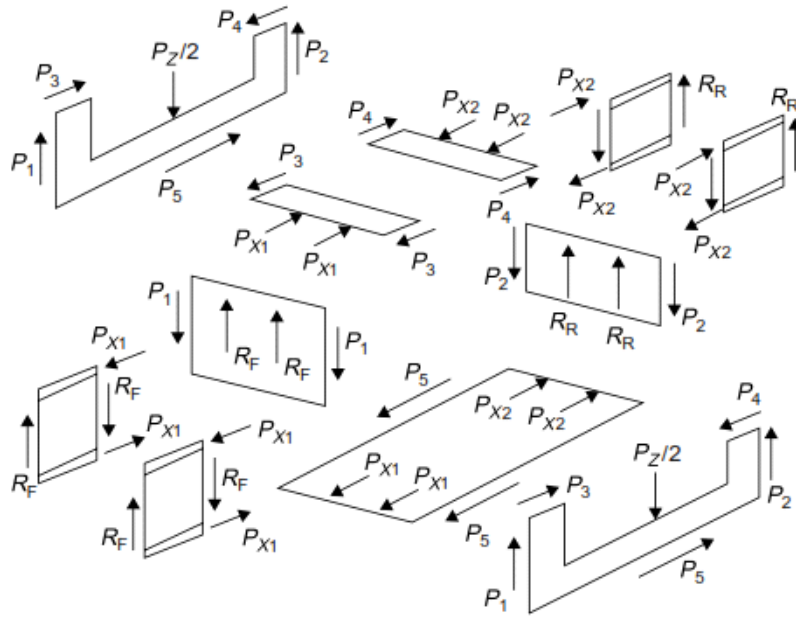


Figure 3-17 Simplified bending load case for open vehicle [2]

The open vehicle “behaves” like the sedan vehicle, concerning the front and rear ends. Furthermore, the front fenders, the bulkhead and the parcel shelf act in the same way as those at the rear. However, the values of the edge forces are different due to the fact that the sizes a_2 , h_2 , etc. are different. According to Jason C. Brown, A. John Robertson, Stan T. Serpento formula:

Table 3-3 The edge forces in the end structures [2]

	<i>Front</i>	<i>Rear</i>
Upper and lower boom force	$P_{X1} = R_F a_1 / h_1$	$P_{X2} = R_R a_2 / h_2$
Bulkhead side reaction	$P_1 = R_F$	$P_2 = R_R$
Parcel shelf to pillar force	$P_3 = P_{X1} = R_F a_1 / h_1$	$P_4 = P_{X2} = R_R a_2 / h_2$

The floor is in tension, as might be expected in the bending case. Floor edge force P_5 (same on both sides) is present only if P_{X1} and P_{X2} are of different magnitude, so that $P_5 = P_{X2} - P_{X1}$. If this is the case, then the outer sections of the floor are in shear between the lines of action of P_{X1} and P_5 . The sidewalls are the major members carrying bending along the passenger compartment. They need to be stiff in bending because there is no upper sideframe to act as a truss. At the ends, bending moments are fed into the side-wall from forces P_3 and P_4 via the A- and C-pillar fill-in panels and their flanges. The overall shear force and bending moment diagrams for the sidewall are shown in Figure 3-18.

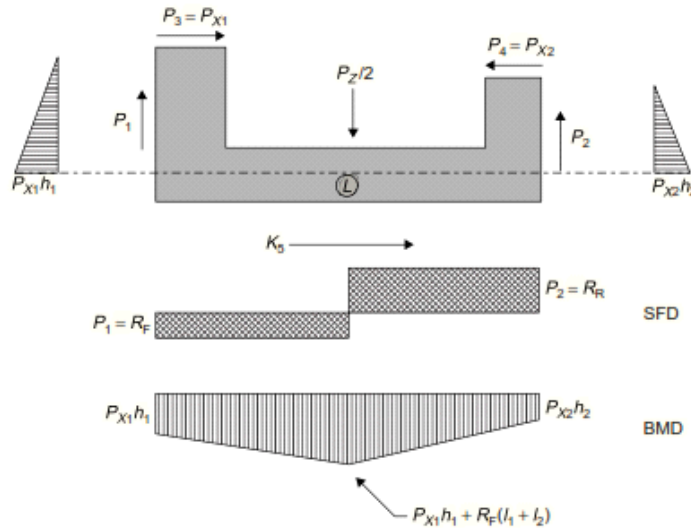


Figure 3-18 Sidewall shear force and bending moment diagrams for simplified bending load case [2]

3.3.2.3 Torsion load case scenario

Due to the lack of a roof this type of vehicle appears to have a disadvantage concerning the torsion load case.

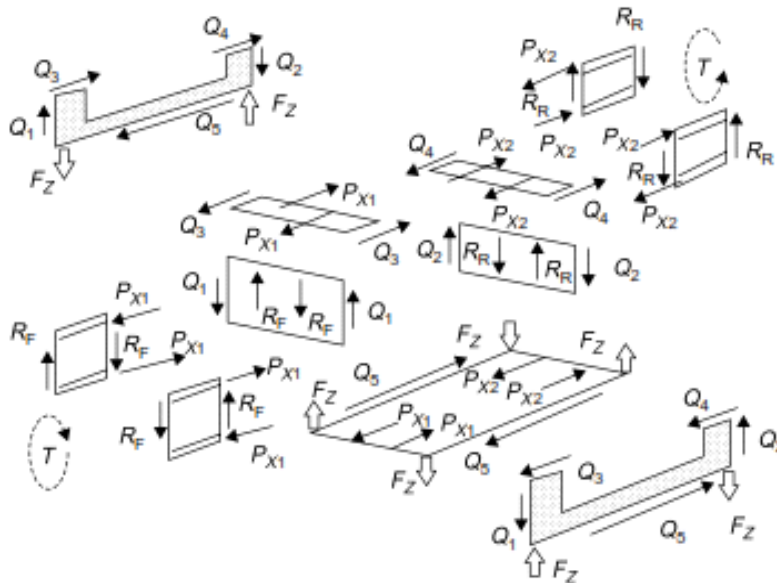


Figure 3-19 Edge loads in torsion load case on open vehicle [2]

During the torsion load case, the parcel shelf, the fender and the bulkhead of an open vehicle act like those in the sedan vehicle. According to Jason C. Brown, A. John Robertson, Stan T. Serpento formula, the equilibrium equations are:

Table 3-4 The equilibrium equations (Torsion load case) [2]

	<i>Front</i>	<i>Rear</i>
Suspension force	$R_F = T/S_F$	$R_R = T/S_R$
Upper and lower boom force	$P_{X1} = R_F a_1/h_1$	$P_{X2} = R_R a_2/h_2$
Bulkhead side reaction	$Q_1 = R_F S_F/B = T/B$	$Q_2 = R_R S_R/B = T/B$
Parcel shelf to pillar force	$Q_3 = P_{X1} S_F/B$	$Q_4 = P_{X2} S_R/B$
Floor (in-plane)	$P_{X1} S_F + P_{X2} S_R - Q_5 B = 0$	

Nevertheless, the sidewall of an open vehicle suffers, for the reason that all the edge forces on the sidewall create moments in the same direction. This type of structure needs out-of-plane loads in order to neutralize the unbalanced moments. These loads can be acted only from the floor (equal and opposite loads F_z). Thus, for these surfaces, the simple structural surfaces (SSS) “in-plane shear panel” theories are not valid. Consequently, extra measures and techniques are required to minimize the flexibility in torsion of this structure.

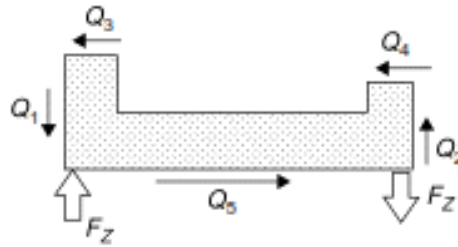


Figure 3-20 Open vehicle sidewall in torsion load case [2]

3.3.2.4 Torsion stiffening measures for open car structures

Many different approaches have been tried over the years to improve the torsion stiffness of open vehicles, with varying degrees of success. It is important, not only to achieve increased stiffness, but to do so without an excessive weight penalty. The particular approach used will depend on the type of open vehicle under consideration. Stiffening measures for purpose-built open sports cars are likely to be different from those used in “cabriolet conversions” of mass produced integral sedans [2].

Two widely used methods are:

- a) Adding or building in a torsionally stiff grillage type structure into the vehicle floor.
- b) Finding areas within the vehicle body which can be “boxed in” to give torsionally stiff elements. It is then necessary to provide adequate structural connections from the torsionally stiff box to the rest of the body.

Since many open vehicles have a “sporty” aspect, an additional approach is to add a “roll-bar” or a “T-roof” to the vehicle to tie the two sides together in torsion. In a sense, this is an attempt to replace part of the roof structure removed in the first place. It also amounts to adding cross-members to the vehicle, and this is another approach which has been used also. Such methods are usually not very effective on their own, but they

are often incorporated as subsidiary methods to be used in association with the major approaches listed above.

The torsional stiffening approaches outlined in (a) and (b) will now be discussed with examples.

(a) Torsionally stiff grillage in floor

Several different versions of this are available, they include:

- Cruciform braced members in the floor. It has the advantage that the members used in the brace do not themselves need to be torsionally stiff, so that open sections can be used.
- Torsionally stiff tubular members in the floor. These may take the form of longitudinal “backbone” members, or sometimes they may be laterally positioned.
- A full “grillage” of tubular interconnected members, each with good local torsion and bending stiffness and with joints which are good at transmitting torsion and bending.

Tubular “backbone” members: This approach is often used in specialist sports cars, conceived from the outset as open vehicles. They often consist of a separate longitudinal “backbone chassis frame” with added bodywork. These could be termed “longitudinally aligned torsion boxes”. Torsion stiffness for this comes from a large cross-section area of the tube. The torsion constant J for this is proportional to the enclosed area squared (A_E^2), so a large tube ($\sim 300 \times 200$ mm) gives a certain amount of stiffening. It is essential that the backbone be of closed section, since open sections are very flexible in torsion. The Lotus sheet steel backbone structure, and the TVR backbone, made of bays of triangulated tubes.

Another good example of this approach is the Chevrolet Corvette. The structure of this consists of a closed central tube which is structurally tied to long hydroformed outboard longitudinals, so that it is a mixture of the “backbone” and “punt” types. Note that all of the examples in this section are specialist sports cars with separate frames.

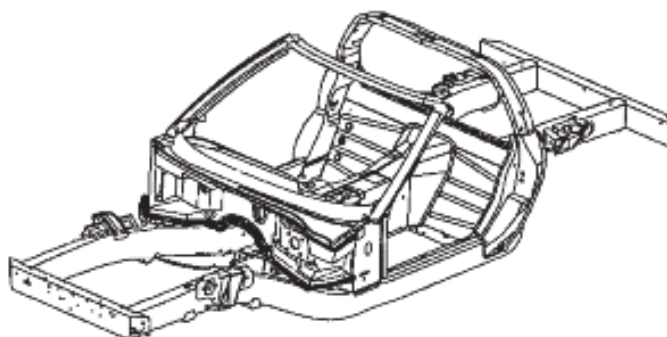


Figure 3-21 Chevrolet corvette structure (courtesy of General Motors Corporation) [2]

Full underfloor grillage structure: This is an approach more commonly used in “cabriolet conversions” of integral body vehicles, because it is relatively easy to incorporate existing closed members (such as the rocker) into the required grillage. The integral structure of a Japanese “micro-car” was turned into a cabriolet by removing the roof. To restore torsional stiffness inevitably lost by removing the roof, the floor of the vehicle was converted into a grillage. The longitudinal rockers were turned into multi-cell box members by the addition of additional sheet steel closing plates. The enclosed area A_E of these members was thereby increased by 3.5 times. Good torsional connection to the dash was achieved by “butterfly” ends on the fronts of the enlarged rockers, welded to the dash. A new closed section middle floor cross-member was also created by adding closing plates to the seat cross-member. A roll-hoop, and an additional rear cross-member were also incorporated.

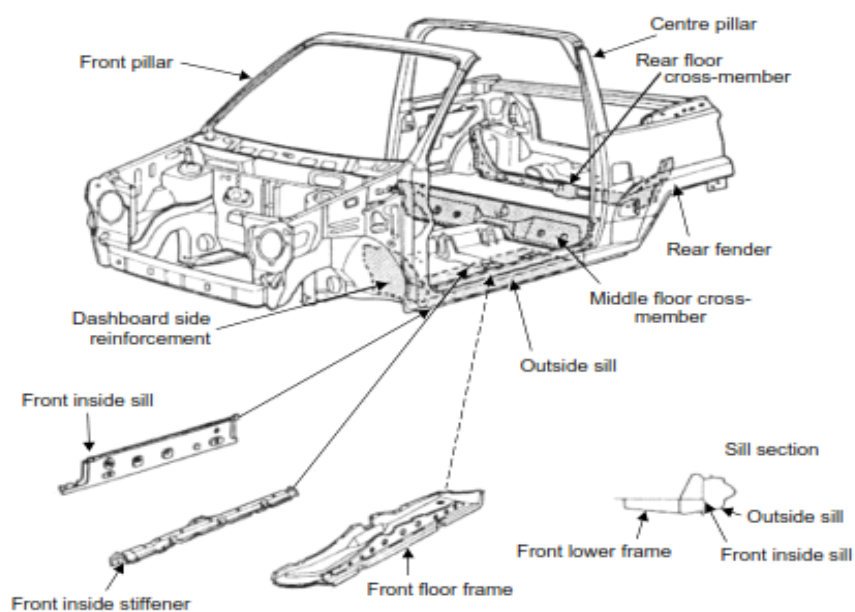


Figure 3-22 City car cabriolet conversion (courtesy Honda UK Ltd and Automotive Engineering magazine) [2]

It was reported (Automotive Engineering magazine 1984) that the cabriolet had the same torsion stiffness as the sedan, with the cabriolet body-in-white weighing 60 kg more than that of the closed vehicle. Such weight increases are by no means unusual in “cabriolet conversions”. They simply underline the difficulty in achieving high torsion stiffness in open vehicles.

(b) Addition of a “closed-simple structural surfaces-box”, using space and components which are there for other purposes

Such boxed-in regions usually run across the car, tying the two sides together torsionally. The sidewalls act as “levers” applying torsion to the box. As such, these could be called “laterally aligned torsion boxes”. This method is also applicable to longitudinally aligned boxes if an appropriately shaped structure is available. Boxes in either direction are capable of providing torsion stiffness.

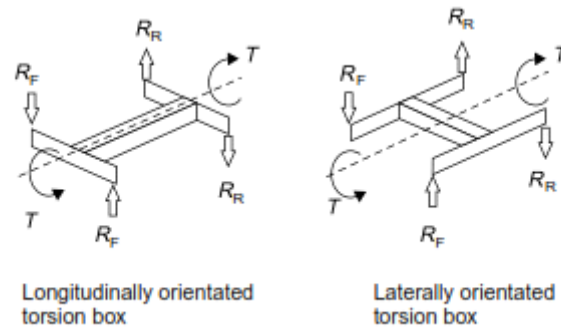


Figure 3-23 Longitudinally and laterally orientated torsion box [2]

Typical areas used for such boxes are:

- “Boxing in” the luggage compartment or the engine compartment. This is done by ensuring that all openings in the region are surrounded by good, complete ring frames with stiff corner joints, and by ensuring structural continuity of the other sides of the box.
- In the region of the engine bulkhead, parcel shelf and (wide) lower A-pillars. An additional ring frame is added, consisting of the instrument panel, wider lower A-pillar, and a floor cross-member (possibly under the floor). It is essential that all four corners of this frame have good joints and that the frame is well connected to the rest of the box.
- In the region under the rear seat or near the fuel tank (there is often a step in the floor at this point, with a certain amount of available space).

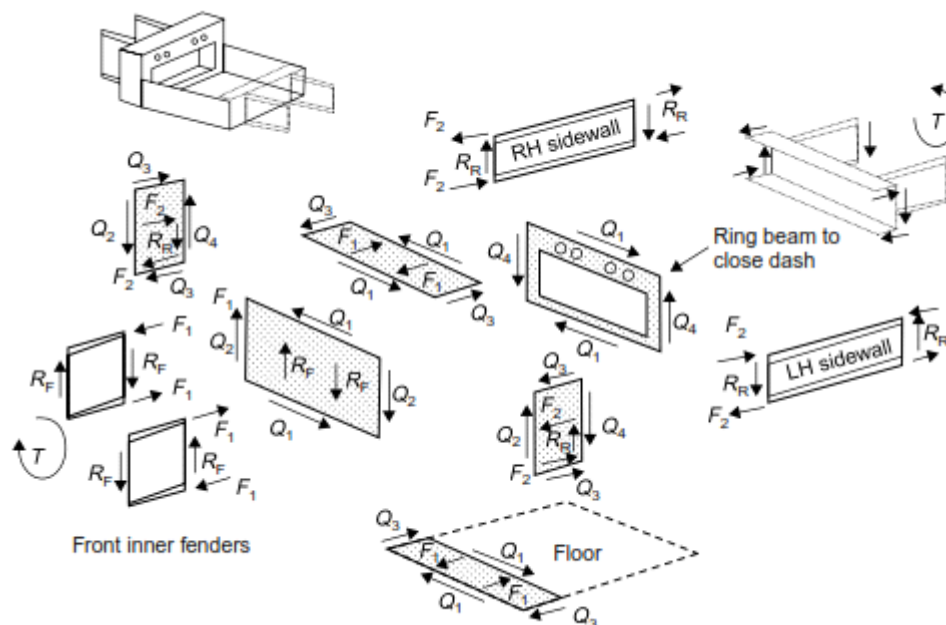


Figure 3-24 Example of open vehicle with torsion box on dash region [2]

4 CAD / COMPUTER-AIDED DESIGN

Computer-aided design (CAD) is the use of computer programs to create two- or three-dimensional (2D or 3D) graphical representations of physical objects. CAD software may be specialized for specific applications [9] [10]. CAD is widely used for computer animation and special effects in movies, advertising, and other applications where the graphic design itself is the finished product. CAD is also used to design physical products in a wide range of industries, where the software performs calculations for determining an optimum shape and size for a variety of product and industrial design applications.

In product and industrial design, CAD is used mainly for the creation of detailed 3D solid or surface models, or 2D vector-based drawings of physical components. However, CAD is also used throughout the engineering process from conceptual design and layout of products, through strength and dynamic analysis of assemblies, to the definition of manufacturing methods. This allows an engineer to both interactively and automatically analyze design variants, to find the optimal design for manufacturing while minimizing the use of physical prototypes.

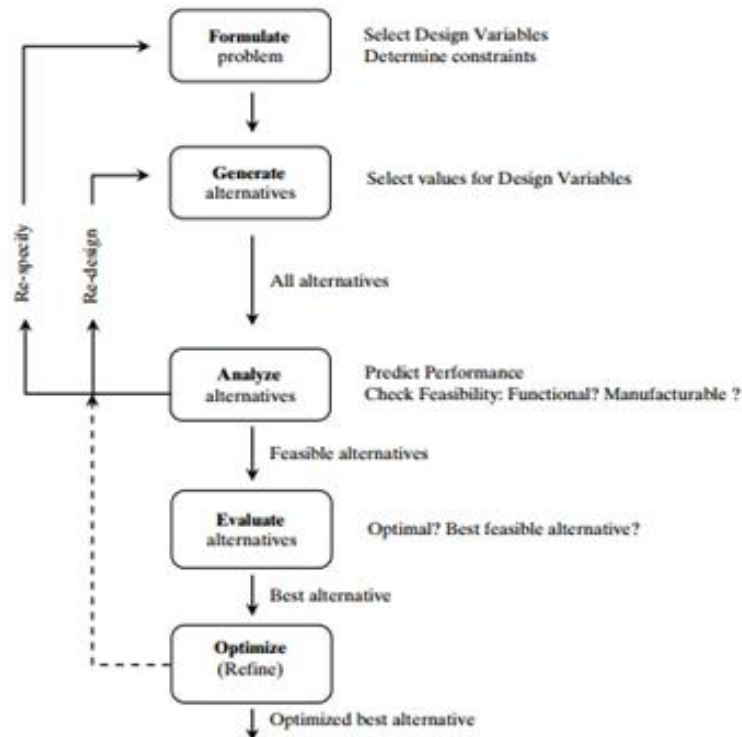
Benefits of CAD

The benefits of CAD include lower product development costs, increased productivity, improved product quality and faster time-to-market.

- Better visualization of the final product, sub-assemblies and constituent parts in a CAD system speeds the design process.
- CAD software offers greater accuracy, so errors are reduced.
- A CAD system provides easier, more robust documentation of the design, including geometries and dimensions, bills of materials, etc.
- CAD software offers easy re-use of design data and best practices.

4.1 Parametric design

Parametric design includes a number of decision-making processes, just like the other phases of design. The processes use information (input) from prior phases to arrive at logical decisions (output). Systematic parametric design has five major steps.



- Step 1:** Formulate the parametric design problem.
Step 2: Generate alternative designs.
Step 3: Analyze/predict the performance of the alternatives.
Step 4: Evaluate the performance of each alternative.
Step 5: Optimize/refine.

Figure 4-1 Parametric design decision-making processes [11]

Parametric design has become an increasingly popular approach to Computer-aided Design (CAD). The popularity of this approach is due, on the one hand, to the generation of unusual forms, often with complex geometries and increased technical sophistication; on the other hand, by virtue of the recognition of these designs being novel, useful and, arguably, creative - important goals in non-routine design [11].

The ground of parametric design is the generation of geometry from the definition of a family of initial parameters and the design of the formal relations they keep with each other. It is about the use of variables and algorithms to generate a hierarchy of mathematical and geometric relations that allow you to generate a certain design, but to explore the whole range of possible solutions that the variability of the initial parameters may allow. The benefits of this process are immediate. It is a huge leap in the quality of our process. On the other hand, parametric design is fundamental when minimizing the effort needed to create and test design variants. Generating an automated process eliminates tedious repetitive tasks, the need for complicated calculations on the fly, the possibility of human error, and generates huge shifts in the outcomes with slight variations of the original parameters. It is the difference between using the "Cube" command one thousand times, entering center point and dimensions, or customizing the design of a "Group of Variable Height Cubes" command out of our own predefined variability rules [12].

First Figure (Figure 4-2) shows a set of two objects with their dimensioned relationships. This example can be referred to as an “explicit design”. Any of the dimensioned parameters can be changed, but only through a sequence of erasures and redrawing.

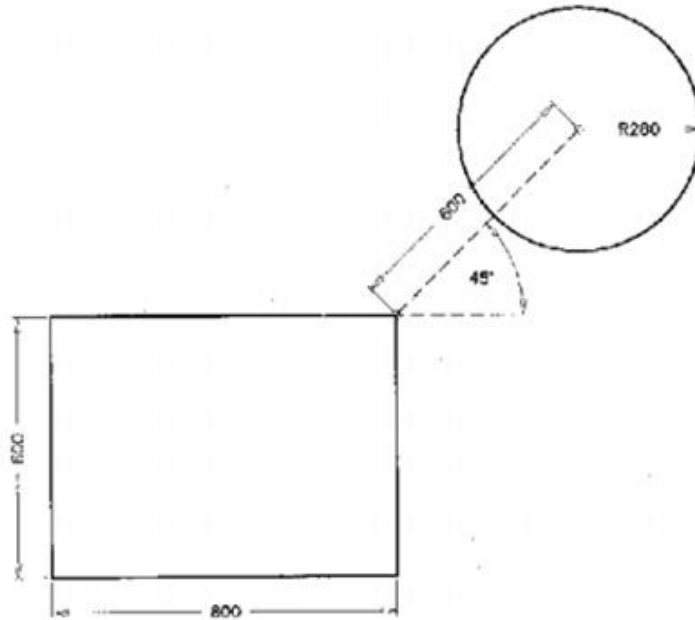


Figure 4-2 "Explicit design" [12]

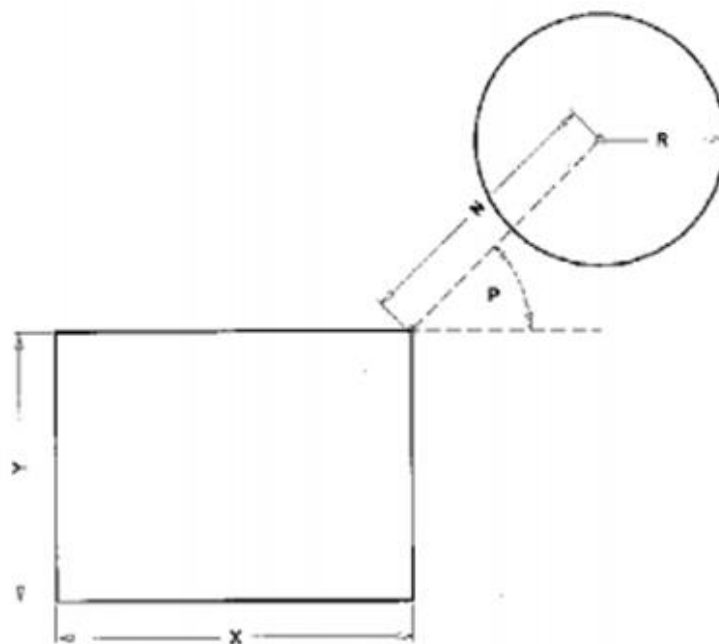


Figure 4-3 Parametrically generated model [12]

A parametrically generated model can be “updated” by identifying one or more of the parameters and changing their values. Figure 4-3 is an example of a parametrically generated model and shows the difference in philosophy between explicit and associative geometry.

All the designs which are going to be presented, are produced with the use of specialised designing package PRO ENGINEER, by the company Parametric Technology Corporation (PTC).

4.2 Eco Racer chassis 2014

ER14 (Eco Racer) is the name of the current car model of the research team. The following sections illustrate the chassis design and the design of the rest of the mechanical parts placed on it [13].

4.2.1 Chassis design

In this section, the chassis design is presented through a series of figures from different aspects.

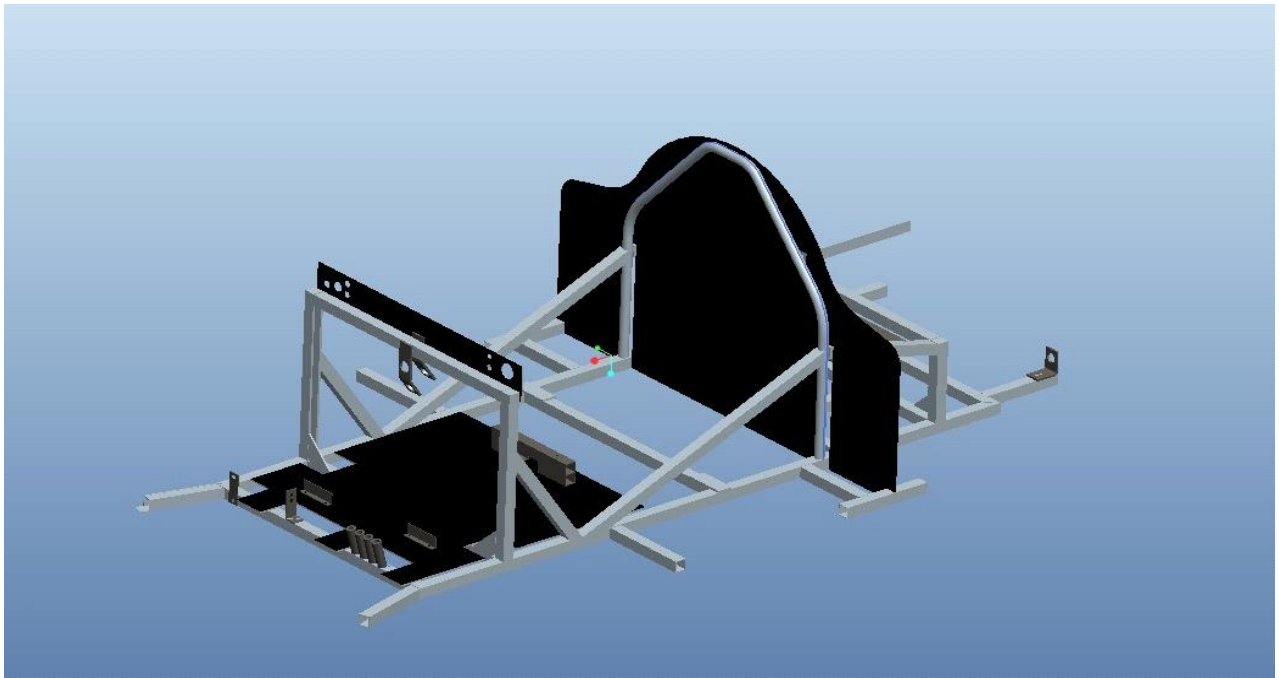


Figure 4-4 ER14 design (View 1)

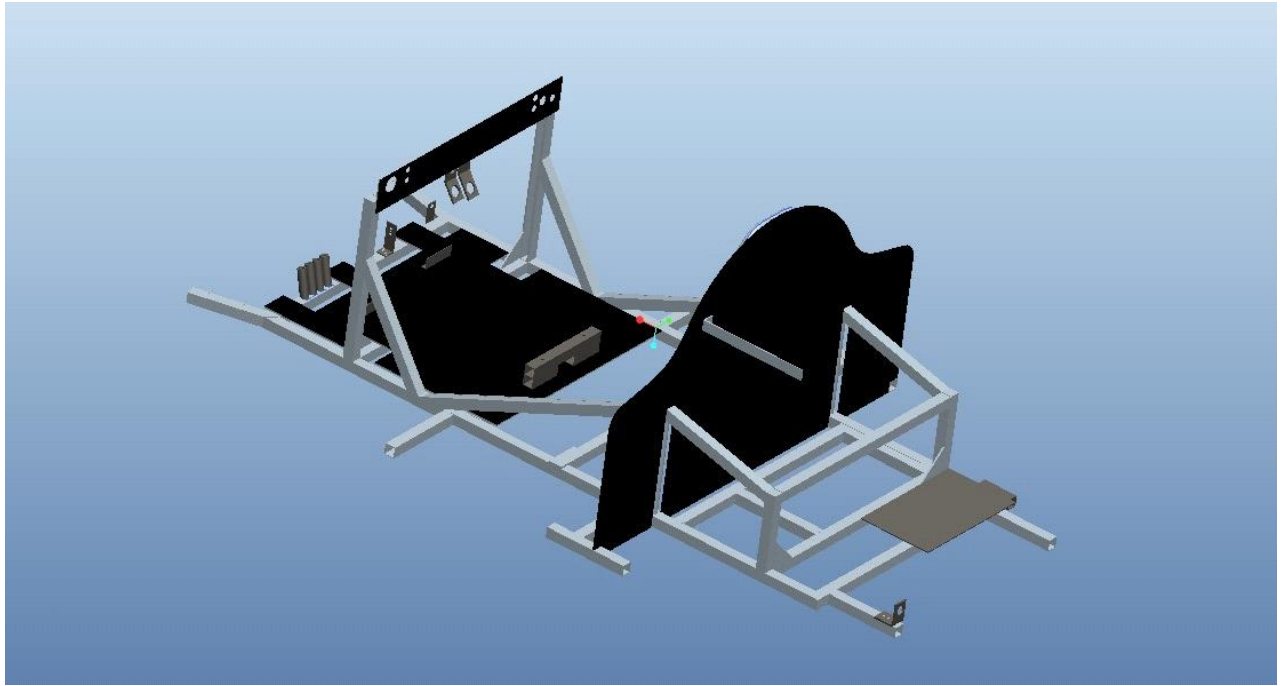


Figure 4-5 ER14 design (View 2)

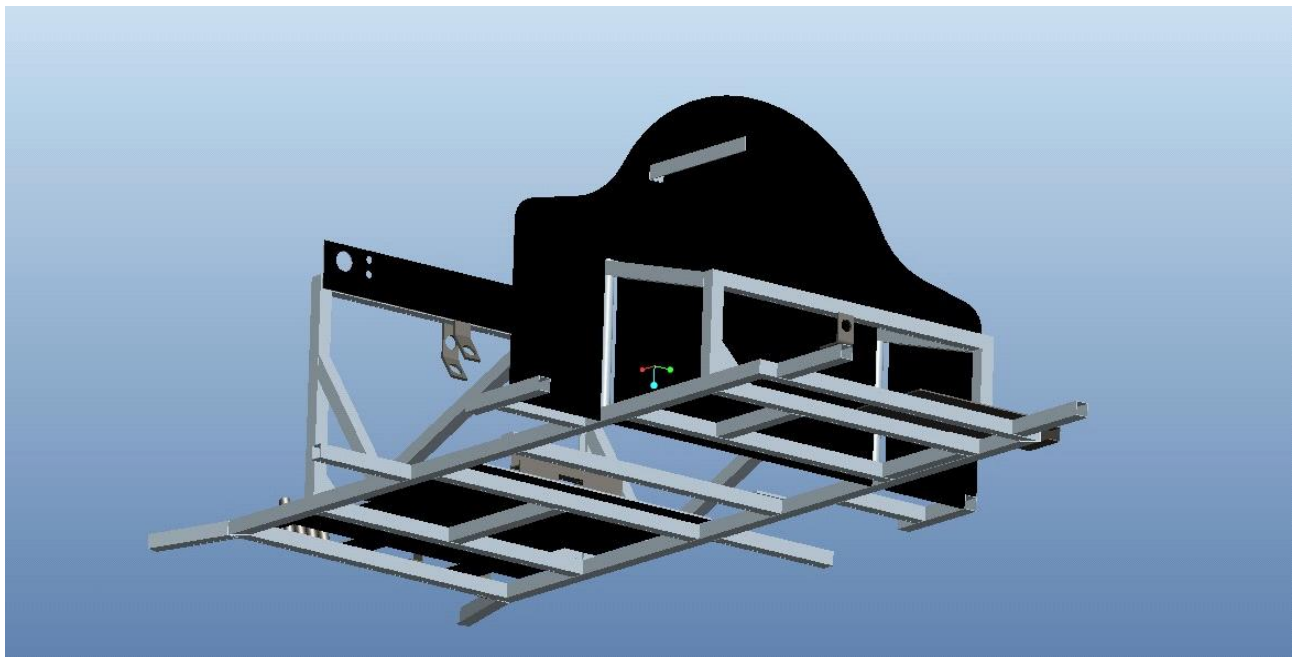


Figure 4-6 ER14 design (View 3)

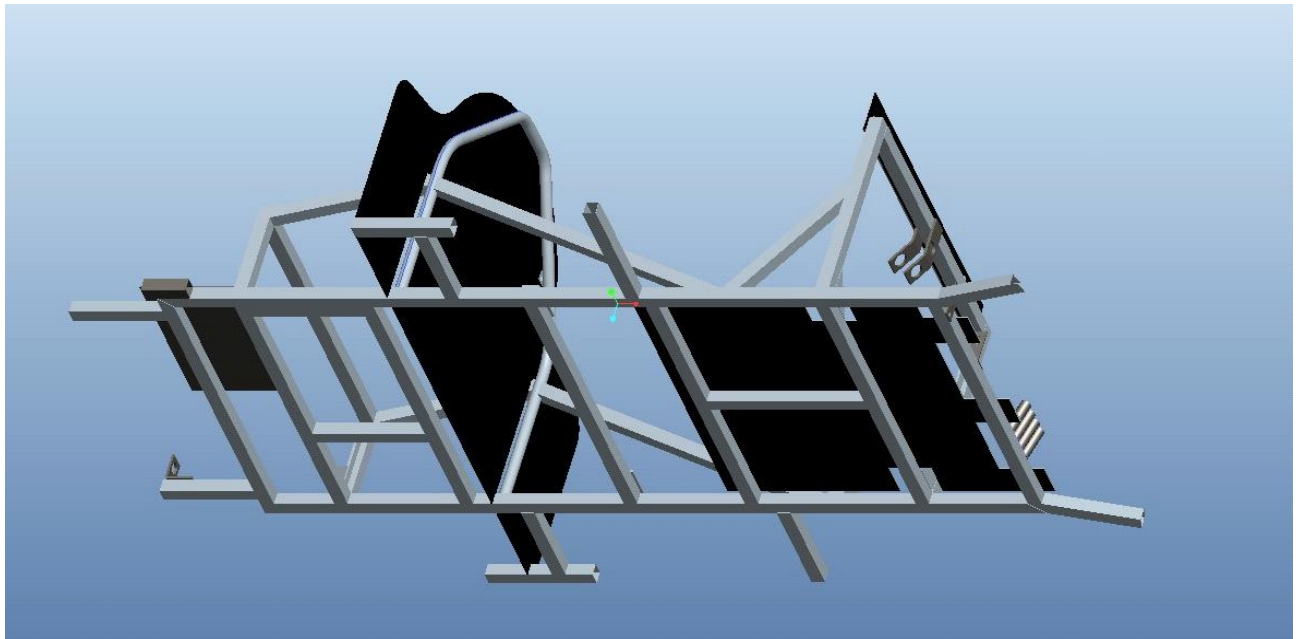


Figure 4-7 ER14 design (View 4)

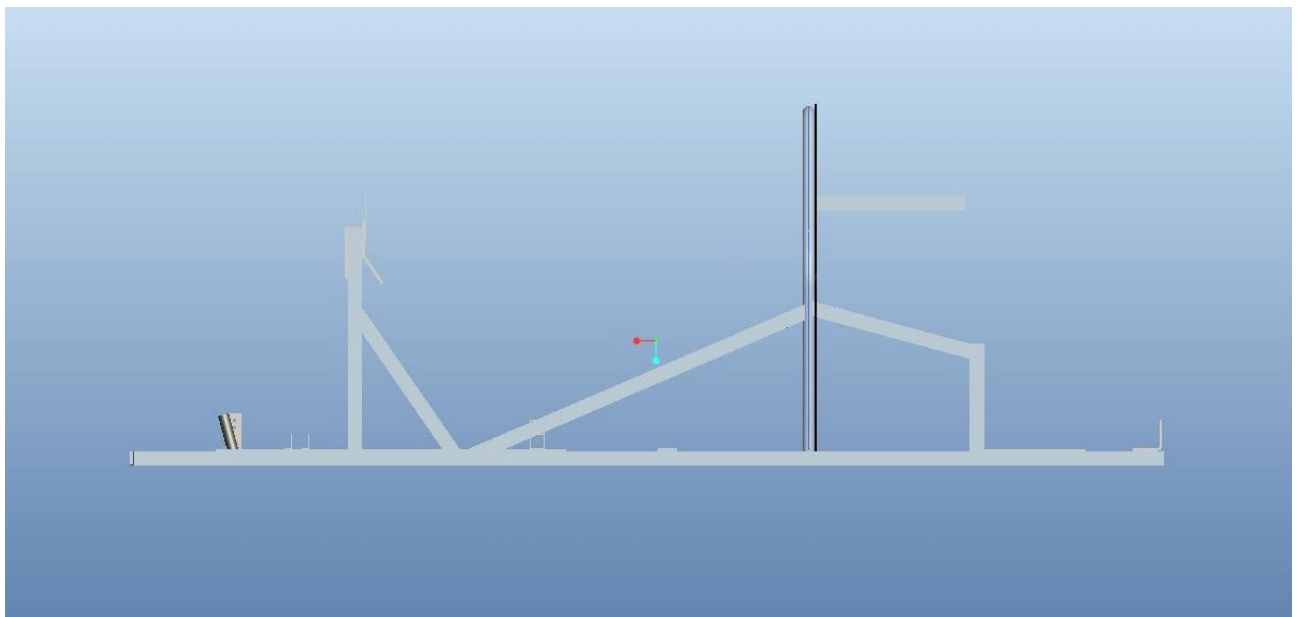


Figure 4-8 ER14 design (View 5)



Figure 4-9 ER14 during manufacturing

4.2.2 Design of the parts around the chassis

In this section, the different parts placed on the chassis are presented. These include the front spindle base, the front spindle, the rear semi-axle kit and the body panel.

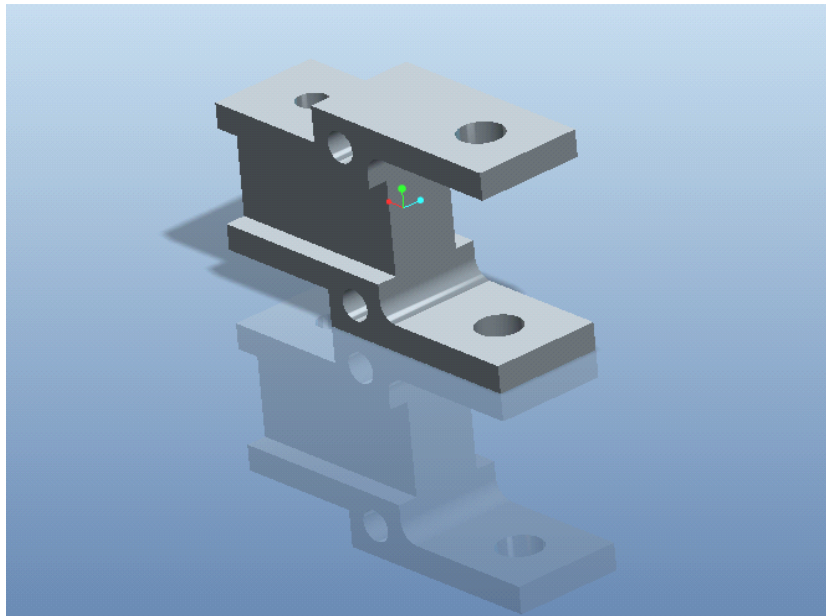


Figure 4-10 Front spindle base

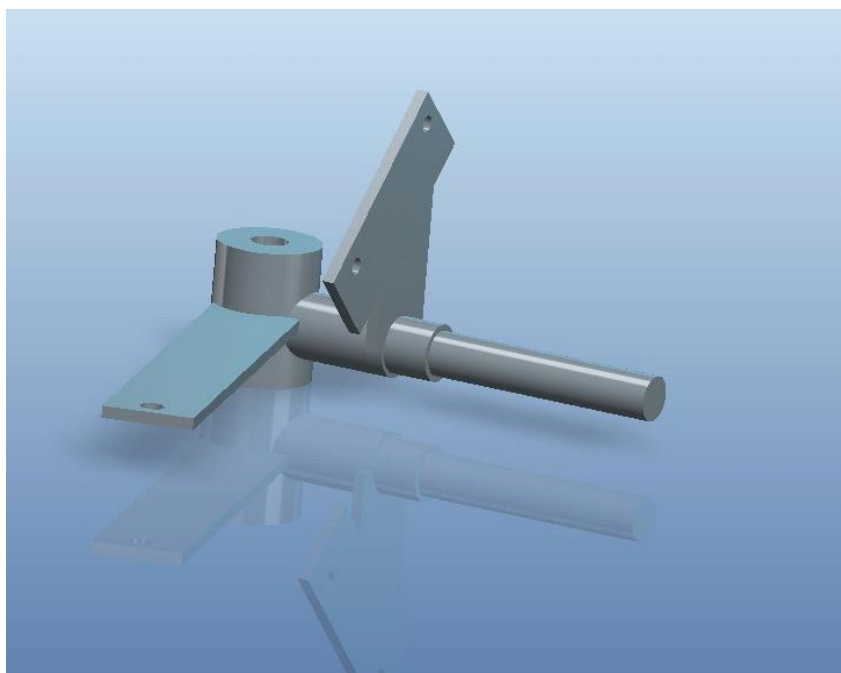


Figure 4-11 Front spindle

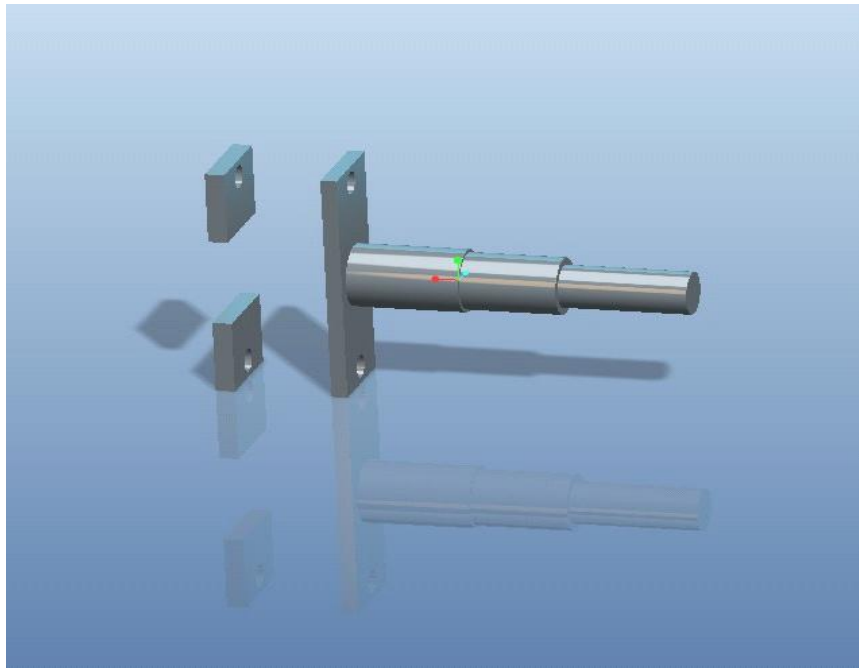


Figure 4-12 Rear semi-axle kit



Figure 4-13 Body panel (View 1) [12]

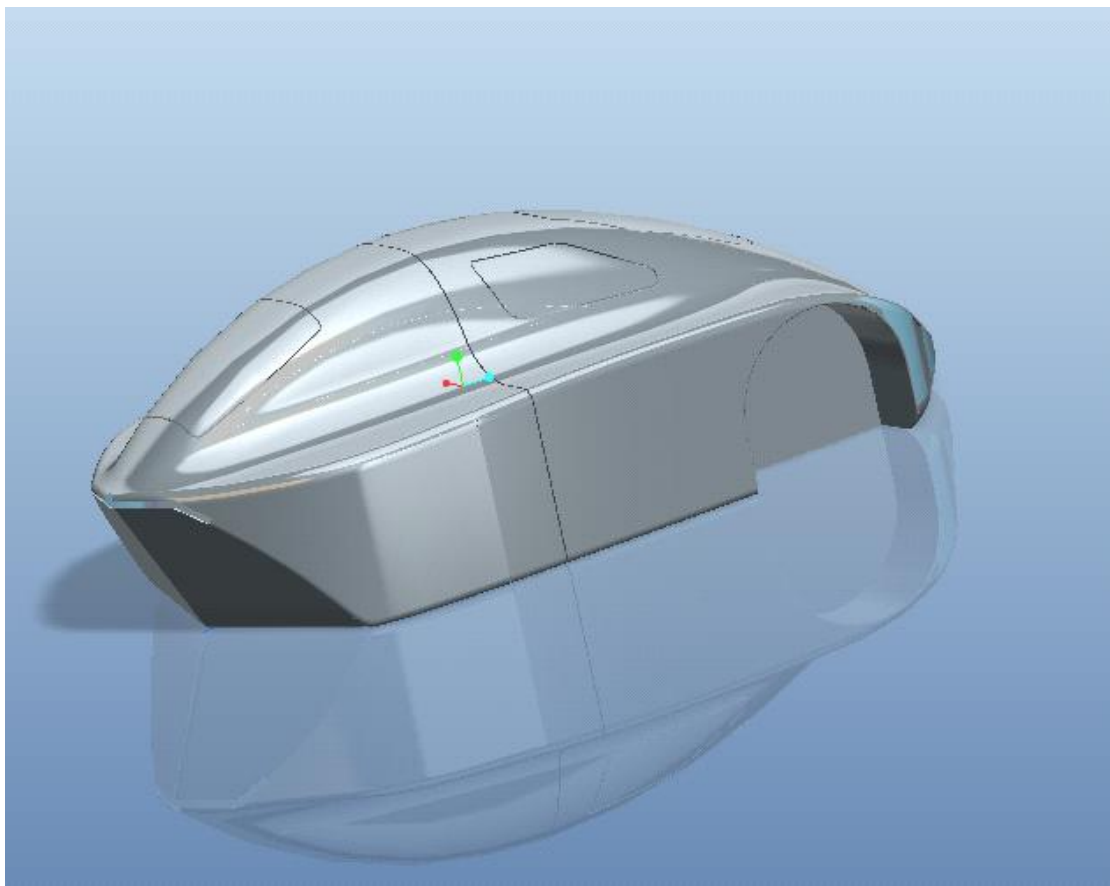


Figure 4-14 Body panel (View 2) [12]

4.3 New chassis design

Firstly, the ergonomic limitations taken into consideration during the design process are figured out. After that, the process is ready to start. It took more than 20 different designs of different types of chassis, in order to evaluate which one fits better in our case. Having made the choice, two of these evolutionary design stages are illustrated later on in the thesis. The final stage of the designing process and the remaining parts that will be placed on the final design, are presented in the following images.

4.3.1 Ergonomics

One of the most determining factors in the competition is the driver. The driver can be aided in his performance by ensuring that all controls can be easily reached, he has a comfortable seating position and that visibility over the front of the chassis is sufficient. Besides being comfortable, the driver must be safe at all times. This mainly involves the existence of a roll bar and dimensional demands for the chassis to allow for quick driver egress in case of accidents or in case of fire. These regulations are often with respect to a so called 95th percentile male. This is a statistical representation meaning that at least 95 percent of the male population must be able to drive the car safely [14] [15] [16] [17].

The variables used in looking for a good seating position of the driver are the following:

- The vertical and horizontal position of the steering wheel
- The horizontal position and angle of the seat with respect to the horizontal
- The horizontal and vertical position of the pedal assembly
- The height and horizontal position of the dashboard and front roll hoop

The goals were:

- ➔ Reclined seat back angle with respect to the horizontal: lower the overall center of gravity without compromising the drivers comfort.
- ➔ Create a seat thigh angle, to prevent the driver from shoving into his or her restraint harness when braking (the restraint harness is mounted in between the drivers legs).
- ➔ Safe chassis with low mass.
- ➔ Steering wheel location in such a way that:
 - a) the drivers can turn the steering wheel without hitting his or her legs.
 - b) the driver can operate the pedals without hitting the steering wheel with his or her legs.
- ➔ Dashboard/front roll hoop such that: the driver can see ahead of the car and especially ahead of the front wheels.
- ➔ Dash/floor and dash/seat clearance sufficient to pass the tests. The ground clearance must be at least 10 cm.
- ➔ Suitably shaped field in order to enter the various components on the vehicle. Area suitable to fit the engine and the fuel cell in the rear of the vehicle, just behind the driver. Appropriate areas for battery lights and steering system.
- ➔ Position of the pedal assembly so that all drivers can easily reach them.
- ➔ Determine the dashboard/front roll hoop height in such a way that the helmet clearance rule for a 95th percentile male is met (see Figure 4-15).

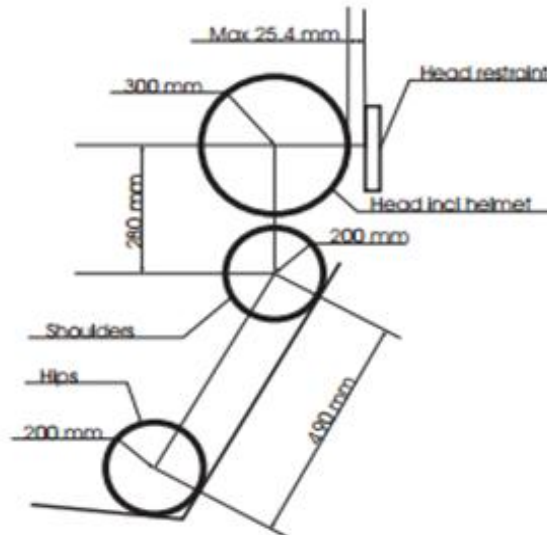


Figure 4-15 95th percentile male driver template [15]

We can see the 95th percentile male sketched on our chassis (Figure 4-16). We observe that there is a small slope to the back in the spot where the driver's hips would be, in order to place the driver's seat above it correctly.

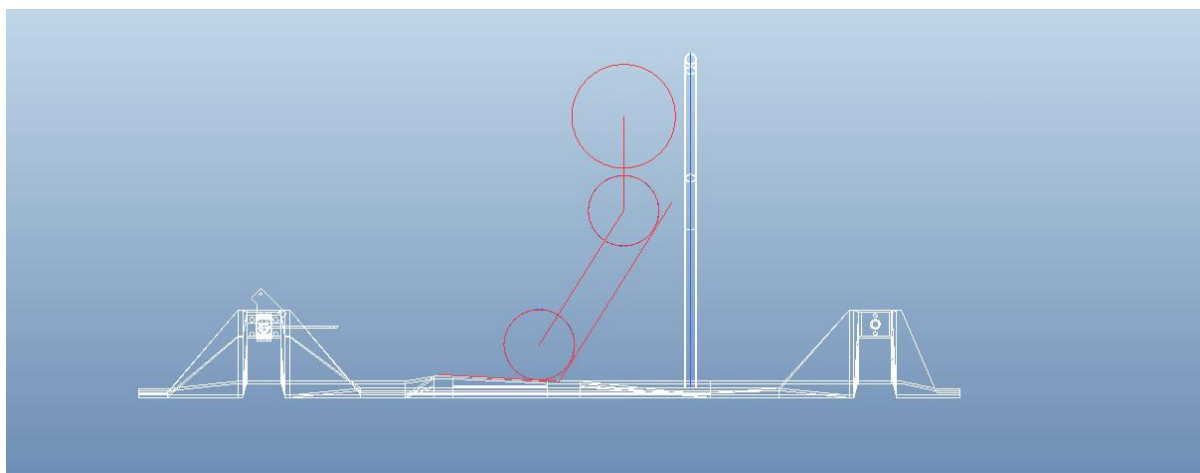


Figure 4-16 95th percentile male sketch on our new chassis design

DIMENSIONS

- a) The total vehicle height must be between 100 cm and 130 cm.
- b) The total body width, excluding rear view mirrors, must be between 120 cm and 130 cm.
- c) The total vehicle length must be between 220 cm and 350 cm.
- d) The track width must be at least 100 cm for the front axle and 80 cm for the rear axle, measured between the midpoints where the tyres touch the ground.
- e) The wheelbase must be at least 120 cm.
- f) The Driver's compartment must have a minimum height of 88 cm and a minimum width of 70 cm at the Driver's shoulders.
- g) The ground clearance must be at least 10 cm with the driver (and necessary ballast) in the vehicle.
- h) The maximum vehicle weight (excluding the Driver) is 205 kg.

CHASSIS/MONOCOQUE SOLIDITY

- a) Teams must ensure that the vehicle chassis or monocoque is designed wide and long enough to effectively protect the driver's body in the case of collisions or rollovers. A monocoque is a construction that supports structural load by using an object's external skin as opposed to using a frame.
- b) The vehicle chassis must be equipped with an effective roll bar that extends 5 cm around the driver's helmet when seated in normal driving position with the safety belts fastened. If this position impairs the driver visibility it will be deemed that the roll bar is not adequate. The effectiveness of the roll bar and driver's visibility will be validated simultaneously, i.e. the driver must not be in such position that he or she must raise their head or torso above the roll bar to pass the visibility test.
- c) This roll bar must extend in width beyond the driver's shoulders when seated in normal driving position with the safety belts fastened. It is permissible to either use a tubular or panel type roll bar. If a 'tubular roll bar' is used, it must be made of metal. A panel roll bar is the rigid partition separating the cockpit from the engine compartment. Such a panel roll bar must be an integral part of the vehicle chassis or integrated in a monocoque.

- d) Any roll bar must be capable of withstanding a static load of 700 N (~ 70 kg) applied in a vertical, horizontal or perpendicular direction, without deforming (i.e. in any direction).

PROPULSION AND ENERGY STORAGE SYSTEM ISOLATION

A permanent Bulkhead must completely separate the vehicle's propulsion and energy storage systems from the driver's compartment. This means engines, fuel cells, fuel tanks, batteries (both propulsion and auxiliary), hydrogen cylinders, Super Capacitors, etc. must be placed outside the driver's compartment behind the bulk head. The purpose of this bulkhead is that in the event of a fuel leak or fire, it prevents liquids and/or flames and/or smoke reaching the driver. Pay particular attention to avoid any gaps and holes between the body and the bulk head. It is recommended to seal gaps with materials such as metal/aluminium sheeting or aluminium tape.

DRIVER POSITION

For safety reasons, the head-first driving position is prohibited. The driver position should be such that the helmet is 5 cm below the roll bar AND that the visibility for the driver is unimpaired at the same

VEHICLE ACCESS

It is imperative for Drivers, fully harnessed, to be able to vacate their vehicles at any time without assistance in less than 10 seconds. The opening release mechanism must be easily and intuitively operable from the inside and the outside of the vehicle.

Figure 4-17 shows some essential rules that we will apply in our new model:

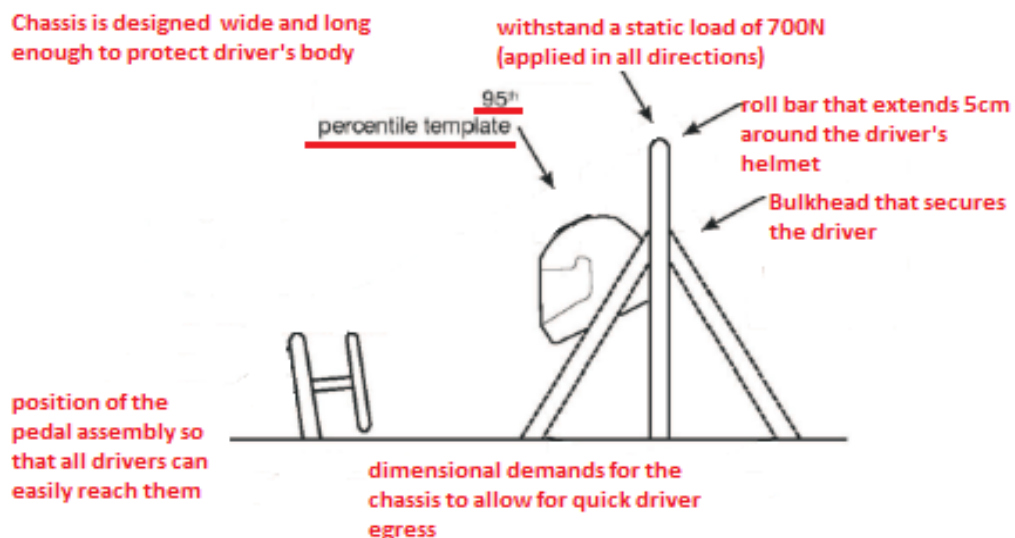


Figure 4-17 Major Ergonomic Rules in our new chassis design

4.3.2 New chassis' design stages

The first model is a parametrically generated model, which we can update by changing one or more of its parameters values. Changing these values, we create some optimal steps for the final chassis design. Two of the steps are presented below [13].

4.3.2.1 First design stage

The first design stage can be observed here.

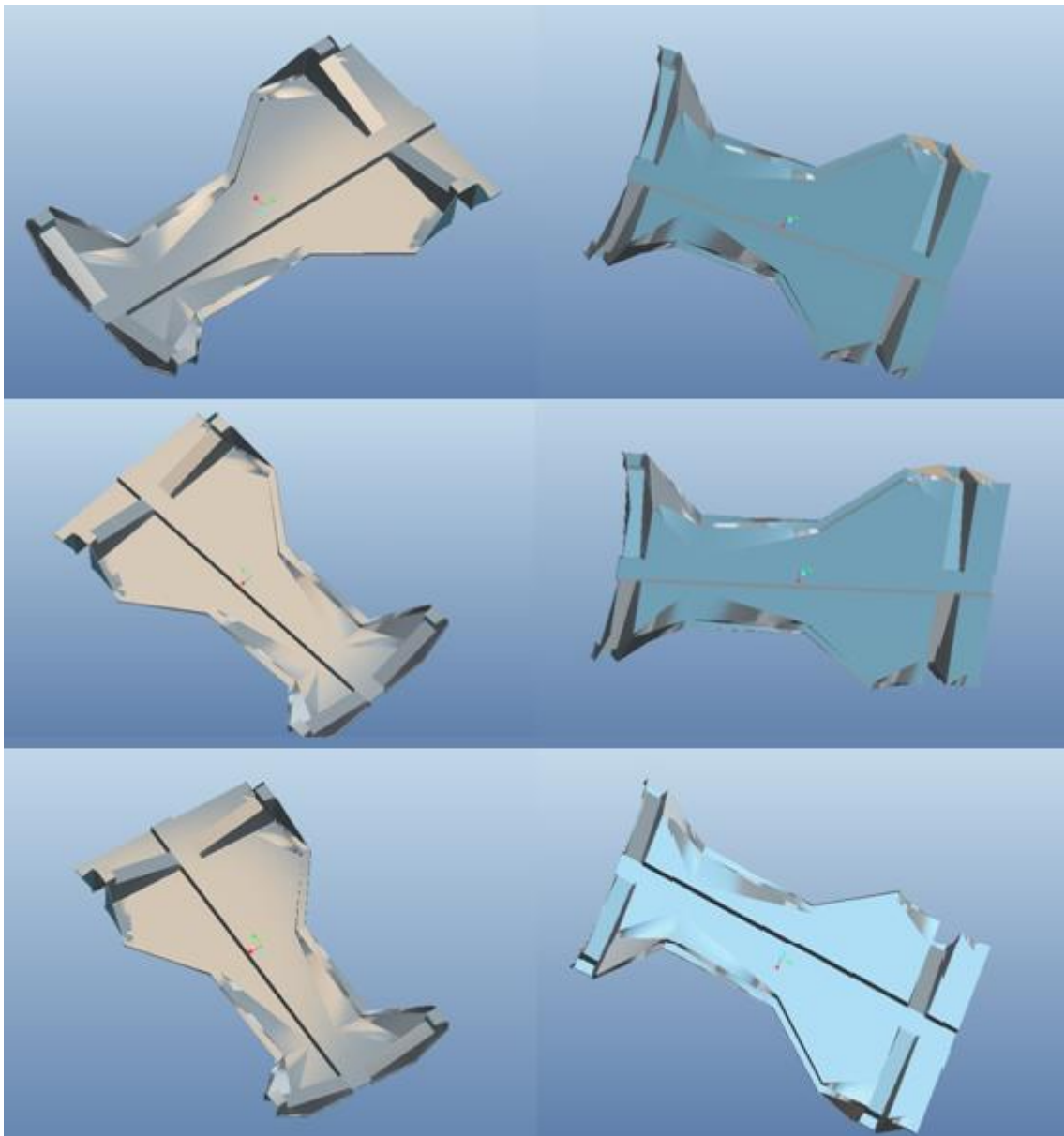


Figure 4-18 New Chassis First Design Stage

4.3.2.2 Second design stage

The second design stage can be observed below.

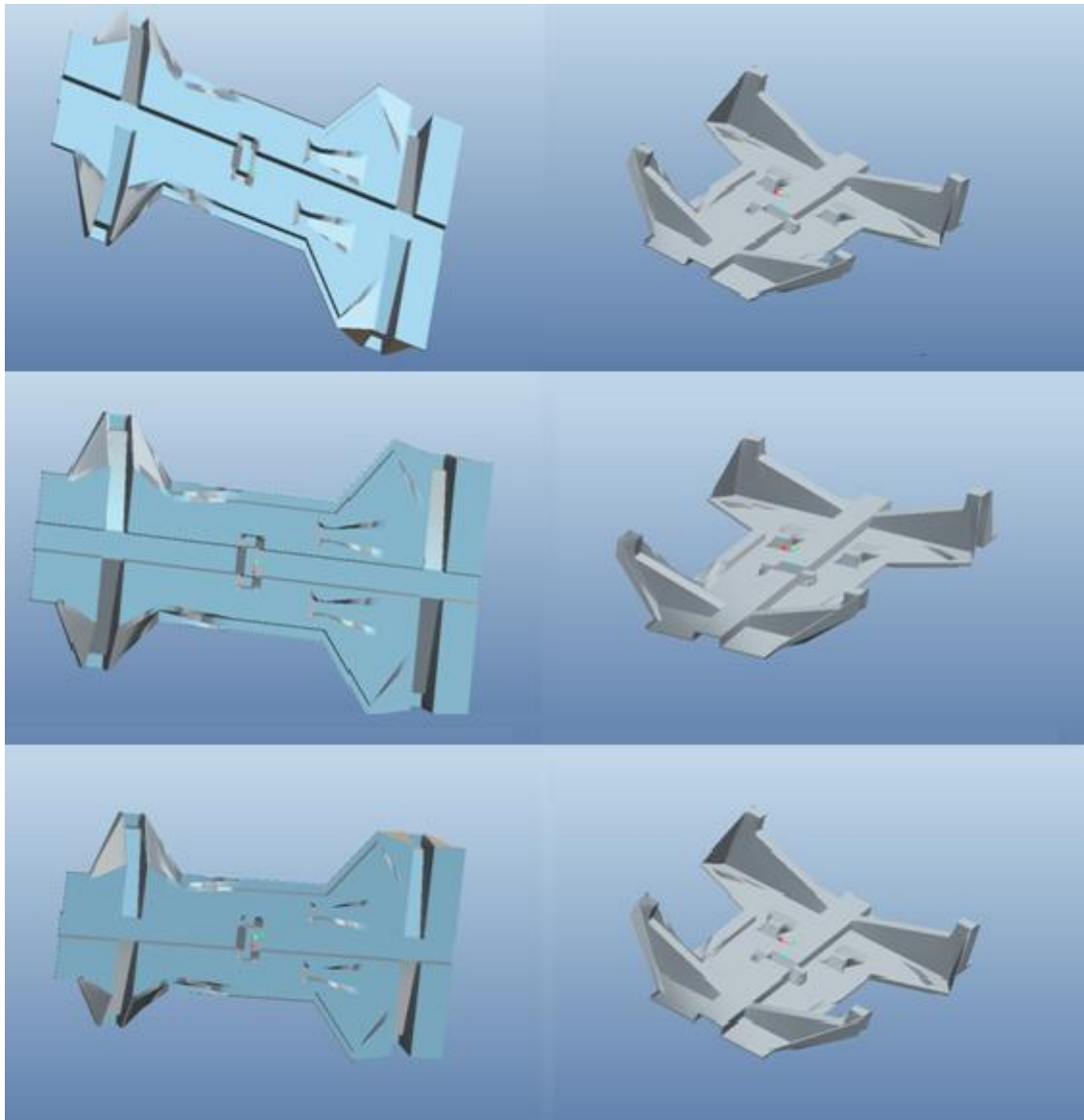


Figure 4-19 New Chassis Second Design Stage

4.3.2.3 Final design stage

First and foremost, the entire frame was designed considering the strength of the chassis, its low mass, ergonomics and aesthetics. The new chassis is a parametrically generated model, which can be updated by identifying one or more of its parameters and then changing their values. To do so, we use variables and algorithms to generate a hierarchy of mathematical and geometric relations. Below, the final chassis design is presented with different angles [13].

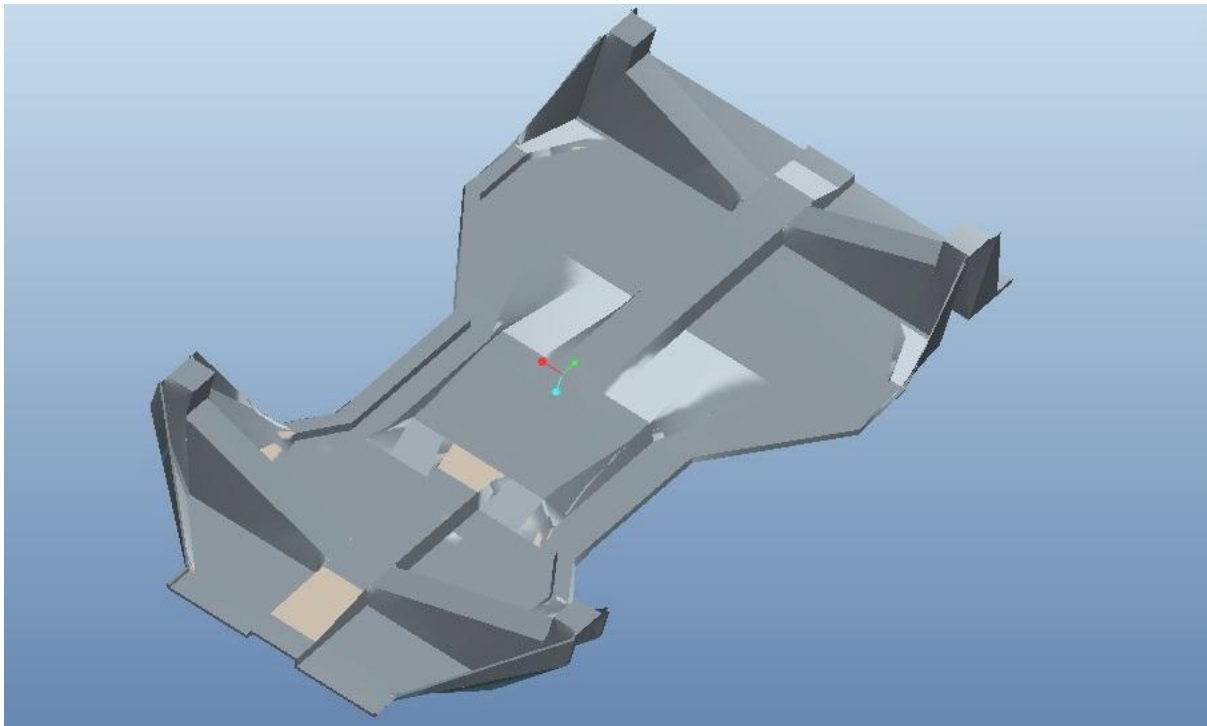


Figure 4-20 New Chassis design (View 1)

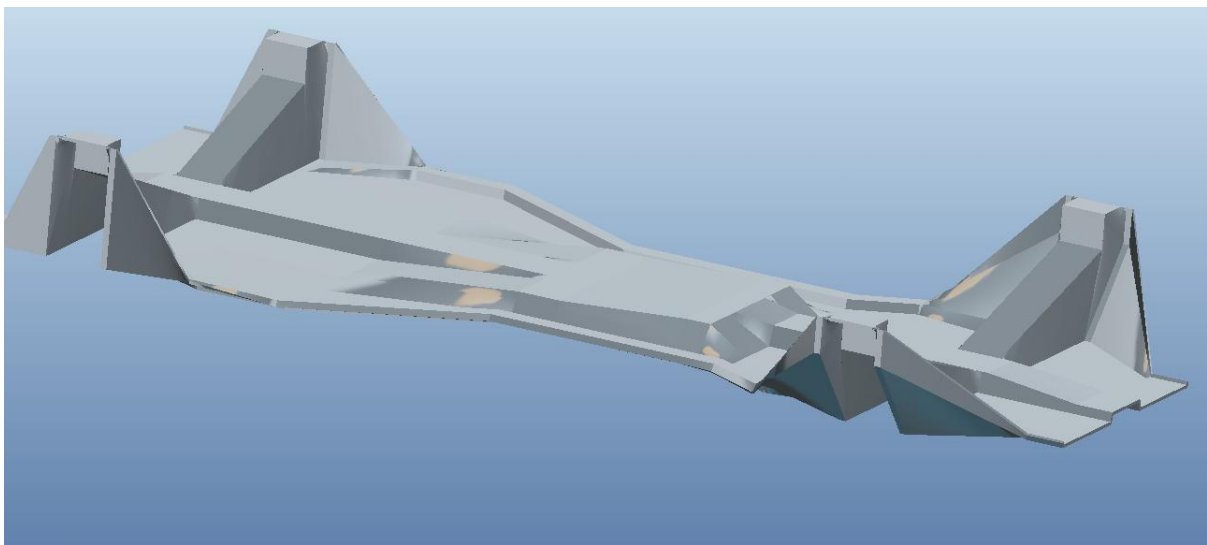


Figure 4-21 New Chassis design (View 2)

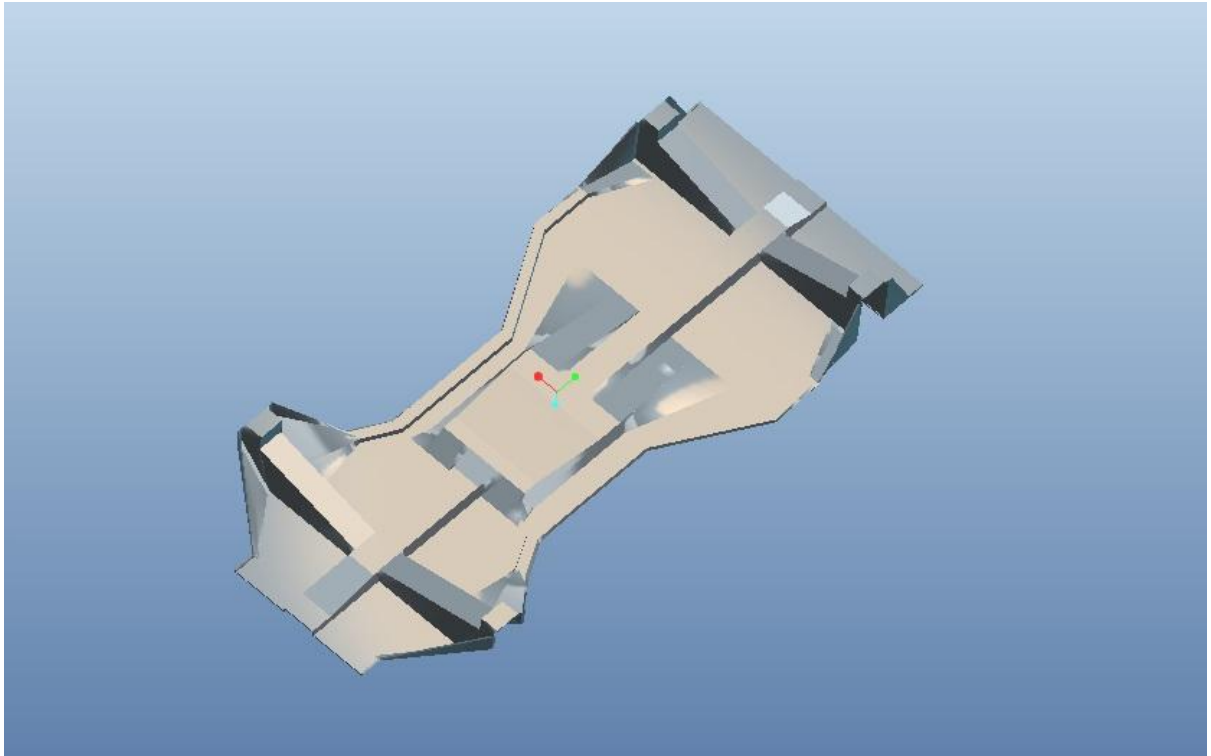


Figure 4-22 New Chassis design (View 3)

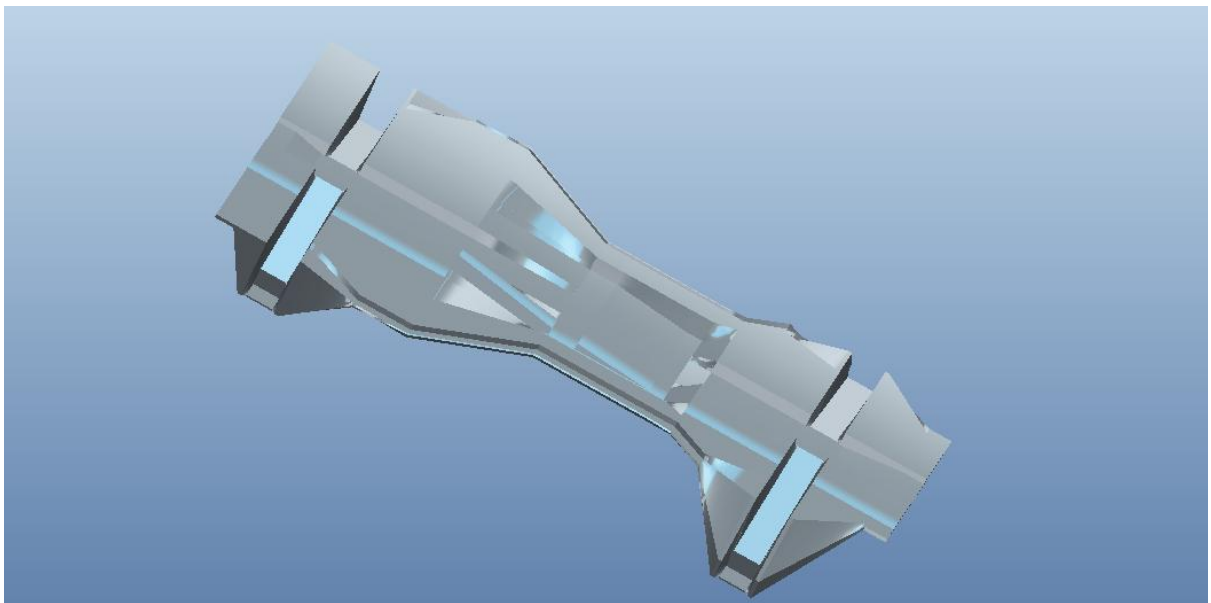


Figure 4-23 New Chassis design (View 4)

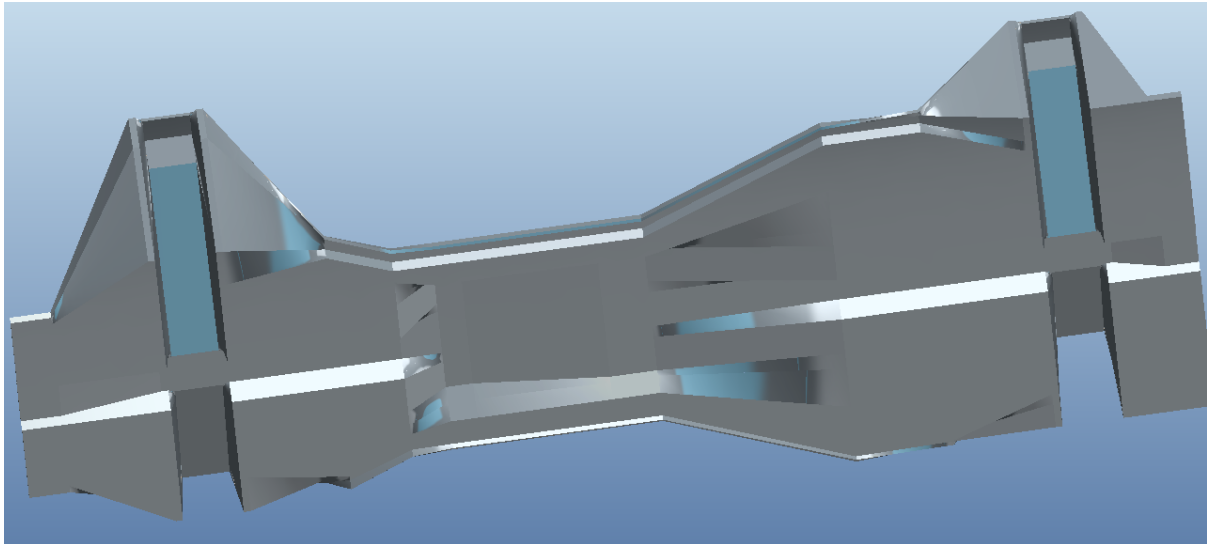


Figure 4-24 New Chassis design (View 5)

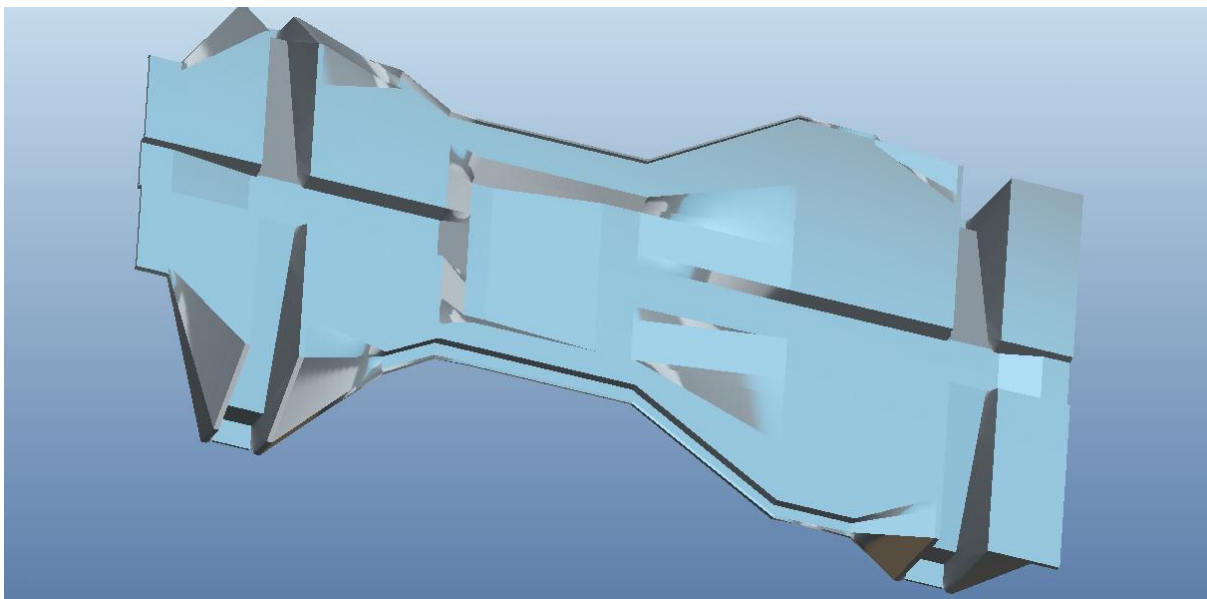


Figure 4-25 New Chassis design (View 6)

4.3.3 Design of the parts around the new chassis

In this section, the different parts placed on the chassis are presented. These include the front spindle base, the front spindle, the rear semi-axle kit and the body panel.

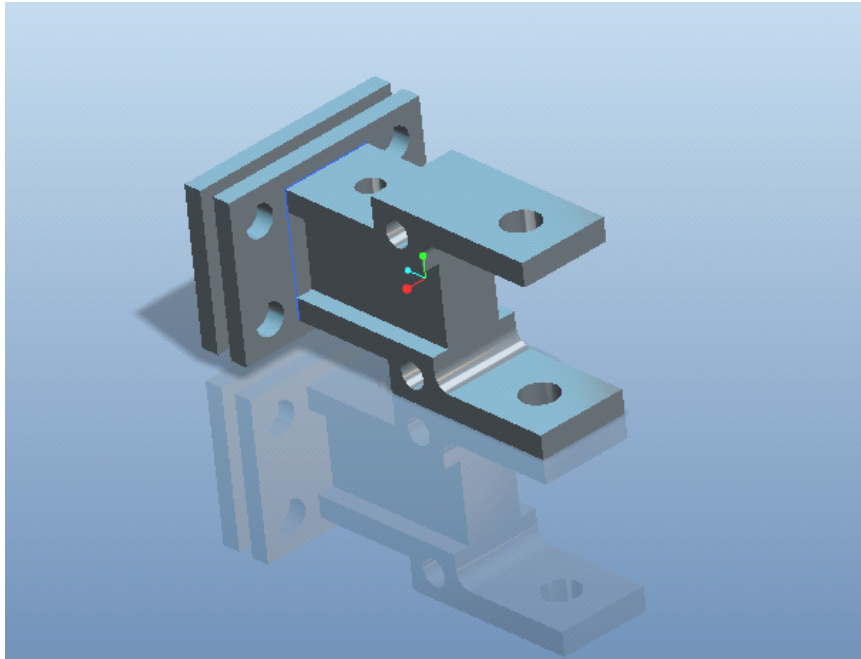


Figure 4-26 Front spindle base

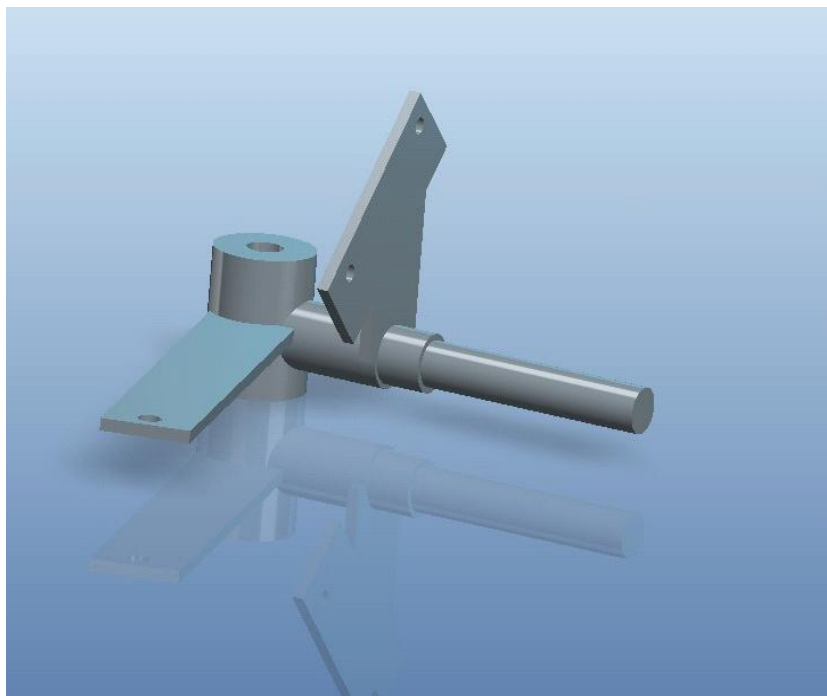


Figure 4-27 Front spindle

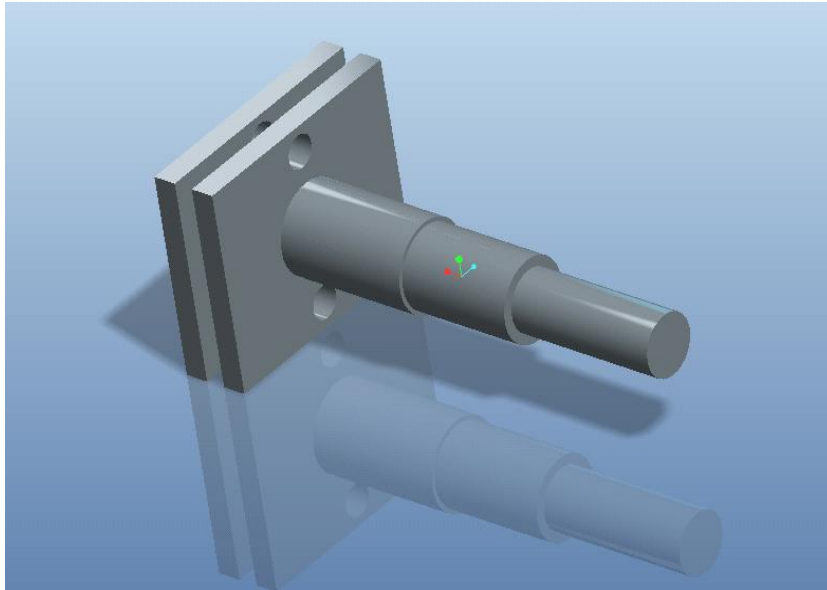


Figure 4-28 Rear semi-axle kit

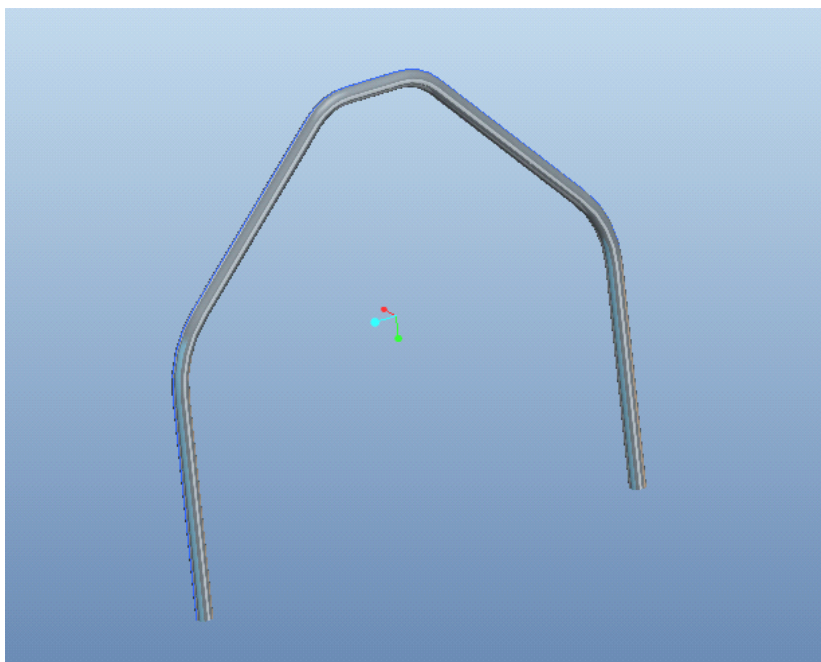


Figure 4-29 Roll Bar



Figure 4-30 Body Panel (View 1) [12]

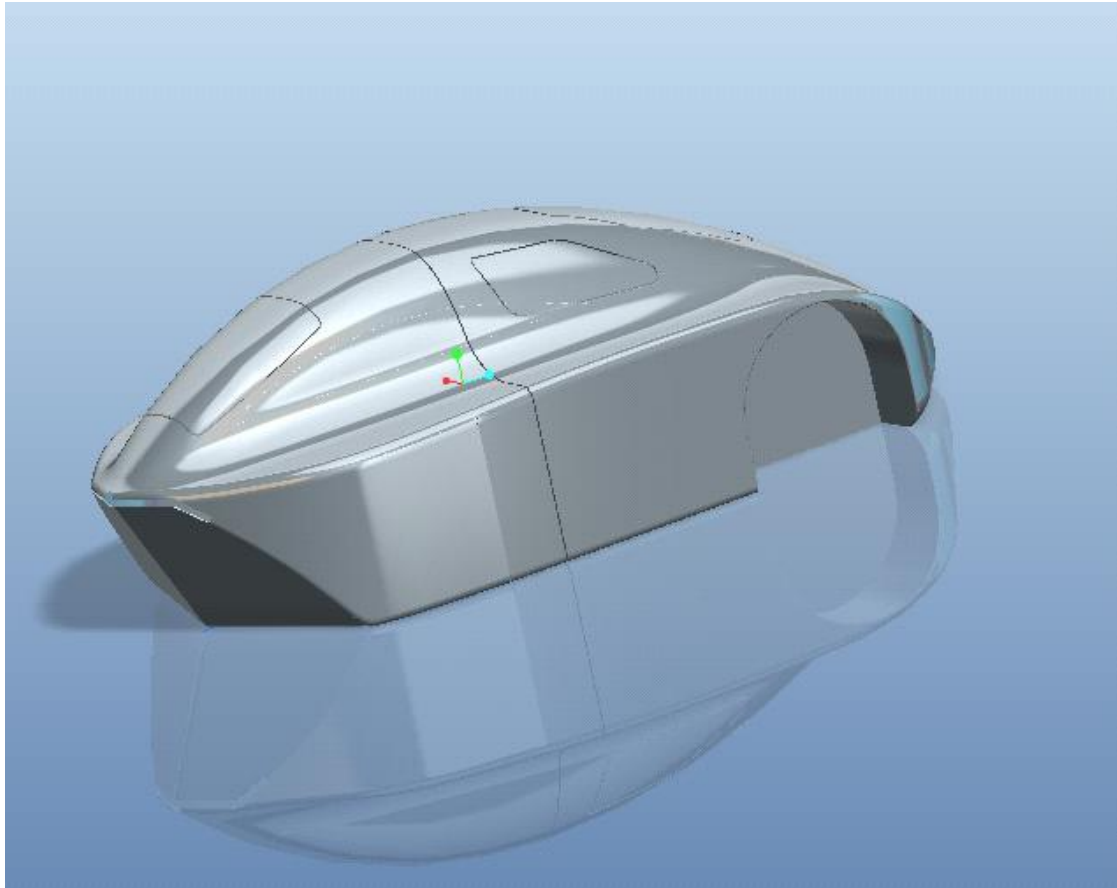


Figure 4-31 Body Panel (View 2) [12]

5 MECHANICAL PROPERTIES OF CHOSEN MATERIALS

In the next sections, the mechanical properties of the chosen materials are determined. Firstly, we work out the mechanical properties of the previous chassis material (aluminium), and after that, in order to specify the mechanical properties of the composite (carbon fiber) material, several required computations are described. Apart from that, the mechanical properties of the parts around the previous as well as the new chassis material are presented.

5.1 Mechanical properties of previous chassis

The previous chassis was constructed by 30"X30" 6082-T6 aluminium hollow sections with 1.5 mm wall thickness, welded together accurately.

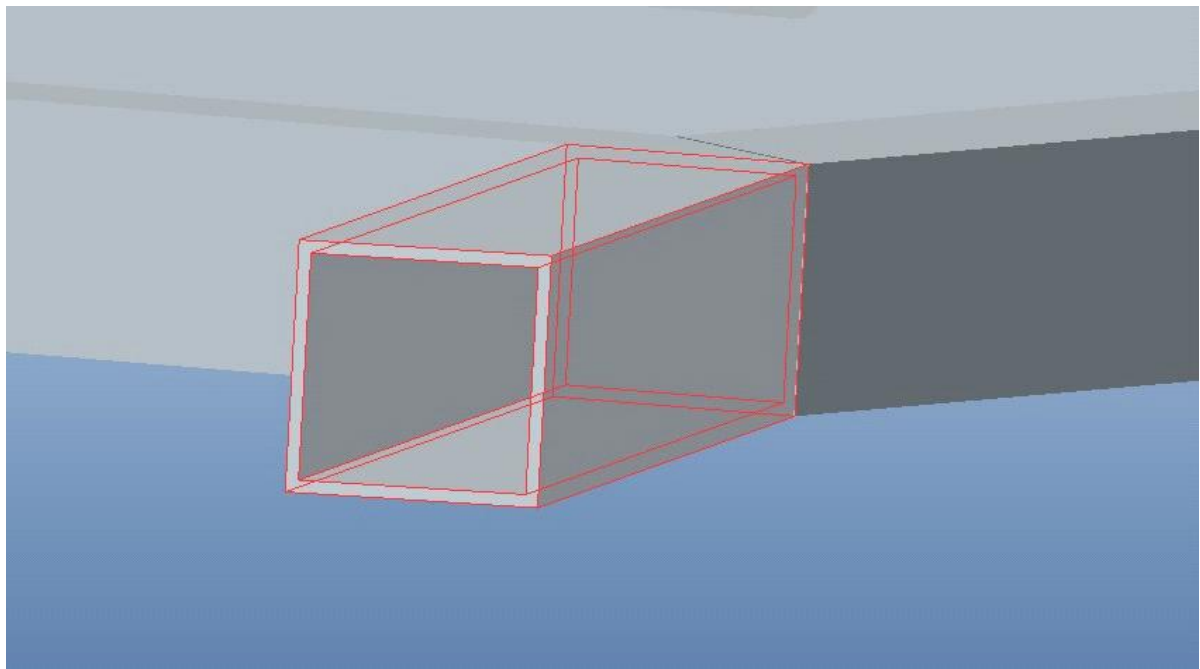


Figure 5-1 6082-T6 aluminium hollow sections

The mechanical characteristics of aluminium 6082-T6 [18]:

Young modulus = $70 \cdot 10^9$ Pa
Poisson ratio : 0.33
Density $\rho = 2.7$ g /cc
yield strength = 255 MPa

This is one type of aluminium whose yield strength is increased up to five times than that of the common types while maintaining the same mass. Generally, the main selection criteria of this material was the great strength, low mass, the great workability and weldability.

5.1.1 Mechanical properties of the parts around the previous chassis

In the front end structure, the spindle base is made of Aluminium 6082- T6 and the spindle of AISI 9000 Series Steel. The rear end structure is made of AISI 9000 Series Steel [18].

Table 5-1 Mechanical and physical properties of AISI 9000 Series Steel [18]

Physical Properties	Metric
Density	7.75 - 7.87 g/cc
Mechanical Properties	Metric
Hardness, Brinell	163 - 514
Hardness, Knoop	204 - 405
Hardness, Rockwell B	89.0 - 100
Hardness, Rockwell C	15.0 - 41.0
Hardness, Vickers	192 - 397
Tensile Strength, Ultimate	770 - 1780 MPa
Tensile Strength, Yield	440 - 1560 MPa
Elongation at Break	10.0 - 22.0 %
Modulus of Elasticity	200 - 209 GPa
Bulk Modulus	140 - 170 GPa
Poissons Ratio	0.270 - 0.300
Machinability	40.0 - 70.0 %
Shear Modulus	78.0 - 82.0 GPa
Izod Impact	9.00 - 119 J

5.2 Mechanical properties of new chassis

The material choice for the new chassis design and the determination of its properties are shown below.

5.2.1 Material choice

We chose the carbon fiber as construction material. The following points highlight the principal advantages and characteristics of carbon fiber [19] [20]:

- **Strength / Light Weight:** For the same strength, carbon composites are 80% lighter than steel and 60% lighter than aluminium.
- **Stiffness:** Carbon composites exhibit higher stiffness to weight ratios than conventional materials.
- **Fatigue:** Carbon Composites resist degradation in high fatigue applications much better than conventional materials.
- **Corrosion Resistance:** Carbon composites are essentially inert even in corrosive environments.
- **Energy Dampening:** Carbon Composites can be constructed around foam cores that will enable tremendous vibration dampening characteristics.
- **Thermal Expansion:** This property can be tailored to match surrounding structures thereby minimizing thermal stress.
- **Production Flexibility:** Carbon composites can be easily formed into complex shapes.
- **Durability:** Properly designed and fabricated, carbon composites exhibit very long life characteristics even in harsh operating environments.

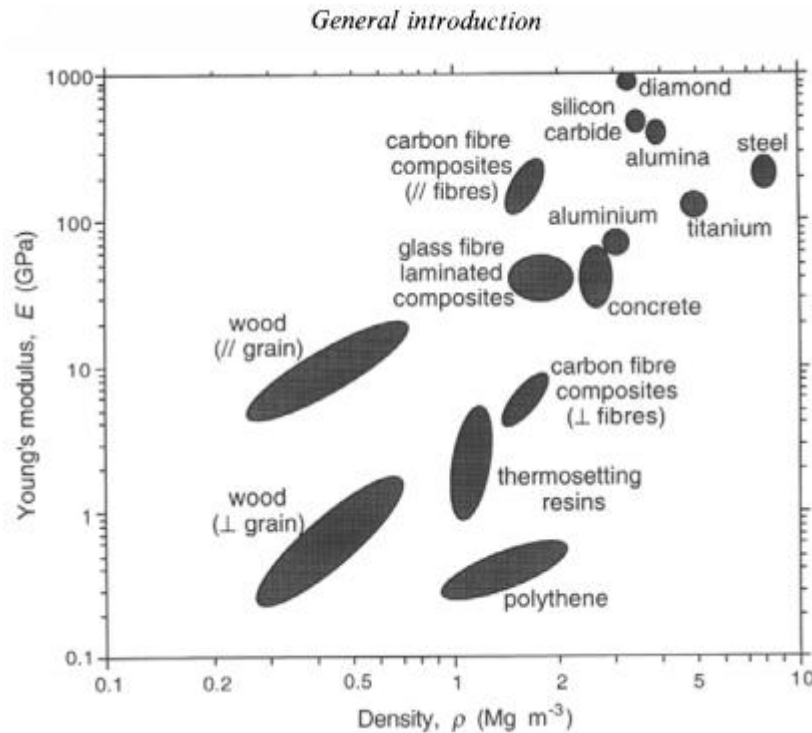


Figure 5-2 Data for some engineering materials in the form of areas on a map of Young's modulus E against density ρ [19]

Carbon fiber composites are extremely versatile. The properties of a carbon fiber composite structure depend on the selection of the components and how they are arranged. The two principal elements of a carbon composite structure are the matrix and the fibers. Fiber can be individual strands or multiple strands braided. The selection of the fiber, its orientation and its layering play a dominant role in determining the characteristics of the finished structure. The matrix serves to keep the fiber in the desired position. In addition, the matrix imparts important properties to the composite structure. Certain ingredients may be added to the matrix during production that will provide additional desired properties.

5.2.2 Designing with composites

Composite materials (Figure 5-3), consist of two or more materials with different mechanical and chemical properties. The individual materials are easily distinguishable, when they are combined, and are divided into two categories, the reinforcements and the fillers. The reinforcements provide the good properties (strength, stiffness, etc) to the composites and the fillers support the reinforcements so as to maintain mutual relative position. The combination of these categories produces incredible mechanical properties. Undoubtedly, the designer has the ability to choose the appropriate mixture of reinforcements and fillers in order to achieve the desired mechanical properties. [21] [22].

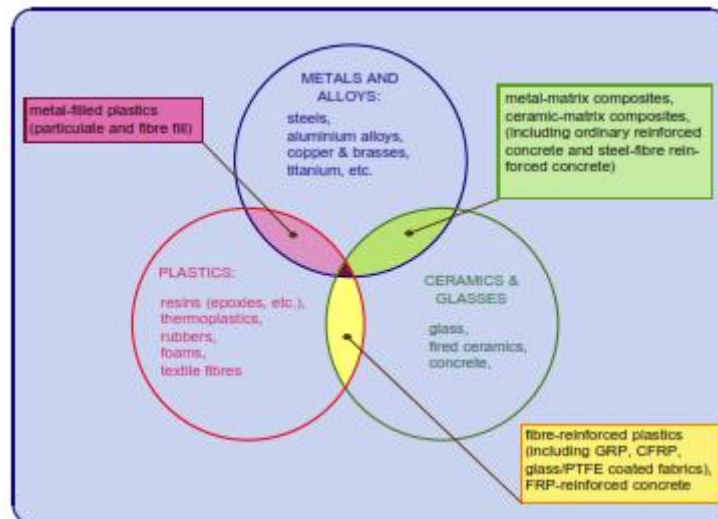


Figure 5-3 Relationships between classes of engineering materials, showing the evolution of composites [23]

Laminates composed of fillers and reinforcements, in fiber (fabric) form. According to their use, there are various fillers and reinforcements, that obviously, have different mechanical properties, thermal expansion and resistance. The most common fillers (resins) are:

- Polyester
- Vinyl ester
- Epoxy
- Phenol formaldehyde
- Polyimide
- Polyamide
- Polypropylene
- Polyether ether ketone

The most famous fibers are:

- Glass
- Carbon
- Aramid
- Hybrid boron

In order to achieve special properties, they used various types of reinforcement fabrics such as weaves cloth, twill or satin or single-shift and bi-axial or mat with binder [23] [24] [25].

5.2.2.1 Unidirectional fiber composites

Unidirectional Carbon Fiber Reinforced Plastic (CFRP) plies means that a large percentage of the fibers has the same orientation. These plies allow for higher specific moduli in the main fiber direction.

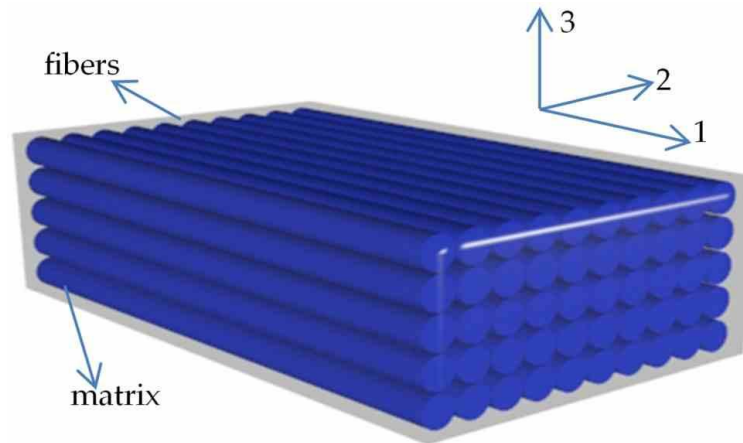


Figure 5-4 Unidirectional fiber composites

5.2.2.1.1 Elastic properties of fiber composites

The elastic properties of a unidirectional fiber composite are evaluated with the use of the most accurate methods. Consequently, the longitudinal tensile modulus, the transverse tensile modulus, the Poisson ratio, the shear modulus and the compression modulus are analytically calculated [26].

5.2.2.1.1.1 Longitudinal tensile modulus

Assuming that the structure is a simple beam, as in Figure 5-5, consisting of fiber and matrix that deform together, a method of estimating the stiffness of a unidirectional composite is performed.

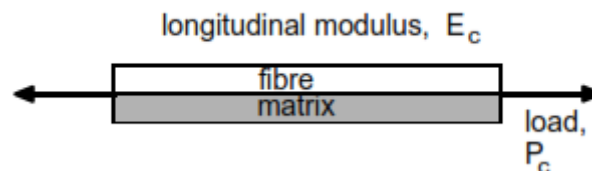


Figure 5-5 Simplified parallel model of unidirectional composite [23]

We also assume, that the deformation of the polymer matrix is time independent, and the length of the beam is L . Then, the sum of the volume fractions is:

$$V_f + V_m = 1$$

- where V_f the volume fraction of the fiber and V_m the volume fraction of the matrix.

The load on the composite is shared between the two phases, so that:

$$P_c = P_f + P_m$$

and the strain in the two phases is the same as that in the composite, $\epsilon_c = \epsilon_f = \epsilon_m$ (an “iso-strain” condition). Since stress = load/area [26]:

$$\sigma_c A_c = \sigma_f A_f + \sigma_m A_m$$

- where A_f the cross-sectional area of the fiber and A_m the cross-sectional area of the matrix.

From the iso-strain condition, dividing through by the relevant strains:

$$\frac{\sigma_c A_c}{\varepsilon_c} = \frac{\sigma_f A_f}{\varepsilon_f} + \frac{\sigma_m A_m}{\varepsilon_m}$$

$$\text{or } E_c = E_f V_f + E_m(1 - V_f).$$

- where E_f the elastic modulus of the fiber and E_m the elastic modulus of matrix.

This equation makes the assumption that $\nu_f = \nu_m$ (equal Poisson ratios), and is referred to as the Voigt estimate, well known as the rule of mixtures. The Hill's estimation, for the unidirectional composite characteristics, in 1964, is a model with better accuracy. It shows that the composite characteristics are greater than those calculated by the rule of mixtures. This change is proportional to:

$$(\nu_f - \nu_m)^2$$

Figure 5-6, shows the validity of the mixture rule for the longitudinal modulus of two different composites.

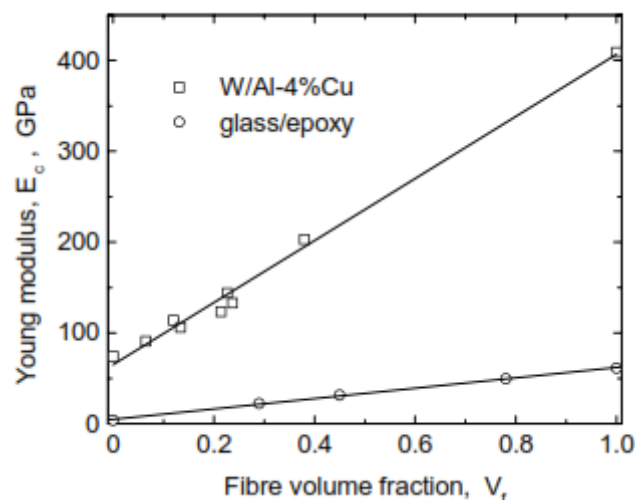


Figure 5-6 Confirmation of the rule-of-mixtures relationship for the Young moduli, E_c , of unidirectional composites consisting of tungsten wires in Al-4%Cu alloy and glass rods in epoxy resin [23]

5.2.2.1.2 Transverse tensile modulus

In the same way, the transverse tensile modulus, E_t , is determined (Figure 5-7), using the same constraints as previously.

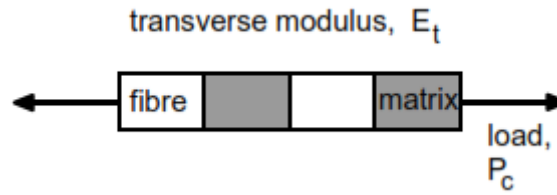


Figure 5-7 Simple series model of a composite [23]

An “iso-stress” model is used:

$$\sigma_c = \sigma_f = \sigma_m$$

The total extension is given by the equation:

$$\varepsilon_c L_c = \varepsilon_f L_f + \varepsilon_m L_m$$

We consider that the cross-sections L, V , are the same, $L = V$. We consider also that:

$$V_f + V_m = 1$$

From the iso-stress condition, dividing through by the relevant strains:

$$\frac{\varepsilon_c}{\sigma_c} = \frac{\varepsilon_f V_f}{\sigma_f} + \frac{\varepsilon_m V_m}{\sigma_m}$$

$$\text{or } \frac{1}{E_t} = \frac{V_f}{E_f} + \frac{V_m}{E_m}$$

This is the inverse rule of mixtures (Reuss estimate):

$$E_t = \frac{E_f E_m}{E_m V_f + E_f (1 - V_f)}$$

5.2.2.1.1.3 Poisson ratio

As far as the isotropic materials, the Poisson ratio (ν) can be calculated by:

$$\nu = -\varepsilon_2 / \varepsilon_1$$

- where ε_2 is the lateral strain and ε_1 is the longitudinal strain.

As far as the unidirectional composite layers, two Poisson ratios should be considered. According to Voigt and Reuss, the major Poisson ratio, ν_{12} , relates to the lateral strain, when a stress is applied in the longitudinal direction and the minor Poisson ratio, ν_{21} , relates to the longitudinal strain, when a stress is applied in the lateral direction. The major Poisson ratio can be calculated by:

$$\nu_{12} = \nu_f V_f + \nu_m (1 - V_f)$$

In addition, the minor Poisson ratio, ν_{21} , is related with the major Poisson ratio, ν_{12} . The minor Poisson ratio is given by:

$$\nu_{21} / E_2 = \nu_{12} / E_1.$$

5.2.2.1.1.4 Shear modulus

Figure 5-8 shows a unidirectional composite lamina loaded in shear. The result of this force is a displacement to a parallelogram.

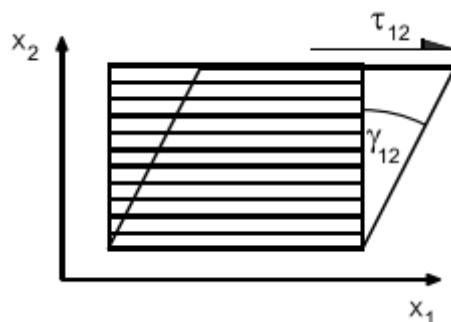


Figure 5-8 Definition of a shear relative to the x_1x_2 Cartesian axes [23]

We can assume that the fibers and matrix carry the same stress:

$$\tau_{12} = G_{12} \gamma_{12} = G_f \gamma_f = G_m \gamma_m$$

- where τ_{12} is the shear stress in the longitudinal axis.

Therefore, the shear modulus in x-axis, G_{12} , is given by:

$$\frac{1}{G_{12}} = \frac{V_f}{G_f} + \frac{(1-V_f)}{G_m}.$$

If the fiber volume fraction is not very large, the matrix shear stiffness dominates the composite shear modulus.

5.2.2.1.1.5 The compression modulus

Piggott and Harris experimented on the compression modulus of composite materials, which consist of polyester matrix along with reinforced materials such as glass, Kevlar-49, and two types of carbon fiber. The conclusion of their research proves that the V_f is linear up to only about 50 vol% of reinforcement, and that beyond this the rate of increase of stiffness falls. The consequence of a V_m decrease is that the matrix fails to hold the fiber from deforming.

Figure 5-9 represents that the rule of mixtures can be followed precisely, only in the case of fiber glass reinforcement. The slopes, dE_c/dV_f , of the curves for the two carbon-fiber composites are vaguely lower than the 1:1 rule-of-mixtures values, whilst the aramid fiber slopes are far lower than the RoM ones.

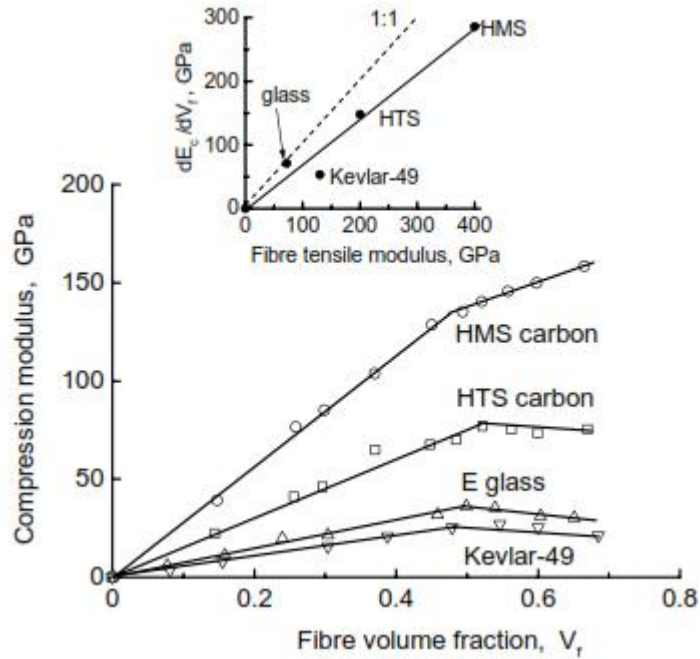


Figure 5-9 Variation of the compression moduli of polyester-matrix composites with volume fraction of four species of reinforcing fibers [23]

5.2.2.1.1.6 The anisotropic properties of a thin lamina

When the orientation between the longitudinal and the transverse axis is altered, the properties of unidirectional composites change. This variation regarding angle exists because of their anisotropic behaviour and it is essential to be determined by a designer.

Several engineering materials are considered as isotropic. This means that they have similar properties in all directions (plastics, metals, ceramics, etc.). For the characterization of an isotropic material the elastic constants should be defined. These constants are the Young modulus (E), the shear or rigidity modulus (G), the bulk modulus (K) and the Poisson ratio (ν). However, only two of these are independent properties (for example, if E and ν are known, the other two constants can be calculated).

$$G = \frac{E}{2(1+\nu)} \quad K = \frac{E}{3(1-2\nu)}$$

These equations are used only for isotropic materials.

Figure 5-10 shows an anisotropic thin composite lamina. The fibers are aligned in the x_1 direction and transverse to the x_2 direction.

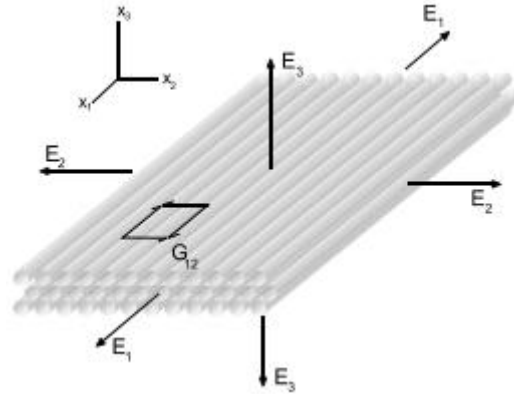


Figure 5-10 Definition of elastic constants for an anisotropic thin composite lamina [23]

Three Young's modulus, E_1 , E_2 , E_3 , three shear modulus, G_{12} , G_{13} , G_{23} , and six Poisson ratios, ν_{12} , ν_{21} , ν_{13} , ν_{31} , ν_{23} , ν_{32} , are required for the characterization of an anisotropic material. Nonetheless, the E_3 value is approximately equal with the E_2 value as well as the G_{13} is not practically different than G_{12} . The G_{23} value usually differs from G_{13} and G_{12} . Likewise, the ν_{12} value is similar to that of ν_{13} . Although $\nu_{12} \gg \nu_{21}$, considering the Poisson ratios, it is obvious that $G_{12} = G_{21}$ applies, considering the shear modulus etc. What is obtained by this research, is that a unidirectional lamina reacts to another in a more complicated way than how an isotropic material would.

5.2.2.1.2 The strength of fibers composites

The definition of the fiber composites strength is more complicated than the elastic properties definition. The fiber composite failure depends on many aspects of the composite construction, such as:

- The type of the fiber and its distribution.
- The aspect ratio l/d of the fiber.
- The quality of the interfacial adhesive bond between the fibers and the matrix.

Because of the complex nature of failure in many types of composite, considerations of strength and toughness are closely inter-related. We should bear in mind when designing with composites that the strength and toughness may not be independent.

5.2.2.1.2.1 Longitudinal tensile strength

Assuming that the structure is a simple unidirectional composite lamina, as in Figure 5-11, consisting of fiber and matrix that deform together, a method of estimating the stress on the composite is performed.

$$(\sigma)_c = (\sigma)_f V_f + (\sigma)_m (1 - V_f)$$

- where $(\sigma)_f$ are the fibers stress levels and $(\sigma)_m$ the matrix stress levels and are equal to $E_{f\varepsilon}$ and $E_{m\varepsilon}$, respectively. (where ε is the composite strain)

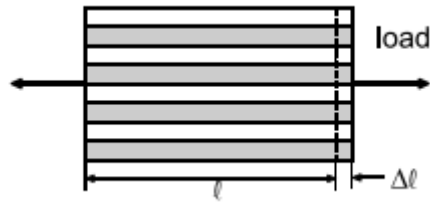


Figure 5-11 A simple unidirectional composite lamina under tensile load [23]

5.2.2.1.2.2 Transverse tensile strength

Perpendicular to the reinforcing fibers most composites are weak and failure is controlled by rupture or plastic flow of the matrix, or by fiber/matrix decohesion: the precise mechanism will depend on the capacity of the matrix for plastic deformation and the strength of the fiber/matrix bond. If the matrix is a metal or polymer, its intrinsic yield strength will govern the transverse behaviour of a composite containing only a few fibers. If this yielding is restricted to the ligaments between the fibers, the transverse strength of the composite might be estimated from a crude rule-of-mixtures model in which the deforming matrix cross-section is obtained from a knowledge of V_f and the reinforcement geometry.

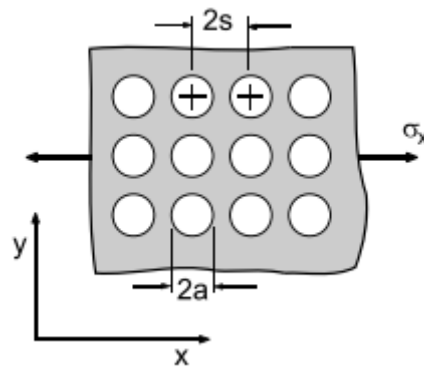


Figure 5-12 Kies's model (1962) for strain magnification during transverse loading of a unidirectional composite [23]

For the square array shown in Figure 5-12, for example, the effective volume fraction of the deforming matrix normal to the fibers is:

$$V_m(\text{eff}) = 1 - \sqrt{\frac{4V_f}{\pi}}$$

Assuming no contribution from the fibers, the transverse strength of the composite is then:

$$\sigma_t = \sigma_{my} \left(1 - \sqrt{\frac{4V_f}{\pi}} \right)$$

As the volume fraction increases, however, the relatively undeformable fibers impose an increasing degree of constraint on the matrix.

5.2.2.1.2.3 Compression strength

Studies of the compression behaviour of composites have been complicated by the fact that when testing small, free blocks of material, failure modes occur which are not necessarily determined by fiber behaviour, and the compression strength of a composite often appears to be lower than its tensile strength. As in the case of wood compressed

along the grain, longitudinal splitting and/or kinking of the sample often occur, as illustrated schematically in Figure 5-13, at stresses well below the equivalent tensile load-bearing ability of the composite.

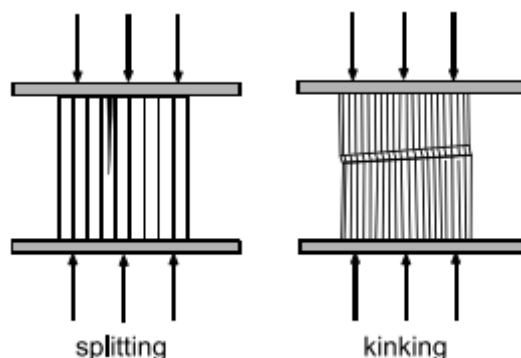


Figure 5-13 Schematic illustration of compression failure modes in unidirectional composites [23]

Measurements to obtain the true compression strength are difficult to carry out. In an early model for compression strength, Rosen (1965) proposed that failure was initiated by matrix instabilities that lead to co-operative, in-plane buckling of the reinforcement. The model was developed for lamellar composites with reinforcing plates, rather than fibers, and, except at low V , it predicted failure by a shear mode at a stress:

$$\sigma_{\text{comp}} = \frac{G_m}{1 - V_f}$$

- where G_m is the matrix shear modulus.

5.2.2.1.2.4 Shear strength

Most laminated continuous-fiber composites contain planes of weakness between the laminations and along fiber/matrix interfaces. In shear the composite strength will be dominated by these weaknesses unless the stress direction intersects the fibers. Shear stresses at the interfaces between the plies can seldom be avoided by lay-up design because of the anisotropies of neighbouring plies. These interlaminar shear stresses are usually high at edges, as shown by Pipes and Pagano (1970), and often give rise to delaminations which propagate into the composite from the edges, significantly reducing the laminate tensile strength (Pagano and Pipes, 1971). Delamination is a major cause of failure in laminated composites, and one of the concerns of the designer is to ensure that shear stresses are diffused safely away from stress concentration points.

Interlaminar shear failure is most readily seen in the three-point bending of short beams, a method commonly used to measure what is usually referred to as the interlaminar shear strength, or ILSS, although this is often regarded as unsatisfactory because the state of stress is not pure shear.

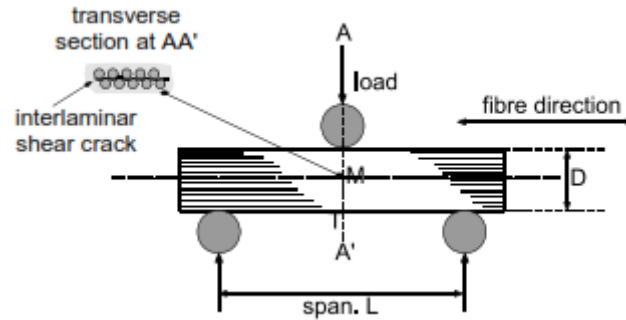


Figure 5-14 Schematic illustration of interlaminar shear failure in a unidirectional laminate [23]

In the diagram in Figure 5-14, if the level of horizontal shear stress at the midplane point M reaches the interlaminar shear strength, τ_{IL} , of the composite before the tensile stress level at T reaches the composite strength, σ_c , then the beam will fail. If the beam is longer than a certain critical length, however, it will fail in a normal bending mode by a tensile failure initiating at the mid-point of the outer face. As long as the failure mode is interlaminar shear, the failure load is independent of length, but when the tensile failure mode predominates, the failure load falls rapidly in inverse ratio to the span of the beam. The critical span-to-depth ratio for the transition can be found by equating the expressions for the tensile and shear stresses in the beam.

The tensile stress at T is $3PL/2B(D)^2$, while the shear stress at the neutral plane is $3P/4BD$ (the standard formulae for the bending beam, with B = width, D = thickness, and L = length). Equating these, we have:

$$\frac{\sigma_c}{\tau_{IL}} = \frac{3PL}{2BD^2} / \frac{3P}{4BD} = \frac{2L}{D}$$

and the beam will therefore fail in interlaminar shear at the neutral plane if $L/D < \sigma_c/2\tau$. For a typical unidirectional CFRP laminate with $\sigma_c = 1.5\text{GPa}$ and $\tau_{IL} = 50\text{MPa}$, a shear failure will occur in bending at span-to-depth ratios less than about 15:1, and when the short-beam shear test is used to evaluate the ILSS, it is usually recommended that a span-to-depth ratio of about 5 is used.

5.2.2.2 Multi-ply laminates

Unidirectional composites are rarely used in practice because of the high level of anisotropy demonstrated by Figure 5-15.

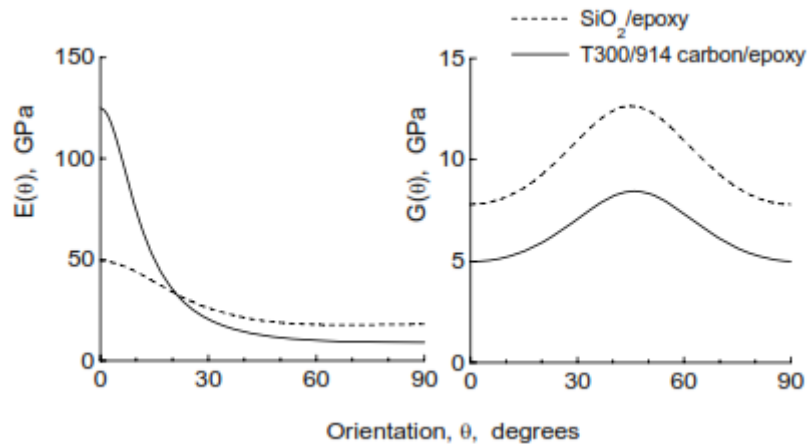


Figure 5-15 Dependence of Young's modulus, $E(\theta)$ and the shear modulus, $G(\theta)$, on the angle, θ , between the fibers and the stress axis for a carbon-fiber composite and a silica/epoxy composite [23]

In practice it is more sensible to make use of the versatility of composite materials by arranging the fibers in different directions to suit the design requirements. There are various ways in which this is done, depending on the level of sophistication of the required product. It is useful at this stage, however, to refer to the most common procedure for producing high performance laminates, which is to stack groups of single-ply lamina cut at various angles from the continuous sheet of "prepreg"—a continuous layer of fibers pre-impregnated with resin which is then dried (but not cured) - and then hot-press them between the heated platens, flat or shaped, of a press. The stacking sequence of such a laminate is described in short-hand form by formulae of the following kind:

- $(0)_{12}$ - a unidirectional composite with 12 plies.
- $(0,90)_{2s}$ - a cross-plyed laminate with four pairs of 0/90 lamina arranged symmetrically (indicated by the "s") $(0,90,0,90,90,0,90,0)$.
- $[(\pm 45,0,2,90_2)_2]_s$ - a quasi-isotropic laminate with 24 plies arranged symmetrically $(+45,-45,0,0,90,90,+45,-45,0,0,90,90,90,90,0,0,45,+45,90,90,0,0,-45,+45)$, the external ± 45 plies providing protection against impact damage.

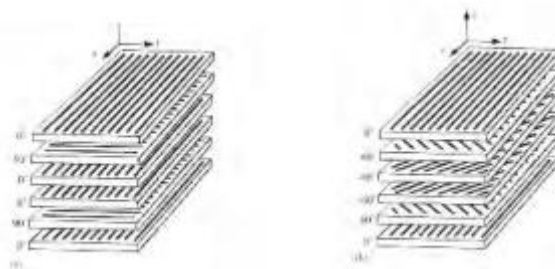


Figure 5-16 Multi-ply laminates [24]

The choice of laminating sequence may vary widely, depending upon the particular design requirements, but an indication of the potential for modifying the lay-up to achieve a desired result can be seen by comparing the orientation dependence of the stiffness of a unidirectional laminate with the stiffness of a series of composites of lay-up $\pm\theta$, where in each case θ varies from 0 to $\pi/2$, as shown in Figure 5-16.

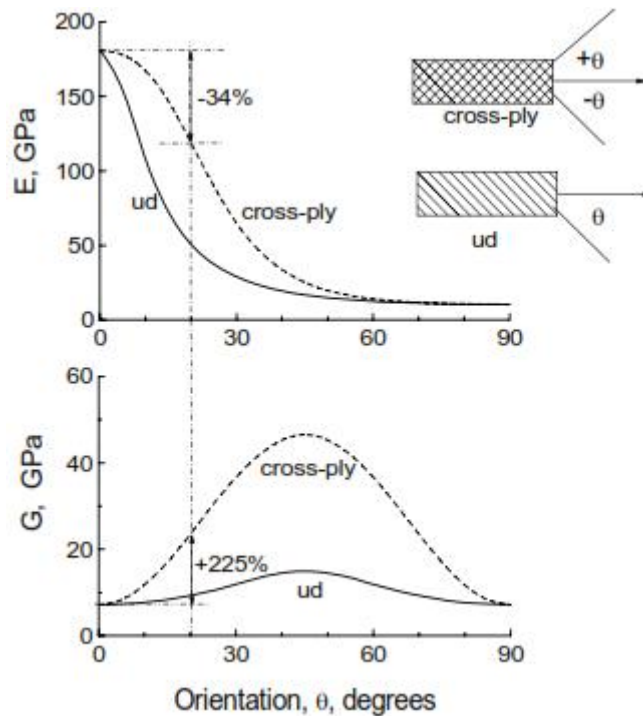


Figure 5-17 The effect of cross-laminating on Young’s modulus and the shear modulus of a T300/5208 carbon-fiber/epoxy composite [23]

5.2.2.2.1 Tensile & shear modulus of multi-ply laminates.

Cross-laminating is a compromise solution which results in improved torsional and transverse rigidity at the expense of some loss in longitudinal stiffness. It can be seen, for example, that by using a ±20° laminate instead of a unidirectional composite, for only a 34% loss in axial stiffness, the torsional rigidity may be doubled. The extent of the axial stiffness reduction caused by cross-laminating is greater the stiffer the reinforcing filaments.

Nielsen and Chen (1968) demonstrated the significance of this by showing the effect of randomising the fiber distribution in the plane of the laminate. The modulus, E(θ), is randomised over all θ:

$$E = \frac{\int_0^{\pi/2} E(\theta) d\theta}{\int_0^{\pi/2} d\theta}$$

The solution to this equation, also obtained in Mathcad, for a pair of composites with different modulus ratios, E_f/E_m is shown in Figure 5-18.

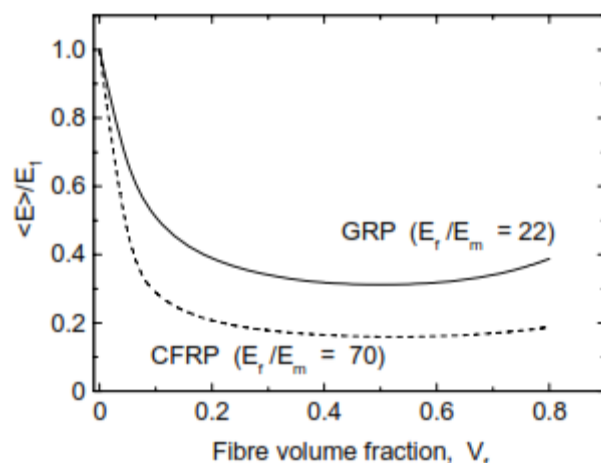


Figure 5-18 Effect of randomising the fiber orientations on the stiffnesses of CFRP and CRP laminates [23]

For most practical purposes (Hull, 1981) the solution can be approximated reasonably closely by:

$$\langle E \rangle = \frac{3}{8}E_1 + \frac{5}{8}E_2$$

- where E_1 and E_2 are the known or calculated longitudinal and transverse moduli for a unidirectional lamina.

An analogous approximate expression can be obtained for the shear modulus of a random continuous-fiber composite:

$$\langle G \rangle = \frac{1}{8}E_1 + \frac{1}{4}E_2$$

Multi-ply laminates usually, but not always, consist of regular arrays of plies of the same material and of the same thickness. When a laminate contains equal numbers of plies in each orientation, it is said to be balanced. A $(0,90)_3$ laminate is thus a balanced laminate, but such a laminate would have 0° and 90° plies on opposite faces and may behave in unexpected ways if loaded in other than the 0° and 90° directions. Laminates that are arranged to have the plies on either side of a mid-plane matching in both material and orientation are described as symmetric: such laminates have the advantage that they remain flat after curing and during deformation. Symmetric laminates are therefore preferred for most purposes, but careful tailoring of a laminate lay-up can be used deliberately to produce a material that will change shape in some desired manner under stress.

A preliminary estimate of the elastic response of a general multi-ply laminate can often be obtained by a netting analysis (Cox, 1952; Krenchel, 1964) which sums the contributions from each group of fibers lying at a specific angle, θ , to the applied stress. If we assume that the fibers are continuous and that there are no elastic Poisson constraints ($\nu_f = \nu_m$), each group of fibers (a proportion α of the total fiber content) can be considered to have a reinforcing efficiency:

$$a_n \cos^4 \theta$$

and an overall composite efficiency factor, factor, η_θ , can be defined as:

$$\eta_\theta = \sum a_n \cos^4 \theta.$$

The approximate composite modulus can then be obtained from a modified rule of mixtures as:

$$E_c = \eta_\theta E_f V_f + E_m (1 - V_f)$$

Shear and transverse behaviour is ignored, however, and the limitation of the model is therefore that it allows no stiffness contribution from transverse fibers and ignores interlayer constraints. Values of the efficiency factor, η_θ for a range of fiber distributions are shown in Figure 5-19. For a 3-D random array η_θ is about 1/6.

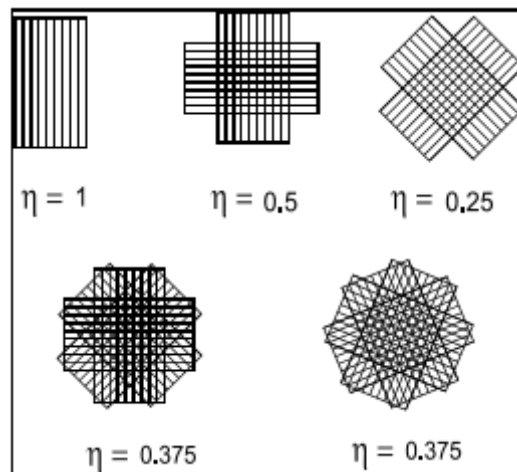


Figure 5-19 Values of the Krenchel efficiency factor for various fiber groupings [23]

5.2.2.2 The strengths of multi-ply laminates

The Krenchel model is utilized for the approximation of the strengths of multi-ply laminates. The efficiency factor, η_θ , is determined by:

$$\eta_\theta = \sum a_n \cos^4 \theta.$$

The efficiency factor is used in a mixture-rule calculation:

$$\sigma_c = \eta_\theta \sigma_{fu} V_f + \sigma_m (1 - V_f)$$

5.2.2.3 Calculation of monocoque's carbon fiber properties

The characterization of orthotropic materials is obtained, when Young's modulus E , Poisson's ratio ν and shear G have been determined, in x , y , z axis. Tensile strength in x axis, tensile strength in y axis and compressive strength in x axis are also needed. For the estimation of these constants, the above methods are used, for unidirectional fibers. To achieve good material properties, a number of tests are required to be held.

The percentage of fiber/resin can be found, by weighing the dry fiber before impregnation. After that, the ratio (fiber/resin), according to density, can be recalculated:

$$\text{Volume fraction of fiber: } V_f = (W_f / d_f) / [(W_f / d_f) + (W_m / d_m)] \quad \text{and}$$

$$\text{Volume fraction of epoxy: } V_m = 1 - V_f$$

- where d_f density of fiber and d_m density of resin, W_f weight of fiber and W_m weight of resin

If we know the volume ratio of resin and fiber, material properties can be calculated:

Table 5-2 Properties of unidirectional CFRP

PROPERTIES OF UNIDIRECTION CFRP	VALUE	UNIT
Elastic modulus E_x	380.1	Gpa
Elastic modulus E_y	28.26923077	GPa
Elastic modulus $E_z=E_y$	28.26923077	GPa
Poisson ratio ν_{xy}	0.336	
Poisson ratio ν_{yz}	0.024989375	
Poisson ratio $\nu_{xz}=\nu_{xy}$	0.336	
Shear modulus G_{xy}	4.212926249	Gpa
Shear modulus G_{yz}	13.79001161	GPa
Shear modulus $G_{xz}=G_{xy}$	4.212926249	GPa
Tensile strength σ_x	2539.4	Mpa
Tensile strength σ_y	8.250759874	Mpa
Compressive strength σ_{comp_x}	4.722222222	Gpa

In our case, we will use multi-ply laminates. Therefore, we will calculate the properties of our CFRP with the equations of multi-ply laminates, that were referred to above and CFRP can be considered as an isotropic material. For the characterization of isotropic materials Young's modulus E , Poisson constant ν and shear G are needed. The tensile strength also needs to be defined.

Table 5-3 Properties of multi-ply laminates

Properties of Multi-ply laminates	VALUE	UNIT
Elastic modulus	160.2057692	Gpa
Shear modulus	54.57980769	Gpa
Tensile strength	971.4	Mpa
Poisson ratio	0.467628561	

5.2.3 Mechanical properties of the parts around the new chassis

The materials used for the parts placed on the new chassis are essentially the same with those used on the previous one.

6 MASS AND CENTER OF GRAVITY CALCULATION

In the following sections, the mass and the center of gravity of the previous and the new chassis respectively are calculated.

6.1 Previous chassis

We begin with the calculation of the mass and the center of gravity of the previous chassis.

6.1.1 Mass definition

Given the density 0.27kg/mm^3 the program directly gives us the chassis mass with an accuracy of 0.00001. Therefore, the mass value is 10.849641kg. Furthermore, the program gives us its volume and its surface area.

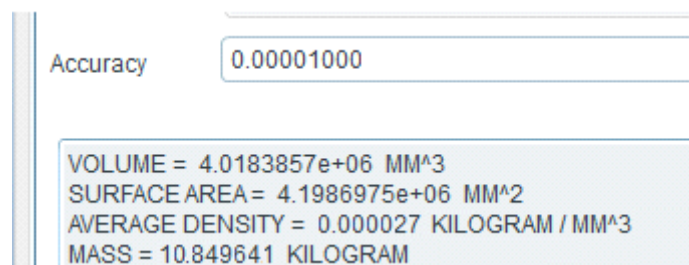


Figure 6-1 Previous chassis's mass

6.1.2 Center of gravity determination

Pro engineer can also provide the center of gravity of the chassis, in relation with the point defined by us. This point is positioned in the center of the axis (0, 0, 0) assuming that the distance on the x axis is measured from the imaginary line that crosses the front of the chassis. We also assume that the distance of the y axis is measured by the line on the left of the chassis, and on the z axis by the line that crosses the bottom of the chassis.

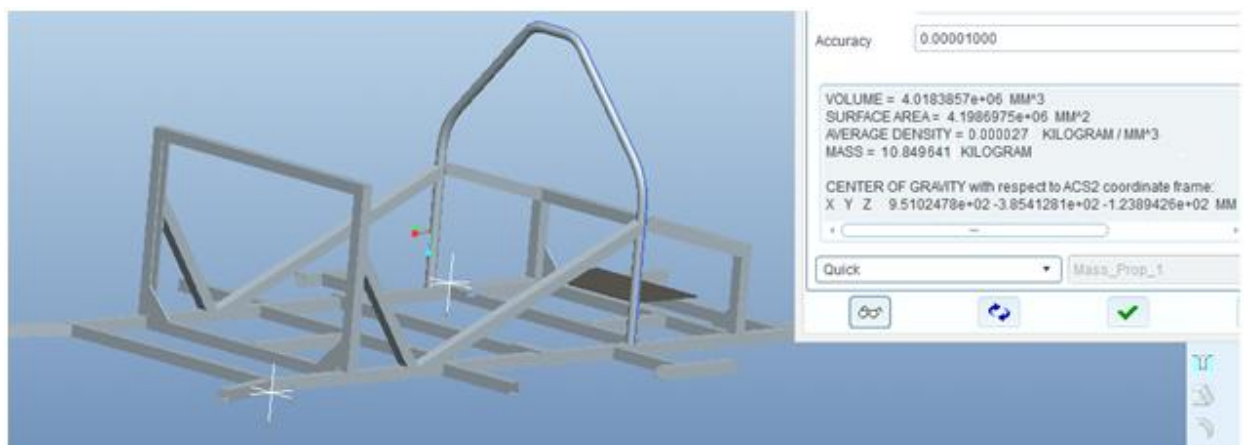


Figure 6-2 Center of gravity determination of ER14

In order to calculate the gravity center of the vehicle, a certain methodology described in the bibliography is followed [27] [28] [29] [30] [31] [32] [33] [34]. The Microsoft Excel program is also used.

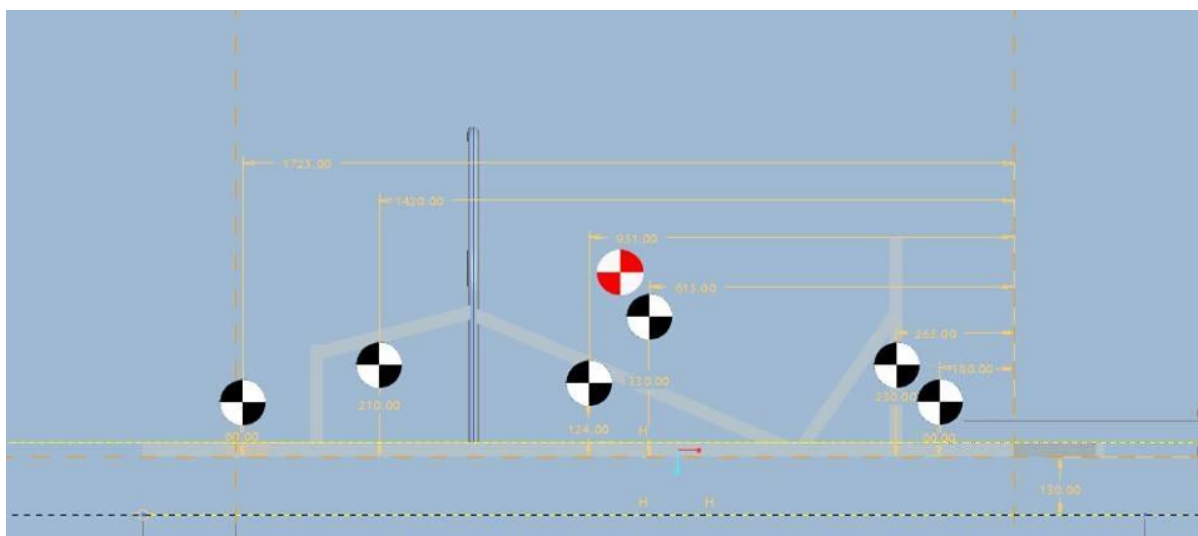


Figure 6-3 Center of Gravity of ER14

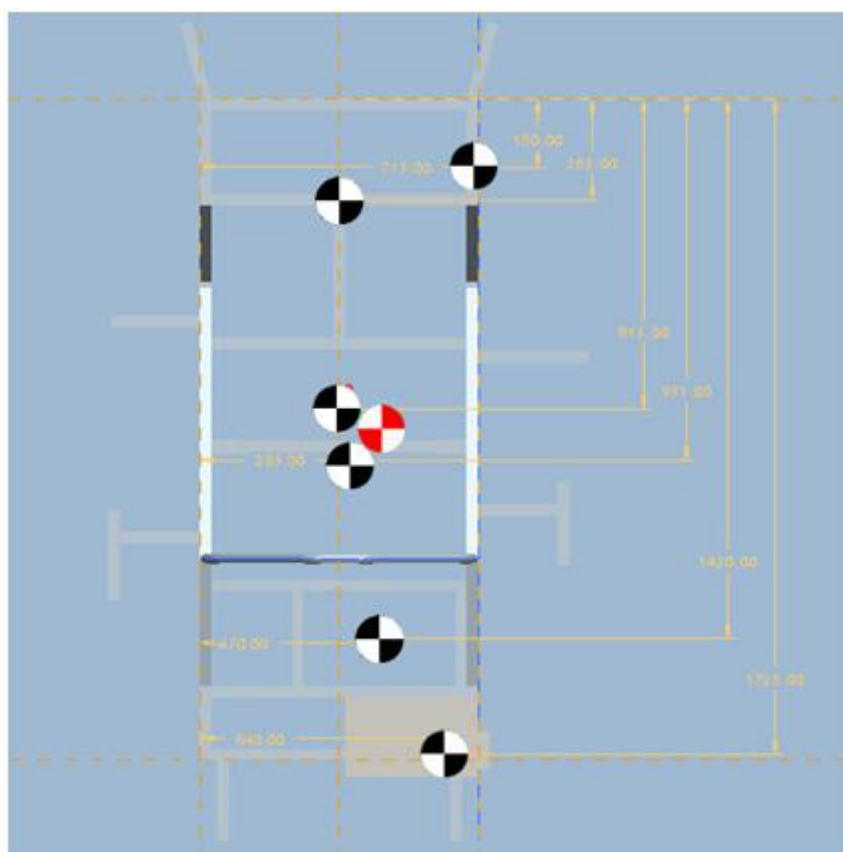


Figure 6-4 Center of Gravity of ER14

The different centers of gravity of the vehicle's parts are added up, and form the main center of gravity. These centers are described in the Table 6-1. The wheels' mass is omitted because it has no effect on finding the gravity center.

Table 6-1 The different centers of gravity of the vehicle's parts are added up and form the main center of gravity

PART	m(kg)	FROM FRONT		FROM LEFT		FROM THE GROUND	
		Lxi(mm)	m*Lxi	Lyj(mm)	m*Lyj	Lzi(mm)	m*Lzi
BATTERY LIGHT	2	180	360	715	1430	210	420
STEERING SYSTEM	7	265	1855	365	2555	360	2520
DRIVER + SEAT	75	815	61125	365	27375	460	34500
CHASSIS	10.85	951	10318.35	385	4177.25	254	2755.9
FUEL CELL	12	1420	17040	470	5640	340	4080
ELECTRIC MOTOR	3	1725	5175	640	1920	210	630
MASS WITHOUT WHEELS	109.85		95873.35		43097.25		44905.9

Center of mass $x = 95873.35 / 109.85 = 872.766$
 Center of mass $y = 43097.25 / 109.85 = 392.3281748$
 Center of mass $z = 44905.9 / 109.85 = 408.7929$

Table 6-2 Previous vehicle's center of gravity

CENTER OF MASS x	CENTER OF MASS y	CENTER OF MASS z	
(mm)	872.766	392.3281748	408.7929
(m)	0.87277	0.392328175	0.408793

As stated earlier, the distances on the x axis are measured with the imaginary line that crosses the front of the chassis. Also, the distances of the y axis are measured by the line on the left of the chassis, and on the z axis by the line that crosses the bottom of the chassis.

Extensive calculation of center of gravity

$$L_{KB}W_{total} = Lx_1W_1 + Lx_2W_2 + Lx_3W_3 + Lx_4W_4 + Lx_5W_5 + Lx_6W_6$$

$$L_{KB}W_{total} = Ly_1W_1 + Ly_2W_2 + Ly_3W_3 + Ly_4W_4 + Ly_5W_5 + Ly_6W_6$$

$$L_{KB}W_{total} = Lz_1W_1 + Lz_2W_2 + Lz_3W_3 + Lz_4W_4 + Lz_5W_5 + Lz_6W_6$$

Therefore, the results are: $L_{KBx} = 872.766$, $L_{KBy} = 392.328$ and $L_{KBz} = 408.7929$.

6.2 New chassis

We begin with the calculation of the mass and the center of gravity of the new chassis.

6.2.1 Mass definition

Therefore, the new chassis mass value is 5.38 kg. Furthermore, the program gives us its volume and its surface area.

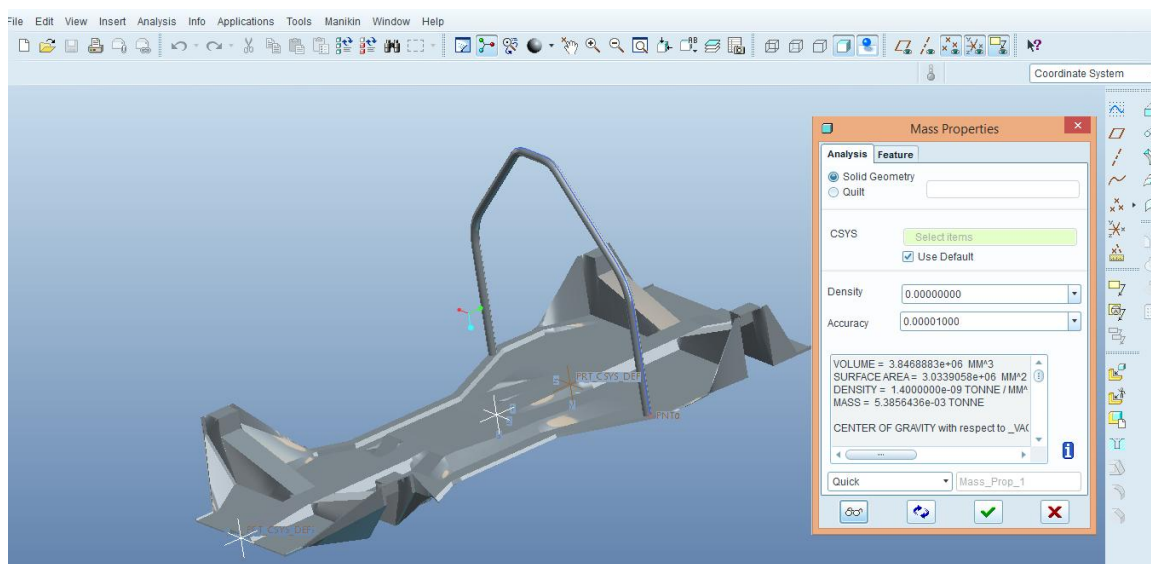


Figure 6-5 Mass definition of the new chassis

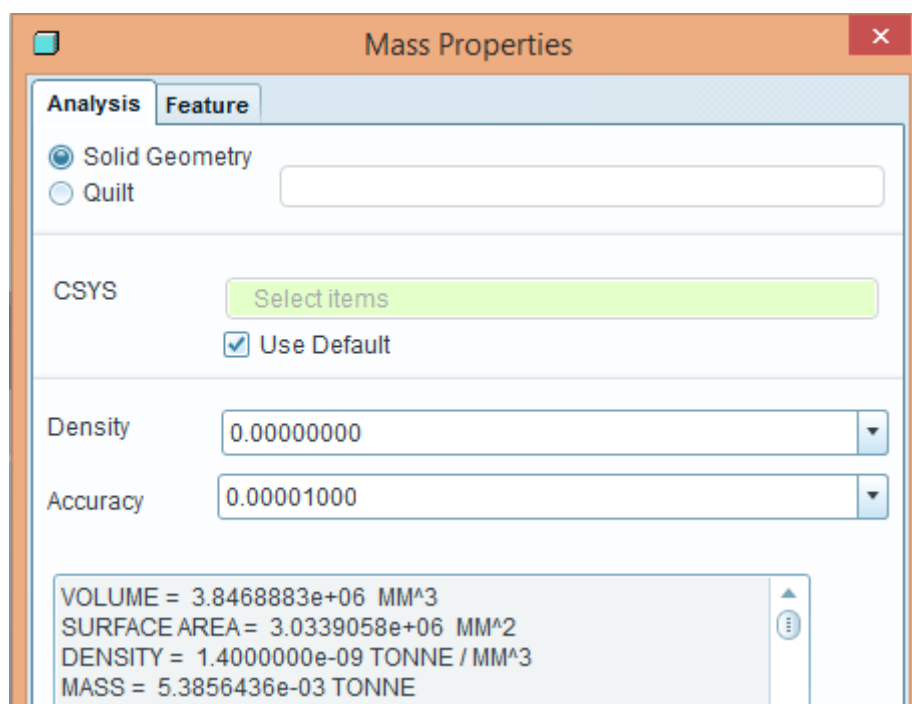


Figure 6-6 New chassis' mass

6.2.2 Center of gravity determination

Using the same procedure, we calculated the center of gravity of the new vehicle. The results are shown in the Table 6-3 below.

Table 6-3 New vehicle's center of gravity

<u>CENTER OF MASS x</u>	<u>CENTER OF MASS y</u>	<u>CENTER OF MASS z</u>	
(mm)	867.9001114	391.177869	419.624954
(m)	0.867900111	0.39117787	0.41962495

7 CHASSIS CHARACTERISTICS

Further below, we can see the collective tables of the basic characteristics of the previous and the suggested chassis, as well as their designs that will be modeled.

7.1 Previous chassis

The collective Table 7-1 depicts the basic characteristics of the previous chassis:

Table 7-1 Previous chassis characteristics

CHASSIS TYPE	SPACE FRAME	DIMENSIONS
CHASSIS MATERIAL	Aloy 6082-T6	x= 1740mm
CHASSIS WEIGHT	10.85 kg	y= 730mm
TOTAL VEHICLE WEIGHT	155.1 kg	z= 740mm

In the next image, we can see the previous chassis design with the βάσεις ψαλιδιων και τα ψαλιδια, without the unnecessary parts that don't concern our analysis. We will use this design later, in order to test its strength.

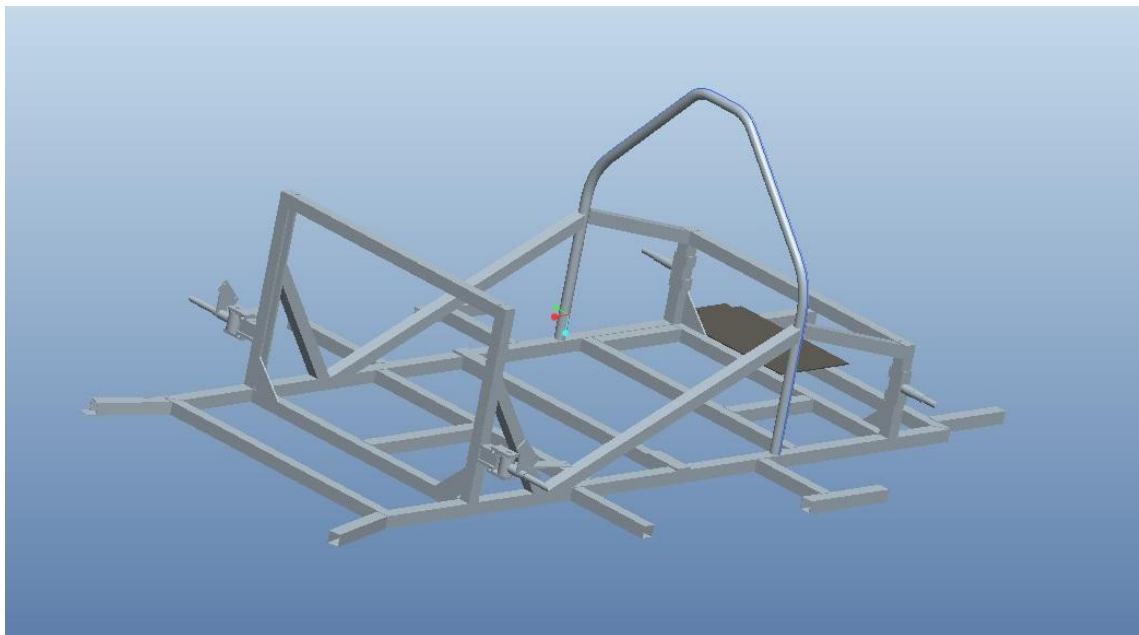


Figure 7-1 The previous chassis design to be tested

7.2 New chassis

The collective Table 7-2 illustrates the basic characteristics of the proposed chassis:

Table 7-2 New chassis characteristics

CHASSIS TYPE	MONOCOQUE	DIMENSIONS
CHASSIS MATERIAL	CARBON FIBER	x= 1740mm
CHASSIS WEIGHT	5.38 kg	y= 730mm
TOTAL VEHICLE WEIGHT	149.64 kg	z= 740mm

In the next image, we can see the new chassis design with the βασεις ψαλιδων και τα ψαλιδια, without the unnecessary parts that don't concern our analysis. We will use this design later, in order to test its strength.

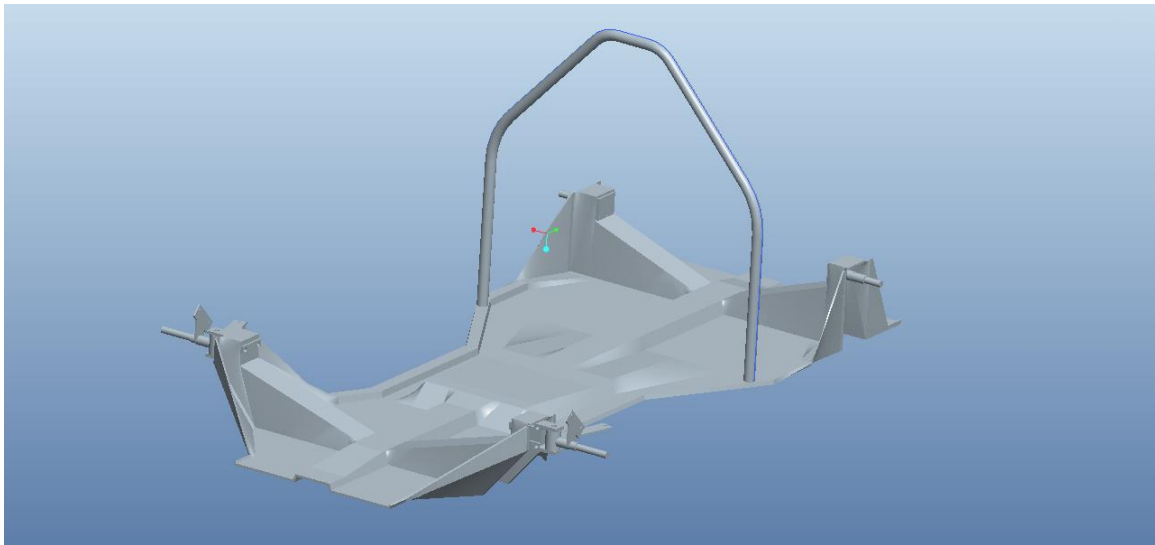


Figure 7-2 The suggested chassis design to be tested

8 VEHICLE DYNAMICS

Vehicle dynamics is concerned with the movements (acceleration, braking, ride, and turning) of vehicles-automobiles, trucks, buses, etc. on a road surface. Dynamic behaviour is determined by the forces imposed on the vehicle from the tires, gravity, and aerodynamics. However, the forces that stress the vehicle structure will only be dealt with in this research. The chassis is studied to determine what forces will be produced by each of these sources at a particular manoeuvre and trim condition. For that purpose it is essential to establish a rigorous approach to modelling the systems and the conventions that will be used to describe motions [35] [27] [36] [37] [38] [39] [40] [41] [42].

8.1 Introduction to vehicle dynamics

A motor vehicle is made up of many components distributed within its exterior envelope. Yet, for many of the more elementary analyses applied to it, all components move together. For example, under braking, the entire vehicle slows down as a unit; thus it can be represented as one lumped mass located at its center of gravity (CG) with appropriate mass and inertia properties. For acceleration, braking, and most turning analyses, one mass is sufficient. For ride analysis, it is often necessary to treat the wheels as separate lumped masses. In that case the lumped mass representing the body is the "sprung mass," and the wheels are denoted as "unsprung masses". For single mass representation, the vehicle is treated as a mass concentrated at its center of gravity (CG). The point mass at the CG, with appropriate rotational moments of inertia, is dynamically equivalent to the vehicle itself for all motions in which it is reasonable to assume the vehicle to be rigid [35].

8.1.1 Vehicle fixed coordinate system

On-board, the vehicle motions are defined with reference to a right-hand orthogonal coordinate system (the vehicle fixed coordinate system) which originates at the CG and travels with the vehicle [43] [44]. By SAE convention [45] [35] the coordinates are:

- x - Forward and on the longitudinal plane of symmetry
- y - Lateral out the right side of the vehicle
- z - Downward with respect to the vehicle
- p - Roll velocity about the x axis
- q - Pitch velocity about the y axis
- r - Yaw velocity about the z axis

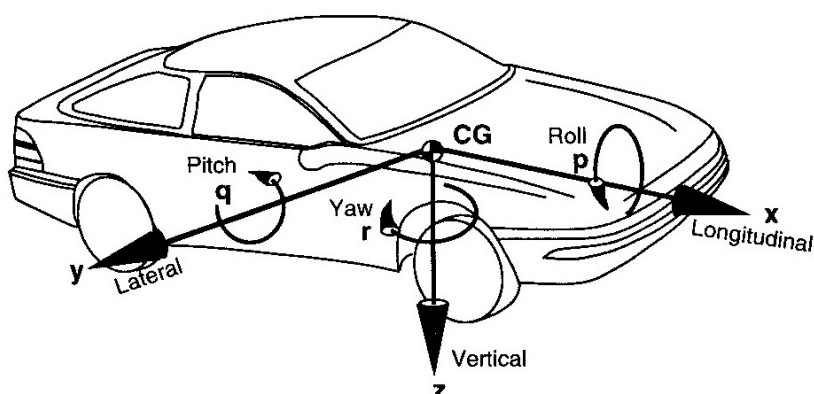


Figure 8-1 SAE Vehicle Axis System [2]

Vehicle motion is usually described by the velocities (forward, lateral, vertical, roll, pitch and yaw) with respect to the vehicle fixed coordinate system, where the velocities are referenced to the earth fixed coordinate system.

8.1.2 Earth fixed coordinate system

Vehicle attitude and trajectory through the course of a manoeuvre are defined with respect to a right-hand orthogonal axis system fixed on the earth. It is normally selected to coincide with the vehicle fixed coordinate system at the point where the manoeuvre is started. The coordinates [35] are:

X - Forward travel

Y - Travel to the right

Z - Vertical travel (positive downward)

ψ - Heading angle (angle between x and X in the ground plane)

ν - Course angle (angle between the vehicle's velocity vector and X axis)

β - Sideslip angle (angle between x axis and the vehicle velocity vector)

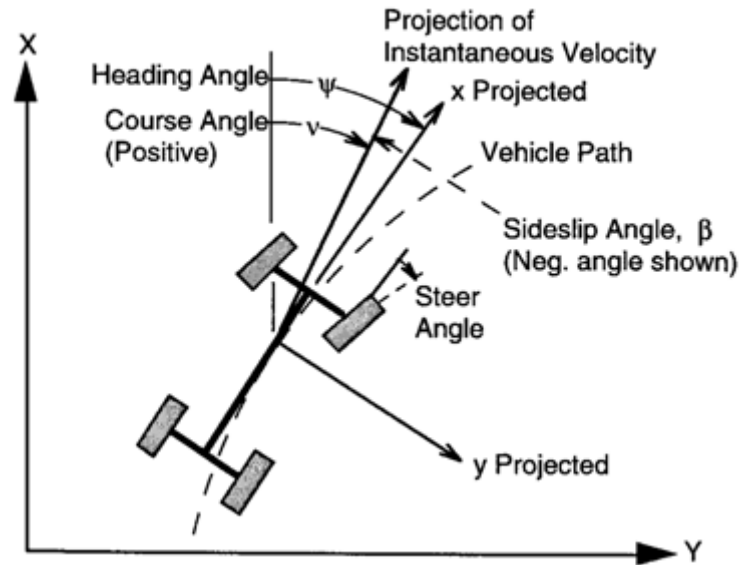


Figure 8-2 Vehicle in an Earth Fixed Coordinate System [2]

8.1.3 Euler angles

The relationship of the vehicle fixed coordinate system to the earth fixed coordinate system is defined by Euler angles. Euler angles are determined by a sequence of three angular rotations. Beginning at the earth fixed system, the axis system is first rotated in yaw (around the z axis), then in pitch (around the y axis), and then in roll (around the x axis) to line up with the vehicle fixed coordinate system. The three angles obtained are the Euler angles. It is necessary to adhere strictly to the defined sequence of rotations, because the resultant attitude will vary with the order of rotations [35] [44].

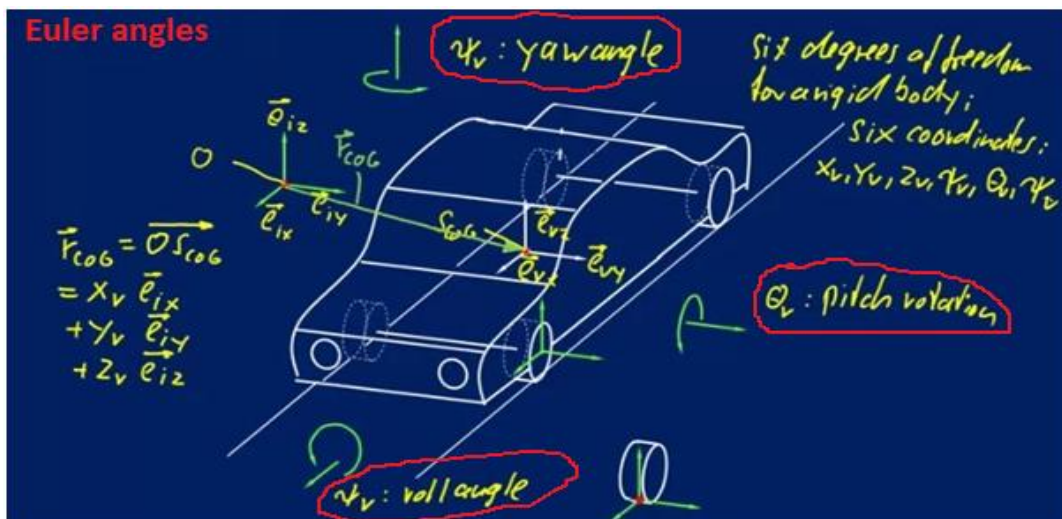


Figure 8-3 Euler angles [44]

Forces and moments are normally defined as they act on the vehicle. Thus a positive force in the longitudinal (x-axis) direction on the vehicle is forward. The force corresponding to the load on a tire acts in the upward direction and is therefore negative in magnitude (in the negative z-direction). Given these definitions of coordinate systems

and forces, it is now possible to begin formulating equations by which to analyze and describe the behaviour of a vehicle [35].

8.2 Deformation modes

As already mentioned in the 2nd and 3rd chapter, the first step to designing a vehicle frame, or any structure, is to understand the different loads acting on the structure as well as the deformation modes that these loads cause. The main deformation modes for an automotive chassis are given in as [5] [7]:

- 1) Longitudinal torsion
- 2) Vertical bending
- 3) Lateral bending
- 4) Horizontal lozenging

8.2.1 Longitudinal torsion

Torsion loads result from applied loads acting on one or two oppositely opposed corners of the car. The frame can be thought of as a torsion spring connecting the two ends where the suspension loads act. Torsional loading and the accompanying deformation of the frame and suspension parts can affect the handling and performance of the car. The resistance to torsional deformation is often quoted as stiffness in foot-pounds per degree.

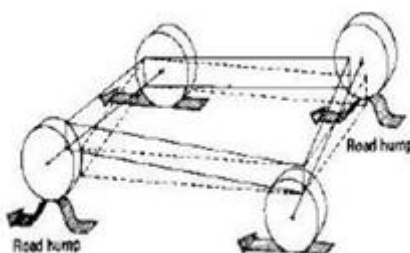


Figure 8-4 Longitudinal Torsion [7]

8.2.2 Vertical bending

The weight of the driver and components mounted to the frame, such as the engine and other parts, are carried in bending through the car frame. The reactions are taken up at the axles. Vertical accelerations can raise or lower the magnitude of these forces.

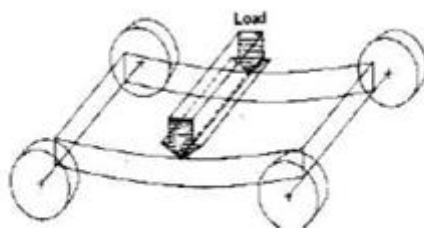


Figure 8-5 Vertical Bending [7]

8.2.3 Lateral bending

The weight of the driver and components mounted to the frame, such as the engine and other parts, are carried in bending through the car frame. The reactions are taken up at the axles. Vertical accelerations can raise or lower the magnitude of these forces.

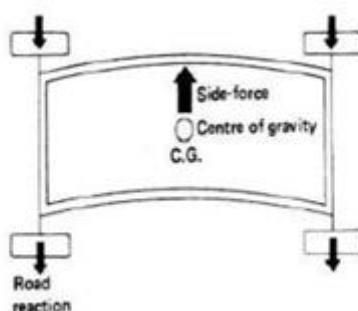


Figure 8-6 Lateral Bending [7]

8.2.4 Horizontal lozengeing

Forward and backward forces applied at opposite wheels cause this deformation. These forces may be caused by vertical variations in the pavement or the reaction from the road driving the car forward. These forces tend to distort the frame into a parallelogram shape as shown in the Figure 8-7.



Figure 8-7 Horizontal Lozengeing [7]

Below, the loads which cause these deformation modes will be shown. Some of them are static, towing, tractive, braking, cornering, aerodynamic and ride loads, as well as load transfer from cornering, from braking, and from accelerating.

8.3 Dynamic axle loads

Determining the axle loadings on a vehicle under arbitrary conditions is a first simple application of Newton's Second Law. It is an important first step in analysis of acceleration and braking performance because the axle loads determine the tractive effort obtainable at each axle, affecting the acceleration, gradeability, maximum speed, and drawbar effort. Consider the vehicle shown, in which most of the significant forces on the vehicle are shown [35].

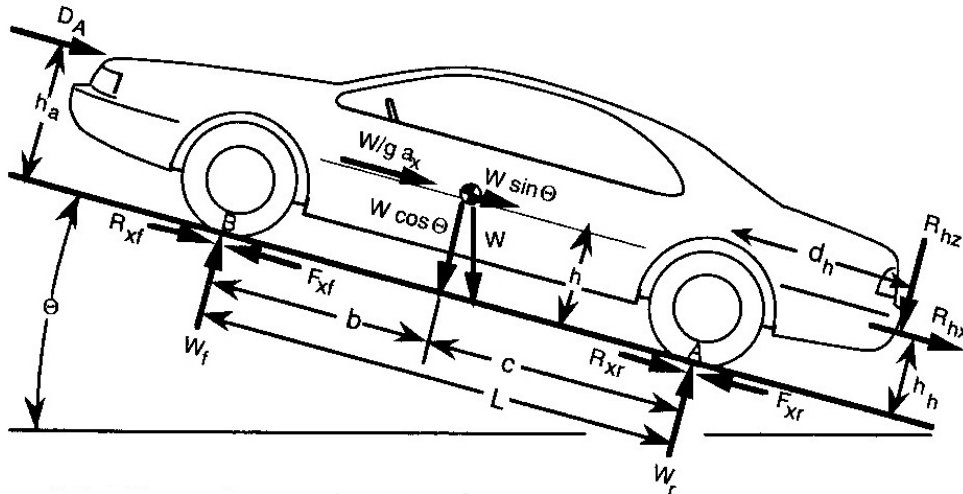


Figure 8-8 Arbitrary forces acting on a vehicle [35]

- W is the weight of the vehicle acting at its CG with a magnitude equal to its mass times the acceleration of gravity. On a grade it may have two components, a cosine component which is perpendicular to the road surface and a sine component parallel to the road.
- If the vehicle is accelerating along the road, it is convenient to represent the effect by an equivalent inertial force known as a "d' Alembert force" (Jean le Rond d' Alembert, 1717-1783) denoted by $W/g \cdot a_x$ acting at the center of gravity opposite to the direction of the acceleration [46].
- The tires will experience a force normal to the road, denoted by W_f and W_r representing the dynamic weights carried on the front and rear wheels.
- Tractive forces, F_{xf} and F_{xr} or rolling resistance forces, R_{xf} and R_{xr} may act in the ground plane in the tire contact patch.
- D_A is the aerodynamic force acting on the body of the vehicle. It may be represented as acting at a point above the ground indicated by the height, h_a , or by a longitudinal force of the same magnitude in the ground plane with an associated moment (the aerodynamic pitching moment) equivalent to D_A times h_a .
- R_{hz} and R_{hx} are vertical and longitudinal forces acting at the hitch point when the vehicle is towing a trailer.

The loads carried on each axle will consist of a static component, plus load transferred from front to rear (or vice versa) due to the other forces acting on the vehicle. The load on the front axle can be found by summing torques about the point "A" under the rear tires. Presuming that the vehicle is not accelerating in pitch, the sum of the torques at point A must be zero. By the SAE convention, a clockwise torque about A is positive. Then:

$$W_f L + D_A h_a + \frac{W}{g} a_x h + R_{hx} h_h + R_{hz} d_h + W h \sin \Theta - W c \cos \Theta = 0$$

Note that an uphill attitude corresponds to a positive angle Θ , such that the sine term is positive. A downhill attitude produces a negative value for this term.

We can solve the W_f equation about point A and the W_r equation about point B. The axle load expressions then become:

$$W_f = (W c \cos \Theta - R_{hx} h_h - R_{hz} d_h - \frac{W}{g} a_x h - D_A h_a - W h \sin \Theta) / L$$

$$W_r = (W b \cos \Theta + R_{hx} h_h + R_{hz} (d_h + L) + \frac{W}{g} a_x h + D_a h_a + W h \sin \Theta) / L$$

8.3.1 Static loads

When the vehicle sits statically on level ground, the load equations simplify considerably [35]. The sine is zero and the cosine is one, and the variables R_{hx} , R_{hz} , a_x and D_A are zero. Thus:

$$W_{fs} = W \frac{c}{L}$$

$$W_{rs} = W \frac{b}{L}$$

8.3.2 Weight transfer from acceleration

When the vehicle is accelerating on level ground at a low speed, such that D_A is zero (and presuming no trailer hitch forces), the loads on the axles [35] are:

$$W_f = W \left(\frac{c}{L} - \frac{a_x h}{g L} \right) = W_{fs} - W \frac{a_x h}{g L}$$

$$W_r = W \left(\frac{b}{L} + \frac{a_x h}{g L} \right) = W_{rs} + W \frac{a_x h}{g L}$$

Thus, when the vehicle accelerates, load is transferred from the front axle to the rear axle in proportion to the acceleration (normalized by the gravitational acceleration) and the ratio of the CG height to the wheelbase.

8.4 Braking performance



Figure 8-9 Braking Performance [44]

The Conservation of Energy

The braking system exists to convert the energy of a vehicle in motion into thermal energy, more commonly referred to as heat. From basic physics, the kinetic energy of a body in motion is defined as [47]:

$$\text{Kinetic Energy} = \frac{1}{2} \times m_v \times v_v^2$$

- where m_v = the mass (commonly thought of as weight) of the vehicle in motion.
- where v_v = the velocity (commonly known as speed) of the vehicle in motion.

Typical Modern Automotive Brake System

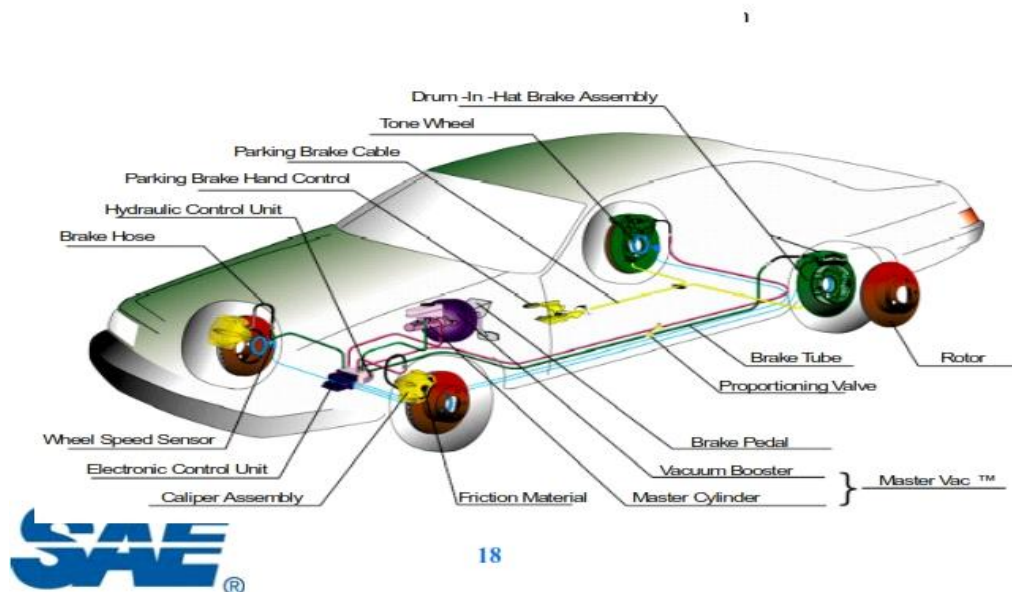


Figure 8-10 Typical Modern Automotive Brake System [47]

Ideally, this energy is completely absorbed by the braking system. While this is not entirely the case, for a stopping event at maximum deceleration most of the vehicle's kinetic energy is converted into thermal energy as defined by [48]:

$$\frac{1}{2} \times m_v \times v_v^2 \Rightarrow m_b \times C_p \times \Delta T_b$$

- where m_b = the mass of the braking system components which absorb energy
- where C_p = the specific heat of the braking system components which absorb energy (a constant based on material properties).
- where ΔT_b = the temperature rise experienced by the braking system components which absorb energy.

Note that for most single-stop events, the rotors serve as the primary energy absorbing components.

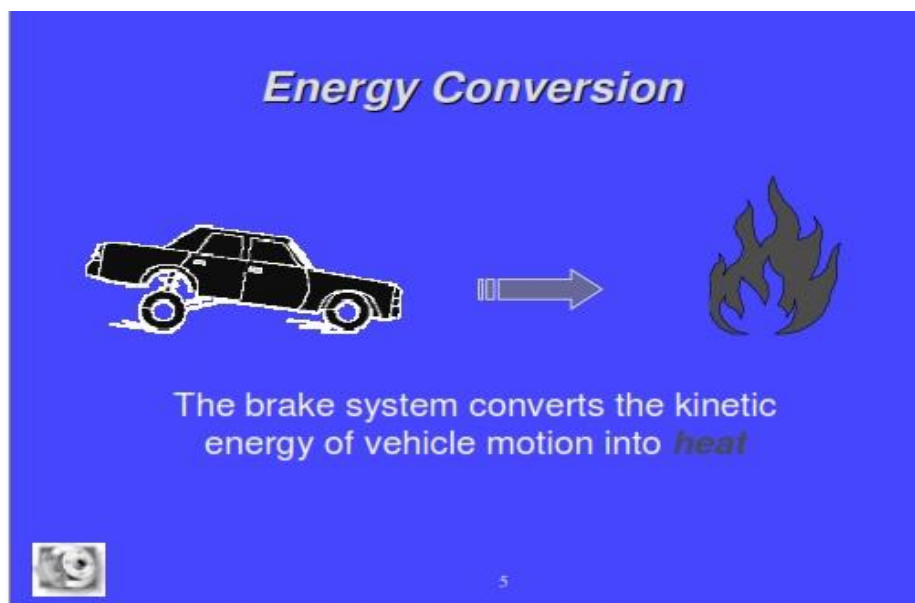


Figure 8-11 Energy Conversion [49]

It follows then that the temperature rise of the braking system is directly proportional to the mass of the vehicle in motion. More importantly perhaps, the temperature rise of the braking system is directly proportional to the square of the velocity of the vehicle in motion. In other words, doubling speed will theoretically quadruple brake temperatures:

In practical application, tire rolling resistance, aerodynamic drag, grade resistance, and other mechanical losses will also play an energy-absorbing role, but value is still placed in establishing this fundamental relationship as a limiting condition.

8.4.1 Calculation of the torque generated by the rotor

Now, the torque generated by the rotor, beginning by the brake pedal will be calculated. The images below help one to understand the system [48]:

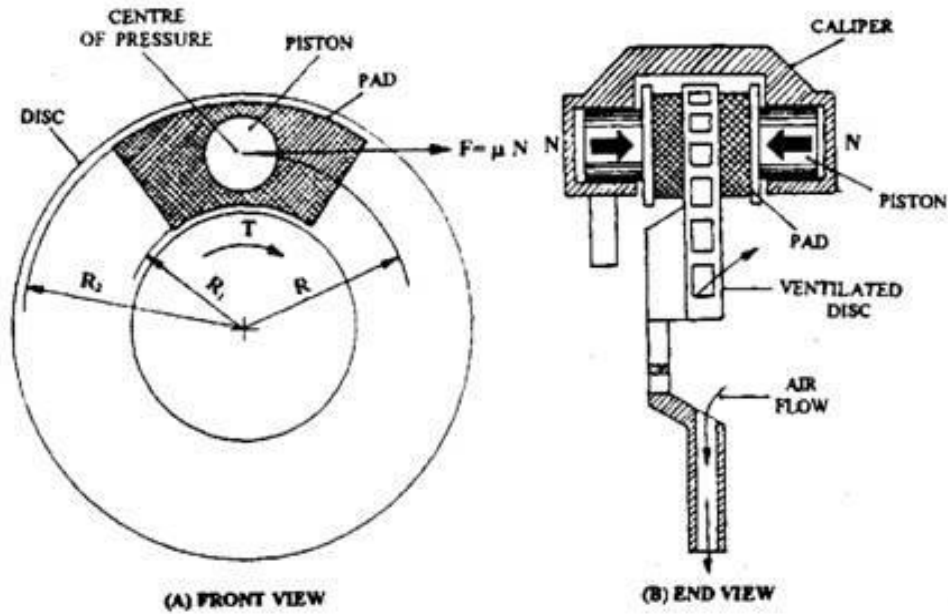


Figure 8-12 Front and end view of the rotor [47]

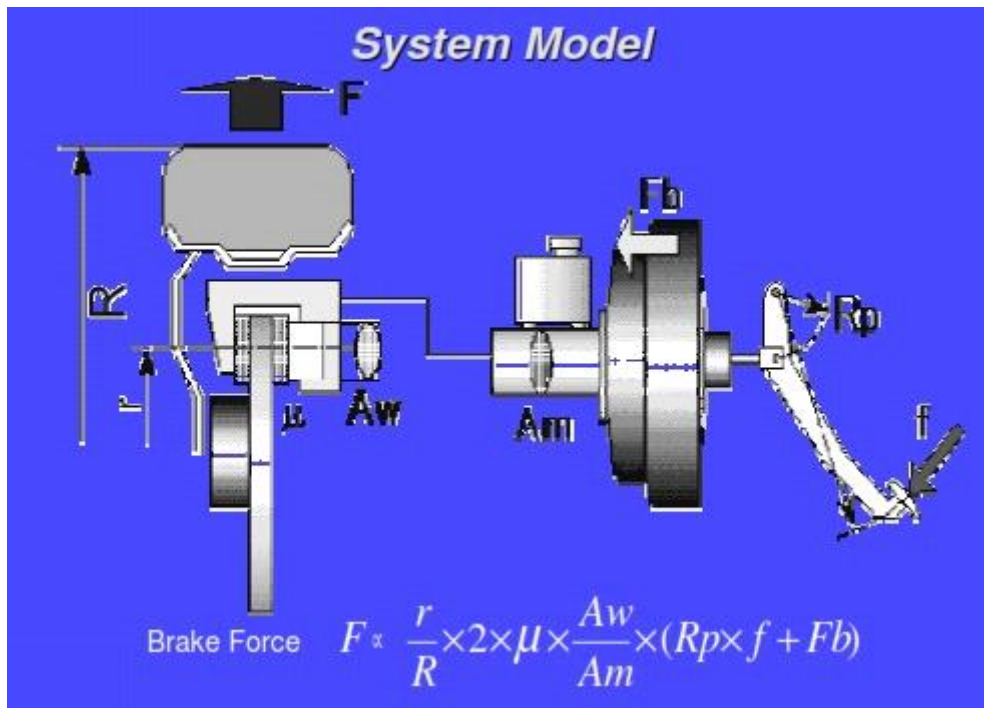


Figure 8-13 Brake force generated by the rotor [49]

The Brake pedal

The brake pedal exists to multiply the force exerted by the driver’s foot. From elementary statics, the force increase will be equal to the driver’s applied force multiplied by the lever ratio of the brake pedal assembly [47]:

$$F_{bp} = F_d \times \{L_2 \div L_1\}$$

- where F_{bp} = the force output of the brake pedal assembly.
- where F_d = the force applied to the pedal pad by the driver.
- where L_1 = the distance from the brake pedal arm pivot to the output rod clevis attachment.
- where L_2 = the distance from the brake pedal arm pivot to the brake pedal pad.

Note that this relationship assumes 100% mechanical efficiency of all components in the brake pedal assembly. In practical application, the mechanical deflection of components and friction present in physical interfaces prevents this condition.

For example, as we can see on the photo [48], a driver input force of 100 N is multiplied by a 4:1 ratio into 400 N of output force. This output force becomes the input force for the power brake unit or booster. The travel of the drivers foot will of course be 4 times the travel of the booster input pushrod. Pedal ratios on most vehicles today vary between 3:1 and 5:1.

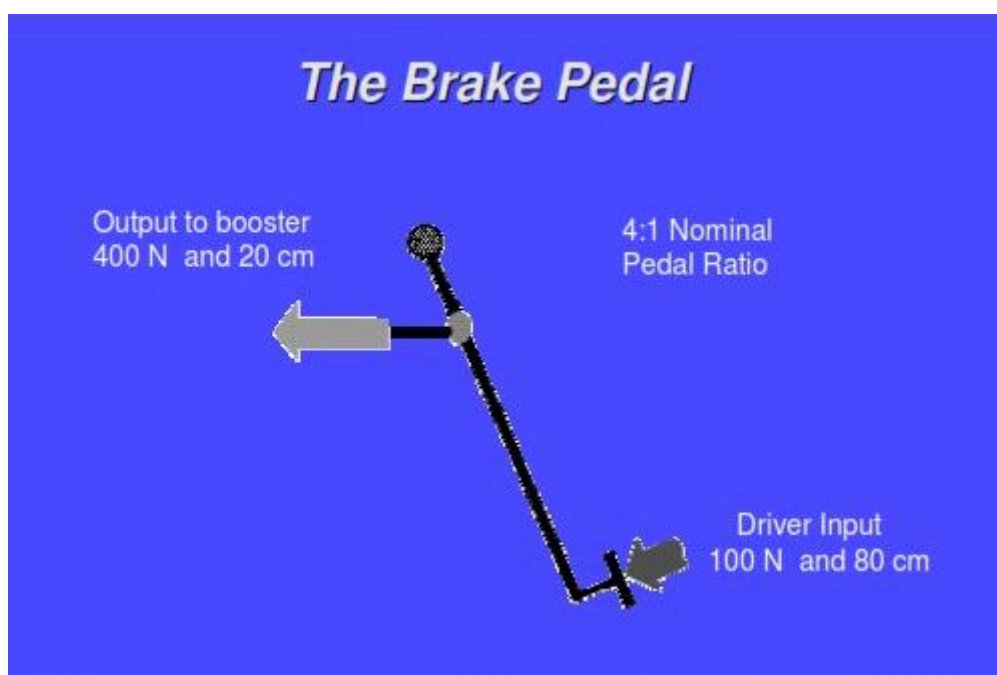


Figure 8-14 The Brake Pedal [49]

Ergonomics in the design of a brake system can play an important role in the ease with which the driving public can optimally use the braking capabilities built into a vehicle. Aside from positioning of the brake pedal, the effort and displacement properties of the pedal during braking are recognized as influential design variables. In the 1950s when power brake systems first came into general use, there was little uniformity among manufacturers in the level of effort and pedal displacement properties of the systems. In 1970 the National Highway Traffic Safety Administration sponsored research to determine ergonomic properties for the brake pedal that would give drivers the most effective control [49]. The research identified an optimum range for pedal force gain—the rela-

tionship between pedal force and deceleration. The photo shows the results from the NHTSA study indicating the optimal gain values by the shaded area [35].

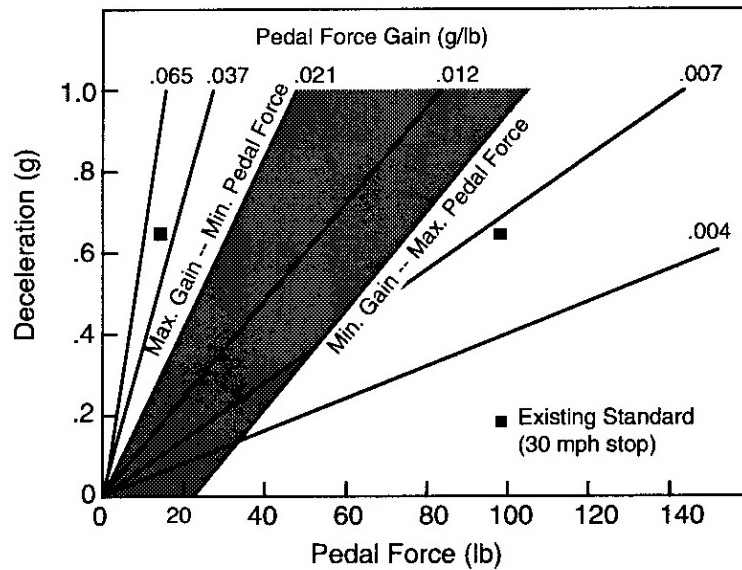


Figure 8-15 Optimal pedal force gain properties [35]

The Master Cylinder

It is the functional responsibility of the master cylinder to translate the force from the brake pedal assembly into hydraulic fluid pressure. Assuming incompressible liquids and infinitely rigid hydraulic vessels, the pressure generated by the master cylinder will be equal to [47]:

$$P_{mc} = \frac{F_{bp}}{A_{mc}}$$

- P_{mc} = the hydraulic pressure generated by the master cylinder
- A_{mc} = the effective area of the master cylinder hydraulic piston

Note that this relationship assumes 100% hydraulic efficiency of all components in the master cylinder assembly. In practical application, fluid properties, seal friction, and compliance the physical components prevents this condition.

Brake fluids, Brake Pipes, and Hoses

It is the functional responsibility of the brake fluid, brake pipes, and hoses to transmit the hydraulic fluid pressure from the master cylinder to the calipers located at the wheel ends. Out of necessity, part of this subsystem must be constructed from flexible (compliant) materials, as the wheel ends are free to articulate relative to the vehicle’s unsprung mass (most commonly known as the body structure). However, again assuming incompressible liquids and infinitely rigid hydraulic vessels, the pressure transmitted to the calipers will be equal to [47]:

$$P_{cal} = P_{mc}$$

- where P_{cal} = the hydraulic pressure transmitted to the caliper

Note that this relationship assumes 100% hydraulic efficiency of all brake fluid, brake pipes, and hoses. In practical application, fluid properties and the compliance inherent in flexible brake hoses prevent this condition.

The Caliper, Part I

It is the first functional responsibility of the caliper to translate the hydraulic fluid pressure from the pipes and hoses into a linear mechanical force. Once again assuming incompressible liquids and infinitely rigid hydraulic vessels, the one-sided linear mechanical force generated by the caliper will be equal to [47]:

$$F_{cal} = P_{cal} \times A_{cal}$$

- where F_{cal} = the one-sided linear mechanical force generated by the caliper
- where A_{cal} = the effective area of the caliper hydraulic piston(s) found on one half of the caliper body

Note that this relationship assumes 100% hydraulic efficiency of all components in the caliper assembly. In practical application, fluid properties, seal friction, and compliance the physical components prevents this condition.

The Caliper, Part II

It is the second functional responsibility of the caliper to react the one-sided linear mechanical force in such a way that a clamping force is generated between the two halves of the caliper body. Regardless of caliper design (fixed body or floating body), the clamping force will be equal to, in theory, twice the linear mechanical force as follows [47]:

$$F_{clamp} = F_{cal} \times 2$$

- where F_{clamp} = the clamp force generated by the caliper

Note that this relationship assumes 100% mechanical efficiency of all components in the caliper assembly. In practical application, mechanical deflection and, in the case of floating caliper bodies, the friction in the caliper slider assembly components prevents this condition.

The Brake Pads

It is the functional responsibility of the brake pads to generate a frictional force which opposes the rotation of the spinning rotor assembly. This frictional force is related to the caliper clamp force as follows:

$$F_{friction} = F_{clamp} \times \mu_{bp}$$

- where F_{clamp} = the frictional force generated by the brake pads opposing the rotation of the rotor.
- where μ_{bp} = the coefficient of friction between the brake pad and the rotor.

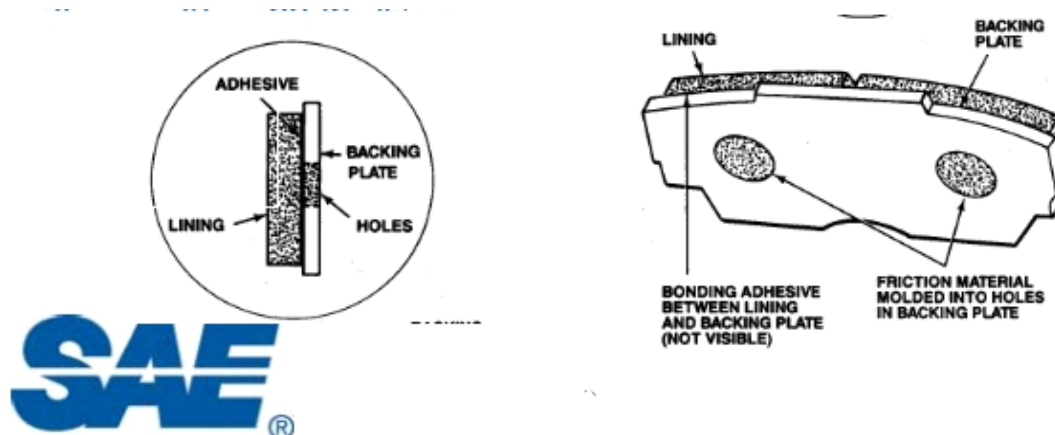


Figure 8-16 Brake pads [47]

Note that this relationship assumes 100% mechanical efficiency of all components at the brake pad interface. In practical application, mechanical deflection (compressibility) of the brake pad materials and friction found between the brake pad and the caliper body components prevents this condition. In addition, it should be noted that the coefficient of friction between the brake pad and the rotor is not a single fixed value, but rather changes dynamically with time, temperature, pressure, wear, and such.

The Rotor

While the rotor serves as the primary heat sink in the braking system, it is the functional responsibility of the rotor to generate a retarding torque as a function of the brake pad frictional force. This torque is related to the brake pad frictional force as follows [47]:

$$T_r = F_{friction} \times R_{eff}$$

- where T_r = the torque generated by the rotor.
- where R_{eff} = the effective radius (effective moment arm) of the rotor (measured from the rotor center of rotation to the center of pressure of the caliper pistons).

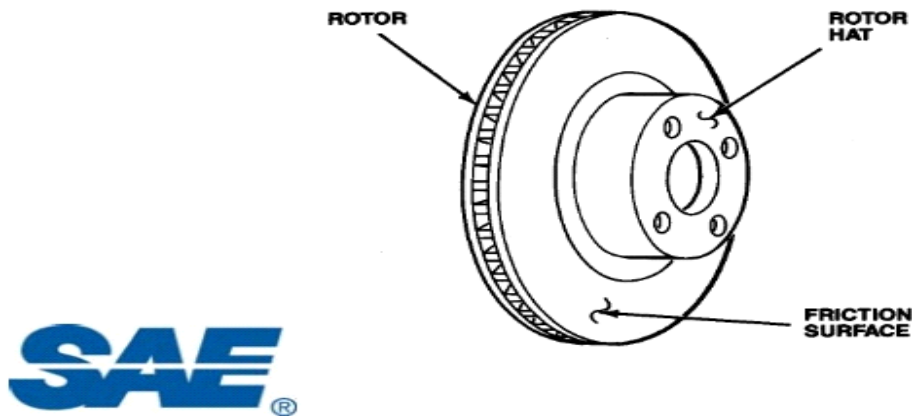


Figure 8-17 The rotor [47]

Because the rotor is mechanically coupled to the hub and wheel assembly, and because the tire is assumed to be rigidly attached to the wheel, the torque will be constant throughout the entire rotating assembly as follows [47]:

$$T_t = T_w = T_r$$

- where T_t = the torque found in the tire.
- T_w = the torque found in the wheel.

Note that this relationship assumes 100% mechanical efficiency of all components at the wheel end. In practical application, mechanical deflection and relative motion between the rotating components prevents this condition.

The Tire

Assuming that there is adequate traction (friction) between the tire and the road to accommodate the driver's braking request, the tire will develop slip in order to react the torque found in the rotating assembly. The amount of slip generated will be a function of the tire's output characteristics (the mu-slip relationship), but the force reacted at the ground will be equal to [47]:

$$F_{\text{tire}} = \frac{T_t}{R_t}$$

- where F_{tire} = the force reacted between the tire and the ground (assuming friction exists to support the force).
- where R_t = the effective rolling radius (moment arm) of the loaded tire.

Up to this point our analysis has consisted of a single wheel brake assembly; however, because modern vehicles have one wheel brake assembly at each corner of the car, there are actually four tire forces being reacted during a typical stopping event. Because of this condition, the total braking force generated is defined as the sum of the four contact patch forces as follows [47]:

$$F_{total} = \sum F_{tire\ LF, RF, LR, RR}$$

- where F_{total} = the total braking force reacted between the vehicle and the ground (assuming adequate traction exists).

8.4.2 Weight transfer from deceleration

Deceleration of a vehicle in motion

Based on the work of Sir Isaac Newton, if a force is exerted on a body it will experience a commensurate acceleration. Convention dictates that accelerations which oppose the direction of travel are called decelerations. In the case of a vehicle experiencing a braking force, the deceleration of the vehicle will be equal to [47]:

$$a_v = \frac{F_{total}}{m_v}$$

- where a_v = the deceleration of the vehicle

Kinematics Relationships of Vehicles Experiencing Deceleration

The general equation for braking performance may be obtained from Newton's Second Law written for the x-direction:

$$M a_x = - \frac{W}{g} D_x = - F_{xf} - F_{xr} - D_A - W \sin \Theta$$

- where w = Vehicle weight
- where g = Gravitational acceleration
- where $D_x = -a_x$ = Linear deceleration
- where F_{xf} = Front axle braking force
- where F_{xr} = Rear axle braking force
- where D_A = Aerodynamic drag
- where H = Uphill grad

Simple and fundamental relationships can be derived for the case where it is reasonable to assume that the forces acting on the vehicle will be constant throughout a brake application [35]. The simple equations that result provide an appreciation for the basic relationships that govern braking maneuvers. From the above equation:

$$D_x = \frac{F_{xt}}{M} = - \frac{dV}{dt}$$

- where F_{xt} = The total of all longitudinal deceleration forces on the vehicle (+)
- where V = Forward velocity.

This equation can be integrated (because F_{xt} is constant) for a deceleration (snub) from initial velocity, V_0 to final velocity, V_f :

$$\int_{V_0}^{V_f} dV = -\frac{F_{xt}}{M} \int_0^{t_s} dt$$

$$V_0 - V_f = \frac{F_{xt}}{M} t_s$$

- where t_s = Time for the velocity change

Because velocity and distance are related by $V = dx/dt$, we can substitute for "dt" in equation $Dx = -dV/dt$, integrate, and obtain the relationship between velocity and distance:

$$\frac{V_0^2 - V_f^2}{2} = \frac{F_{xt}}{M} X$$

- where x = Distance traveled during the deceleration

In the case where the deceleration is a full stop, then V_f is zero, and X is the theoretical stopping distance, SD. Then [47]:

$$SD = \frac{V_0^2}{2 \frac{F_{xt}}{M}} = \frac{V_0^2}{2 D_x}$$

- where V_0 = the velocity of the vehicle
- where D_x = the deceleration of the vehicle

Note that this equation assumes a step-input deceleration from a fixed speed followed by a linear and constant rate of deceleration until the vehicle comes to rest. In practical application, deceleration cannot be achieved instantaneously, nor can deceleration be assumed to be constant for the duration of a stopping event.

And the time to stop is:

$$t_s = \frac{V_0}{\frac{F_{xt}}{M}} = \frac{V_0}{D_x}$$

Thus, all other things being equal, the time to stop is proportional to the velocity, whereas the distance is proportional to the velocity squared (i.e., doubling the velocity doubles the time to stop, but quadruples the distance required)

Determining Parameters Related to Vehicle Static Weight Distribution

When either at rest or under conditions of zero acceleration, a vehicle will have a fixed distribution of mass (more commonly referred to as weight) which results in the four corners of the vehicle each suspending a fixed percentage of the total. In the side view, the sum of the left front and right front weights will equal the front axle weight and the sum of the left rear and right rear weights will equal the rear axle weight. If these values are known, then one can quickly calculate the static weight distribution as follows [47]:

$$\text{Percent front weight} = \frac{V_f}{V_t} \times 100$$

&

$$\text{Percent rear weight} = \frac{V_r}{V_t} \times 100$$

- where V_f = the front axle vertical force (weight)
- where V_r = the rear axle vertical force (weight)
- where V_t = the total vehicle vertical force (weight)

If the static weight distribution is known, then calculating the longitudinal position of the vehicle's center of gravity (CG) is simply a function of geometry as follows:

$$CG_{f,x} = \frac{V_r}{V_t} \times WB$$

&

$$CG_{r,x} = \frac{V_f}{V_t} \times WB$$

- where $CG_{f,x}$ = distance from the front axle to the CG
- where $CG_{r,x}$ = distance from the rear axle to the CG.
- where WB = the vehicle wheelbase (distance from the front axle to the rear axle)

From these relationships, it naturally follows that:

$$CG_{f,x} + CG_{r,x} = WB$$

Dynamic Impacts of Vehicles Experiencing Deceleration

The braking decelerations achievable on a vehicle are simply the product of application level and the brake gains (torque/pressure) up to the point where lockup will occur on

one of the axles. Lockup reduces the brake force on an axle, and results in some loss of ability to control the vehicle. It is well recognized that the preferred design is to bring both axles up to the lockup point simultaneously. Yet, this is not possible over the complete range of operating conditions to which a vehicle will be exposed. Balancing the brake outputs on both the front and rear axles is achieved by "proportioning" the pressure appropriately for the foundation brakes installed on the vehicle. Proportioning then adjusts the brake torque output at front and rear wheels in accordance with the peak traction forces possible.

The first-order determinants of peak traction force on an axle are the instantaneous load and the peak coefficient of friction. During braking, a dynamic load transfer from the rear to the front axle occurs such that the load on an axle is the static plus the dynamic load transfer contributions [35].

Whenever a vehicle experiences a deceleration, the effective normal force (again, more commonly referred to as weight) reacted at the four corners of the vehicle will change. While the total vehicle normal force remains constant, the front axle normal force during a deceleration event will increase while the rear axle normal force will decrease by the same amount. As the following equation demonstrates, the magnitude is a function of deceleration and vehicle geometry [47]:

$$WT = \left(\frac{a_v}{g} \right) \times \left(\frac{h_{cg}}{WB} \right) \times V_r$$

- where WT = the absolute weight transferred from the rear axle to the front axle
- where g = the acceleration due to gravity (effectively expressing a_v in units of g's)
- where h = the vertical distance from the CG to ground

Figure 8-18 illustrates the basic brake operation. The weight transfer increases the load on the front wheels [50].

Basic Brake Operation

Weight transfer increases the load on the front wheels while the load on the rear wheels is reduced.

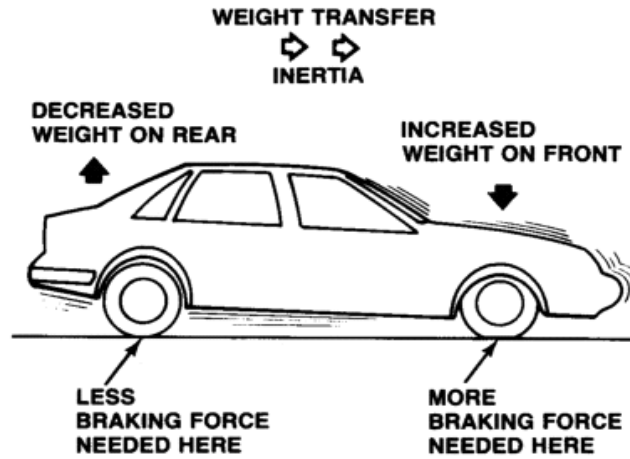


Figure 8-18 Basic Brake Operation [47]

Brake balance is the science of the relationship between the vertical forces on the front and rear tires and the torque applied by the front, and rear brakes at any given instant [48].

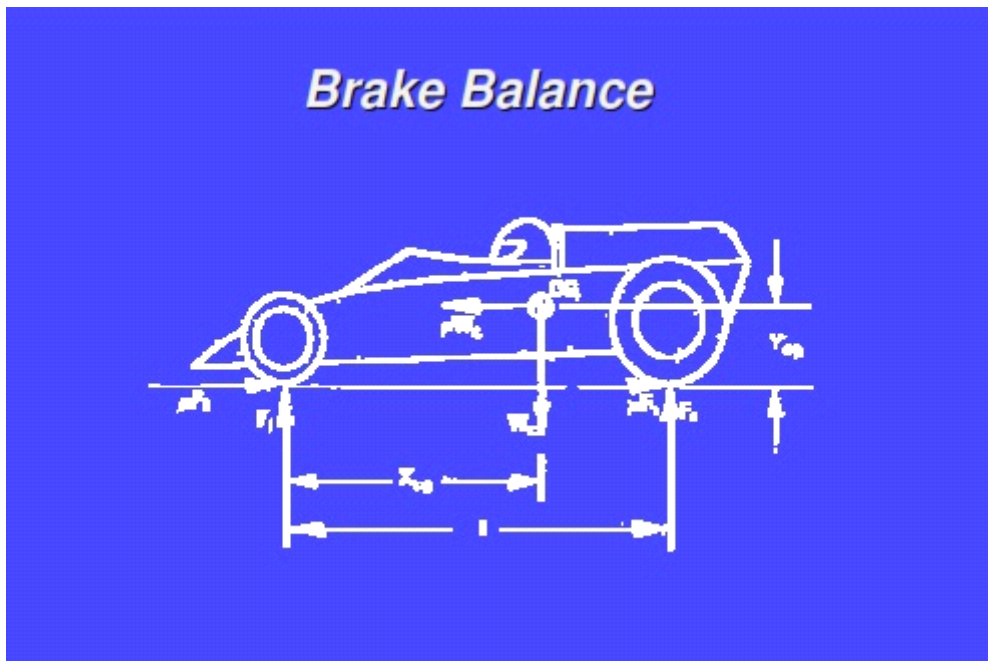


Figure 8-19 Brake Balance [49]

In order to calculate the steady-state vehicle axle vertical forces during a given stopping event, the weight transferred must be added to the front axle static weight and subtracted from the rear axle static weight as follows:

$$V_{f,d} = V_f + WT$$

&

$$V_{r,d} = V_r - WT$$

- where $V_{f,d}$ = the front axle dynamic vertical force for a given deceleration.
- where $V_{r,d}$ = the rear axle dynamic vertical force for a given deceleration.

From these relationships, it naturally follows that for any given deceleration:

$$V_{f,d} + V_{r,d} = V_t$$

Effects of Weight Transfer on Tire Output

As a vehicle experiences dynamic weight transfer, the ability of each axle to provide braking force is altered. Under static conditions, the maximum braking force that an axle is capable of producing is defined by the following relationships [47]:

$$F_{tires,f} = \mu_{peak,f} \times V_f$$

&

$$F_{tires,r} = \mu_{peak,r} \times V_r$$

- where $F_{tires,f}$ = the combined front tire braking forces.
- where $F_{tires,r}$ = the combined rear tire braking forces.
- where $\mu_{peak,f}$ = the maximum effective coefficient of friction between the front tires and the road.
- where $\mu_{peak,r}$ = the maximum effective coefficient of friction between the rear tires and the road.

However, as a result of weight transfer during a deceleration event the maximum braking force that an axle is capable of producing is modified as follows:

$$F_{tires,f} = \mu_{peak,f} \times V_{f,d} = \mu_{peak,f} \times (V_f + WT)$$

&

$$F_{tires,r} = \mu_{peak,r} \times V_{r,d} = \mu_{peak,r} \times (V_r - WT)$$

As shown by the relationships above, weight transfer increases the ability of the front axle to provide braking force while simultaneously decreasing the ability of the rear axle to provide braking force.

Note that in this analysis it is assumed that $\mu_{\text{peak},f}$ and $\mu_{\text{peak},r}$ are independent of deceleration, when in practice they are sensitive to the loading changes brought about by the weight transfer phenomenon. Consequently, as weight is transferred the total vehicle deceleration capability is diminished by a small amount.

Calculating Optimum Brake Balance

In order to achieve optimum brake balance, or to achieve 100% base brake efficiency, the ratio of the front and rear braking forces will be equal to the ratio of the front and rear vertical forces (axle weights). Under static conditions, this leads to:

$$\frac{F_{\text{tires},f}}{V_f} = \frac{F_{\text{tires},r}}{V_r}$$

However, as the brakes are applied the effects of weight transfer must be considered, as the ratio of front and rear vertical forces will change as follows:

$$\frac{F_{\text{tires},f}}{V_{f,d}} = \frac{F_{\text{tires},r}}{V_{r,d}}$$

From this relationship it becomes apparent that while the ratio of the front and rear braking forces is a fixed parameter based on the mechanical sizing of the brake system components, the ratio of the front and rear vertical forces is a variable based on deceleration and vehicle geometry. This dictates that relationship can only be optimized for only one vehicle deceleration level and loading condition (typically at maximum deceleration with the highest percentage of static front weight).

8.5 Cornering performance

The cornering behaviour of a vehicle is an important performance mode often equated with handling. "Handling" is a loosely used term meant to imply the responsiveness of a vehicle to driver input, or the ease of control. As such, handling is an overall measure of the vehicle-driver combination. The driver and vehicle is a "closed-loop" system meaning that the driver observes the vehicle direction or position, and corrects his/her input to achieve the desired motion.

8.5.1 Low-speed turning

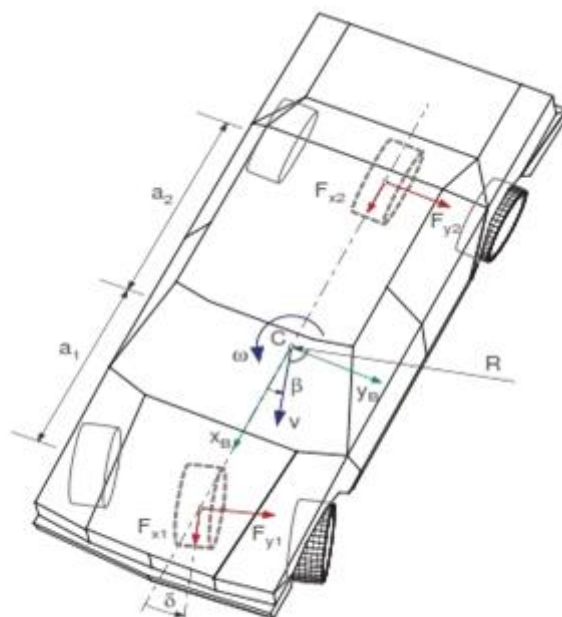


Figure 8-20 Low-speed turning vehicle [51]

The steady-state cornering equations are derived from the application of Newton's Second Law along with the equation describing the geometry in turns (modified by the slip angle conditions necessary on the tires). For purposes of analysis, it is convenient to represent the vehicle by the bicycle model shown in the following Figure 8-21. At high speeds the radius of turn is much larger than the wheelbase of the vehicle. Then small angles can be assumed, and the difference between steer angles on the outside and inside front wheels is negligible. Thus, for convenience, the two front wheels can be represented by one wheel at a steer angle δ , with a cornering force equivalent to both wheels. The same assumption is made for the rear wheels. For a vehicle travelling forward with a speed of V , the sum of the forces in the lateral direction from the tires must equal the mass times the centripetal acceleration. [35].

$$\Sigma F_y = F_{yf} + F_{yr} = M V^2/R$$

- where F_{yf} = Lateral (cornering) force at the front axle
- where F_{yr} = Lateral (cornering) force at the rear axle
- M = Mass of the vehicle
- V = Forward velocity
- R = Radius of the turn

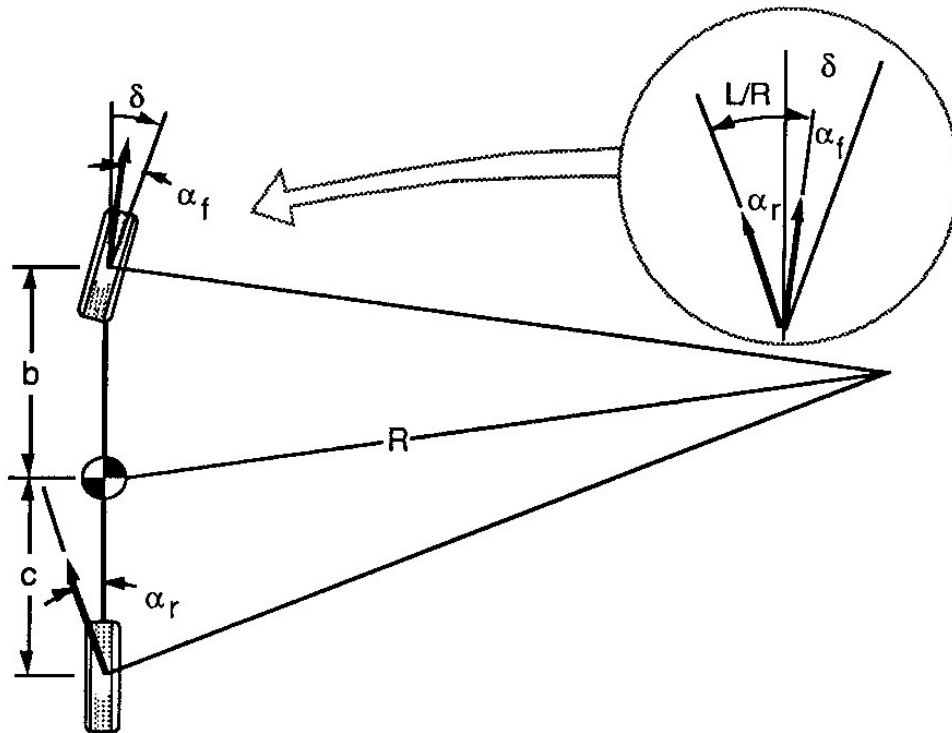


Figure 8-21 Cornering of a bicycle model [35]

8.5.2 Roll moment distribution

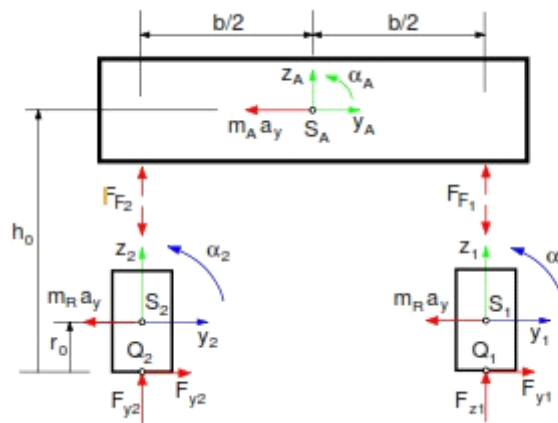


Figure 8-22 Simple vehicle roll moment [43]

Actually, this mechanism is at work on both axles of all vehicles [51] [43]. Whether it contributes to understeer or oversteer depends on the balance of roll moments distributed on the front and rear axles. More roll moment on the front axle contributes to understeer, whereas more roll moment on the rear axle contributes to oversteer. Auxiliary roll stiffeners (stabilizer bars) alter handling performance primarily through this mechanism—applied to the front axle for understeer, and to the rear for oversteer. The mechanics governing the roll moment applied to an axle are shown in the model of Figure 8-23. All suspensions are functionally equivalent to the two springs. The lateral separation of

the springs causes them to develop a roll resisting moment proportional to the difference in roll angle between the body and axle [35]. The stiffness is given by:

$$K_{\phi} = 0.5 K_s s^2$$

- where K_{ϕ} = Roll stiffness of the suspension.
- where K_s = Vertical rate of each of the left and right springs.
- where s = Lateral separation between the springs.

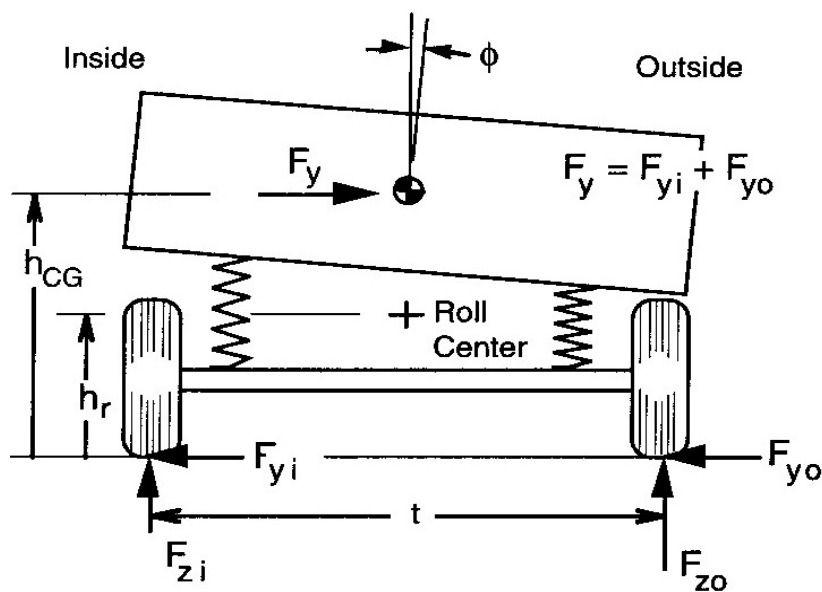


Figure 8-23 Force of a simple vehicle in cornering [35]

(In the case of an independent suspension, the above expression can be used by substituting the rate at the wheel for K_s and using the tread as the separation distance. When a stabilizer bar is present, the roll stiffness of the bar must be added to the stiffness calculated above.)

The suspension is further characterized by a "roll center," the point at which the lateral forces are transferred from the axle to the sprung mass. The roll center can also be thought of as the point on the body at which a lateral force application will produce no roll angle, and it is the point around which the axle rolls when subjected to a pure roll moment.

By writing Newton's Second Law for moments on the axle, we can determine the relationship between wheel loads and the lateral force and roll angle. In addition to the vertical forces imposed at the tires there is a net lateral force, F_y (the sum of the lateral forces on the inside and outside wheels), acting to the right on the axle at its roll center. The body roll acting through the springs imposes a torque on the axle proportional to the roll stiffness, K_{ϕ} , times the roll angle, ϕ . This results in an equation for the load difference from side to side of the form:

$$F_{zO} - F_{zi} = 2 F_y h_r/t + 2 K_\phi \phi/t = 2 \Delta F_z$$

- where F_{zO} = Load on the outside wheel in the tum
- where F_{zi} = Load on the inside wheel in the tum
- where F_y = Lateral force = $F_{yi} + F_{yo}$
- where h_r = Roll center height
- where t = Tread (track width)
- where K_ϕ = Roll stiffness of the suspension
- where ϕ = Roll angle of the body

Note that lateral load transfer arises from two mechanisms:

- 1) $2 F_y h_r/t$ - Lateral load transfer due to cornering forces. This mechanism arises from the lateral force imposed on the axle, and is thus an instantaneous effect. It is independent of roll angle of the body and the roll moment distribution.
- 2) $2 K_\phi \phi/t$ - Lateral load transfer due to vehicle roll. The effect depends on the roll dynamics, and thus may lag the changes in cornering conditions. It is directly dependent on front/rear roll moment distribution.

The second mechanism for us is zero, because we have not springs, we have an un-sprung mass. So our equation is:

$$F_{zO} - F_{zi} = 2 F_y h_r/t$$

8.6 Aerodynamic performance

The aerodynamic forces and torques are most essential for the driving performance of the automobiles at medium and high speeds. The aerodynamics are also important for energy conservation and economic efficiency of cars [52] [35].

<u>Direction</u>	<u>Force</u>	<u>Moment</u>
Longitudinal (x-axis, positive rearward)	Drag	Rolling moment
Lateral (y-axis, positive to the right)	Sideforce	Pitching moment
Vertical (z-axis, positive upward)	Lift	Yawing moment

The aerodynamic resistance is originating from three sources:

- shape resistance due to the turbulence of the air flow at the rear of the vehicle with a strong influence of the design of the vehicle (85%)
- friction resistance due to the shear flow at the car body depending on its surface (10%)
- internal resistance due to the flow through the car body(5%). The inner flow is required for the cooling of the engine and the air ventilation of the passenger compartment.

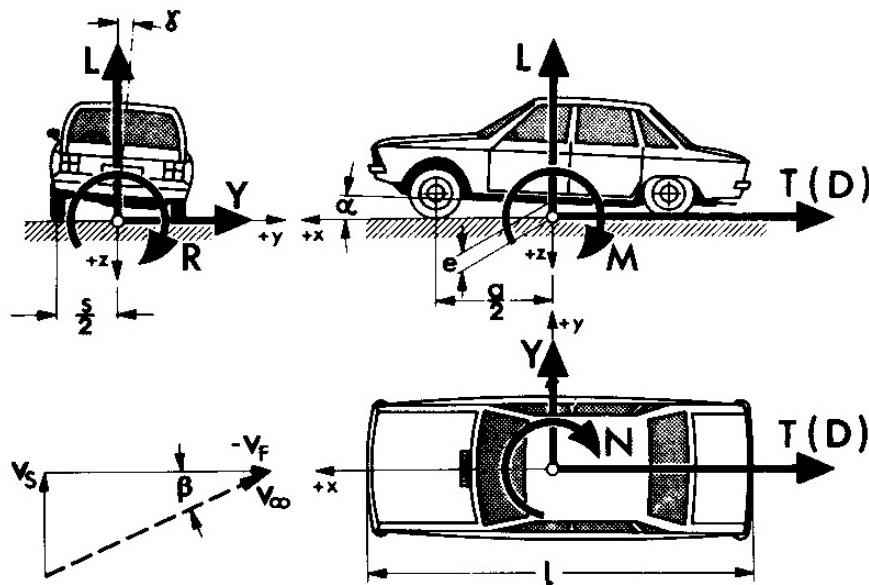


Figure 8-24 Aerodynamic forces and moments acting on a car [35]

The aerodynamic resistance and therefore the aerodynamic forces are mainly resulting from the turbulent flow and they are proportional to the dynamic pressure

$$p_L = \frac{1}{2} \rho v_L^2$$

- where ρ is the air density and v is the velocity of the air relative to the car.

The force which is being resisted on the motion of vehicle while it is travelling at a particular speed is called drag force. This is due to friction of the vehicle body moving through the air [53].

$$F_{ad} = \frac{1}{2} \rho A C_d v^2$$

- where ρ is the density of the air, A is the frontal area, v is the velocity, C_d is a constant called the drag coefficient.

The shape of the vehicle influences the value of the drag coefficient and can be reduced by proper vehicle design. Generally, for a commercial vehicle is about 0.3, but some electric vehicle designs have achieved values as low as 0.19, due to the flexibility in the location of the major components [54]. Our vehicle drag coefficient is 0.21 [53].

The aerodynamic forces and torques depend on dimensionless coefficients c , the characteristic area A of the vehicle and the wheel base l , have to be considered.

The air resistance reads as

$$W_L = c_W A p_L$$

The lifting force as

$$F_L = c_A A p_L$$

The aerodynamic torque is given by

$$M_L = c_M A l p_L$$

Furthermore, for the lateral motion, the side force

$$S_L = c_N A p_L$$

And the yaw torque

$$M_{Lz} = c_{Mz} A l p_L$$

The coefficients c depends as already mentioned strongly on the body design and the direction of the air flow relative to the vehicle. Some air resistance coefficient c for head-on flow is presented in Table 8-1. These coefficients are found experimentally in wind tunnels or evaluated by computational fluid dynamics (CFD) software. All new vehicles are subject to a thorough optimization to reduce the air resistance. As shown, the air resistance force depends not only on the coefficients c_w often used in commercials but also on the front surface A of the vehicle.

Table 8-1 Air resistance coefficients of different vehicles types

Air resistance coefficients of different vehicles types

Type of value	Air resistance coefficient c_W
Passenger car	0.3 - 0.4
Bus	0.6 - 0.7
Truck	0.6 - 1.0
Motor cycle	0.5 - 1.0

In our case, the aerodynamic forces are not a crucial part of the potential damage that would be caused on the chassis. Therefore, it will not be taken into account in our study, because we move with low speed (30km/h maximum speed) and at such speeds, the aerodynamic forces are negligible.

8.7 Ride performance

The vibration environment is one of the more important criteria by which people judge the design and construction "quality" of a car. Being a judgment, it is subjective in nature, from which arises one of the greatest difficulties in developing objective engineering methods for dealing with ride as a performance mode of the vehicle [35].

The lower-frequency ride vibrations are manifestations of dynamic behaviour common to all rubber-tired motor vehicles. Thus, the study of these modes is an important area of vehicle dynamics. As an aid in developing a systematic picture of ride behaviour, it is helpful to think of the overall dynamic system as shown in Figure 8-25. The vehicle is a dynamic system, but only exhibits vibration in response to excitation inputs. The response properties determine the magnitude and direction of vibrations imposed on the passenger compartment and ultimately determine the passenger's perception of the vehicle. Thus, understanding ride involves the study of three main topics:

- Ride excitation sources
- Basic mechanics of vehicle vibration response
- Human perception and tolerance of vibrations

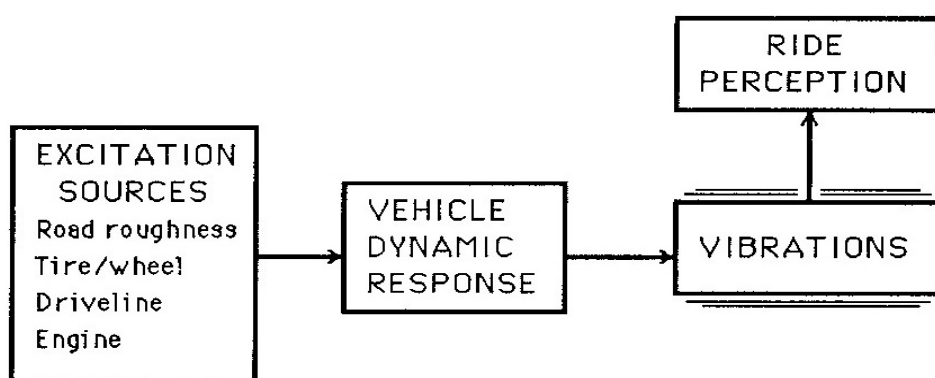


Figure 8-25 The ride dynamic system [35]

In these photos we can distinguish the ride performance of the vehicles:



Figure 8-26 Example of fatigue loading event [2].



Figure 8-27 Example of proving ground event [2].



Figure 8-28 Vertical symmetric (“bending”) load case (courtesy of MIRA UK) [2].



Figure 8-29 Vertical asymmetric (“pure torsion”) load case (courtesy of National Motor Museum, Beaulieu) [2].

In our situation, the road is not rough, but smooth and as a result does not cause vibrations, that is, there is an absence of potholes and bumps. Also, there is no vibrations from driveline because there are not any. Finally, our machine is a small electric motor and the vibrations that are created are negligible, like the vibrations of our tire/wheel.

9 DETERMINE THE WORST CASE STRESS SCENARIO

The vehicle designer needs to know the worst or most damaging loads to which the structure is likely to be subjected, to ensure that the structure will not fail in service due to instantaneous overload and to ensure a satisfactory fatigue life. The considerable attention (through test and analysis) which is paid to fatigue life is outside the scope of this thesis, so, the main interest focuses on instantaneous strength. A commonly used assumption at the early design stage is: "If the structure can resist the worst possible loading which can be encountered, then it is likely to have sufficient fatigue strength" [2].

- Crash cases are often the most difficult and critical to design. These are outside the scope of this thesis, since the structure moves out of the elastic regime into deep collapse.
- The ride loads (vibration environment) is one of the more important criteria by which people judge the design and construction "quality" of a car. Being a judgment, is subjective in nature, from which arises one of the greatest difficulties in developing objective engineering methods for dealing with ride as a performance mode of the vehicle. However, in our case, the track road is not rough. In fact it is quite smooth, so there are not any ride loads [35].
- Towing loads, of course, cannot be neglected, but the vehicle will not need to tow another vehicle.
- Road loads (aerodynamic loads) also stress the vehicle structure. Nevertheless, our forward velocity is very small, lower than 30km/h. After calculations, in the present research case, we observed that these loads were negligible.

9.1 Lateral worst case stress scenario

Cornering loads, of course, overstresses the vehicle structure. Therefore, we need to check the cornering performance of our structure, to understand when it is stressed more.

In general, cornering loads are maximized when the vehicle's speed is maximized and its turning radius is minimized. Looking at the Shell Eco Marathon's track in Rotterdam, we observe that there are five counterclockwise turns [55]. All these turns have approximately the same angle (90°). However, the speed in these corners is not the same. In accordance with the tactics that were followed, we have observed that in the 1st corner we have the maximum speed, and specifically 30 km per hour. Therefore, we will investigate this turn (1st) so as to carry out our study.

The goal of our cornering strategy is to achieve low consumptions and quick round cornering. Figure 9-2 illustrates that our chassis follows our cornering strategy.

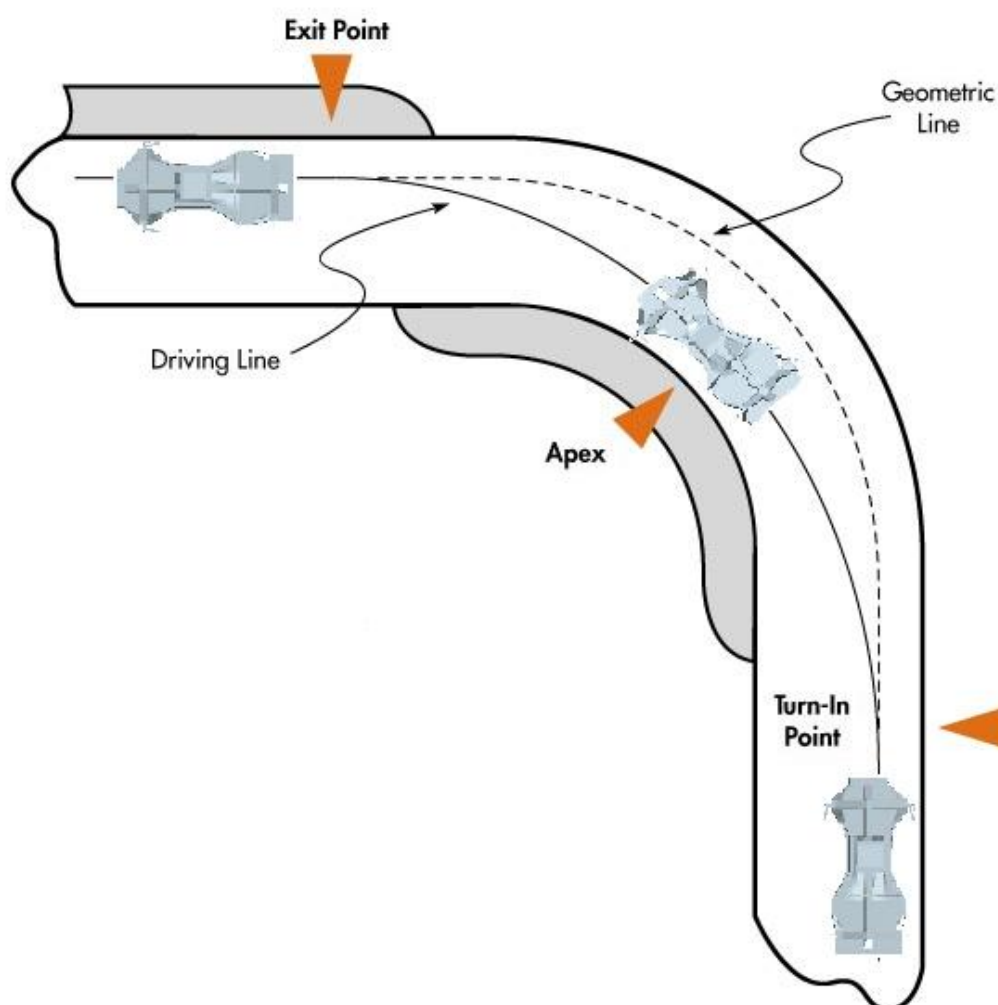


Figure 9-2 Racing line

Apex

The apex is often but not always, the geometric center of the turn. It is the point at which one is the closest to the inside of the corner (clipping point). Hitting the apex allows the car to take the straightest line (low consumption) and maintain the highest speed through out that specific corner. It is also the tightest part of a corner. Therefore, in this point we have the maximum speed and the maximum stress. So, we choose the clipping point for our study because it is the point that we have the cornering worst case stress scenario.

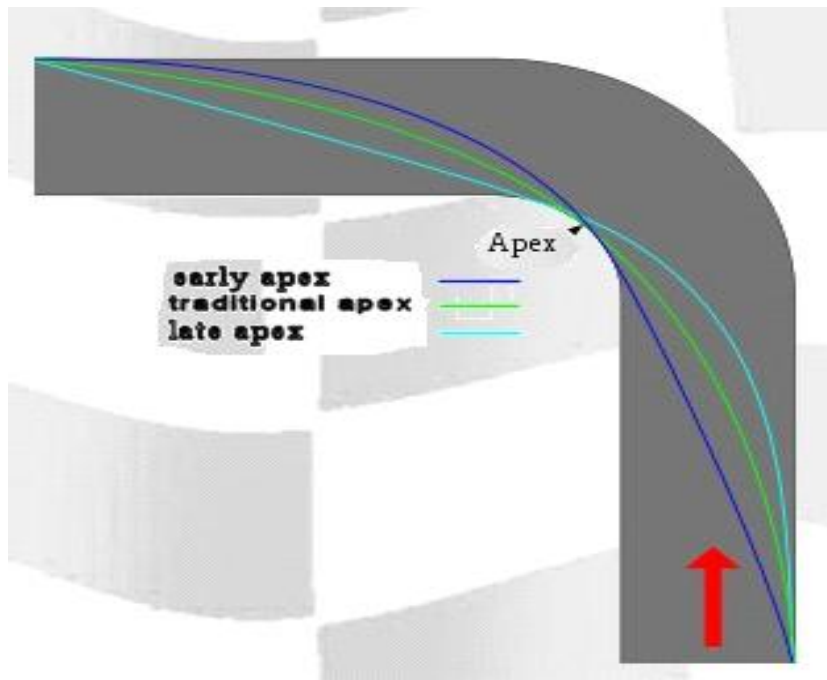


Figure 9-3 Apex. [4]

We considered that the motion of the car follows a parabola (Figure 9-4) and R is the distance between the focus point and the points of the parabola.

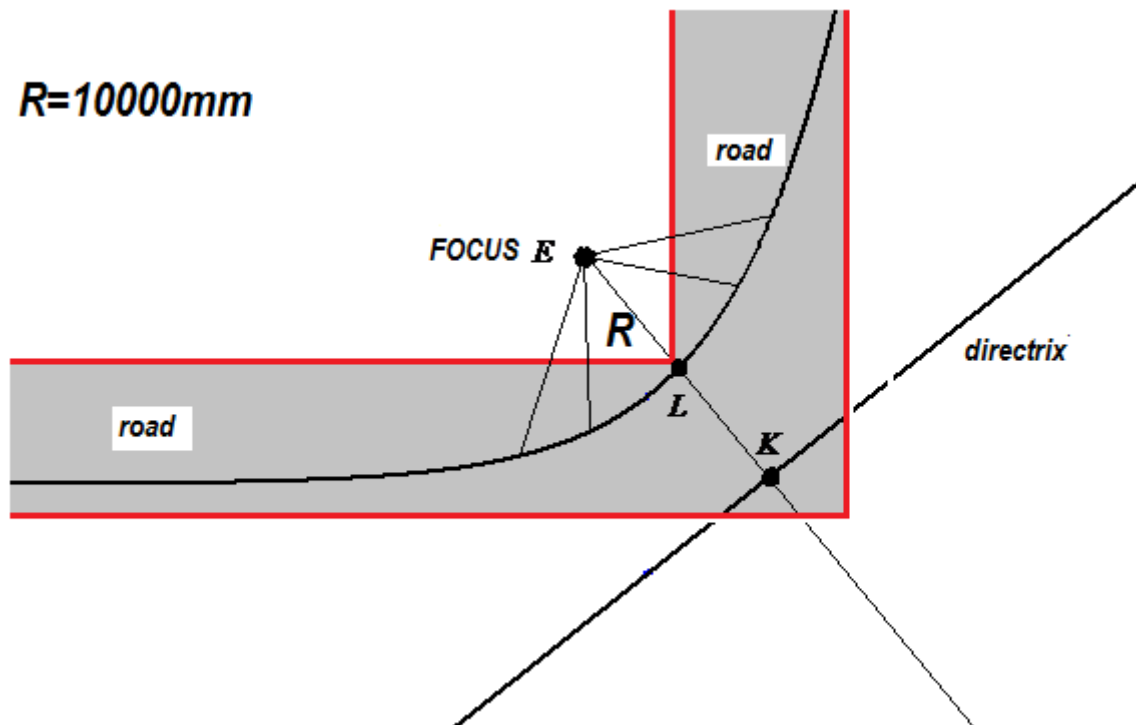


Figure 9-4 The motion of the car follows a parabola

At low speed, the tires need not develop lateral forces. Thus, they roll with no slip angle, and the vehicle must negotiate a turn as illustrated in Figure 9-5.

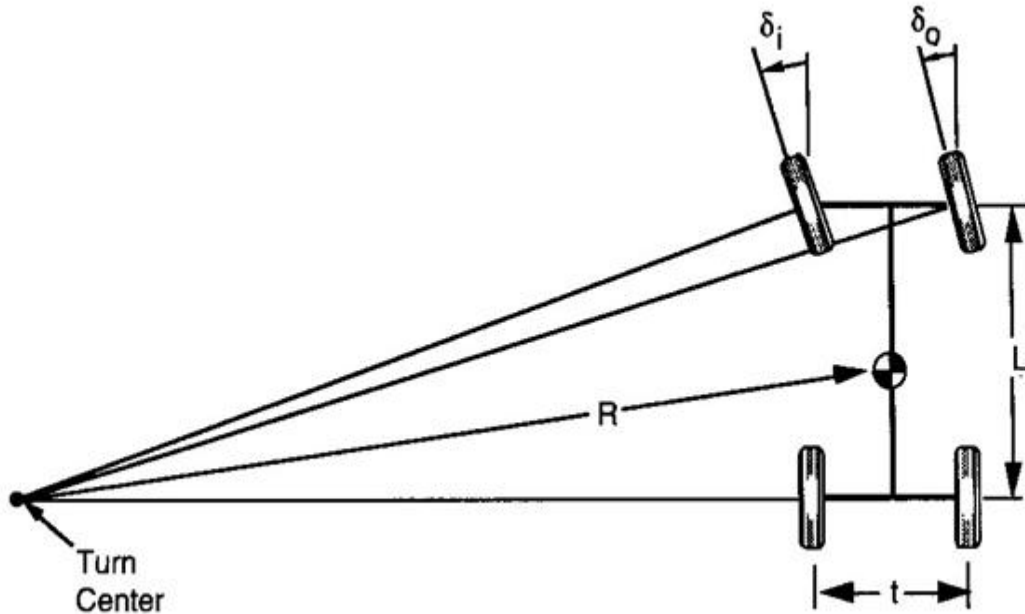


Figure 9-5 Geometry of a turning vehicle. [35]

If the rear wheels have no slip angle, the center of turn must lie in the projection of the rear axle. Likewise, the perpendicular from each of the front wheels should pass through the same point (the center of turn). If they do not pass through the same point, the front tires will "fight" each other in the turn, with each experiencing some scrub (sideslip) in the turn. The ideal turning angles on the front wheels are established by the geometry seen in the Figure 9-5, and define the steering angles for the turn [35].

For proper geometry in the turn (assuming small angles), the steer angles are given by:

$$\delta_o \cong \frac{L}{(R + t/2)}$$

$$\delta_i \cong \frac{L}{(R - t/2)}$$

The average angle of the front wheels (again assuming small angles) is defined [45] as the Ackerman Angle:

$$\delta = L/R$$

The maximum value of δ_o and δ_i is sought. Metrics δ_o and δ_i are maximized when R is minimized.

The car is the moving parable. We know that the distance between the focus point and the points of parabola is equal to the distance between the points of parabola and the directrix. Therefore, the minimum distance between the focus point and the points of the parabola, is the minimum distance between the points of the parabola and the directrix.

$$KL=R=10000 \text{ mm}$$

At this time the vehicle is located in L position:

$$\delta_{0 \max} = \frac{1295}{10000 + 455} = 0,12 \text{ rad} = 6.88^\circ$$

$$\delta_{i \max} = \frac{1295}{10000 - 455} = 0,14 \text{ rad} = 8.02^\circ$$

9.2 Longitudinal worst case stress scenario

Longitudinal loads, also overload the vehicle structure. Thus, we need to find the situation that our chassis is stressed the most. Longitudinal loads are divided into acceleration and braking. Accelerations have been found to be smaller than braking loads [2]. Consequently, our study will focus on braking loads because they cause larger loads than tractive loads. Therefore, the braking performance of our structure should be checked, to understand when the chassis overloaded more during braking.

Thus, a real situation for our vehicle needs to be considered at this point. Supposing that while our vehicle is moving on the track, with its maximum speed, 30km per hour, the preceding vehicle suddenly brakes. Therefore, our driver is forced to brake immediately, to avoid the collision.

Nevertheless, braking force is proportional to the deceleration. Greater slowdown means more force. At this point, we need to find a realistic “deceleration scenario” for urban cars, to determine the deceleration value. Euro NCAP provides motoring consumers with a realistic and independent assessment of the safety performance of some of the most popular cars sold in Europe. One of the tests is the “Autonomous Emergency Braking” (AEB) test, in which many vehicles are evaluated. We will randomly select the FIAT, to see how it behaves in braking tests [17].

FIAT City Brake Control is an autonomous emergency braking which helps a driver avoid a low-speed crash. If the collision becomes imminent, City Brake Control optimises the braking and applies the brakes autonomously. At speeds between 5km/h and 20km/h, the brakes apply a maximum deceleration of 10m/s^2 ; between 20km/h and 30km/h, the maximum deceleration is 6m/s^2 .

In our case we will also suppose, that our driver’s reflexes during braking, are as good as Fiat’s braking control system. This means that in the same situation, our driver would decelerate in the same way. This deceleration, as mentioned above, would be 6m/s^2 , which is the braking of the worst case scenario, in these conditions. This scenario was chosen for our study. Thus, we will subject our vehicle to brake with a deceleration 6m/s^2 from 30km/h to 0km/h.



Figure 9-6 Deceleration because of stationary preceding vehicle

9.3 Combination of cornering and braking worst case stress scenario

In order to demonstrate the strength of our chassis, we only have to show that it withstands the total load worst case. The total load worst case scenario is the combination of cornering worst case stress scenario and braking worst case stress scenario.

Braking during cornering is not advisable as it upsets the cornering balance and will cause problems especially if hard braking is required. At this point one, therefore, needs to study the scenario where the vehicle is turning at the 1st corner with 30km/h and is positioned in the clipping point. At the same time, it encounters a stationary preceding vehicle and decelerates immediately (6m/s^2), to avoid the accident. In this situation our chassis will probably be overstressed.

10 CHASSIS LOAD CALCULATOR (CLC) MODEL

In the chassis load calculator model (CLC), the values of the forces acting on a vehicle structure change depending on the characteristics of the structure. Therefore, what is required is the creation of a model which calculates by itself the forces acting on each chassis structure according to the characteristics of the imported structure. First of all, the chassis load calculator model has been made for academic purposes, as well as to save time during the calculation of forces for each chassis. From the beginning, we know that we will have to design many car structures until the final design is chosen. The possible calculation of the corresponding forces would be time-consuming. Many hours of optimization of this model and many tests are required to ensure the validity and the accuracy of the calculations. The equations that are used to create the models are those which were mentioned in Chapter "Vehicle Dynamics". Initially, for simplicity, this model has been created using computer Excel.

10.1 The dynamics of the Eco Racer chassis 2014

The vehicle receives some static and some dynamic loading. Static loads include forces related to reactions of the total mass of the vehicle while dynamic loads include the forces generated during braking and cornering.

$$L_f + L_r = G$$

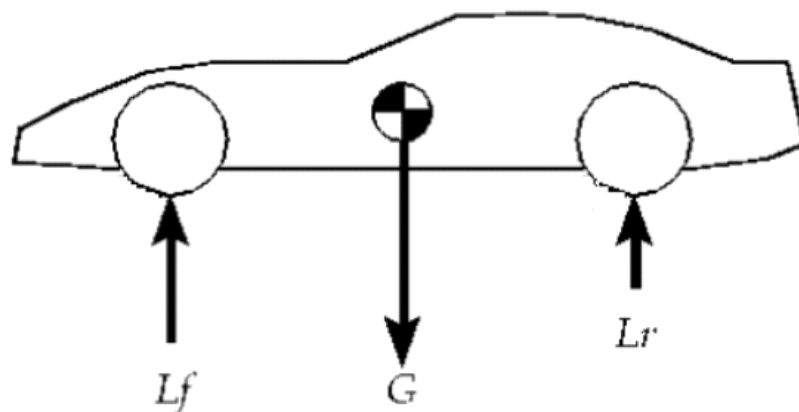


Figure 10-1 Static load distribution on front and rear axle [28].

Table 10-1 Static load distribution on front and rear axle

FROM THE CENTER OF THE FRONT AXLE(mm)	607.766 mm
FROM THE CENTER OF THE REAR AXLE(mm)	687.234 mm
DISTRIBUTION OF MASS ON FRONT AXLE	0.53068 53.07 %
DISTRIBUTION OF MASS ON REAR AXLE	0.46932 46.93 %
WEIGHT ON FRONT AXLE(kg)	82.3089 kg
WEIGHT ON REAR AXLE(kg)	72.7911 kg
STATIC FORCE ON FRONT AXLE(N)	807.45 N
STATIC FORCE ON REAR AXLE(N)	714.081 N

Table 10-2 Static load distribution on left and right wheels

FROM THE LEFT(mm)	392.328 mm
FROM THE RIGHT(mm)	337.672 mm
DISTRIBUTION OF MASS ON THE LEFT	0.46256 46.26 %
DISTRIBUTION OF MASS ON THE RIGHT	0.53744 53.74 %
WEIGHT ON THE LEFT(kg)	71.7437 kg
WEIGHT ON THE RIGHT(kg)	83.3563 kg
STATIC FORCE ON THE LEFT(N)	703.806 N
STATIC FORCE ON THE RIGHT(N)	817.725 N

10.1.1 Vertical dynamics – static load

Vertical static loads act on the vehicle's wheel in response to its weight, when it is stationary. It is observed that this value varies according to the weight distribution on each wheel.

Table 10-3 Vertical dynamics - Static load

STATIC LOAD	
WEIGHT ON LEFT FRONT WHEEL(kg)	38.07313195 kg
WEIGHT ON RIGHT FRONT WHEEL(kg)	44.23573792 kg
WEIGHT ON LEFT REAR WHEEL(kg)	33.67056681 kg
WEIGHT ON RIGHT REAR WHEEL(kg)	39.12056332 kg
STATIC LOAD ON LEFT FRONT WHEEL(N)	373.4974244 N
STATIC LOAD ON RIGHT FRONT WHEEL(N)	433.952589 N
STATIC LOAD ON LEFT REAR WHEEL(N)	330.3082604 N
STATIC LOAD ON RIGHT REAR WHEEL(N)	383.7727262 N

10.1.2 Lateral dynamics – cornering performance

The cornering loads are calculated according to the cornering worst case stress scenario while the vehicle is positioned in the clipping point of the turn.

Table 10-4 The data used for the calculation of lateral dynamics

FIRST FORWARD VELOCITY V (30 km/h->8.33m/s->8333mm/s)	8333 mm/s	8.333 m/s
TURN RADIUS R (mm) 10m*1000= 10000mm	10000 mm	10 m
GRAVITY ACCELARATION g (mm/s ²)	9810 mm/s ²	
ROLL CENTER HEIGHT hr (mm)		280
TREAD (TRACK WIDTH) 0.950-0.040=0.910 (m) ->910mm		910
DISTANCE OF CHASSIS ON Yaxis (mm)		730
TREAD WIDTH (-) DISTANCE OF CHASSIS ON Yaxis (mm)		180
TREAD WIDTH (-) DISTANCE OF CHASSIS ON Yaxis(from one side) (mm)		90

10.1.2.1 Cornering force

The cornering force is calculated:

Table 10-5 Cornering force

CORNERING FORCE	
CORNERING FORCE Fy	1076.997168 N

10.1.2.2 Load transfer from cornering

The load transfer is also calculated:

Table 10-6 Load transfer from cornering

LOAD TRANSFER ON THE RIGHT	662.7674882 N	67.5604 kg
LOAD TRANSFER ON THE LEFT	-662.767488 N	-67.5604 kg

10.1.2.3 New center of gravity during cornering

When stationary, the weight of the car is distributed more or less evenly on all four wheels. However, during cornering the weight is transferred to the outside wheels.

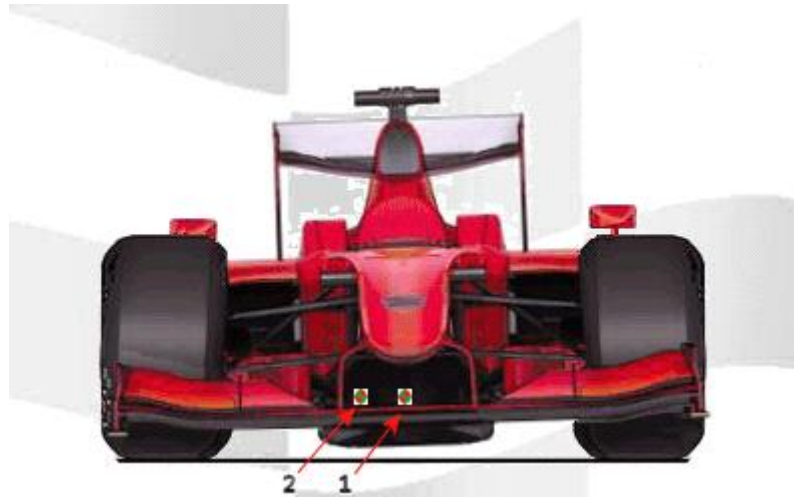


Figure 10-2 Weight transfer during the roll(left corner). [4]

During cornering the mass distribution changes, as well as the center of gravity [34] [33] [56] [4].

Table 10-7 Mass distribution on front and rear axle during cornering

DISTRIBUTION OF MASS ON FRONT AXLE	0.530682591	53.068 %
DISTRIBUTION OF MASS ON REAR AXLE	0.469317409	46.932 %
WEIGHT ON FRONT AXLE(kg)	82.30886987	kg
WEIGHT ON REAR AXLE(kg)	72.79113013	kg
STATIC FORCE ON FRONT AXLE(N)	807.4500134	N
STATIC FORCE ON REAR AXLE(N)	714.0809866	N
WEIGHT ON THE LEFT(kg)	150.9166976	kg
WEIGHT ON THE RIGHT(kg)	4.1833024	kg
STATIC FORCE ON THE LEFT(N)	1480.492803	N
STATIC FORCE ON THE RIGHT(N)	41.03819654	N

Assuming that we do not have mass transfer in the z axis, since we do not have shock absorbers as well as the fact that if there is a mass transfer in the x axis, it will be negligible, then the new COG will be:

Table 10-8 New center of gravity during cornering

NEW CENTER OF MASS (mm)		
CENTER OF MASS x	CENTER OF MASS y	CENTER OF MASS z
872.766045	705.4558015	408.7929

The mass distribution changes during the $\frac{1}{4}$ turn:

Table 10-9 Mass distribution on left and right wheels

DISTRIBUTION OF MASS ON THE RIGHT	96.63778103 %
DISTRIBUTION OF MASS ON THE LEFT	3.36221897 %

10.1.3 Longitudinal dynamics – braking performance

The braking loads are calculated according to the braking worst case stress scenario while the vehicle is positioned in the clipping point of the turn and at the same time decelerates.

Table 10-10 The data used for the calculation of longitudinal dynamics

FINAL FORWARD VELOCITY V2 (mm/s)	0
ABSOLUT VALUE OF VELOCITY CHANGE V2-V (mm/s)	8333
BRAKING TIME (s)	10
BRAKING DISTANCE (mm)	83330
MAXIMUM DECELERATION Dx (mm/s ²)	833.3
WHEELBASE L (mm)	1295
FRONT AREA OF FRONT AXLE (265)	265
Tyre coefficient of friction	0.0025

Table 10-11 Brake system dimensions

Brake System Dimensions

Distance from the brake pedal arm pivot to the output rod clevis attachment L1

Distance from the brake pedal arm pivot to the brake pedal pad L2

Front

Wheel radius	280 mm	
Master cylinder diameter	12.7 mm	
Distance - pushrod to balance bar pivot	30 mm	0.03 m
The effective area of the caliper hydraulic piston found on one half of the calliper body	800 mm ²	
Pad Coefficient of friction	0.35	
Disc diameter	160 mm	0.16 m
Pad depth	3 mm	0.003 m
Gap between top of pad and disc	1 mm	0.001 m

Rear

Wheel radius	280 mm	
Master cylinder diameter	12.7 mm	
Distance - pushrod to balance bar pivot	40 mm	0.04 m
The effective area of the caliper hydraulic piston found on one half of the calliper body	800 mm ²	
Pad Coefficient of friction	0.35	
Disc diameter	160 mm	0.16 m
Pad depth	3 mm	0.003 m
Gap between top of pad and disc	1 mm	0.001 m

Table 10-12 Dynamic characteristics of the vehicle

Cg Height	408.7929 m
Wheelbase	1,295 m
Front wheel rolling radius	280 m
Rear wheel rolling radius	280 m
Weight on Front Axle	82.30887 kg
Weight on Rear Axle	72.79113 kg
Total Weight	155.1 kg
Weight on Front Axle	0.530683 %
Weight on Rear Axle	0.469317 %

10.1.3.1 Braking force

The braking force is calculated:

Table 10-13 Force on balance bar by the driver

Kgf applied to pedal	10 kgf
Force Applied to pedal	98.1 N
Pedal Ratio	4 :1
Force on balance bar	392.4 N

Table 10-14 Braking force calculation

Front		
Balance bar proportion	0.571428571	57.142857 %
Force on M Cyl piston	224.2285714	N
Master/cylinder Area	126.61265	mm ²
Line pressure generated by the master cylinder	1.770980794	N/mm ²
Line hydraulic pressure transmitted to the caliper	1.770980794	N/mm ²
The one sided linear mechanical force generated by the caliper	1416.784635	N
Clamping force on disc generated by the caliper	2833.56927	N
The frictional force generated by the brake pads opposing the rotation of the rotor	991.7492446	N
$F_x = F \cdot \sin 45$	701.2726161	N
$F_y = F \cdot \cos 45$	701.2726161	N
Disc effective radius	77.5	mm
Disc torque, the torque generated by the rotor (both pads 1 wheel)	76860.56646	Nmm
The torque found in the tire=torque wheel=torque by the rotor	76860.56646	Nmm
The force reacted between the tire and the ground (assuming friction exists to support the force)	274.5020231	N
Rear		
Balance bar proportion	0.428571429	42.857143 %
Force on M Cyl piston	168.1714286	N
Master/cylinder Area	126.61265	mm ²
Line pressure generated by the master cylinder	1.328235596	N/mm ²
Line hydraulic pressure transmitted to the caliper	1.328235596	N/mm ²
The one sided linear mechanical force generated by the caliper	1062.588476	N
Clamping force on disc generated by the caliper	2125.176953	N
The frictional force generated by the brake pads opposing the rotation of the rotor	743.8119335	N
$F_x = F \cdot \sin 45$	525.9544621	N
$F_y = F \cdot \cos 45$	525.9544621	N
Disc effective radius	77.5	mm
Disc torque, the torque generated by the rotor (both pads 1 wheel)	57645.42484	Nmm
The torque found in the tire=torque wheel=torque by the rotor	57645.42484	Nmm
The force reacted between the tire and the ground (assuming friction exists to support the force)	205.8765173	N

Table 10-15 Deceleration and stopping distance

Total Force (4 wheels)	960.7570807	N
Deceleration of the vehicle $a = F_{total} / TW$	6.194436368	m/s ² 6194.436 mm/s ²
Stopping distance of the vehicle	5604.940052	mm

As can be seen from the above results, a 6.19m/s² deceleration was achieved, whose value is greater than the maximum value of the Fiat's deceleration (6 m/s²), which was first set as a goal.

10.1.3.2 Load transfer from braking

The load transfer is then calculated:

Table 10-16 Load transfer from braking

Front		
Weight transfer	30.91563432 kg	303.2824 N
Front axle load under braking	113.2245042 kg	
Dynamic front axle load	1110.732386 N	
LOAD TRANSFER FROM BRAKING ON FRONT LEFT WHEEL	1.039451322 kg	10.19702 N
LOAD TRANSFER FROM BRAKING ON FRONT RIGHT WHEEL	29.876183 kg	293.0854 N
Rear		
Weight transfer	-30.9156343 kg	-303.282 N
Rear axle load under braking	41.87549581 kg	
Dynamic rear axle load	410.7986139 N	
LOAD TRANSFER FROM BRAKING ON REAR LEFT WHEEL	-1.03945132 kg	-10.197 N
LOAD TRANSFER FROM BRAKING ON REAR RIGHT WHEEL	-29.876183 kg	-293.085 N

10.1.3.3 New center of gravity during braking and cornering coexistence

During braking the weight is transferred to the front wheels.

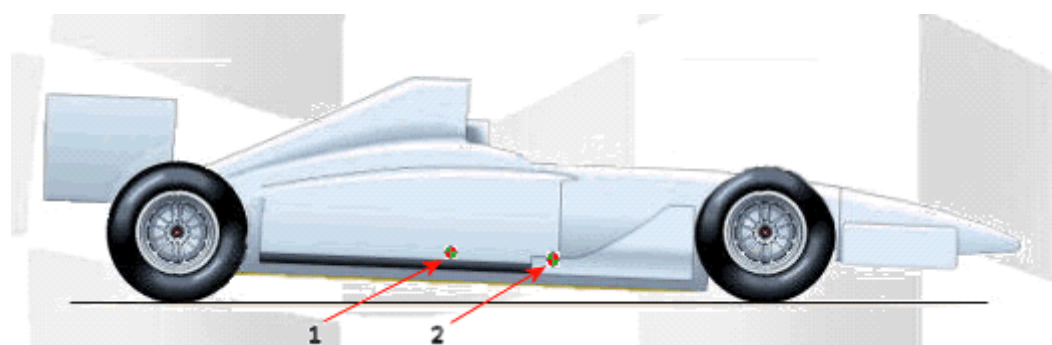


Figure 10-3 Weight transfer during the pitch (decceleration). [4]

At the same time of braking and turning, the mass distribution changes, as well as the center of gravity of the vehicle [34] [33] [56] [4].

Table 10-17 Mass distribution on left and right wheels during braking

WEIGHT ON FRONT AXLE(kg)	113.2245042 kg
WEIGHT ON REAR AXLE(kg)	41.87549581 kg
STATIC FORCE ON FRONT AXLE(N)	1110.732386 N
STATIC FORCE ON REAR AXLE(N)	410.7986139 N
DISTRIBUTION OF MASS ON THE RIGHT	0.96637781 96.638 %
DISTRIBUTION OF MASS ON THE LEFT	0.03362219 3.3622 %
WEIGHT ON THE LEFT(kg)	150.9166976 kg
WEIGHT ON THE RIGHT(kg)	4.1833024 kg
STATIC FORCE ON THE LEFT(N)	1480.492803 N
STATIC FORCE ON THE RIGHT(N)	41.03819654 N

Assuming that we do not have mass transfer in the z axis, since we do not have shock absorbers, as well as the fact that if there is a mass transfer in the y axis, it will be negligible, then the new COG will be:

Table 10-18 New center of gravity during braking and cornering coexistence

NEW CENTER OF MASS (mm)		
CENTER OF MASS x	CENTER OF MASS y	CENTER OF MASS z
614.6374408	705.455802	408.7928994

This is the center of mass that the vehicle has during braking and cornering coexistence. It is observed that after such a sudden stop in a ¼ turn the mass distribution changes:

Table 10-19 Mass distribution on front and rear axles

DISTRIBUTION OF MASS ON FRONT AXLE	0.730009698	73.00096982 %
DISTRIBUTION OF MASS ON REAR AXLE	0.269990302	26.99903018 %

With the new center of mass, the cornering force on each wheel can be found:

Table 10-20 The cornering force on each wheel

WITH THE NEW CENTER OF MASS WE HAVE	
CORNERING FORCE FRONT $F_{yf} = W_f \cdot V^2 / (R \cdot g)$	786.2183779 N
CORNERING FORCE REAR $F_{yr} = W_r \cdot V^2 / (R \cdot g)$	290.7787905 N
CORNERING FORCE ON LEFT FRONT WHEEL (N)	26.43438344 N
CORNERING FORCE ON RIGHT FRONT WHEEL (N)	759.7839944 N
CORNERING FORCE ON LEFT REAR WHEEL (N)	9.776619655 N
CORNERING FORCE ON RIGHT REAR WHEEL (N)	281.0021709 N

10.1.4 Combination load case

Summarizing, the loads that act on each semi-axle of the chassis, in the z axis, are presented in Table 10-21.

Table 10-21 Combination load case

STATIC LOAD ON LEFT FRONT WHEEL(N)	373.4974244 N
STATIC LOAD ON RIGHT FRONT WHEEL(N)	433.952589 N
STATIC LOAD ON LEFT REAR WHEEL(N)	330.3082604 N
STATIC LOAD ON RIGHT REAR WHEEL(N)	383.7727262 N
LOAD TRANSFER FROM CORNERING ON RIGHT FRONT WHEEL(N)	483.8266941 N
LOAD TRANSFER FROM CORNERING ON RIGHT REAR WHEEL(N)	178.9407942 N
LOAD TRANSFER FROM CORNERING ON LEFT FRONT WHEEL(N)	-483.8266941 N
LOAD TRANSFER FROM CORNERING ON LEFT REAR WHEEL(N)	-178.9407942 N
LOAD TRANSFER FROM BRAKING ON FRONT LEFT WHEEL(N)	10.19701747 N
LOAD TRANSFER FROM BRAKING ON FRONT RIGHT WHEEL(N)	293.0853552 N
LOAD TRANSFER FROM BRAKING ON REAR LEFT WHEEL(N)	-10.19701747 N
LOAD TRANSFER FROM BRAKING ON REAR RIGHT WHEEL(N)	-293.0853552 N

Every total dynamic load will be applied to each semi-axle, in the upward direction on the z axis and is calculated by the sum of the above loads:

Table 10-22 Total dynamic loads on each wheel (z axis)

TOTAL DYNAMIC LOAD "STATIC+WEIGHT TRANSFER FROM CORNERING+WEIGHT TRANSFER FROM BRAKING" ON Zaxis'	
TOTAL DYNAMIC LOAD "STATIC+CORNERING+BRAKING" ON FRONT LEFT WHEEL(Z axis) (N)	-100.1322522 N
TOTAL DYNAMIC LOAD "STATIC+CORNERING+BRAKING" ON FRONT RIGHT WHEEL(Z axis) (N)	1210.864638 N
TOTAL DYNAMIC LOAD "STATIC+CORNERING+BRAKING" ON REAR LEFT WHEEL(Z axis) (N)	141.1704488 N
TOTAL DYNAMIC LOAD "STATIC+CORNERING+BRAKING" ON REAR RIGHT WHEEL(Zaxis) (N)	269.6281651 N

10.1.4.1 Transfer the cornering forces

The cornering forces F_y are transferred from the contact patch to the center of the axle [57] [58]. The equivalent system will consist of the cornering forces (F_y) plus the moments (M_x) that are created from the cornering forces. These moments are the result of the cornering forces multiplied by the vertical distance, which is $z=280\text{mm}$.

Table 10-23 Cornering forces and moments from contact patch to the center of axle

CORNERING FORCES F_y		F_y
CORNERING FORCE ON LEFT FRONT WHEEL (N)	26.43438344 N	
CORNERING FORCE ON RIGHT FRONT WHEEL(N)	759.7839944 N	
CORNERING FORCE ON LEFT REAR WHEEL(N)	9.776619655 N	
CORNERING FORCE ON RIGHT REAR WHEEL(N)	281.0021709 N	
MOMENTS M_x FROM CONTACT PATCH TO THE CENTER OF AXLE		M_x
MOMENT FROM CORNERING FORCE ON LEFT FRONT WHEEL	7.401627364 Nm	7401.627364 Nmm
MOMENT FROM CORNERING FORCE ON RIGHT FRONT WHEEL	212.7395184 Nm	212739.5184 Nmm
MOMENT FROM CORNERING FORCE ON LEFT REAR WHEEL	2.737453503 Nm	2737.453503 Nmm
MOMENT FROM CORNERING FORCE ON RIGHT REAR WHEEL	78.68060784 Nm	78680.60784 Nmm

10.1.4.2 Transfer the braking forces

Initially, the braking force needs to be analyzed in x and z axis (F_x , F_z) [57] [58].

Table 10-24 Braking forces

BRAKING FORCES F_x, F_z	F_x	F_z
BRAKING FORCE ON FRONT LEFT AXLE	495.8746223 N	495.8746223 N
BRAKING FORCE ON FRONT RIGHT AXLE	495.8746223 N	495.8746223 N
BRAKING FORCE ON REAR LEFT AXLE	371.9059667 N	371.9059667 N
BRAKING FORCE ON REAR RIGHT AXLE	371.9059667 N	371.9059667 N

The vertical distance of F_z from the end of the axle is calculated as well as the vertical distance of F_x from the center of the axle.

Table 10-25 Vertical distances

$x=(\cos 45)^*0.0075 + 0.0075$	0.012803301 m	12.80330086 mm
$z=(\sin 45)^*0.0075$	0.005303301 m	5.303300859 mm

F_x, F_z are transferred to the axle. The equivalent system will consist of the braking forces (F_x, F_z) plus the moments (M_{y1}, M_{y2}) that are created from the braking forces:

Table 10-26 Braking forces and moments from disc effective radius to the axle

BRAKING FORCES F_x, F_z	F_x	F_z
BRAKING FORCE ON FRONT LEFT AXLE	495.8746223 N	495.8746223 N
BRAKING FORCE ON FRONT RIGHT AXLE	495.8746223 N	495.8746223 N
BRAKING FORCE ON REAR LEFT AXLE	371.9059667 N	371.9059667 N
BRAKING FORCE ON REAR RIGHT AXLE	371.9059667 N	371.9059667 N
MOMENTS FROM DISC EFFECTIVE RADIUS TO THE AXLE	M_{y1}	M_{y2}
MOMENTS FROM BRAKING FORCE ON FRONT LEFT AXLE	2629.77231 Nmm	6348.831978 Nmm
MOMENTS FROM BRAKING FORCE ON FRONT RIGHT AXLE	2629.77231 Nmm	6348.831978 Nmm
MOMENTS FROM BRAKING FORCE ON REAR LEFT AXLE	1972.329233 Nmm	4761.623983 Nmm
MOMENTS FROM BRAKING FORCE ON REAR RIGHT AXLE	1972.329233 Nmm	4761.623983 Nmm

The calculated loads are presented schematically, in the rear, front and side view.

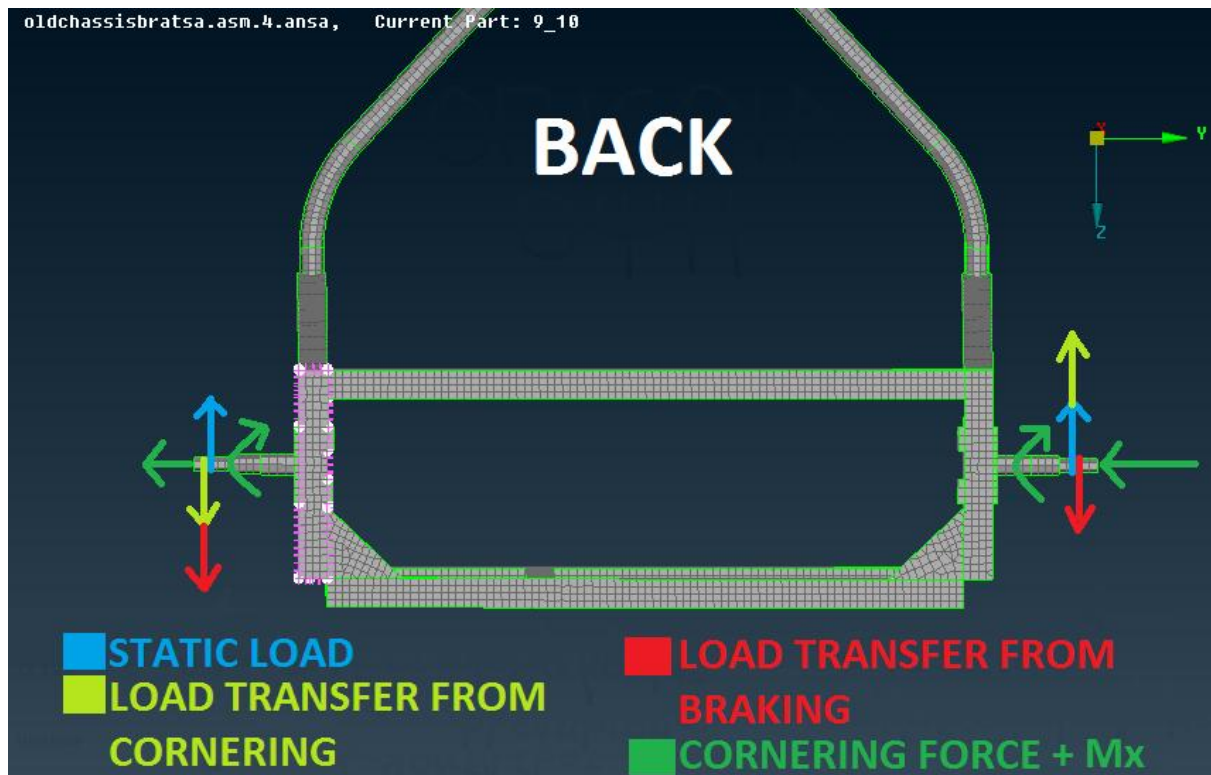


Figure 10-4 Combination load case (Rear view)

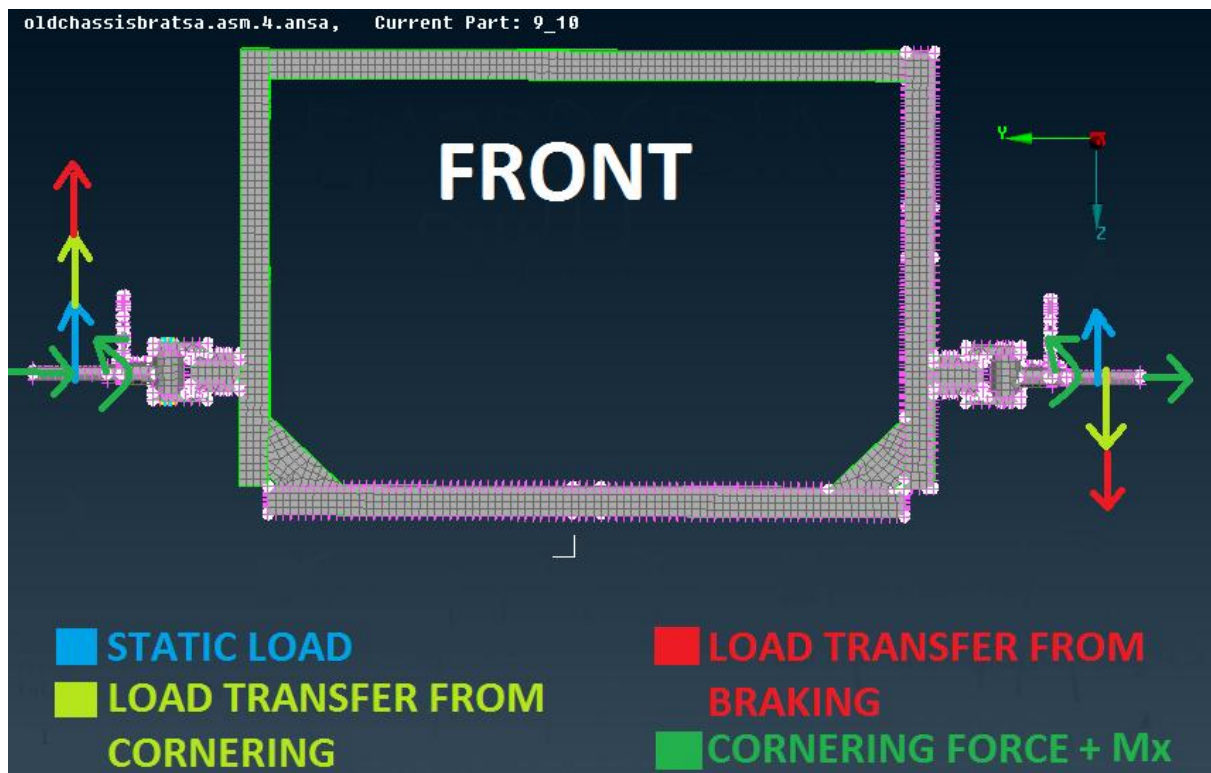


Figure 10-5 Combination load case (Front view)

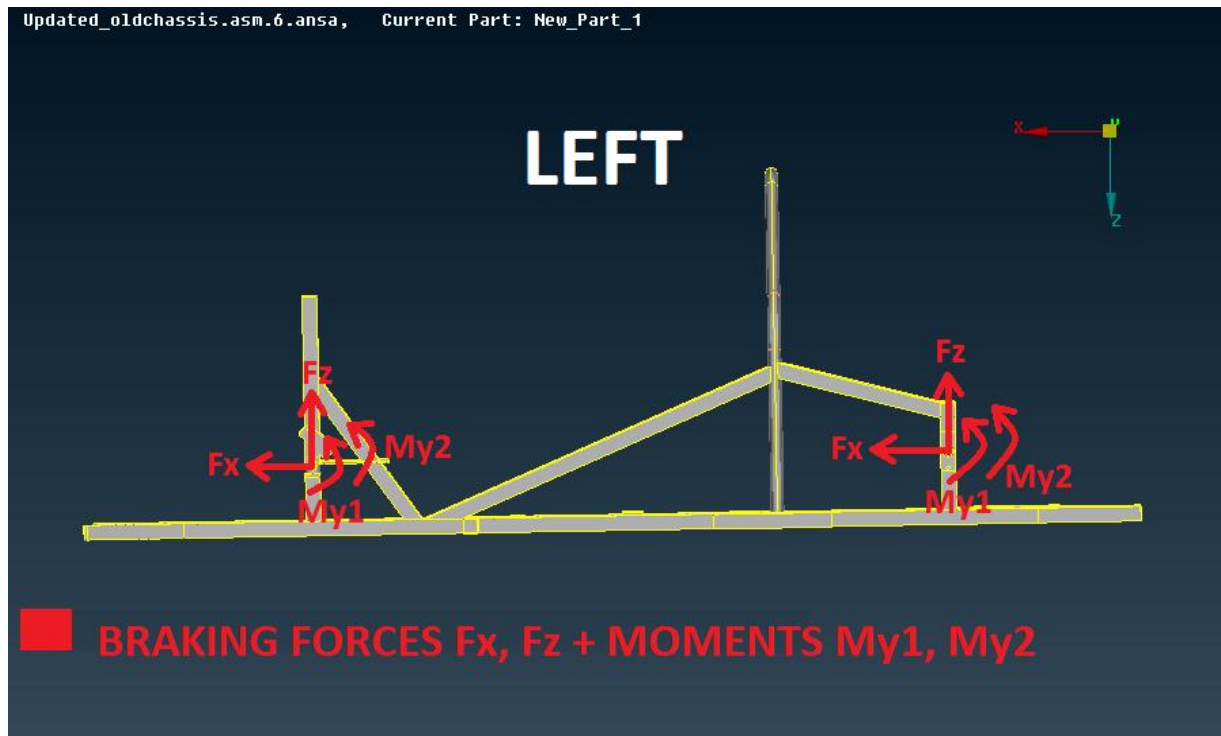


Figure 10-6 Combination load case (Side view)

10.2 Monocoque chassis dynamics

The mass, the center of gravity and other characteristics are different from the space frame characteristics. Consequently, the applied loads values on the monocoque are different from the applied loads values on the space frame. The chassis load calculator model automatically calculates the magnitude and the direction of the loads that are applied on the new vehicle, by providing the characteristics of the new vehicle.

10.2.1 Vertical dynamics – static load

Vertical static loads act on the vehicle’s wheel in response to its weight, when it is stationary. It is observed that this value varies according to the weight distribution on each wheel.

Table 10-27 Vertical dynamics - Static load

STATIC LOAD	
WEIGHT ON LEFT FRONT WHEEL(kg)	37.94744827 kg
WEIGHT ON RIGHT FRONT WHEEL(kg)	43.8111934 kg
WEIGHT ON LEFT REAR WHEEL(kg)	33.05667457 kg
WEIGHT ON RIGHT REAR WHEEL(kg)	38.16468376 kg
STATIC LOAD ON LEFT FRONT WHEEL(N)	372.2644675 N
STATIC LOAD ON RIGHT FRONT WHEEL(N)	429.7878073 N
STATIC LOAD ON LEFT REAR WHEEL(N)	324.2859775 N
STATIC LOAD ON RIGHT REAR WHEEL(N)	374.3955477 N

10.2.2 Lateral dynamics – cornering performance

The cornering loads are calculated according to the cornering worst case stress scenario while the vehicle is positioned in the clipping point of the turn.

10.2.2.1 Cornering force

The cornering force is calculated:

Table 10-28 Cornering force

CORNERING FORCE	
CORNERING FORCE	1062.276124 N

10.2.2.2 Load transfer from cornering

The load transfer is also calculated:

Table 10-29 Load transfer from cornering

LOAD TRANSFER ON CORNERING ON THE RIGHT	653.708384 N	66.6369403 kg
LOAD TRANSFER ON CORNERING ON THE LEFT	-653.708384 N	-66.6369403 kg

10.2.2.3 New center of gravity during cornering

During cornering the mass distribution changes, as well as the center of gravity [34] [33] [4] [56].

Table 10-30 New center of gravity during cornering

NEW CENTER OF MASS (mm)		
CENTER OF MASS x	CENTER OF MASS y	CENTER OF MASS z
867.9001	704.0218581	419.62495

Table 10-31 Mass distribution on left and right wheels

DISTRIBUTION OF MASS ON THE RIGHT	96.44135043 %
DISTRIBUTION OF MASS ON THE LEFT	3.558649571 %

10.2.3 Longitudinal dynamics – braking performance

The braking loads are calculated according to the braking worst case stress scenario while the vehicle is positioned in the clipping point of the turn and at the same time decelerates.

10.2.3.1 Braking force

The braking force of the monocoque is the same as the braking force of the space frame.

10.2.3.2 Load transfer from braking

The load transfer is then calculated:

Table 10-32 Load transfer from braking

Front		
Weight transfer	31.73482621 kg	311.318645 N
Front axle load under braking	113.4934679 kg	
Dynamic front axle load	1113.37092 N	
LOAD TRANSFER FROM BRAKING ON FRONT LEFT WHEEL	1.129331257 kg	11.0787396 N
LOAD TRANSFER FROM BRAKING ON FRONT RIGHT WHEEL	30.60549495 kg	300.239905 N
Rear		
Weight transfer	-31.7348262 kg	-311.318645 N
Rear axle load under braking	39.48653212 kg	
Dynamic rear axle load	387.3628801 N	
LOAD TRANSFER FROM BRAKING ON REAR LEFT WHEEL	-1.12933126 kg	-11.0787396 N
LOAD TRANSFER FROM BRAKING ON REAR RIGHT WHEEL	-30.605495 kg	-300.239905 N

10.2.3.3 New center of gravity during braking and cornering coexistence

At the same time of braking and turning, the mass distribution changes, as well as the center of gravity of the vehicle [56] [34] [33] [4].

Table 10-33 New center of gravity during braking and cornering

NEW CENTER OF MASS (mm)		
CENTER OF MASS x	CENTER OF MASS y	CENTER OF MASS z
599.2597666	704.0218581	419.6249536

Table 10-34 Mass distribution on front and rear axles

DISTRIBUTION OF MASS ON FRONT AXLE	0.74188435	74.188435 %
DISTRIBUTION OF MASS ON REAR AXLE	0.25811565	25.811565 %

With the new center of mass, the cornering force on each wheel can be found:

Table 10-35 The cornering force on each wheel

WITH THE NEW CENTER OF MASS WE HAVE	
CORNERINGFORCEFRONT	788.0860318 N
CORNERING FORCE REAR	274.1900921 N
CORNERING FORCE ON LEFT FRONT WHEEL (N)	28.04522019 N
CORNERING FORCE ON RIGHT FRONT WHEEL(N)	760.0408116 N
CORNERING FORCE ON LEFT REAR WHEEL(N)	9.757464537 N
CORNERING FORCE ON RIGHT REAR WHEEL(N)	264.4326276 N

10.2.4 Combination load case

Summarizing, the loads that act on each semi-axle of the chassis, in the z axis, are presented in Table 10-36.

Table 10-36 Combination load case

STATIC LOAD ON LEFT FRONT WHEEL(N)	372.264467 N
STATIC LOAD ON RIGHT FRONT WHEEL(N)	429.787807 N
STATIC LOAD ON LEFT REAR WHEEL(N)	324.285978 N
STATIC LOAD ON RIGHT REAR WHEEL(N)	374.395548 N
LOAD TRANSFER ON CORNERING FROM RIGHT FRONT WHEEL(N)	484.97602 N
LOAD TRANSFER LOAD CORNERING ON RIGHT REAR WHEEL(N)	168.732364 N
LOAD TRANSFER FROM CORNERING ON LEFT FRONT WHEEL(N)	-484.97602 N
LOAD TRANSFER FROM CORNERING ON LEFT REAR WHEEL(N)	-168.73236 N
LOAD TRANSFER FROM BRAKING ON FRONT LEFT WHEEL(N)	11.0787396 N
LOAD TRANSFER FROM BRAKING ON FRONT RIGHT WHEEL(N)	300.239905 N
LOAD TRANSFER FROM BRAKING ON REAR LEFT WHEEL(N)	-11.07874 N
LOAD TRANSFER FROM BRAKING ON REAR RIGHT WHEEL(N)	-300.23991 N

Every total dynamic load will be applied to each semi-axle, in the upward direction on the z axis and is calculated by the sum of the above loads:

Table 10-37 Total dynamic loads on each wheel (z axis)

TOTAL DYNAMIC LOAD "STATIC+WEIGHT TRANSFER FROM CORNERING+WEIGHT TRANSFER FROM BRAKING" ON Zaxis'	
TOTAL DYNAMIC LOAD "STATIC+CORNERING+BRAKING" ON FRONT LEFT WHEEL(Z axis) (N)	-101.6328125 N
TOTAL DYNAMIC LOAD "STATIC+CORNERING+BRAKING" ON FRONT RIGHT WHEEL(Z axis) (N)	1215.003732 N
TOTAL DYNAMIC LOAD "STATIC+CORNERING+BRAKING" ON REAR LEFT WHEEL(Z axis) (N)	144.4748735 N
TOTAL DYNAMIC LOAD "STATIC+CORNERING+BRAKING" ON REAR RIGHT WHEEL(Zaxis) (N)	242.8880066 N

10.2.4.1 Transfer the cornering forces

The cornering forces F_y are transferred from the contact patch to the center of the axle [57] [58]. The equivalent system will consist of the cornering forces (F_y) plus the moments (M_x) that are created from the cornering forces. These moments are the result of the cornering forces multiplied by the vertical distance, which is $z=280\text{mm}$.

Table 10-38 Cornering forces and moments from contact patch to the center of axle

CORNERING FORCES F_y		F_y
CORNERING FORCE ON LEFT FRONT WHEEL (N)	28.04522019 N	
CORNERING FORCE ON RIGHT FRONT WHEEL(N)	760.0408116 N	
CORNERING FORCE ON LEFT REAR WHEEL(N)	9.757464537 N	
CORNERING FORCE ON RIGHT REAR WHEEL(N)	264.4326276 N	
MOMENTS M_x FROM CONTACT PATCH TO THE CENTER OF AXLE		M_x
MOMENTS FROM CORNERING FORCE ON LEFT FRONT WHEEL	7.852661653 Nm	7852.6617 Nmm
MOMENTS FROM CORNERING FORCE ON RIGHT FRONT WHEEL	212.8114273 Nm	212811.43 Nmm
MOMENTS FROM CORNERING FORCE ON LEFT REAR WHEEL	2.73209007 Nm	2732.0901 Nmm
MOMENTS FROM CORNERING FORCE ON RIGHT REAR WHEEL	74.04113572 Nm	74041.136 Nmm

10.2.4.2 Transfer the braking forces

Initially, the braking force needs to be analyzed in x and z axis (F_x , F_z) [57] [58].

Table 10-39 Braking forces

BRAKING FORCES F_x, F_z	F_x	F_z
BRAKING FORCE ON FRONT LEFT AXLE(N)	701.2726161	701.2726161 N
BRAKING FORCE ON FRONT RIGHT AXLE(N)	701.2726161	701.2726161 N
BRAKING FORCE ON REAR LEFT AXLE(N)	525.9544621	525.9544621 N
BRAKING FORCE ON REAR RIGHT AXLE(N)	525.9544621	525.9544621 N

The vertical distance of F_z from the end of the axle is calculated as well as the vertical distance of F_x from the center of the axle.

Table 10-40 Vertical distances

$x=(\cos 45)^*0.0075 + 0.0075$	0.012803301 m	12.803301 mm
$y=(\sin 45)^*0.0075$	0.005303301 m	5.3033009 mm

F_x , F_z are transferred to the axle. The equivalent system will consist of the braking forces (F_x , F_z) plus the moments (M_{y1} , M_{y2}) that are created from the braking forces:

Table 10-41 Braking forces and moments from disc effective radius to the axle

BRAKING FORCES F_x, F_z	F_x	F_z
BRAKING FORCE ON FRONT LEFT AXLE(N)	701.2726161	701.2726161 N
BRAKING FORCE ON FRONT RIGHT AXLE(N)	701.2726161	701.2726161 N
BRAKING FORCE ON REAR LEFT AXLE(N)	525.9544621	525.9544621 N
BRAKING FORCE ON REAR RIGHT AXLE(N)	525.9544621	525.9544621 N
MOMENTS FROM DISC EFFECTIVE RADIUS TO THE AXLE	M_{y1}	M_{y2}
MOMENTS FROM BRAKING FORCE ON FRONT LEFT AXLE	3719.059667	8978.604288 Nmm
MOMENTS FROM BRAKING FORCE ON FRONT RIGHT AXL	3719.059667	8978.604288 Nmm
MOMENTS FROM BRAKING FORCE ON REAR LEFT AXLE	2789.294751	6733.953216 Nmm
MOMENTS FROM BRAKIN FORCE ON REAR RIGHT AXLE	2789.294751	6733.953216 Nmm

11 CAE / COMPUTER-AIDED ENGINEERING

Computer-aided engineering (CAE) is the use of computer software to simulate performance in order to improve product designs or assist in the resolution of engineering problems for a wide range of industries [9]. This includes simulation, validation, and optimization of products, processes, and manufacturing tools.

A typical CAE process comprises of pre-processing, solving, and post-processing steps. In the pre-processing phase, engineers model the geometry and the physical properties of the design, as well as the environment in the form of applied loads or constraints. Next, the model is solved using an appropriate mathematical formulation of the underlying physics. In the post-processing phase, the results are presented to the engineer for review.

CAE applications support a wide range of engineering disciplines or phenomena including:

- Stress and dynamics analysis on components and assemblies using finite element analysis (FEA)
- Thermal and fluid analysis using computational fluid dynamics (CFD)
- Kinematics and dynamic analysis of mechanisms (multibody dynamics)
- Mechanical event simulation (MES)
- Control systems analysis
- Simulation of manufacturing processes like casting, molding and die press forming
- Optimization of the product or process

Some engineering problems require the simulation of multiple phenomena in order to represent the underlying physics. CAE applications that address such problems are often called multi-physics solutions.

Benefits of CAE

The benefits of CAE include reduced product development cost and time, with improved product quality and durability.

- Design decisions can be made based on their impact on performance.
- Designs can be evaluated and refined using computer simulations rather than physical prototype testing, saving money and time.
- CAE can provide performance insights earlier in the development process, when design changes are less expensive to make.
- CAE helps engineering teams manage risk and understand the performance implications of their designs.
- Integrated CAE data and process management extends the ability to effectively leverage performance insights and improve designs to a broader community.
- Warranty exposure is reduced by identifying and eliminating potential problems. When properly integrated into product and manufacturing development, CAE can enable ear-

lier problem resolution, which can dramatically reduce the costs associated with the product lifecycle.

11.1 FEA / Finite element analysis

Finite element analysis (FEA) is the modeling of products and systems in a virtual environment, for the purpose of finding and solving potential (or existing) structural or performance issues [59] [9]. FEA is the practical application of the finite element method (FEM), which is used by engineers and scientist to mathematically model and numerically solve very complex structural, fluid, and multiphysics problems. FEA software can be utilized in a wide range of industries, but is most commonly used in the aeronautical, biomechanical and automotive industries.

A finite element (FEA) model comprises a system of points, called “nodes”, which form the shape of the design. Connected to these nodes are the finite elements themselves which form the finite element mesh and contain the material and structural properties of the model, defining how it will react to certain conditions. The density of the finite element mesh may vary throughout the material, depending on the anticipated change in stress levels of a particular area. Regions that experience high changes in stress usually require a higher mesh density than those that experience little or no stress variation. Points of interest may include fracture points of previously tested material, fillets, corners, complex detail, and high-stress areas.

FE models can be created using one-dimensional (1D beam), two-dimensional (2D shell) or three-dimensional (3D solid) elements. By using beams and shells instead of solid elements, a representative model can be created using fewer nodes without compromising accuracy. Each modeling scheme requires a different range of properties to be defined, such as:

- Section areas
- Moments of inertia
- Torsional constant
- Plate thickness
- Bending stiffness
- Transverse shear

The triangles (trias) and squares (quads) are the simplest elements used with two degrees of freedom per node (node). Adding and other nodes on the edges or in the center the curves and the fronts modeled best. Three dimensional models are: the isoparametric triangles, tetrahedra and hexahedrons.

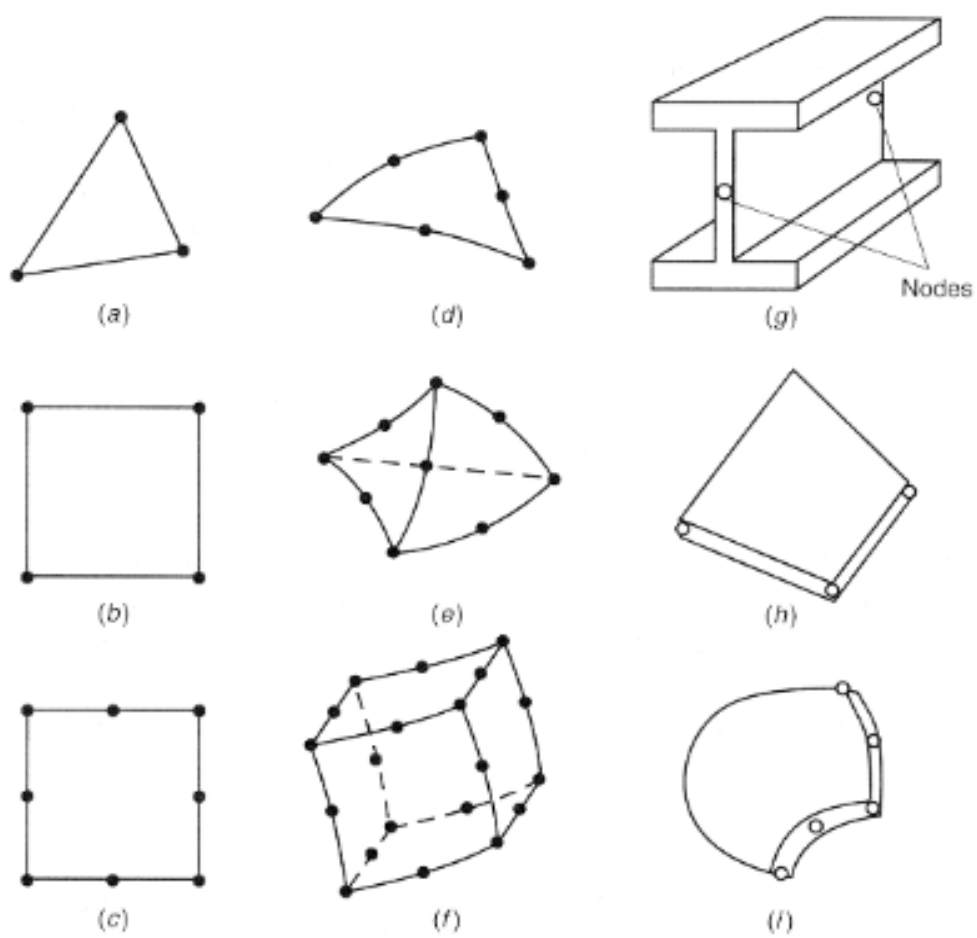


Figure 11-1 Common element types used for meshing. [30]

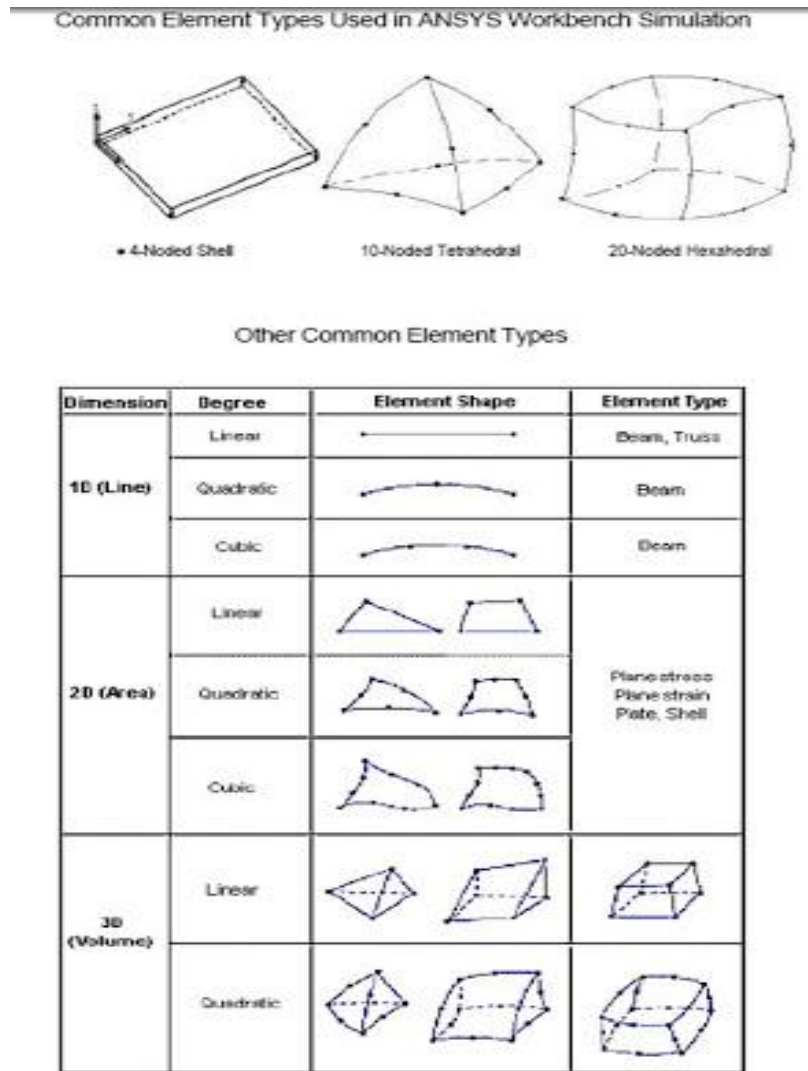


Figure 11-2 Common Element Types Used in ANSYS Workbench Simulation [60]

To simulate the effects of real-world working environments in FEA, various load types can be applied to the FE model, including:

- Nodal: forces, moments, displacements, velocities, accelerations, temperature and heat flux
- Elemental: distributed loading, pressure, temperature and heat flux
- Acceleration body loads (gravity)

Types of analysis include:

- Linear statics: linear analysis with applied loads and constraints that are static
- Nonlinear statics and dynamics: effects due to contact (where one part of the model comes into contact with another), nonlinear material definitions (plasticity, elasticity, etc.) and large displacement (strains that exceed small displacement theory that limits a linear analysis approach)
- Normal modes: natural frequencies of vibration
- Dynamic response: loads or motions that vary with time and frequency
- Buckling: critical loads at which a structure becomes unstable

- Heat transfer: conduction, radiation and phase change

Typical results calculated by the solver include:

- Nodal displacements, velocities and accelerations
- Elemental forces, strains and stresses

Benefits of FEA

FEA can be used in new product design, or to refine an existing product, to ensure that the design will be able to perform to specifications prior to manufacturing. With FEA you can:

- Predict and improve product performance and reliability
- Reduce physical prototyping and testing
- Evaluate different designs and materials
- Optimize designs and reduce material usage

11.2 Theories of failure

Some of them are:

- Maximum Normal Stress Theory
- Maximum Shear Stress Theory
- Von Mises effective stress

Maximum Normal Stress Theory

$$\sigma_1 > \sigma_2$$

Failure occurs when one of the three principal stresses reaches a permissible strength (TS). Failure is predicted to occur when $\sigma_1 = S_t$ and $\sigma_2 < -S_c$. Where S_t and S_c are the tensile and compressive strength. For a biaxial state of stresses

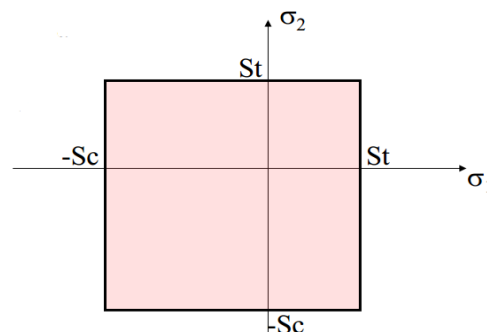
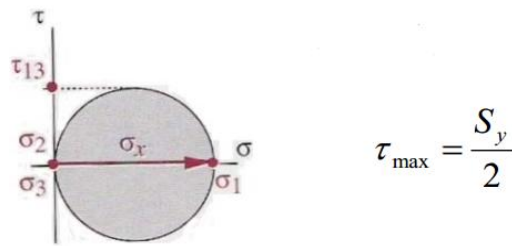


Figure 11-3 Maximum Normal Stress Theory

Maximum Shear Stress Theory

Failure occurs when the maximum shear stress in the part exceeds the shear stress in a tensile test specimen (of the same material) at yield. Hence in a tensile test,



For a general state of stresses:

$$\tau_{\max} = \frac{\sigma_1 - \sigma_3}{2} = \frac{S_y}{2}$$

This leads to a hexagonal failure envelop. A stress system in the interior of the envelop is considered safe.

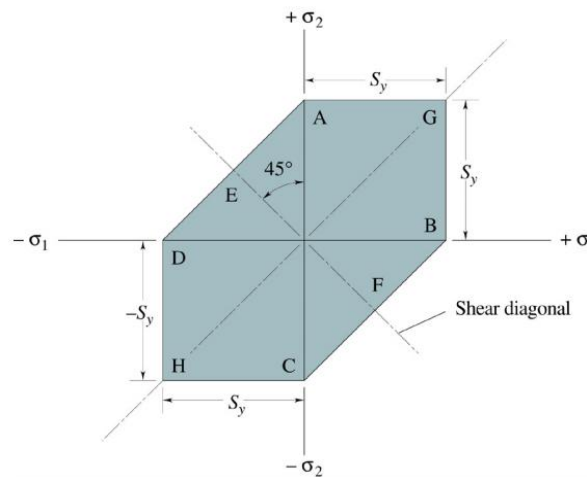


Figure 11-4 Maximum Shear Stress Theory

for design purposes, the failure relation can be modified to include a factor of safety (n):

$$n = \frac{S_y}{\sigma_1 - \sigma_3}$$

Von Mises effective stress

Defined as the uniaxial tensile stress that creates the same distortion energy as any actual combination of applied stresses.

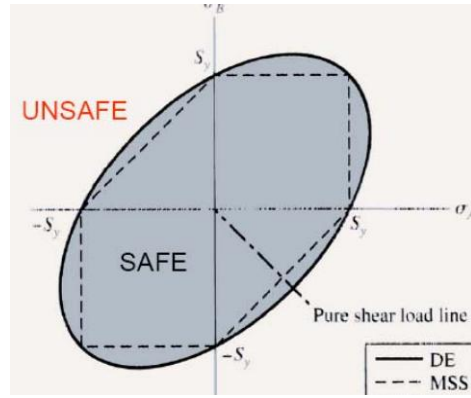


Figure 11-5 Von Mises effective stress

This simplifies the approach since we can use the following failure criterion:

$$\sigma_{VM} \geq S_y$$

$$n = \frac{S_y}{\sigma_{VM}}$$

$$\sigma_{VM} = \sqrt{\frac{(\sigma_x - \sigma_y)^2 + (\sigma_y - \sigma_z)^2 + (\sigma_z - \sigma_x)^2 + 6(\tau_{xy}^2 + \tau_{yz}^2 + \tau_{zx}^2)}{2}}$$

$$\sigma_{VM} = \sqrt{\sigma_x^2 + \sigma_y^2 + \sigma_z^2 - \sigma_x\sigma_y - \sigma_y\sigma_z - \sigma_z\sigma_x + 3\tau_{xy}^2 + 3\tau_{yz}^2 + 3\tau_{zx}^2}$$

11.3 Modelling (Pre-processing)

In this thesis the BETA–CAE systems’ suite was used. The ANSA software, which is the preprocessor of the suite, was applied. This software was employed for the preparation of the model. The ANSYS software was used as the solver, which was developed from the Livermore Software Technology Corporation (LSTC) ANSYS. The ANSYS solver is deemed one of the most specialized of softwares available on the market today [60].

The pre-processor of ANSA is considered as one of the most suitable packages both for the mesh construction, due to its high quality, and its user friendly interface of the software.

To begin with, we insert the appropriate file which was designed with the aid of the Pro Engineer software. The ANSA software embeds a CAD-Translator for almost every commercial software package, making the introduction process of the current CAD file from Pro-Engineer WF5 an easy task.

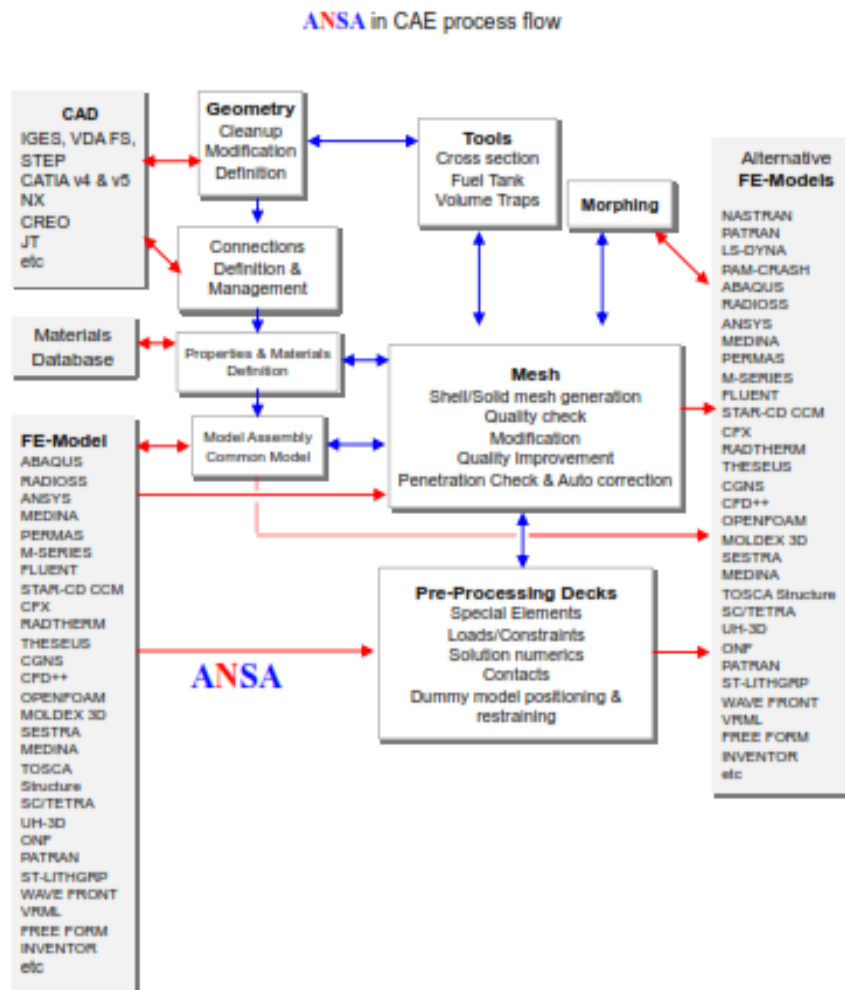


Figure 11-6 Ansa in CAE process flow [61]

11.3.1 Carbon fiber monocoque chassis

Parts

By using different colours we are able to distinguish the 14 different parts of which the carbon fiber monocoque chassis consists.

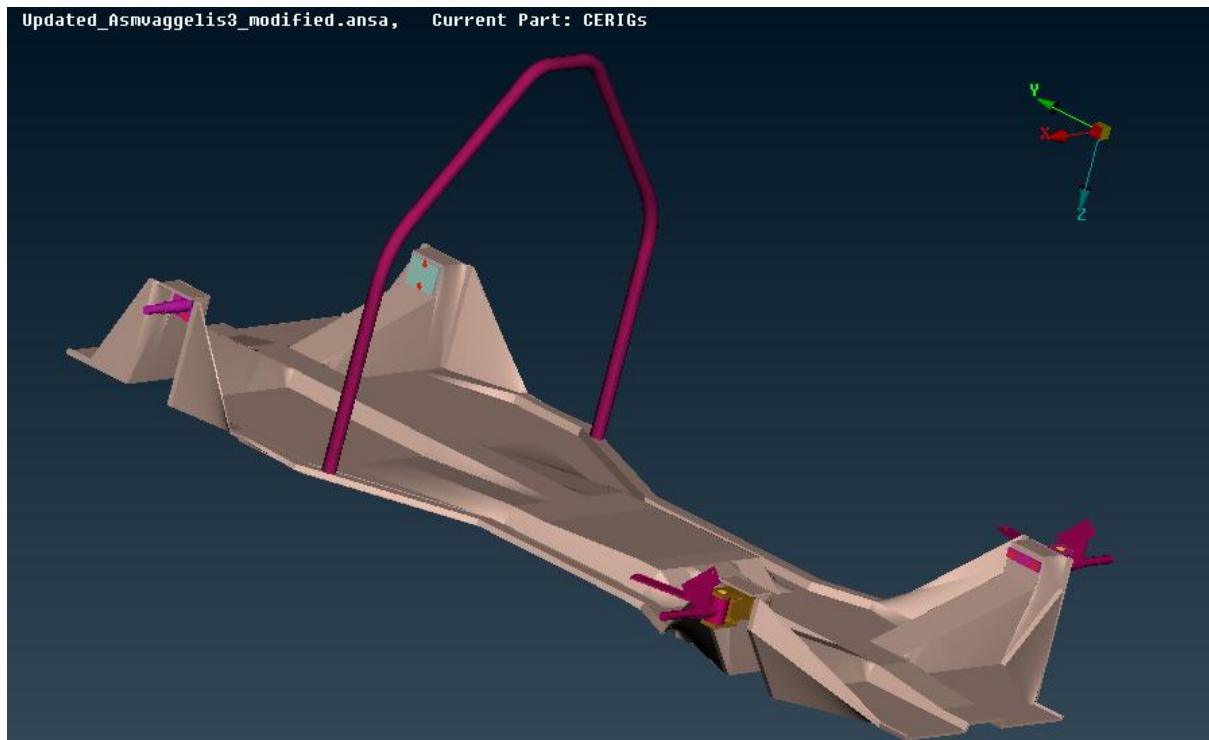


Figure 11-7 Carbon Fiber Monocoque Chassis' Parts (View 1)

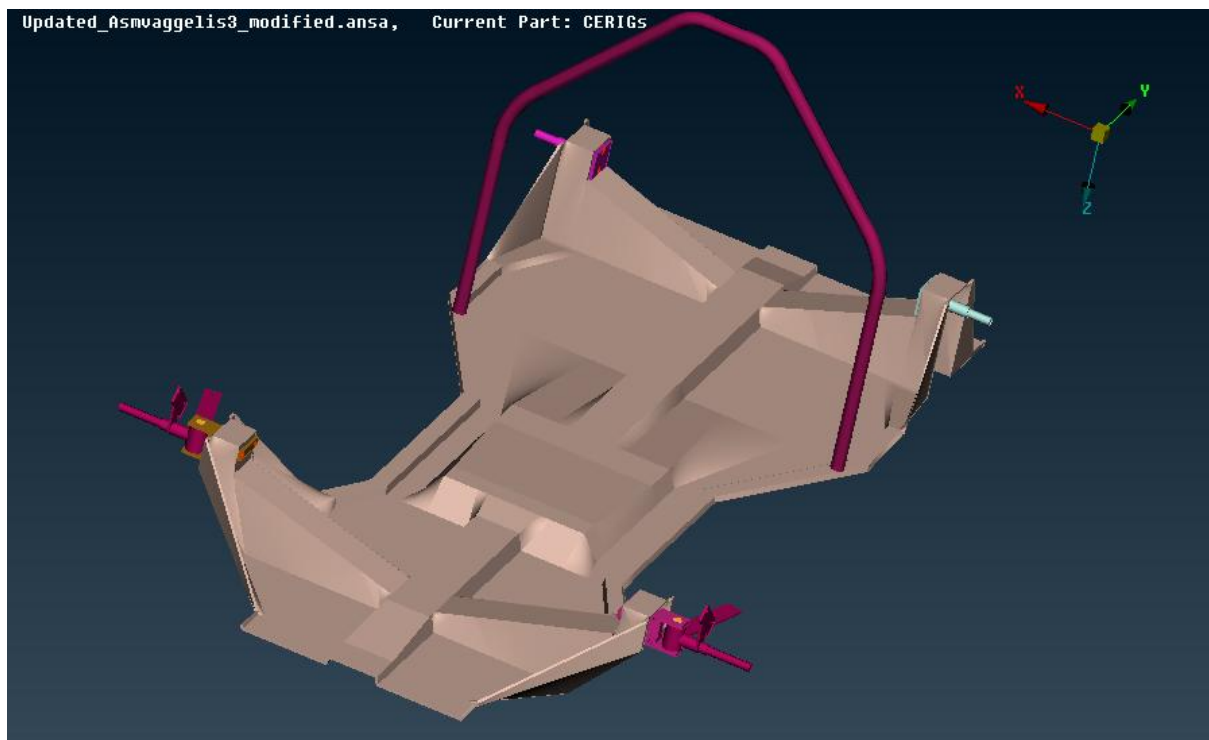


Figure 11-8 Carbon Fiber Monocoque Chassis' Parts (View 2)

11.3.1.1 Clean geometry

By importing the file from Pro-engineer to ANSA, the ANSA software locates geometry problems on some faces (which appear in yellow colour). The next task is to fix them.

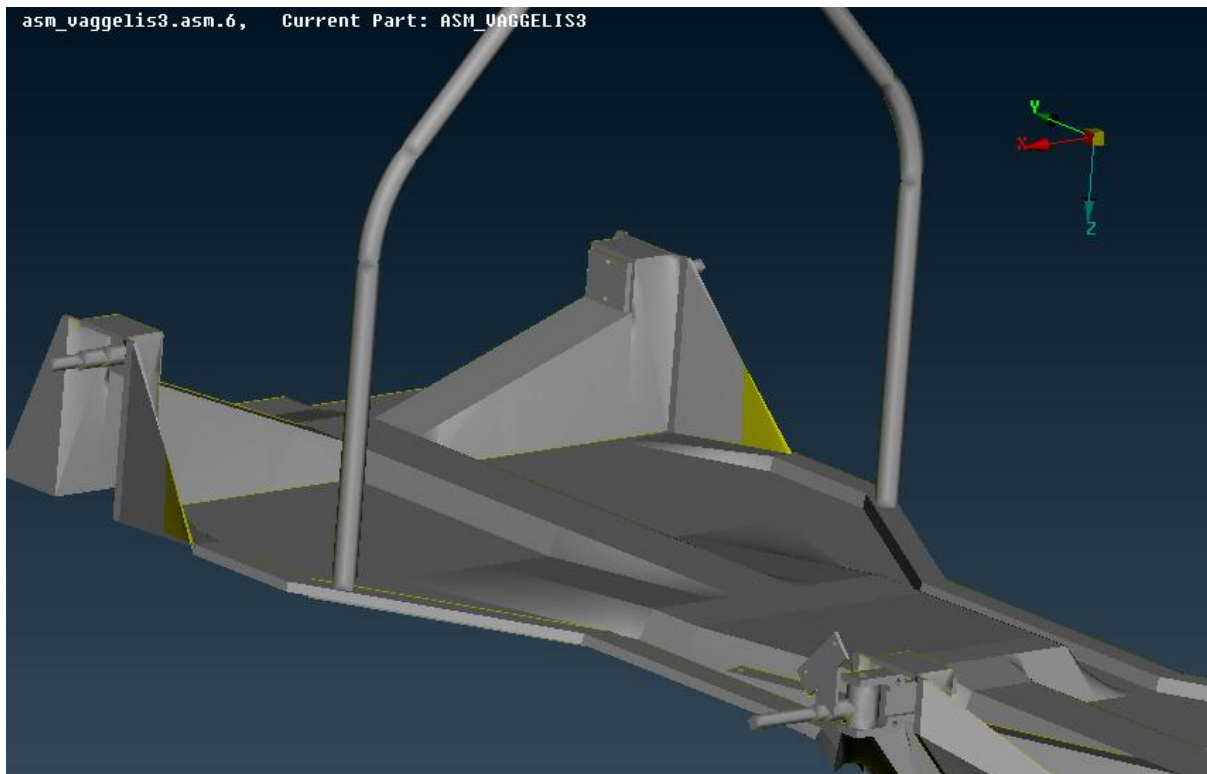


Figure 11-9 Face Problem (View 1)

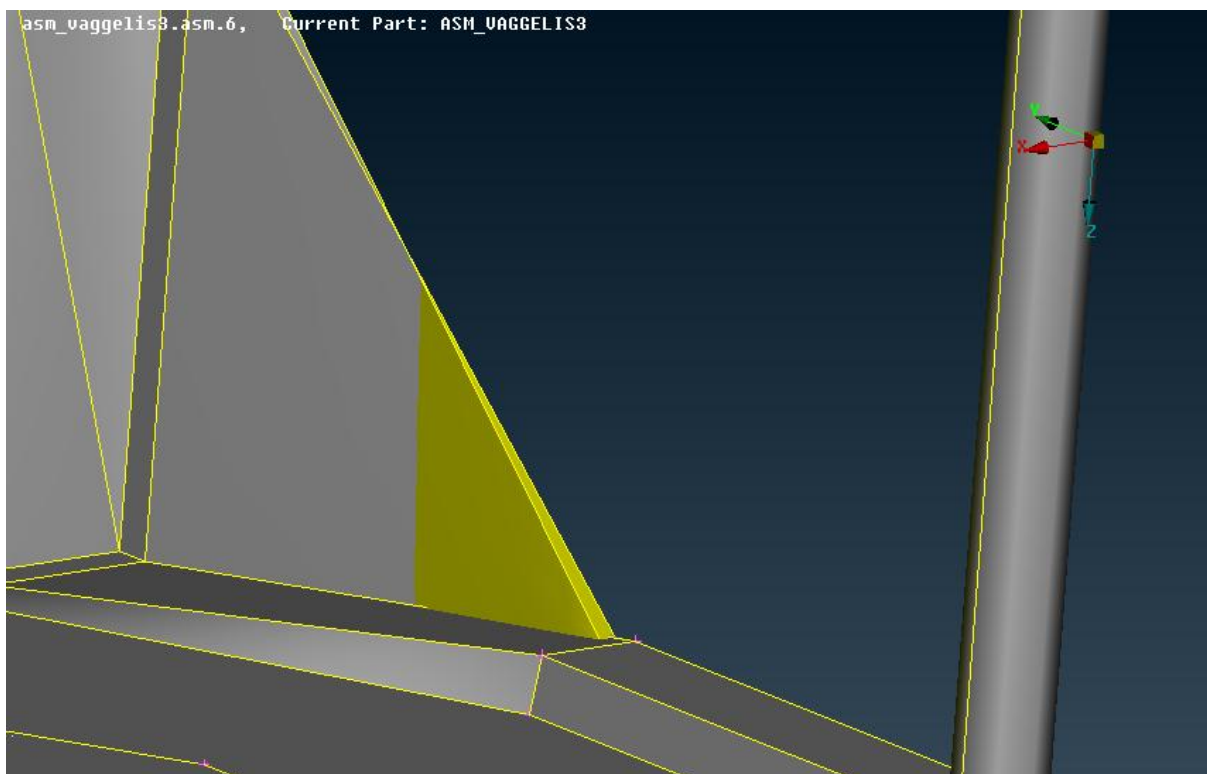


Figure 11-10 Face Problem (View 2)

As can be seen in Figure 11-10, the two faces are intersecting. This is a design error which occurred during the designing process with the pro engineer software. In order to fix it, we must redesign the chassis.

After the re-design process, we observe that the geometry is fixed, and there is no yellow colour any more:

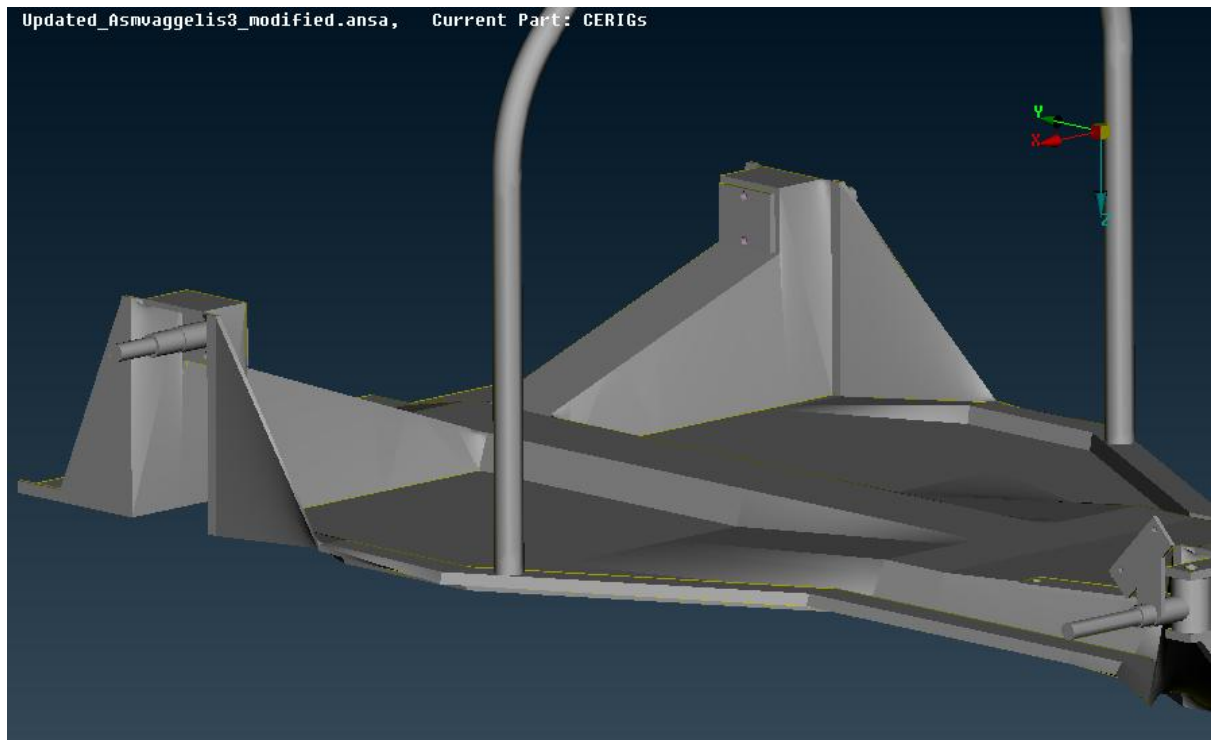


Figure 11-11 Redesign the monocoque to encounter the face problem (View 1)

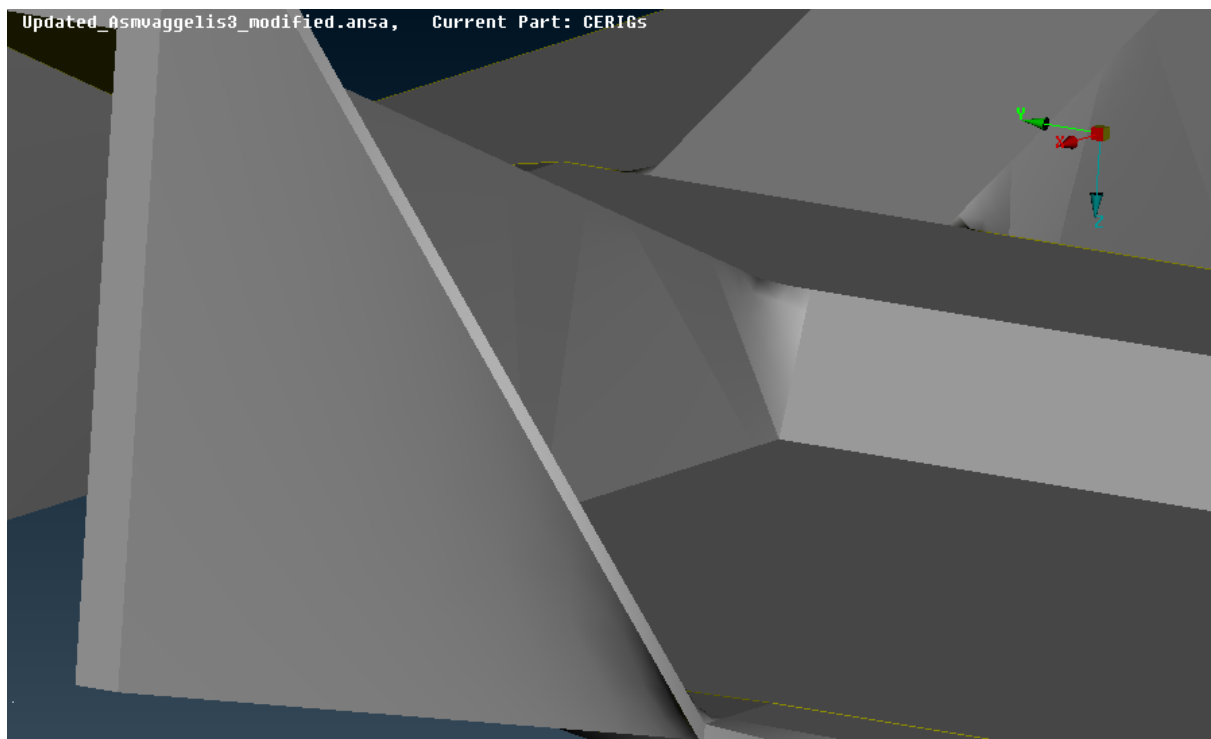


Figure 11-12 Redesign the monocoque to encounter the face problem (View 2)

Geometry check

The next step is to perform a geometry check which will allow us to see if there are any more errors.

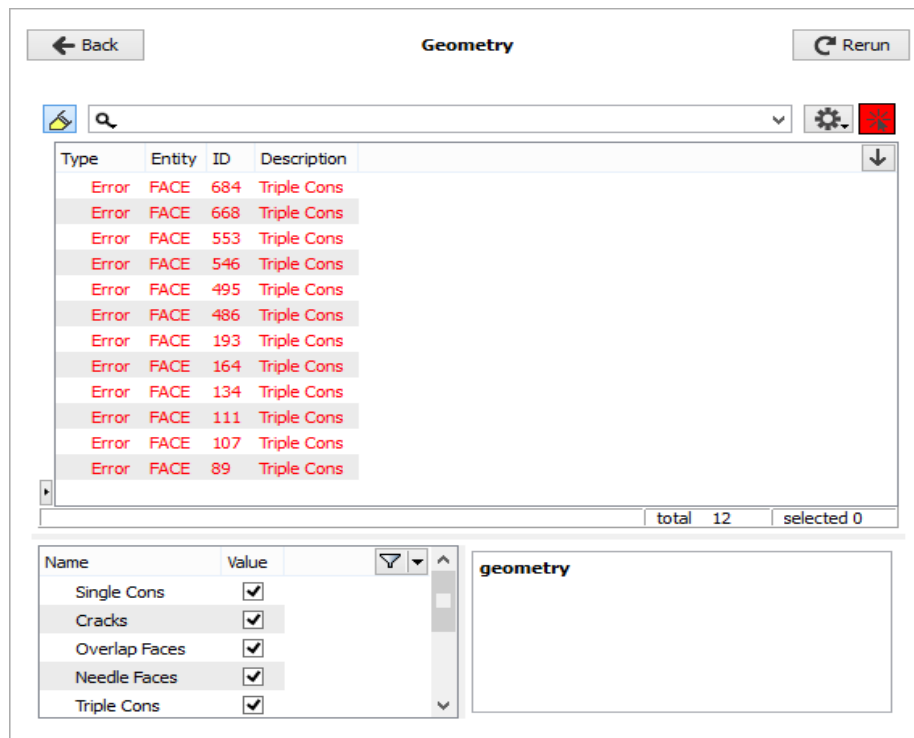


Figure 11-13 Geometry check

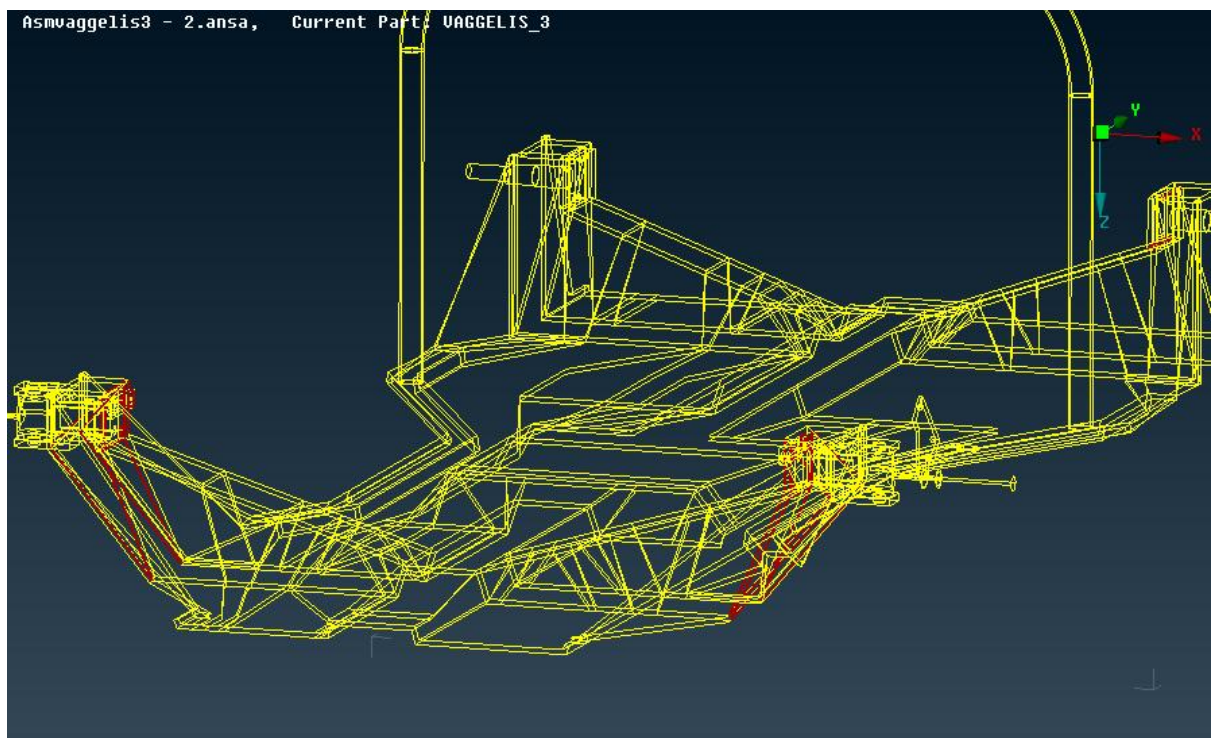


Figure 11-14 Geometry Check on the Monocoque Chassis

Any triple cons errors (cyan in colour) can be observed below.

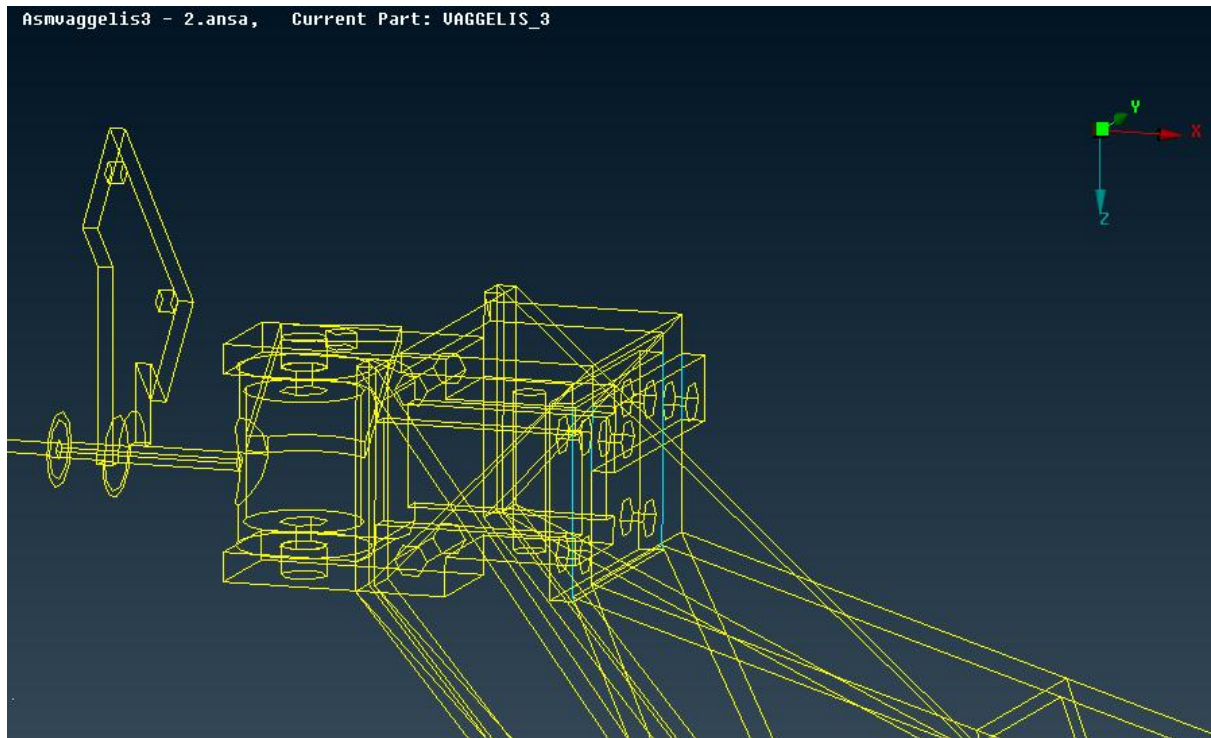


Figure 11-15 Triple Cons on the Monocoque (View 1)

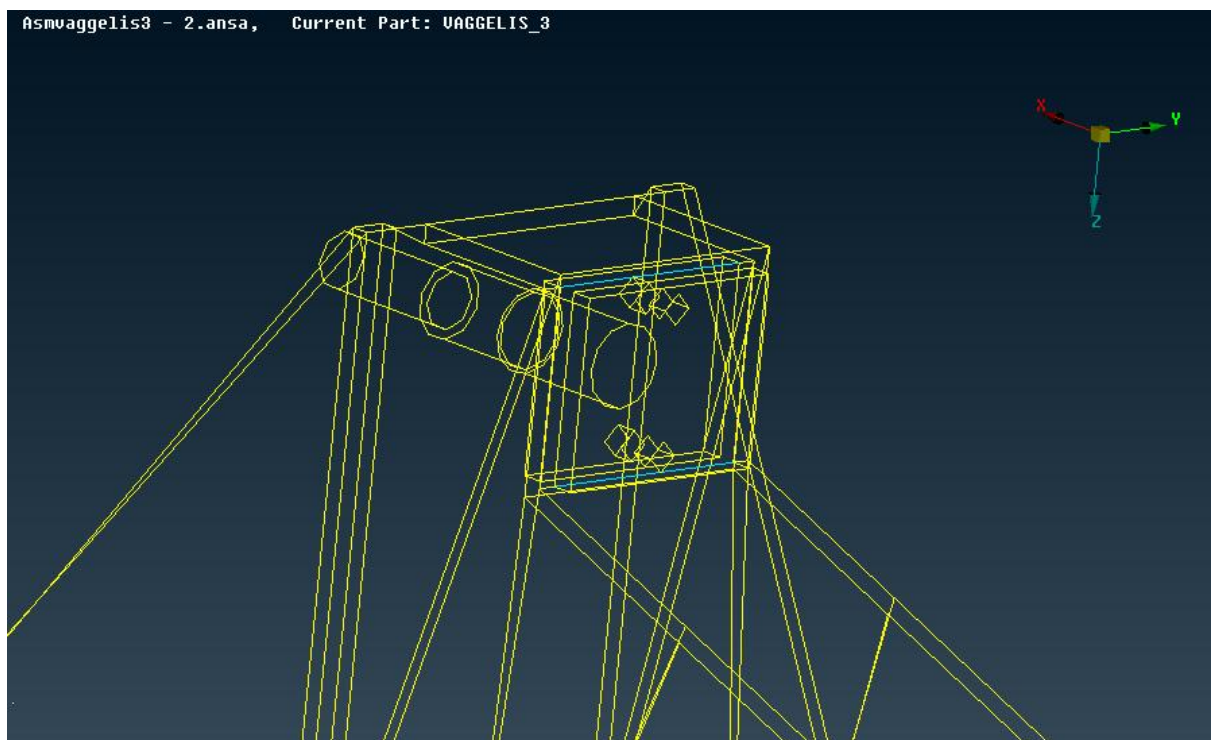


Figure 11-16 Triple Cons on the Monocoque (View 2)

Fix geometry

The geometry errors have been fixed and as a result there are no triple cons errors (cyan in colour) anymore.

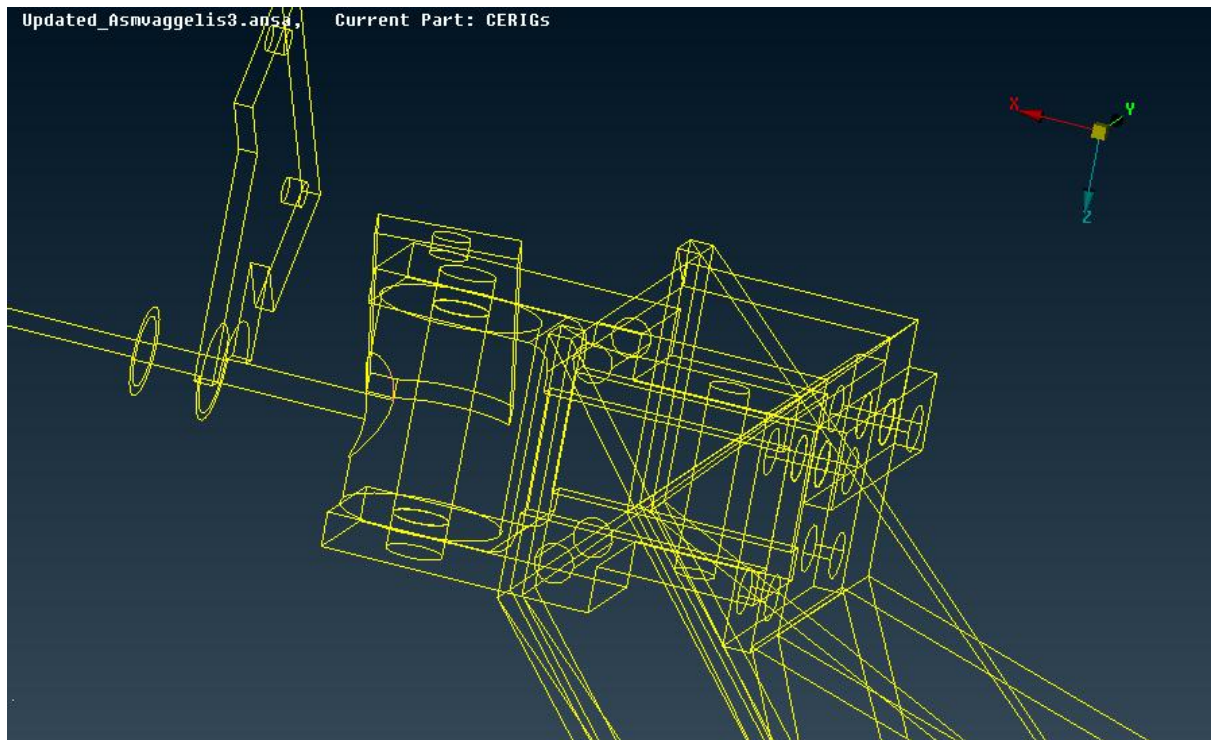


Figure 11-17 Geometry on the Monocoque Fixed (View 1)

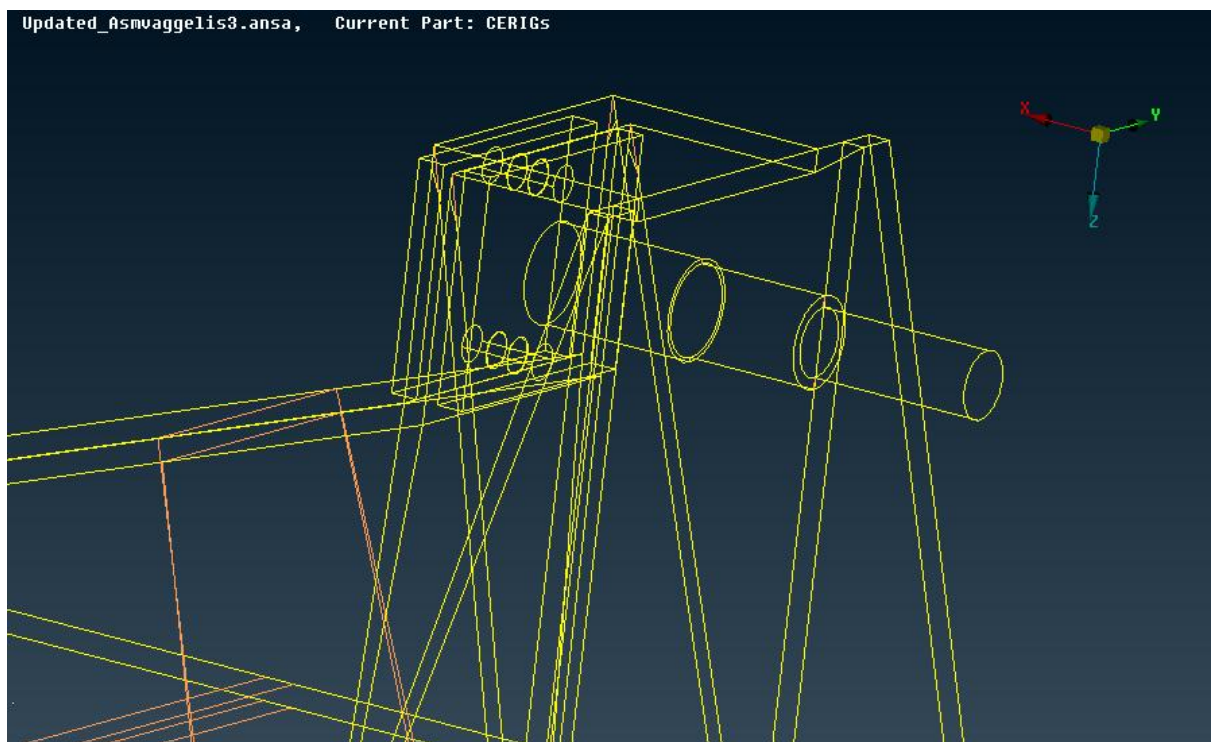


Figure 11-18 Geometry on the Monocoque Fixed (View 2)

Penetration: Intersections check

Following this, the next step is to run a test in order to locate any possible intersections in our model.

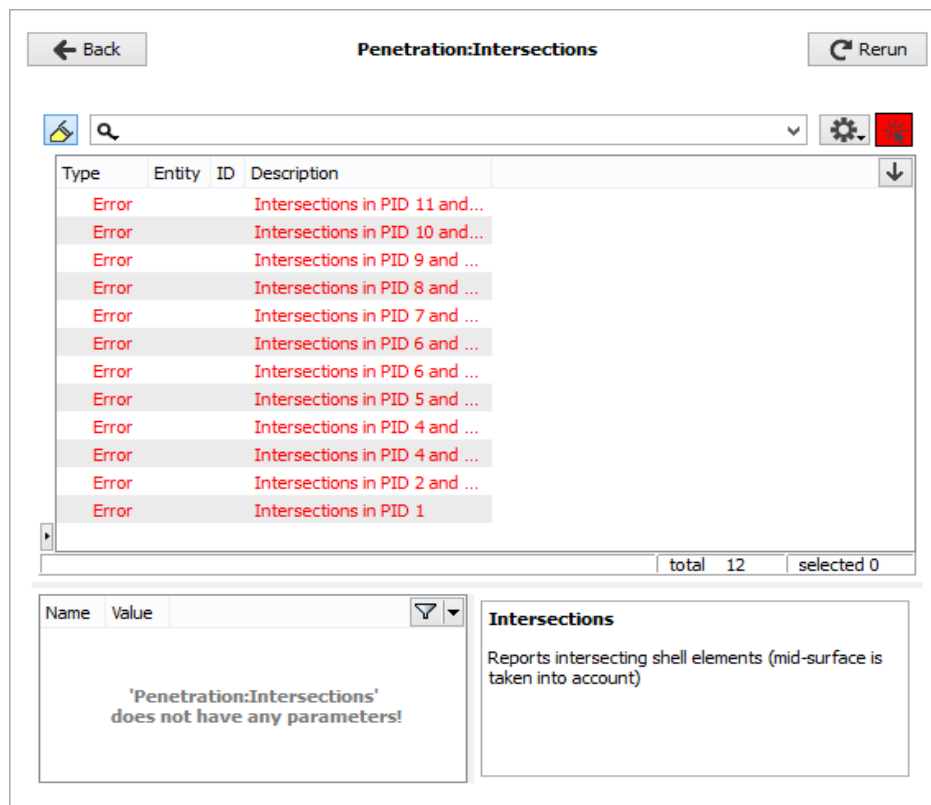


Figure 11-19 Penetration-Intersections check

There are some intersections (red in colour) which can be seen in the figure below (Figure 11-20).

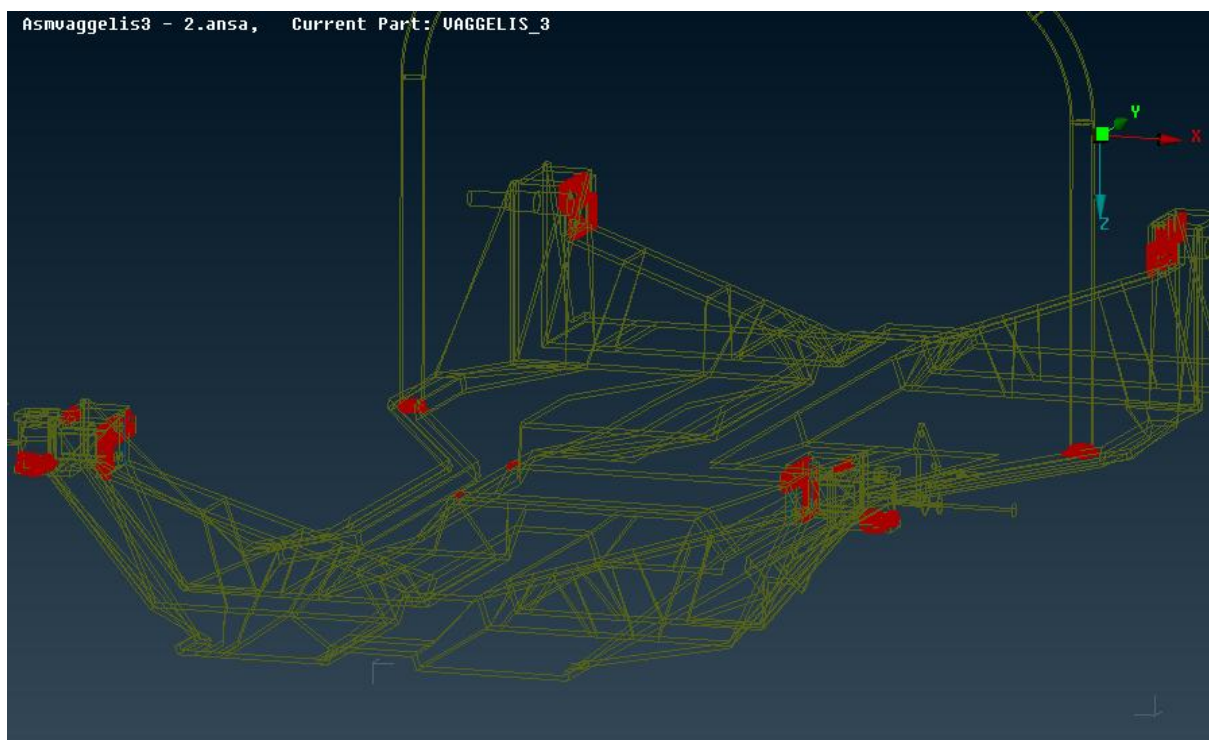


Figure 11-20 Intersections Check on the Monocoque

Fix intersections

The intersections are fixed and this is observed by the absence of the red colour.

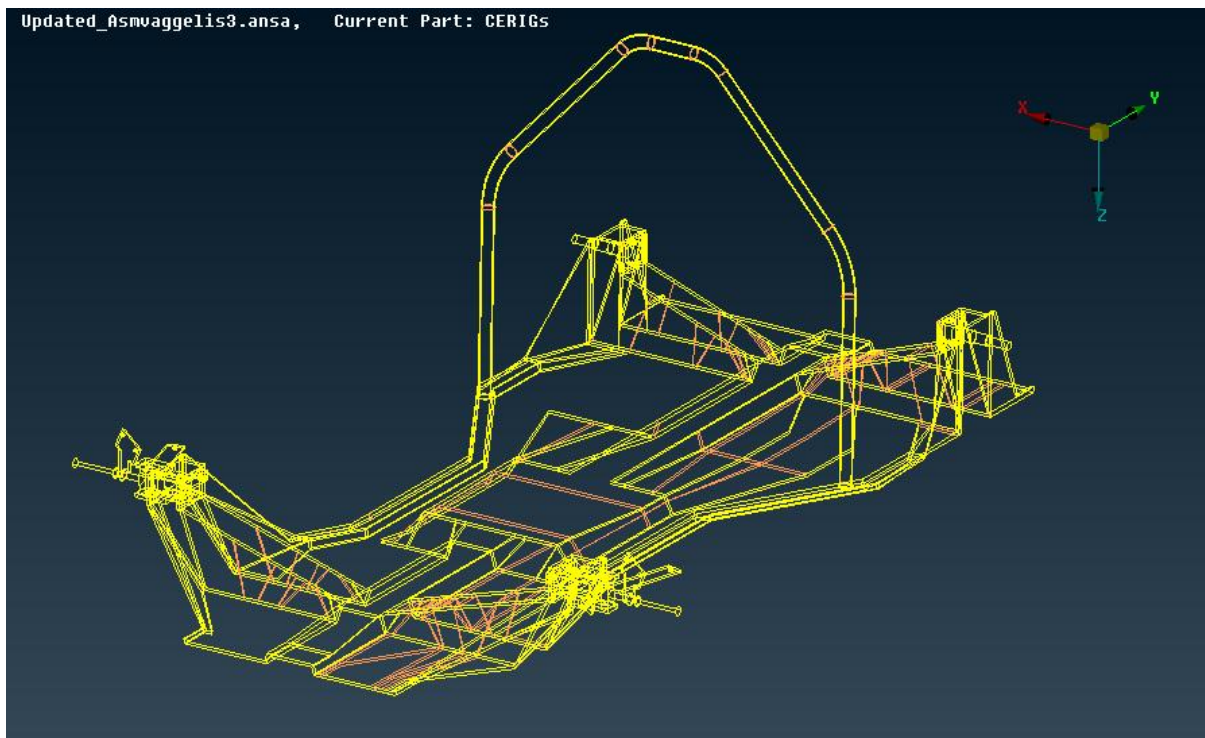


Figure 11-21 Intersections on the Monocoque Fixed

11.3.1.2 Properties and materials definition

First, the chassis materials are defined and then presented in different colours.

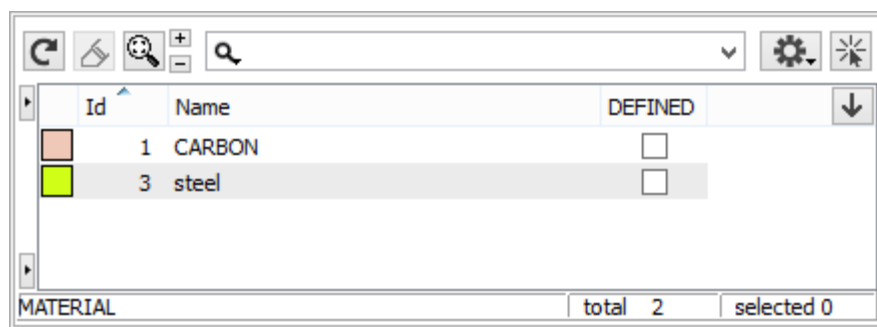


Figure 11-22 Materials definition

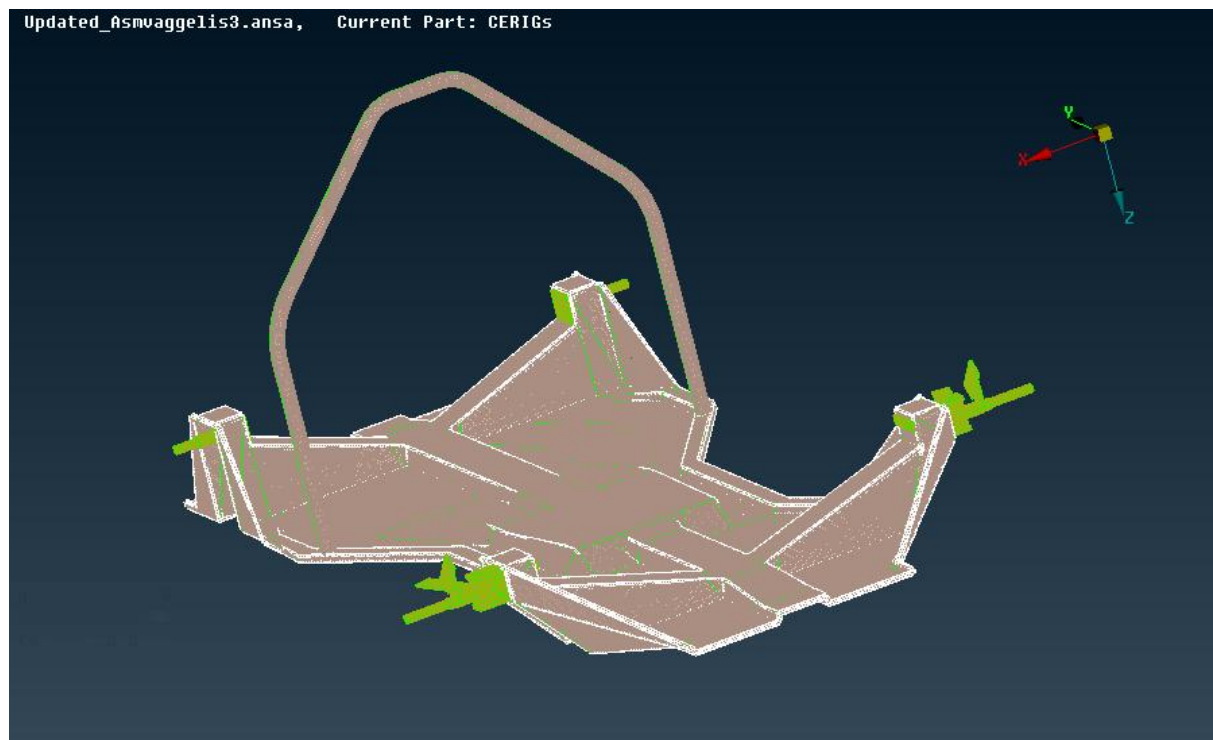


Figure 11-23 Material Definition on the Monocoque Chassis

Then, the carbon fiber characteristics are inserted into the following form. The same is done for the steel characteristics in a similar form.

Name

FROZEN_ID FROZEN_DELETE DEFINED

MATID

EX <input type="text"/>	EY <input type="text"/>	EZ <input type="text"/>	PRXY <input type="text"/>
PRYZ <input type="text"/>	PRXZ <input type="text"/>	NUXY <input type="text"/>	NUYZ <input type="text"/>
NUJZ <input type="text"/>	GXY <input type="text"/>	GYZ <input type="text"/>	GXZ <input type="text"/>
ALPX <input type="text"/>	ALPY <input type="text"/>	ALPZ <input type="text"/>	REFT <input type="text"/>
MU <input type="text"/>	DAMP <input type="text"/>	DENS <input type="text"/>	KXX <input type="text"/>
KY <input type="text"/>	KZZ <input type="text"/>	C <input type="text"/>	ENTH <input type="text"/>
HF <input type="text"/>	EMIS <input type="text"/>	QRATE <input type="text"/>	VISC <input type="text"/>
SONC <input type="text"/>	MURX <input type="text"/>	MURY <input type="text"/>	MURZ <input type="text"/>
MGXX <input type="text"/>	MGY <input type="text"/>	MGZZ <input type="text"/>	RSVX <input type="text"/>
RSVY <input type="text"/>	RSVZ <input type="text"/>	PERX <input type="text"/>	PERY <input type="text"/>
PERZ <input type="text"/>	LSST <input type="text"/>		

OK ColorEdit Cancel

Figure 11-24 Properties definition

11.3.1.3 Meshing

Inside the software, in the field of Mesh Parameters, the maximum and the minimum dimension of the mesh is assigned as 5mm and 3mm respectively. This choice is derived from the need to include a great number of elements inside the mesh. It is also important to mention that the Meshing Scenario of ANSA is created in every single part separately. There are several images below which show the mesh that was created. Additionally, inside these images several characteristics of some areas of the chassis design are depicted in order to make the creation of the mesh more comprehensible. For the creation of the mesh, the command of Shell Mesh was used. With the Shell Mesh com-

mand, an initial mesh at the surfaces of the solid was able to be constructed. Then, by using the already created surface mesh as a base, the volume mesh was derived by the Mesh Volume command.

11.3.1.3.1 Shell meshing

In the beginning, we apply shell meshing to the model. The mesh's density is higher in the highlighted areas compared to the rest of the model.

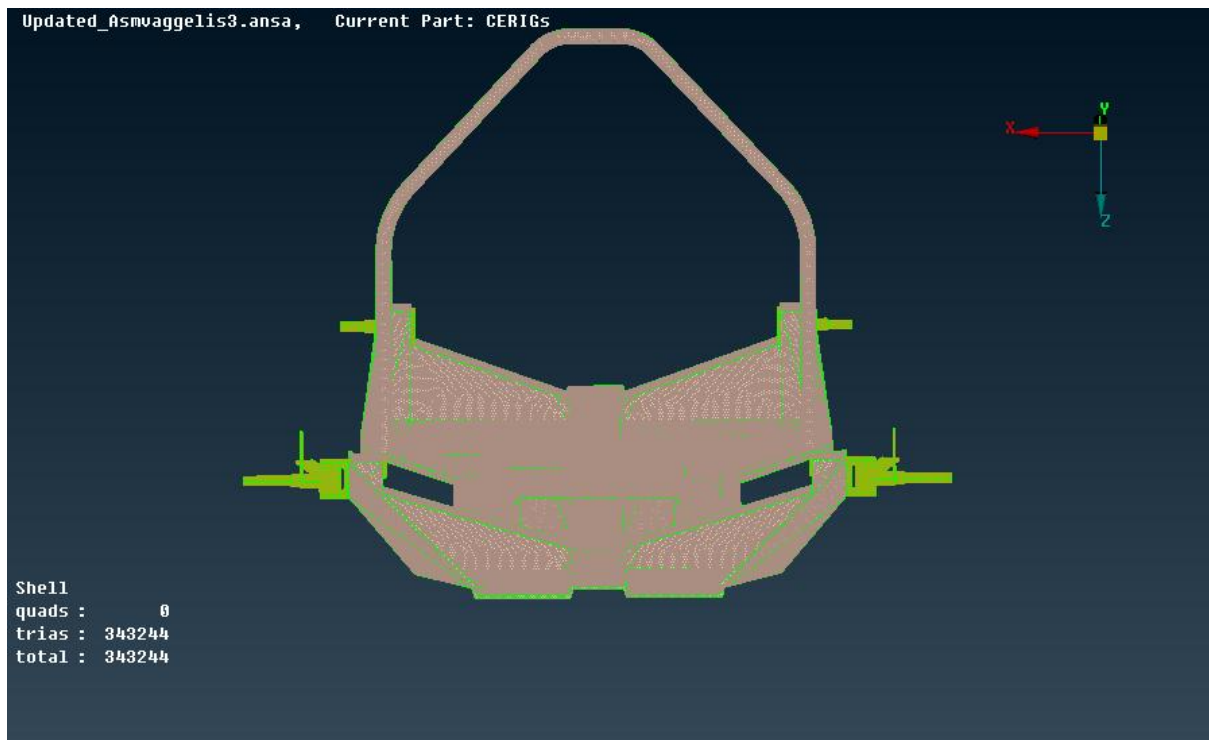


Figure 11-25 Shell Mesh on the Monocoque Chassis

11.3.1.3.2 Volume meshing

The next step is to perform volume meshing. In the following images we observe the volume mesh of our model and its density, as mentioned above.

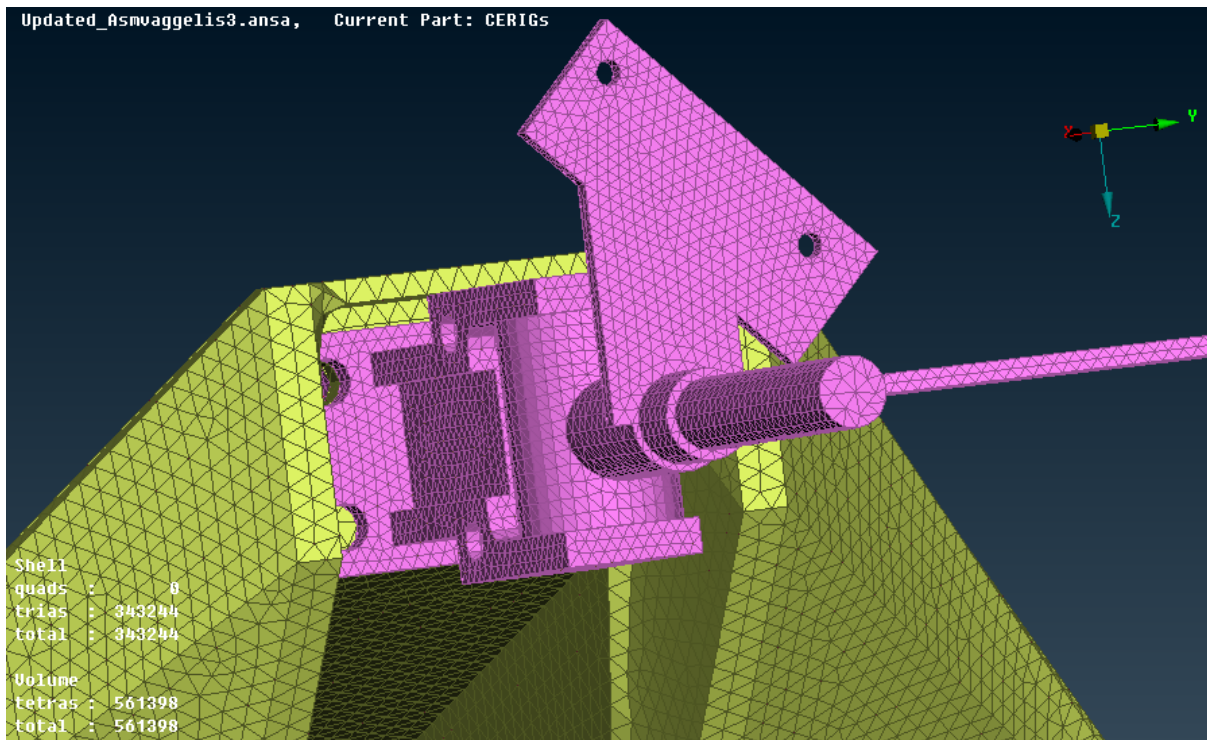


Figure 11-26 Volume Mesh on the Monocoque Chassis (View 1)

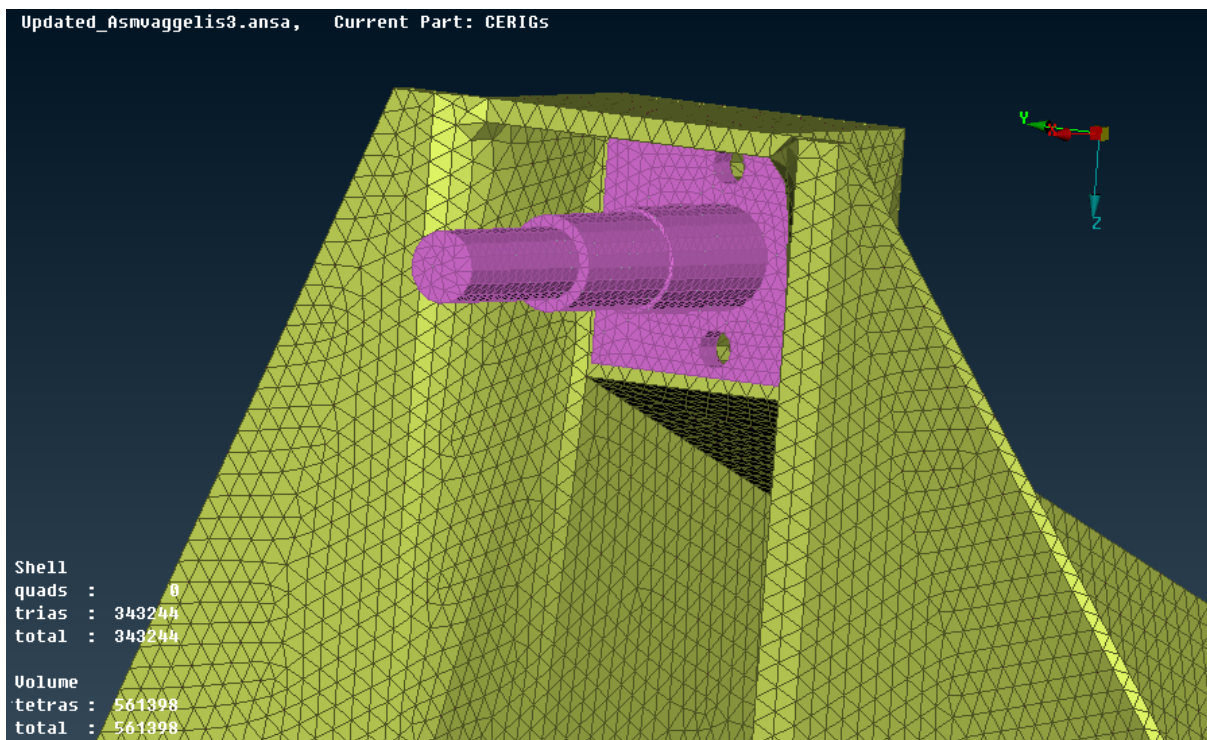


Figure 11-27 Volume Mesh on the Monocoque Chassis (View 2)

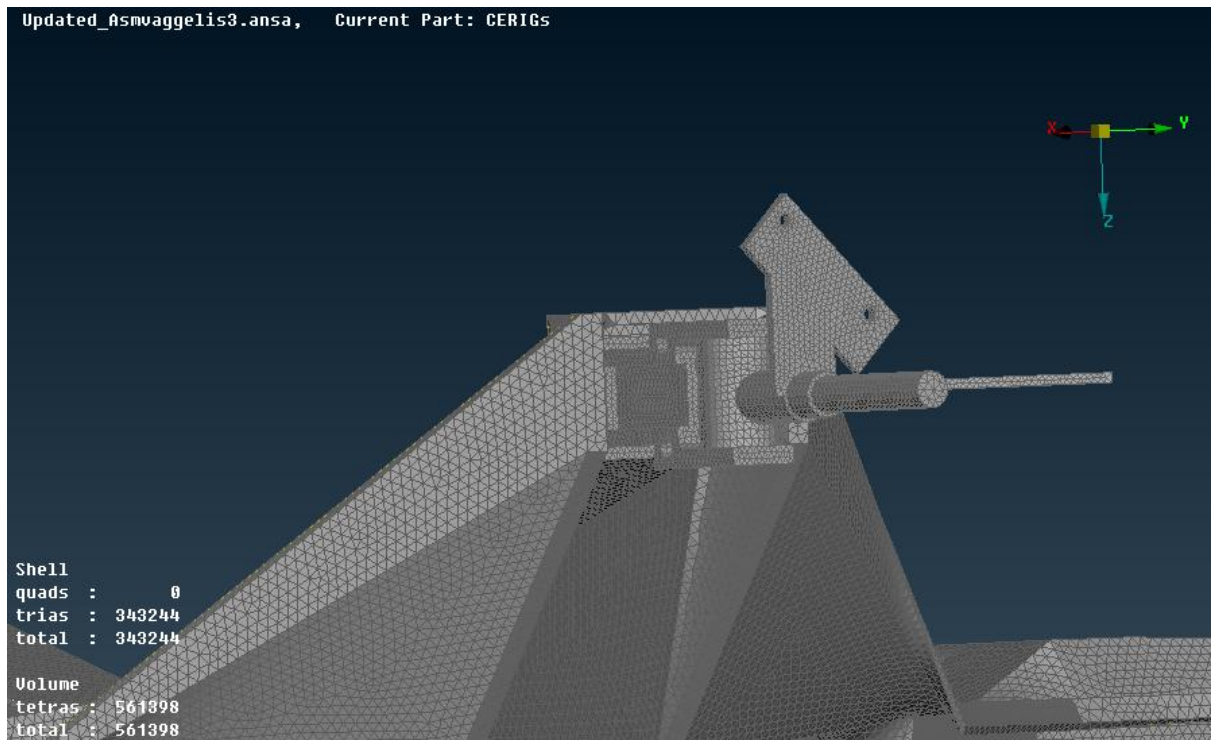


Figure 11-28 Volume Mesh on the Monocoque Chassis (View 3)

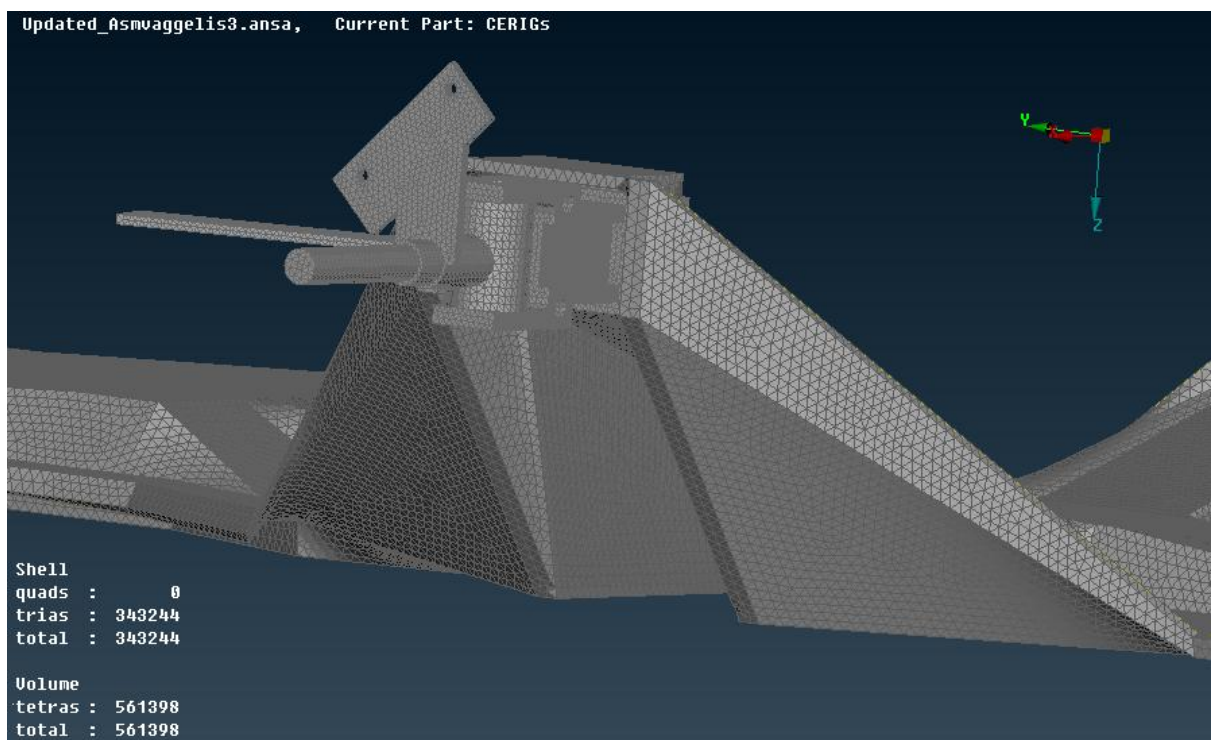


Figure 11-29 Volume Mesh on the Monocoque Chassis (View 4)

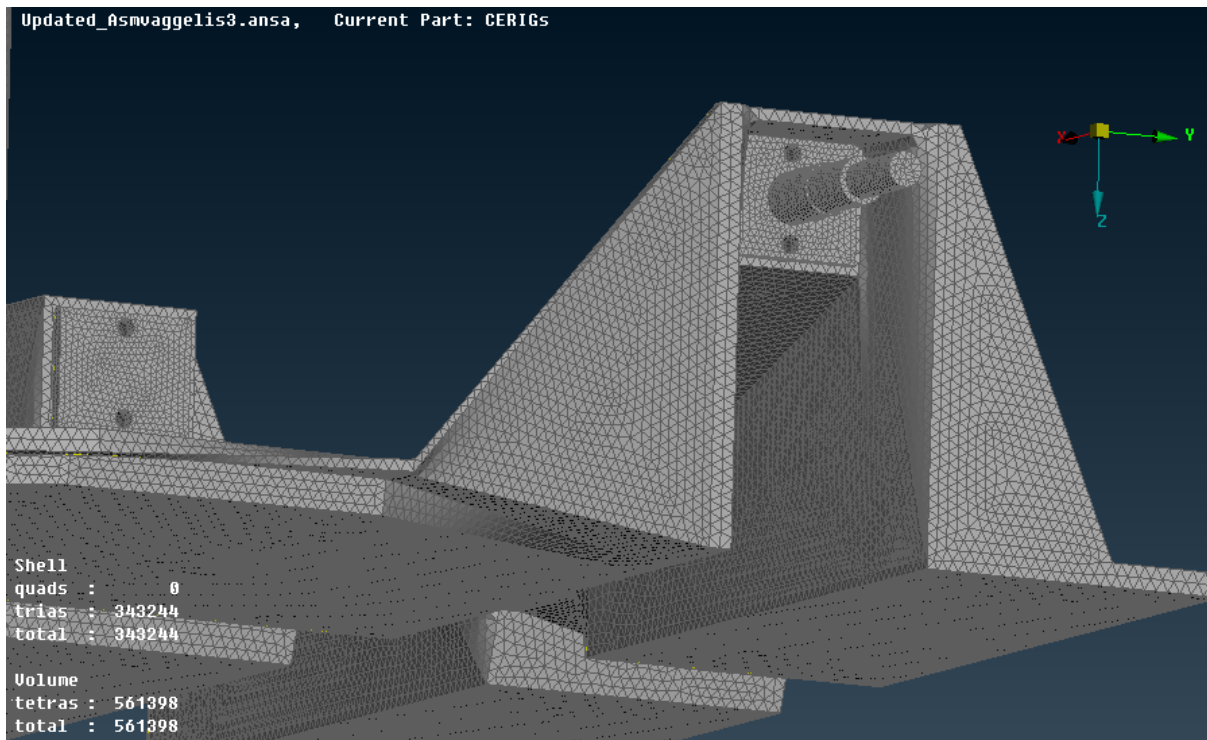


Figure 11-30 Volume Mesh on the Monocoque Chassis (View 5)

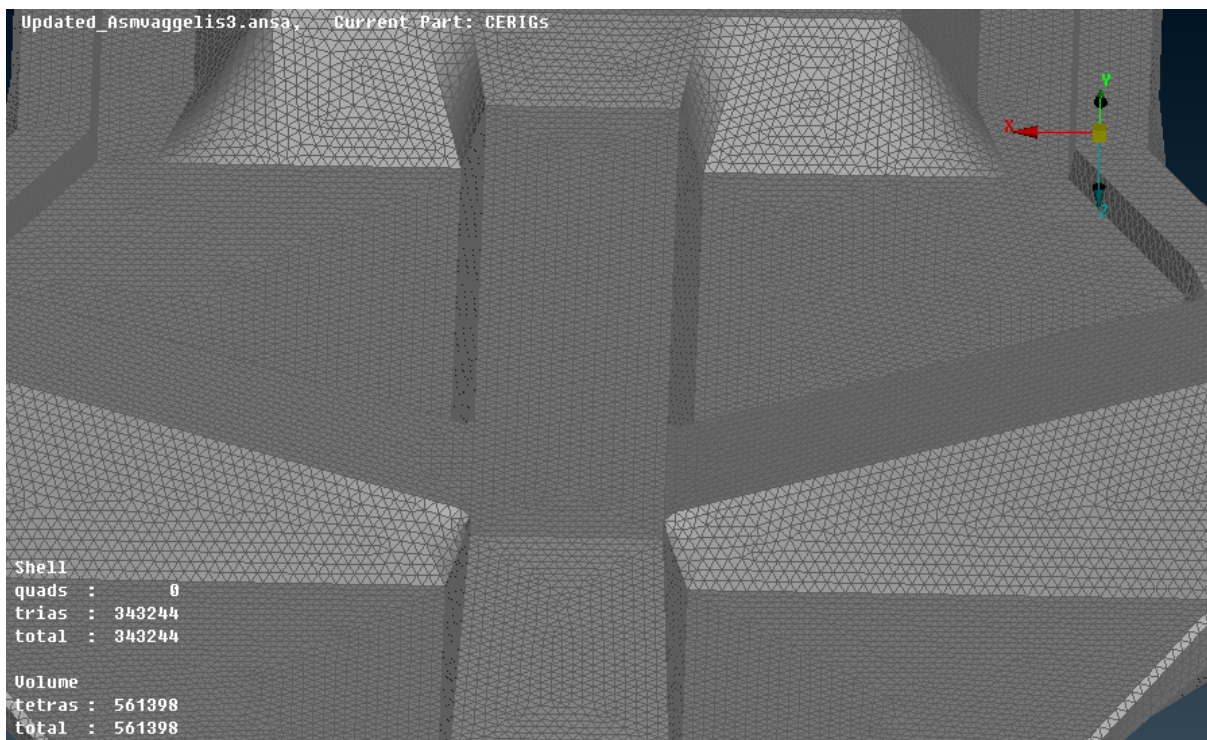


Figure 11-31 Volume Mesh on the Monocoque Chassis (View 6)

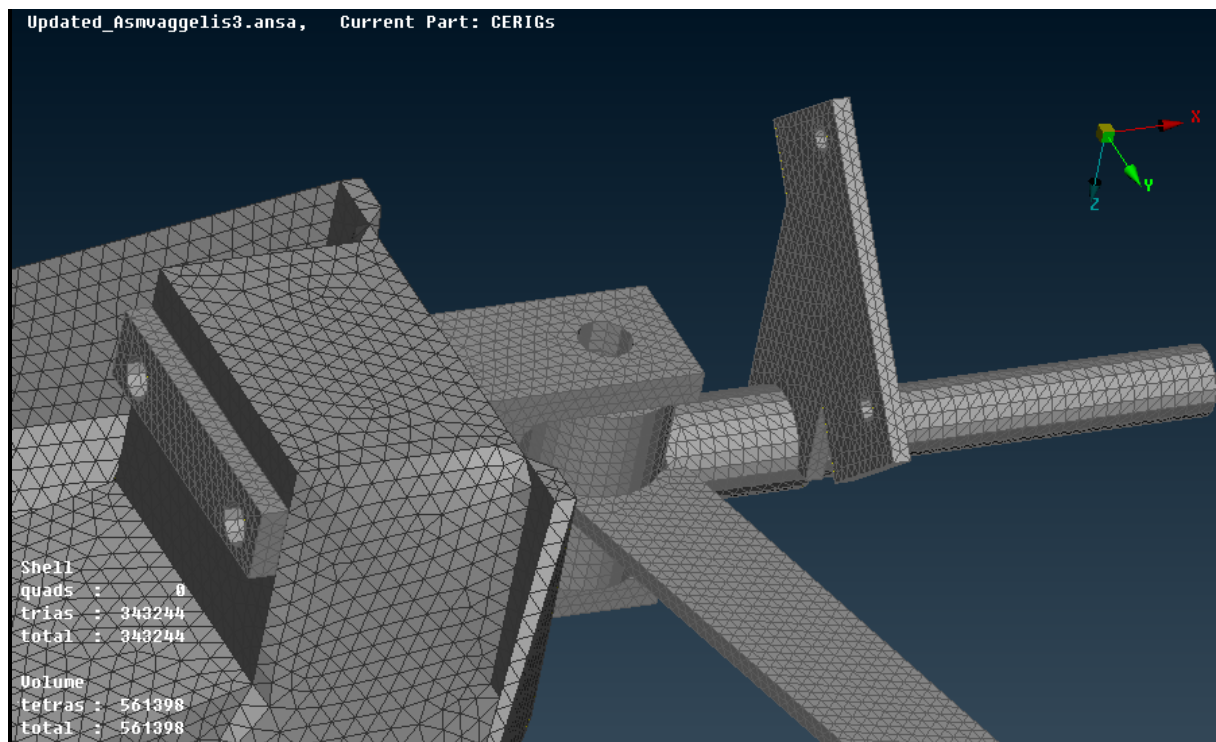


Figure 11-32 Volume Mesh on the Monocoque Chassis (View 7)

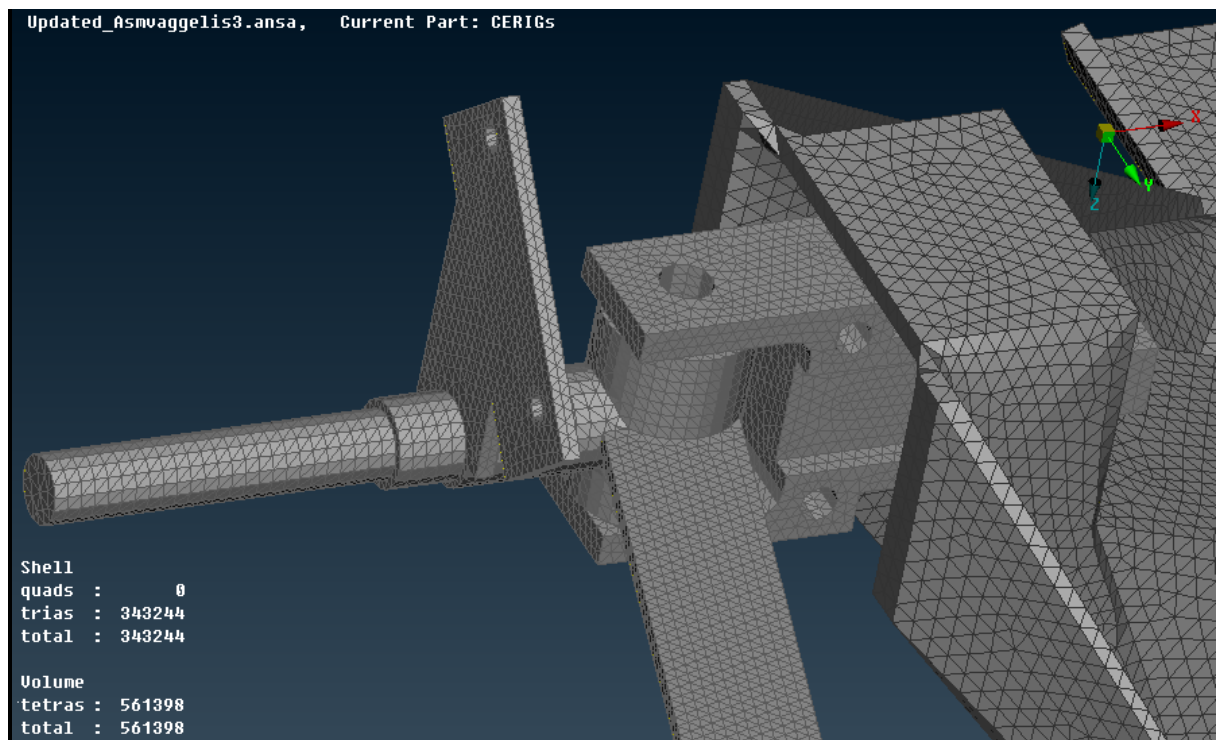


Figure 11-33 Volume Mesh on the Monocoque Chassis (View 8)

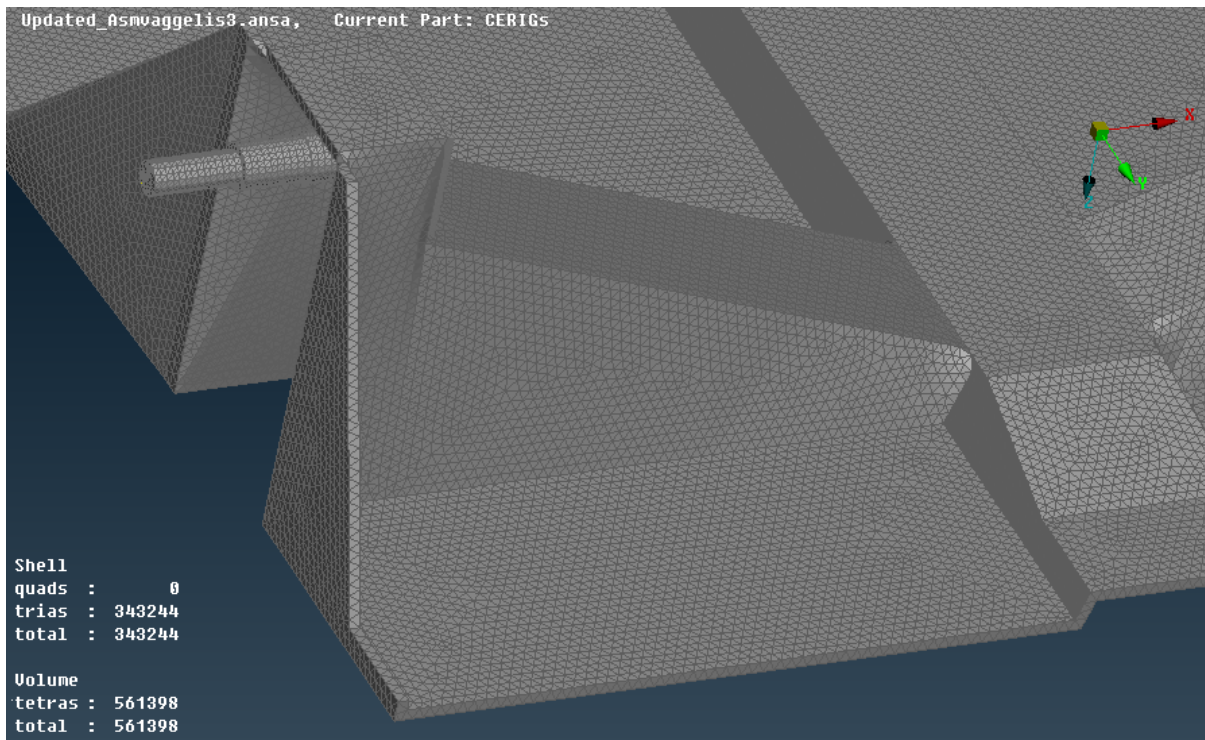


Figure 11-34 Volume Mesh on the Monocoque Chassis (View 9)

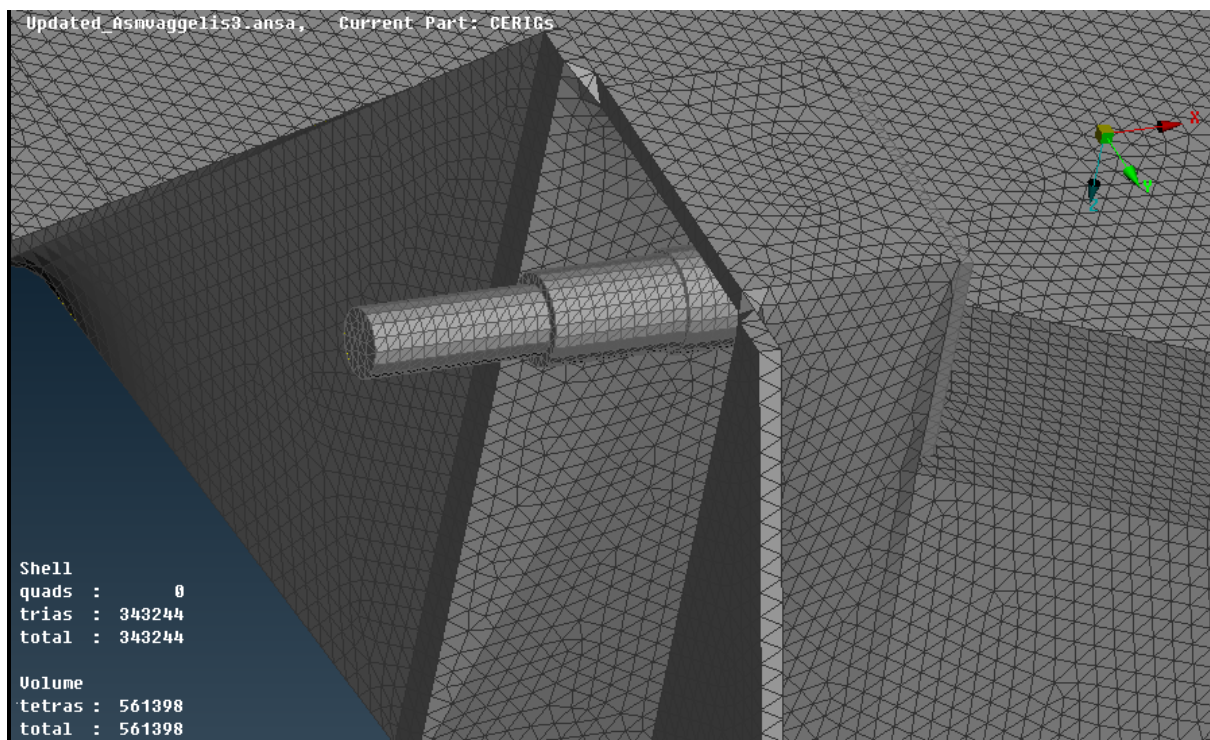


Figure 11-35 Volume Mesh on the Monocoque Chassis (View 10)

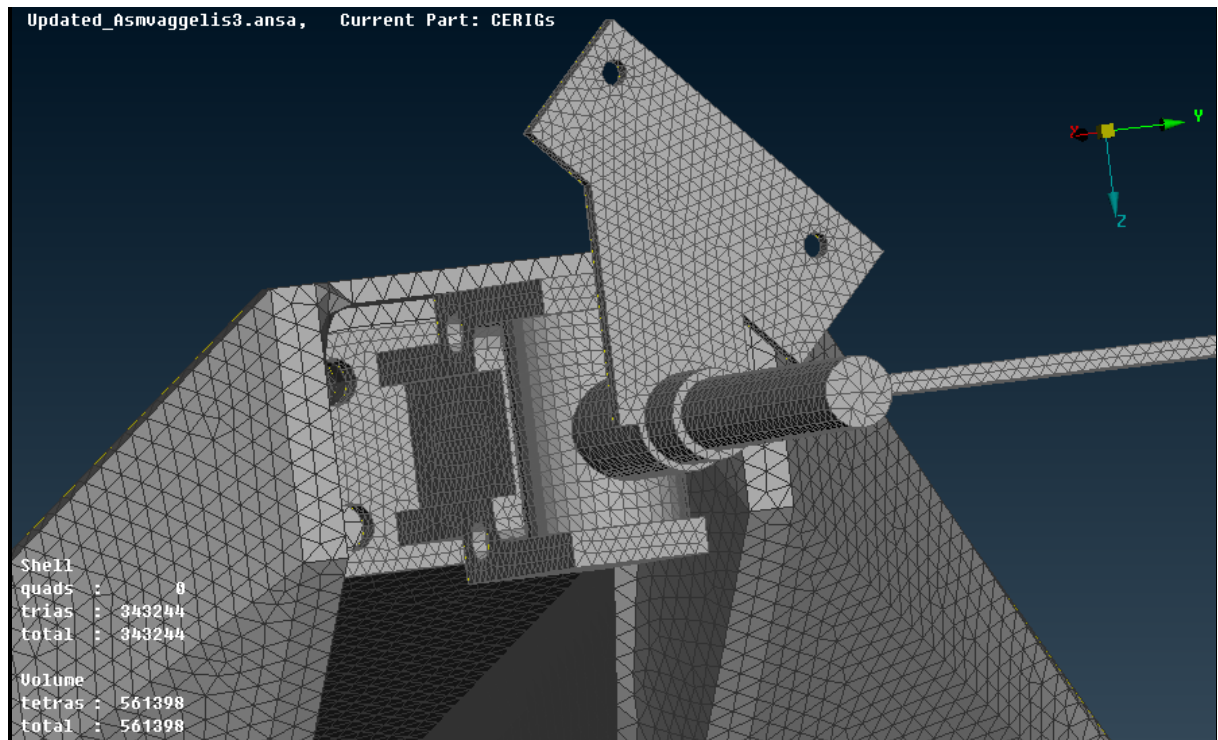


Figure 11-36 Volume Mesh on the Monocoque Chassis (View 11)

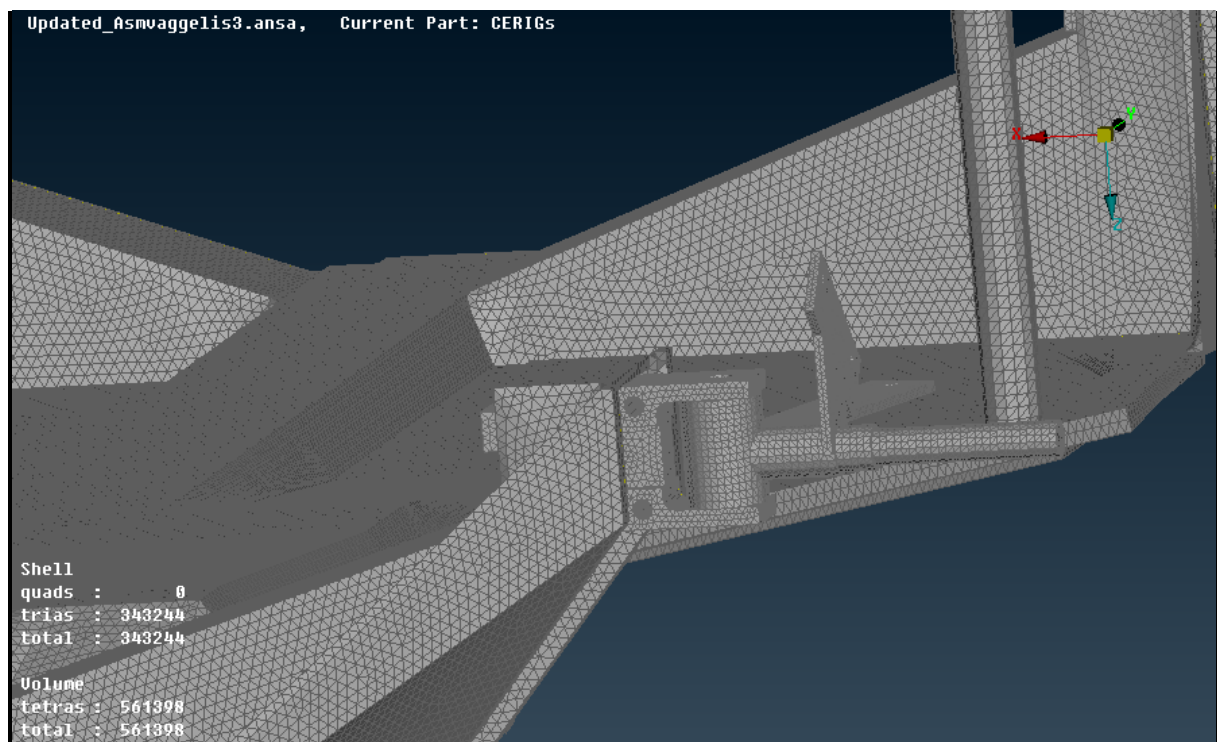


Figure 11-37 Volume Mesh on the Monocoque Chassis (View 12)

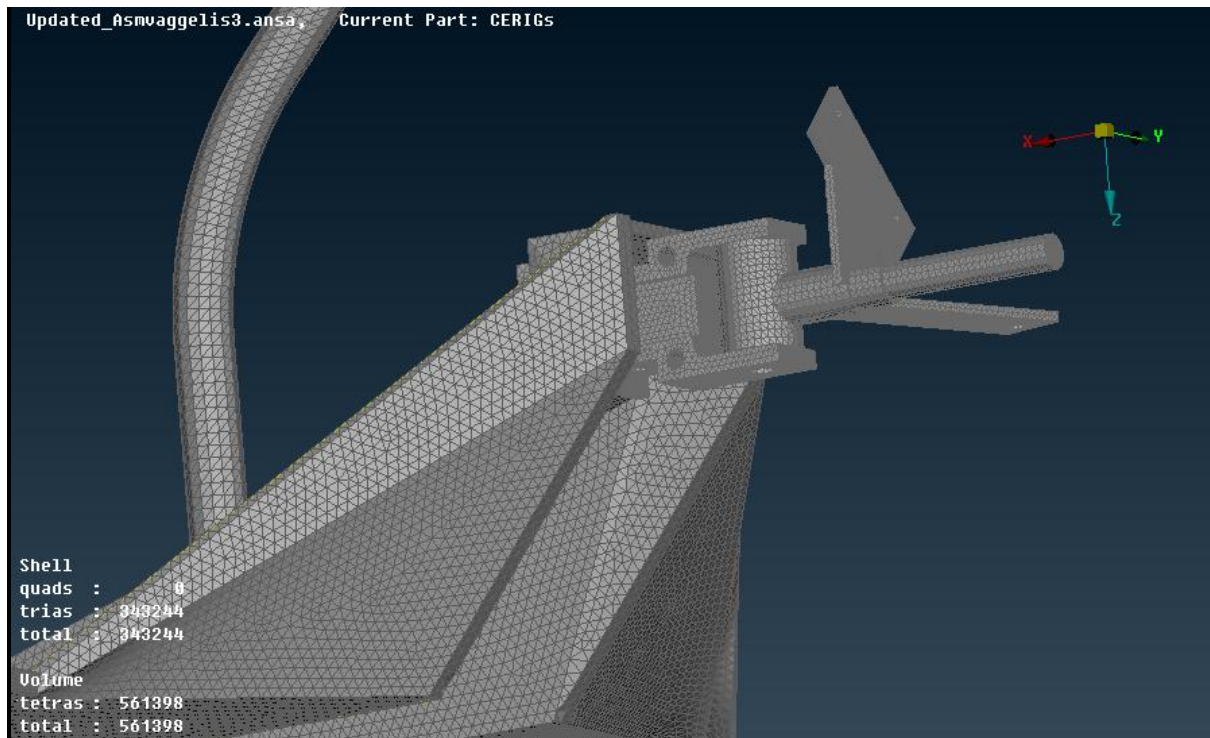


Figure 11-38 Volume Mesh on the Monocoque Chassis (View 13)

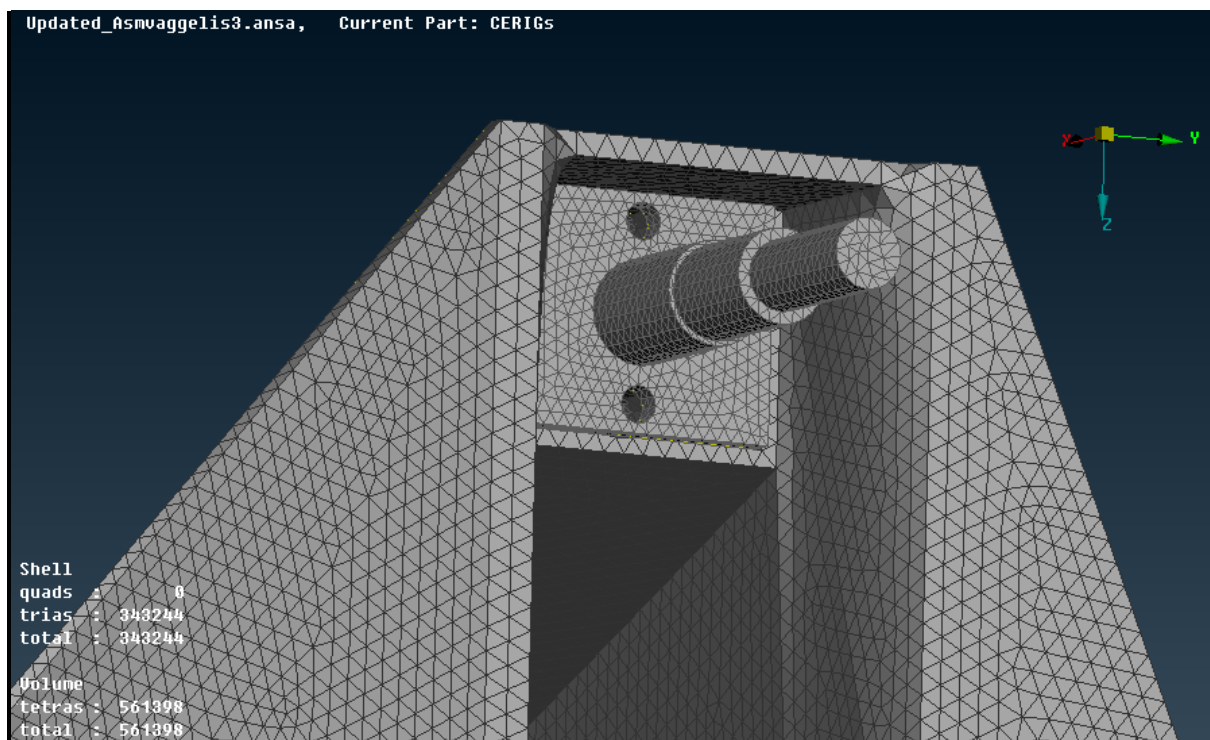


Figure 11-39 Volume Mesh on the Monocoque Chassis (View 14)

11.3.1.3.3 Meshing check

A series of checks take place in order to ensure that our model is functional.

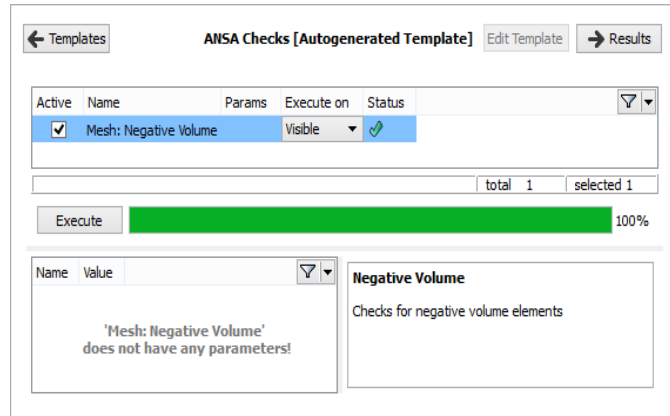


Figure 11-40 Negative volume check

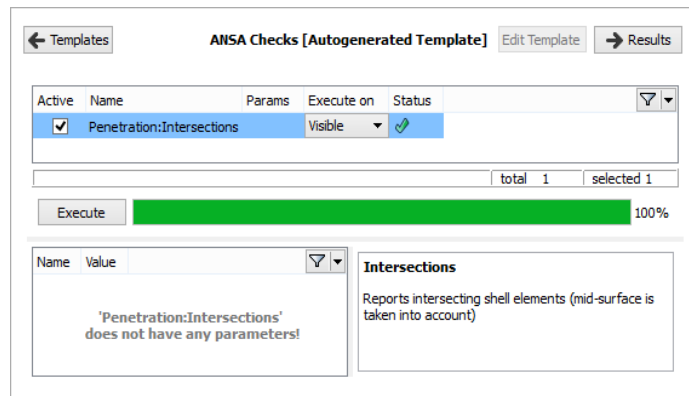


Figure 11-41 Penetration-Intersections check

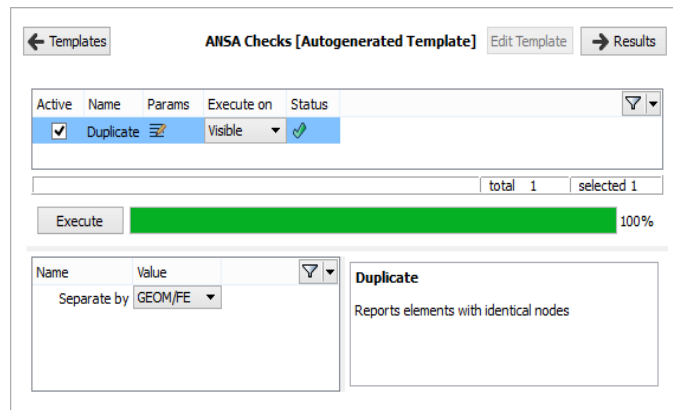


Figure 11-42 Duplicate elements check

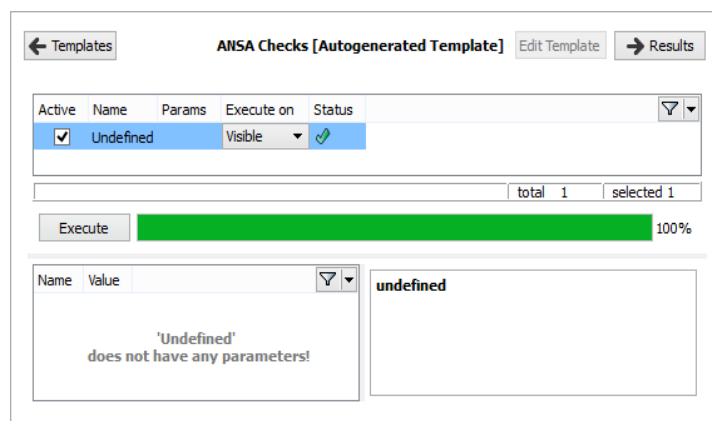


Figure 11-43 Undefined check

From the above figures, it can be seen that our model is error-free and ready for further processing.

11.3.1.4 Connections

The next step is to add the connections to our model. These connections consist of bolt connections and flanges.

11.3.1.4.1 Bolt connections

We place bolt connections, in the areas which have bolts.

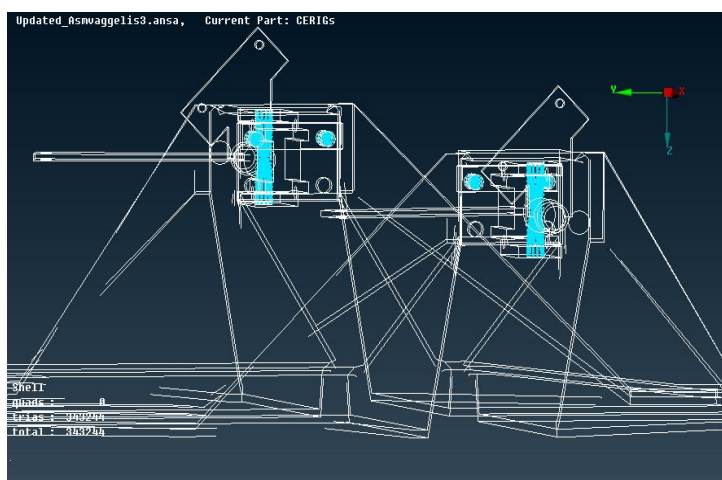


Figure 11-44 Bolt connections on the monocoque Chassis (View 1)

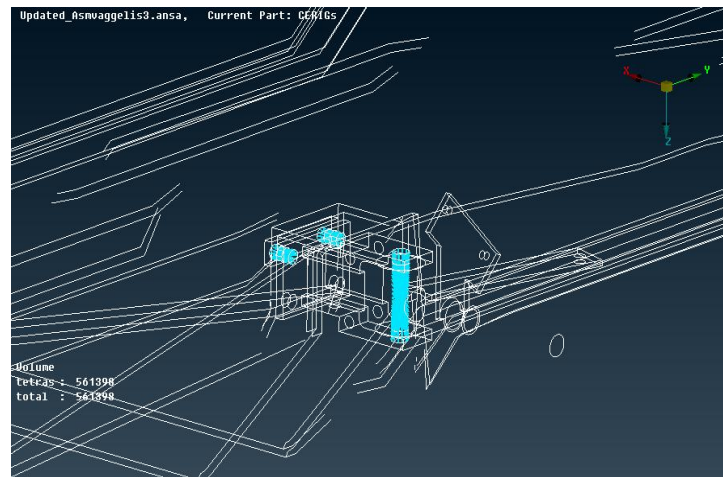


Figure 11-45 Bolt connections on the monocoque Chassis (View 2)

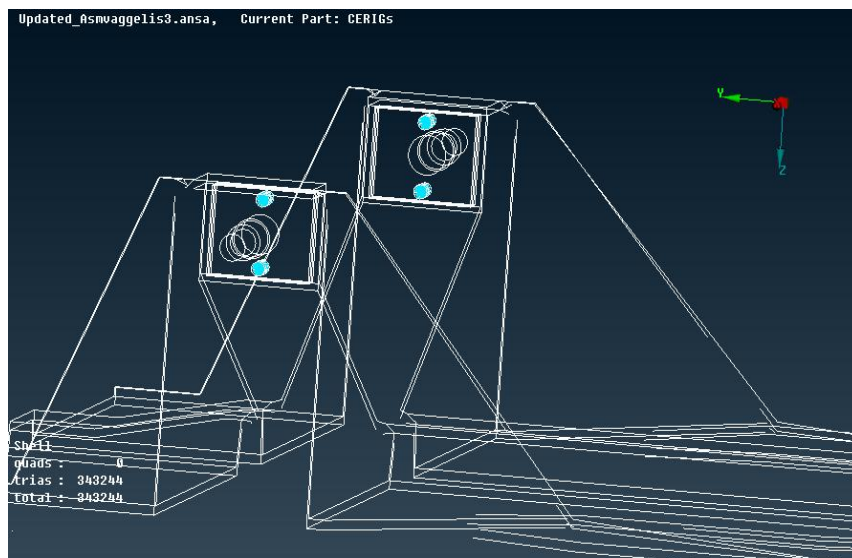


Figure 11-46 Bolt connections on the monocoque Chassis (View 3)

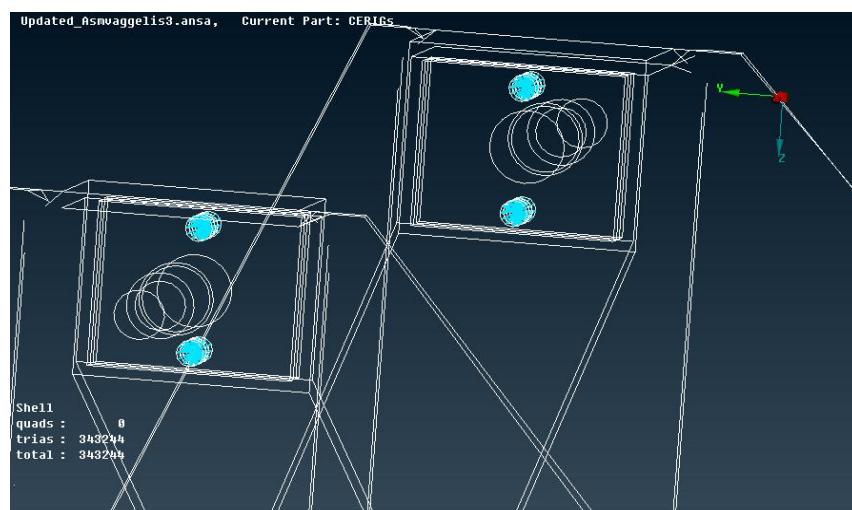


Figure 11-47 Bolt connections on the monocoque Chassis (View 4)

11.3.1.4.2 Contact flanges

In this stage, the contact flanges connections are placed.



Figure 11-48 Contact Flanges on the Monocoque Chassis (View 1)

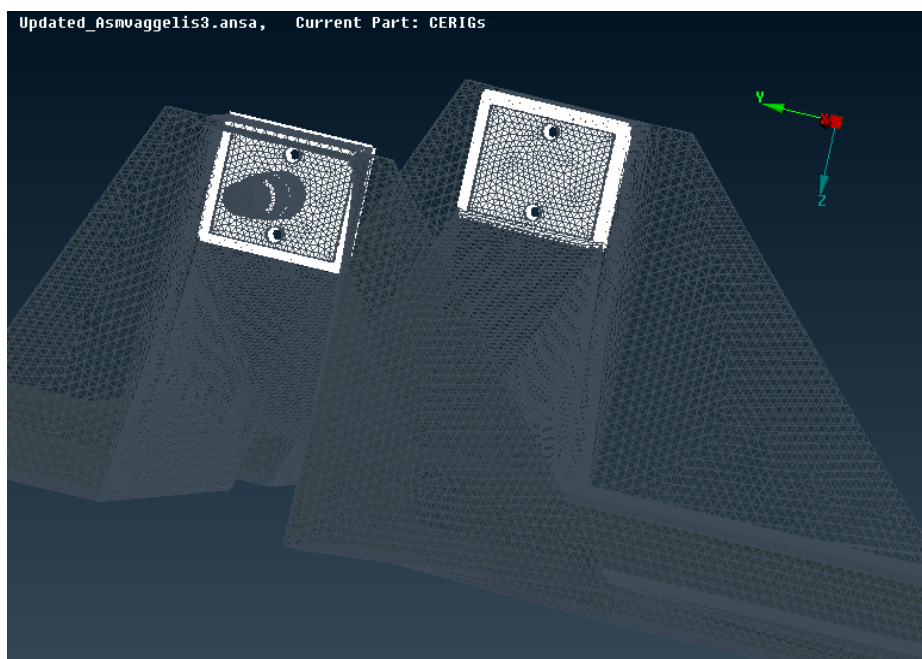


Figure 11-49 Contact Flanges on the Monocoque Chassis (View 2)

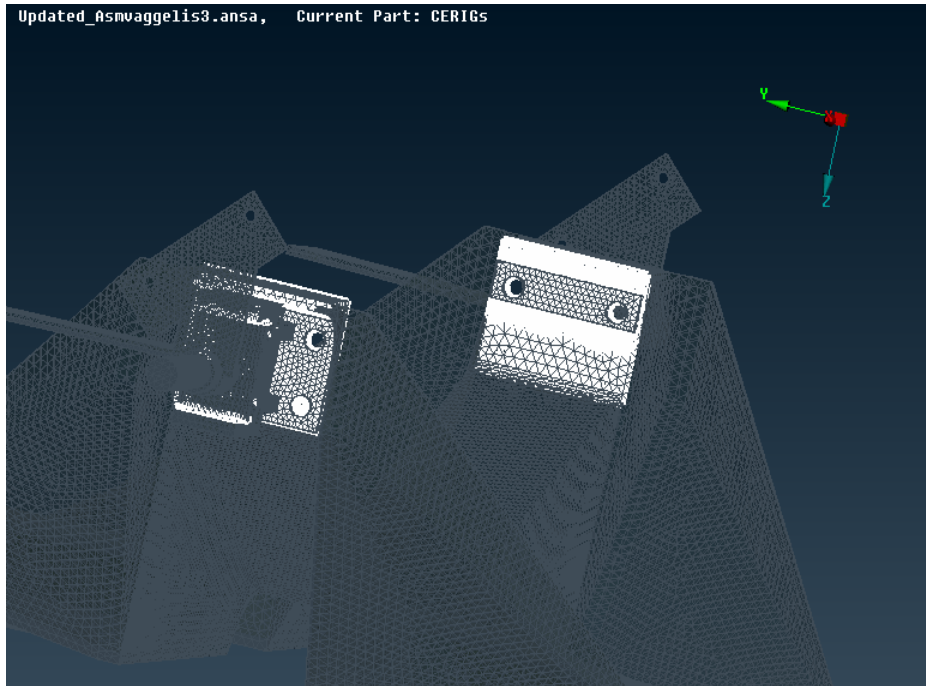


Figure 11-50 Contact Flanges on the Monocoque Chassis (View 3)

11.3.1.5 Loadstep manager

In the loadstep manager, we define just one step which includes:

- the permanent static loads (that is, driver, fuel cell, battery light, steering system, electric motor loads) which always act on our chassis.
- the total dynamic loads on the front axles that act during the coexistence of braking and cornering.
- the loading constraints.

11.3.1.5.1 Loading constraints

Referencing many SAE and other documents, we discovered that the manner in which the vehicle structure is analyzed can yield dramatically varying results on identical structures [62] [63] [64] [65] [8]. To validate the strength of the chassis, we chose the load case, which is cornering and braking. In order to get accurate and meaningful data when the vehicle brakes while taking the corner, we need to consider how the chassis would react in a racing environment.

As a vehicle braked while cornering, an instantaneous weight transfer occurred to the front, outside axle. If the chassis is examined at this very moment, the load is being applied to the front axles of the vehicle and it can be assumed that the rear axles of the vehicle remain fixed. For our application, we hypothesized that a model where the rearmost section of the chassis was constrained with all DOF's (degrees of freedom 123456), and opposite vertical loads were applied to the front axles, it would generate values for chassis strength. We also applied the permanent static loads (driver, fuel cell, battery light, steering system, electric motor loads) to the chassis. In other words, we simulated a model as close to possible to the real world situation. It is important to note, however, that this model does not take into consideration compliance within the suspension, and it is a measure of the strength of the frame structure itself. Figure 11-51 shows the rear constraints:

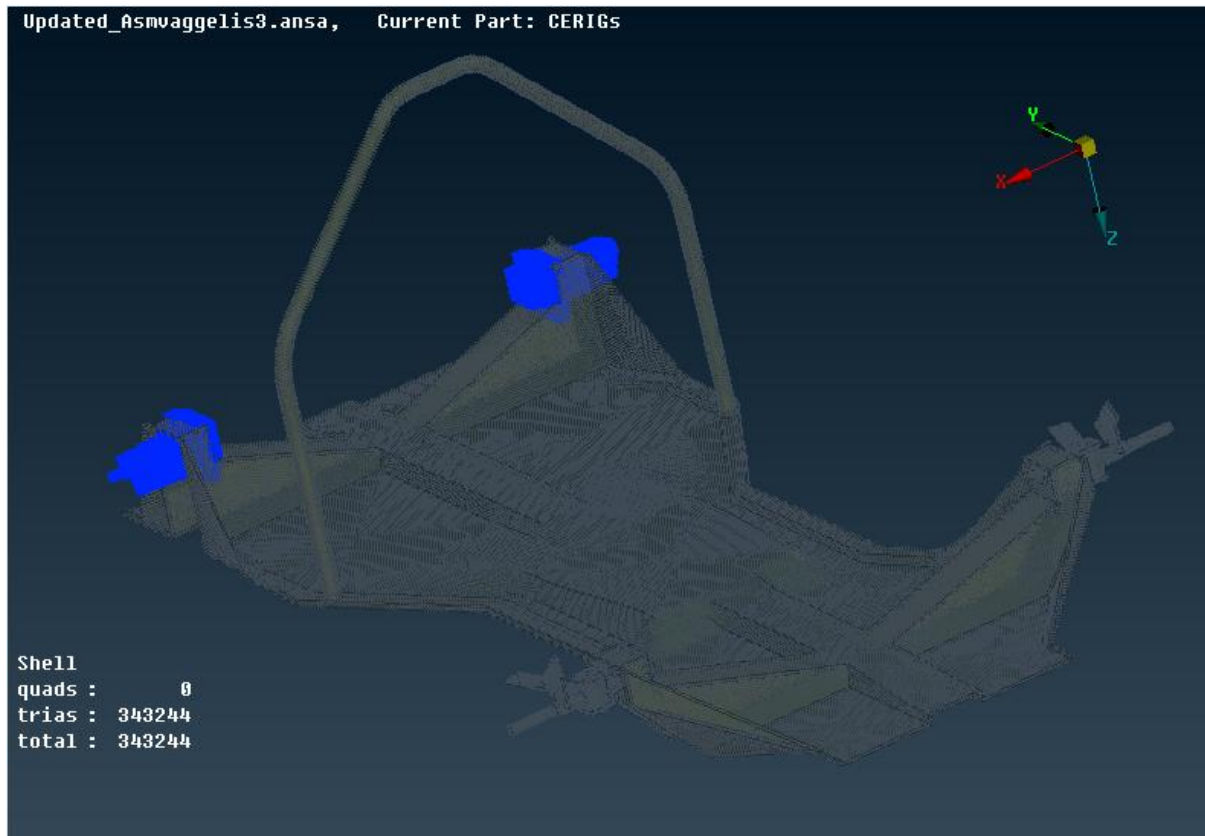


Figure 11-51 Loading Constraints on the Monocoque Chassis

11.3.1.5.2 Permanent static loads

We first apply the permanent static loads (driver, fuel cell, battery light, steering system, electric motor loads) on the monocoque.

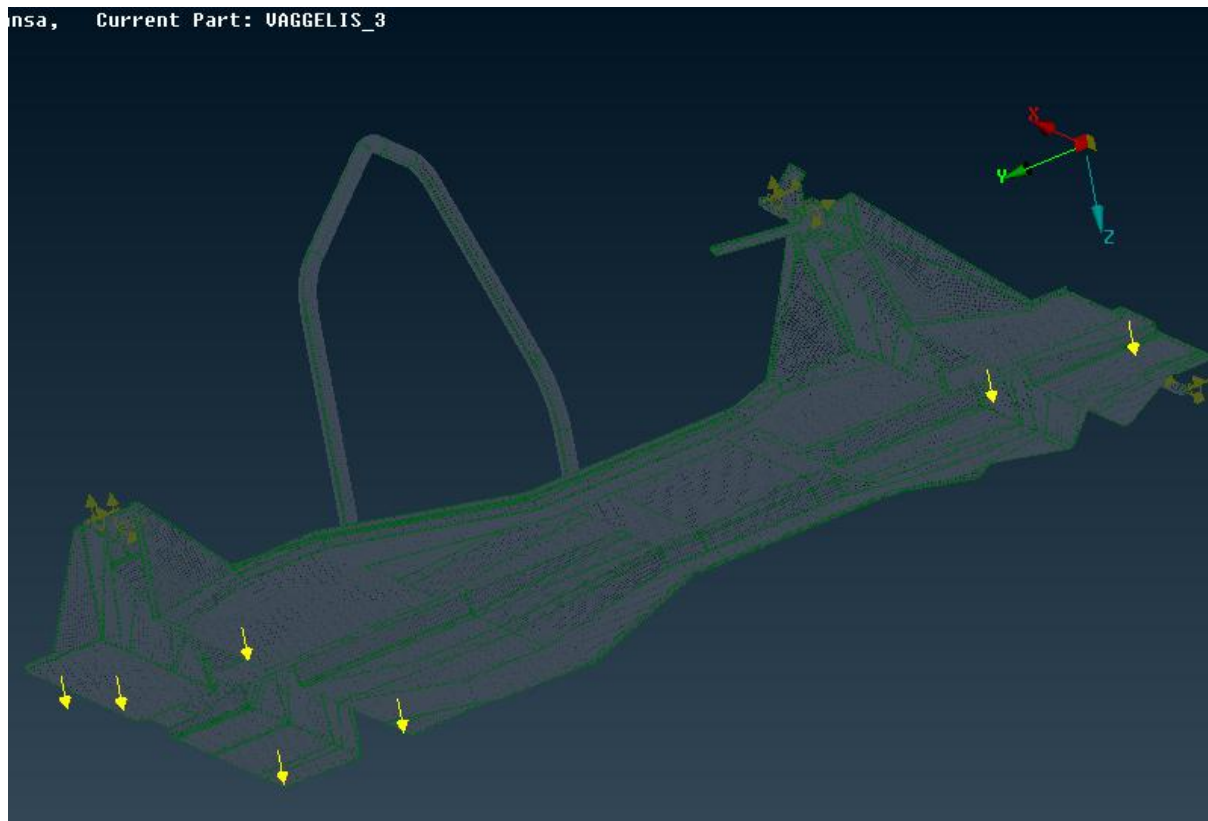


Figure 11-52 Permanent Static Loads on the Monocoque Chassis

During our next step, we calculate the pressure of the driver's body weight (from the table 11-1), dividing the force applied by the driver by the area that the driver's seat takes up on the chassis.

Table 11-1 Pressure applied from the driver's body weight

DRIVER'S SEAT PRESSURE	
kg	75 kg
Force	735.75 N
AREA	19300.095 mm ²
PRESSURE	0.0381216 Mpa

This pressure is applied to the next figures.

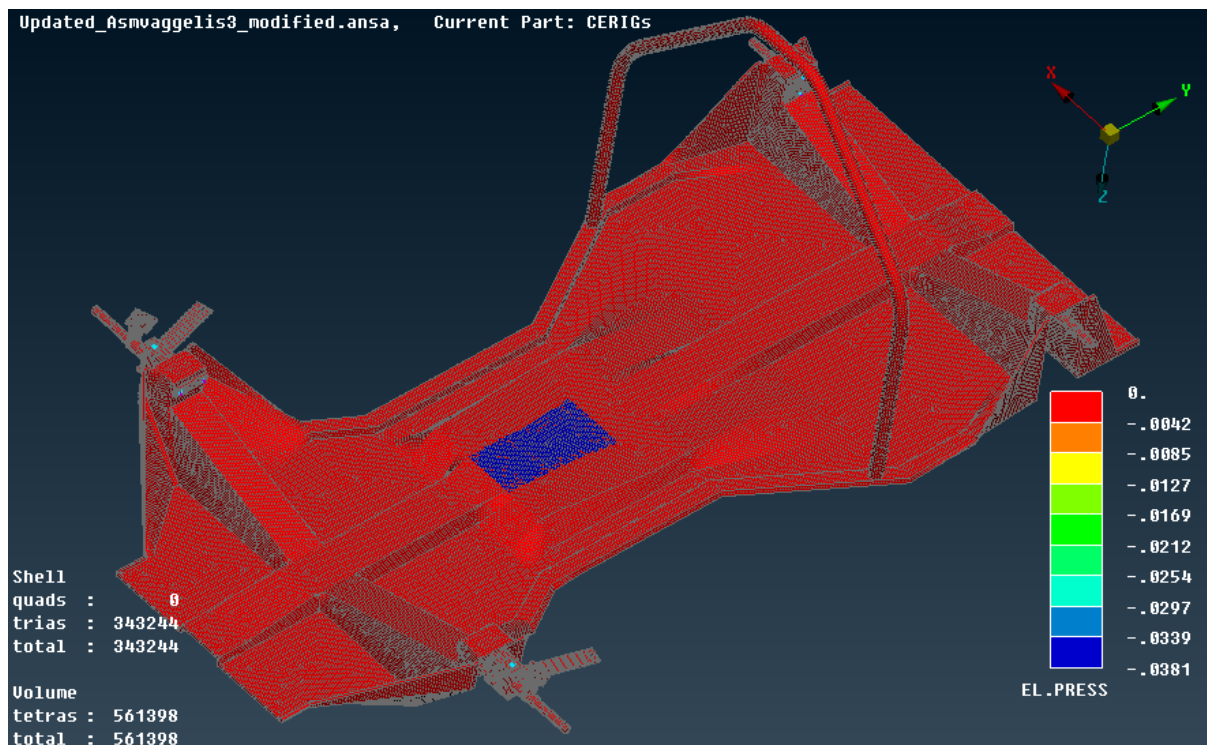


Figure 11-53 Driver's Pressure on the Monocoque Chassis (View 1)

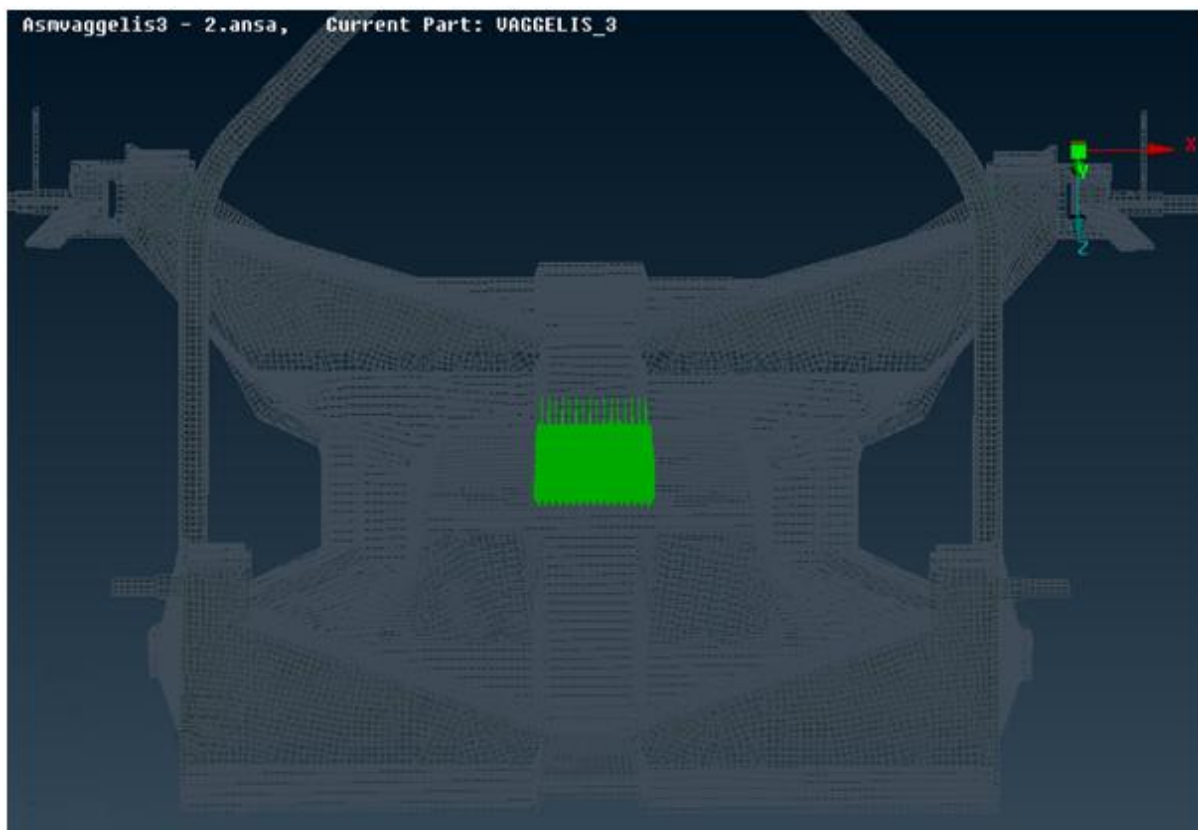


Figure 11-54 Driver's Pressure on the Monocoque Chassis (View 2)

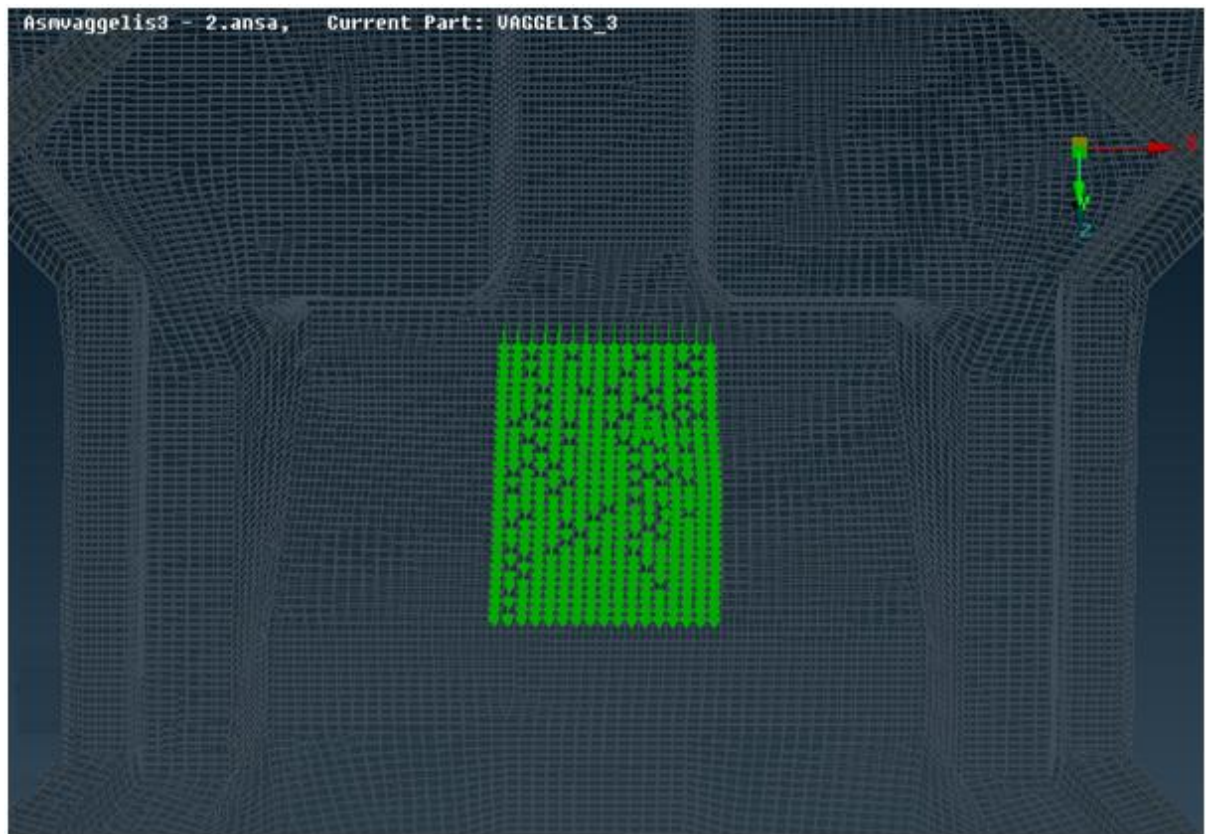


Figure 11-55 Driver's Pressure on the Monocoque Chassis (View 3)

11.3.1.5.3 Front axle loads

The longitudinal, the lateral and the vertical loads are applied, as well as the roll and the pitch moments on the front axles. These loads and moments have already been calculated in a previous chapter.

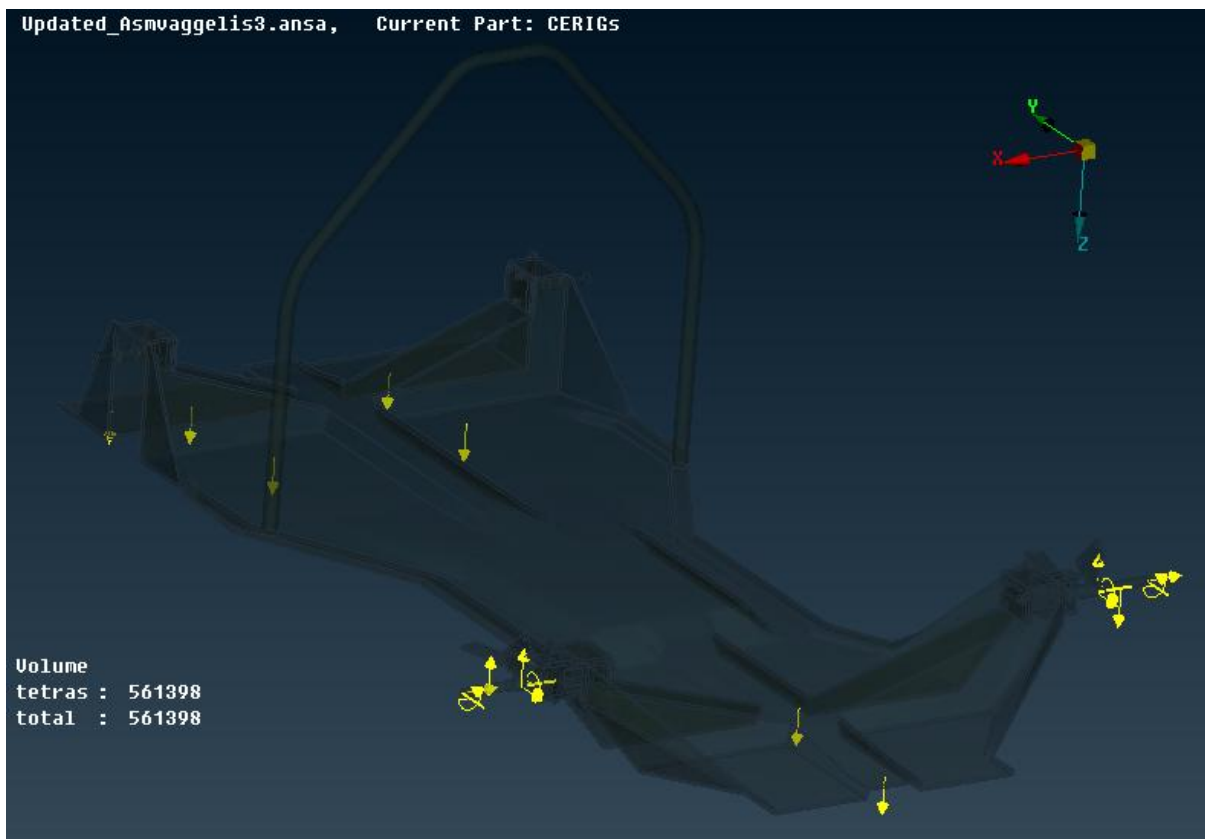


Figure 11-56 Front Axle Loads on the Monocoque Chassis (View 1)



Figure 11-57 Front Axle Loads on the Monocoque Chassis (View 2)



Figure 11-58 Front Axle Loads on the Monocoque Chassis (View 3)



Figure 11-59 Front Axle Loads on the Monocoque Chassis (View 4)

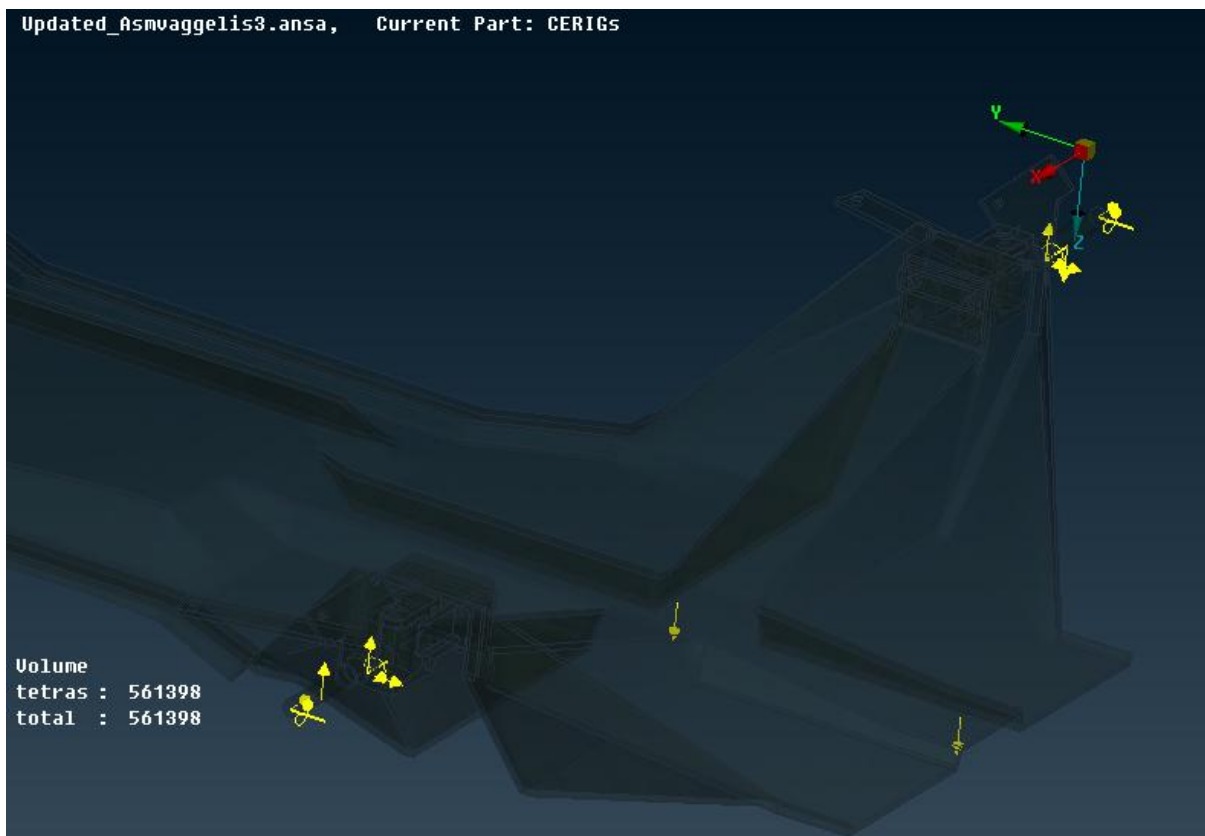


Figure 11-60 Front Axle Loads on the Monocoque Chassis (View 5)

11.3.1.6 Gravity acceleration

In our analysis, we took into consideration the gravity acceleration (9.81m/s^2). We applied this acceleration on the z axis as one can see in the following images.

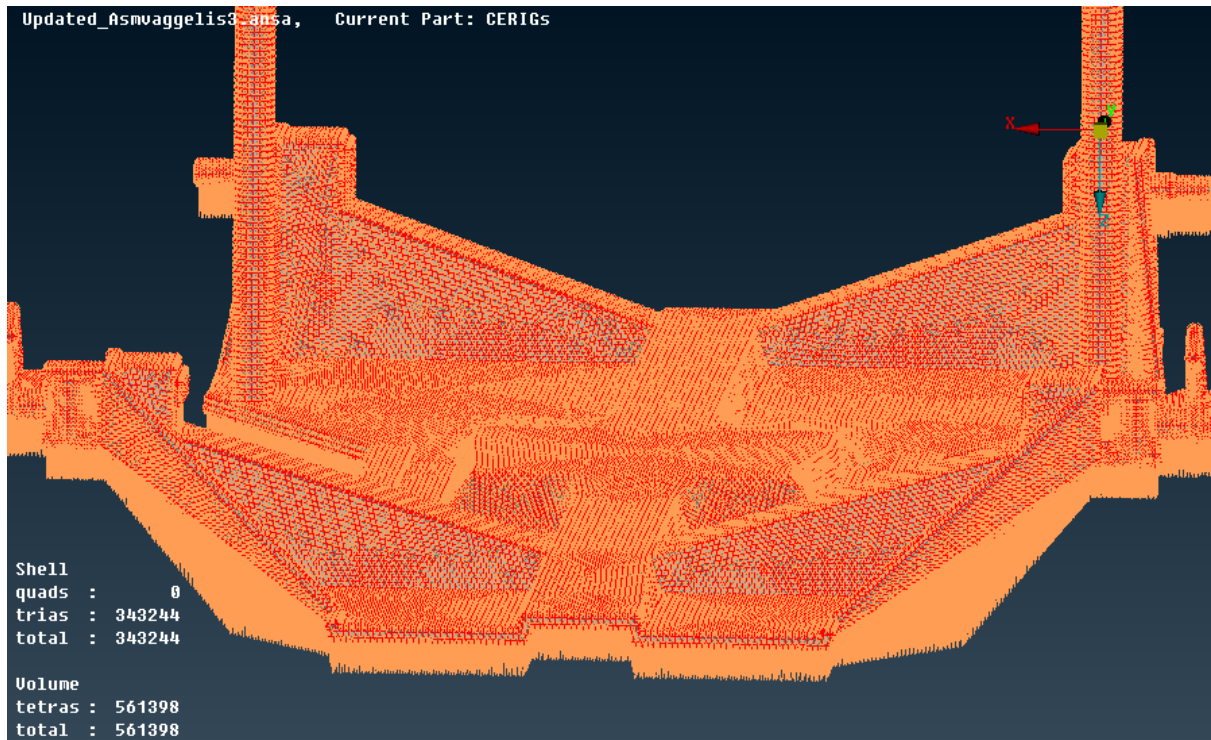


Figure 11-61 Gravity Acceleration on the Monocoque Chassis (View 1)

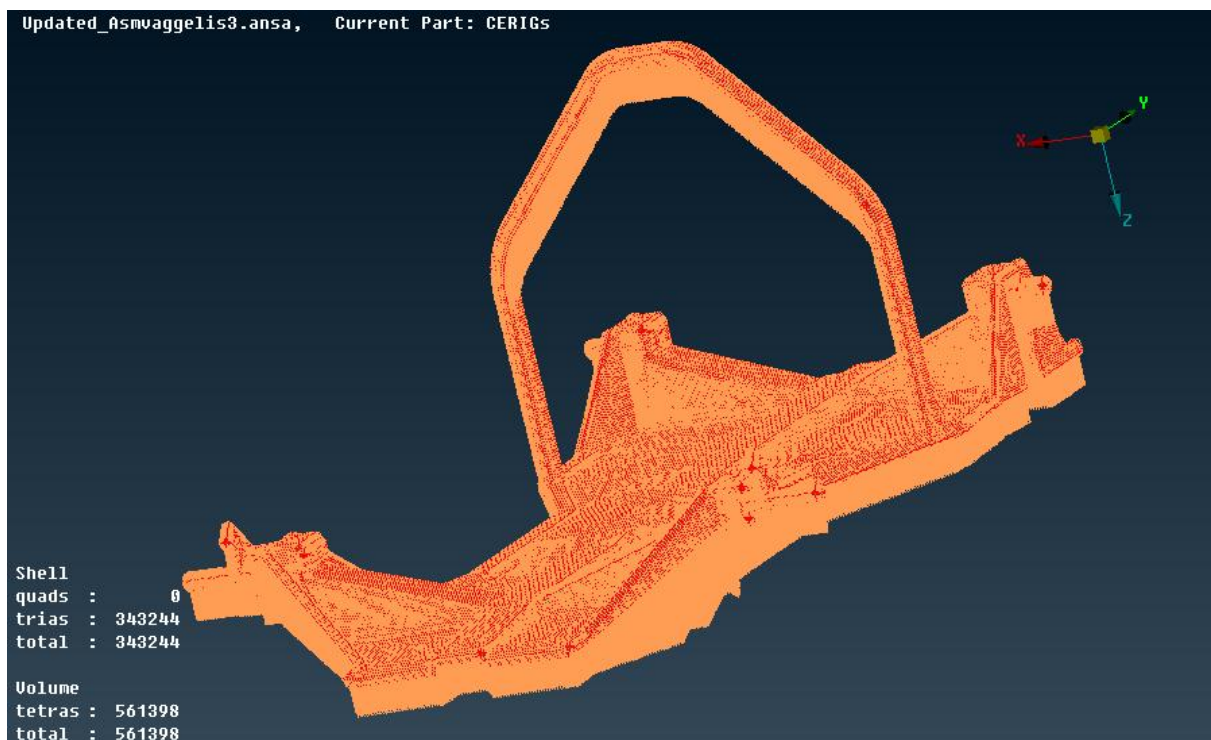


Figure 11-62 Gravity Acceleration on the Monocoque Chassis (View 2)

11.3.2 Aluminium space frame chassis

Parts

By using different colours we are able to distinguish the 48 different parts of which the aluminium space frame chassis consists.

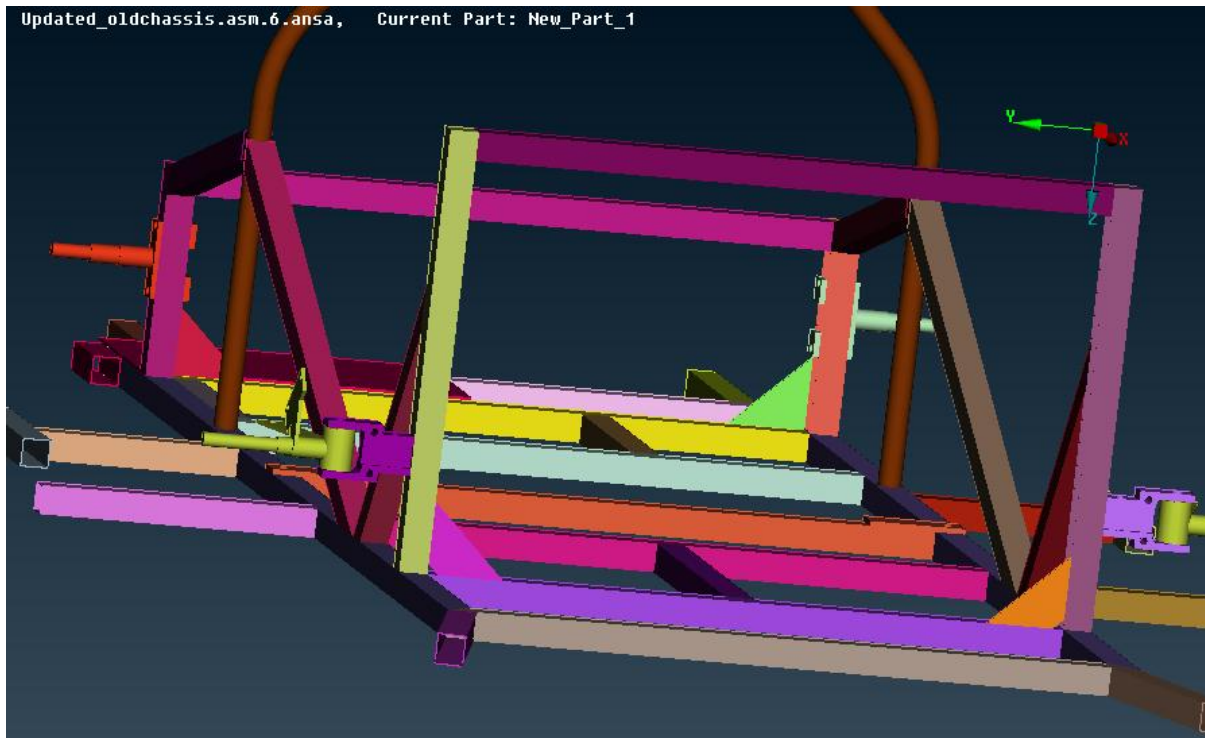


Figure 11-63 Aluminium Space Frame's Parts (View 1)

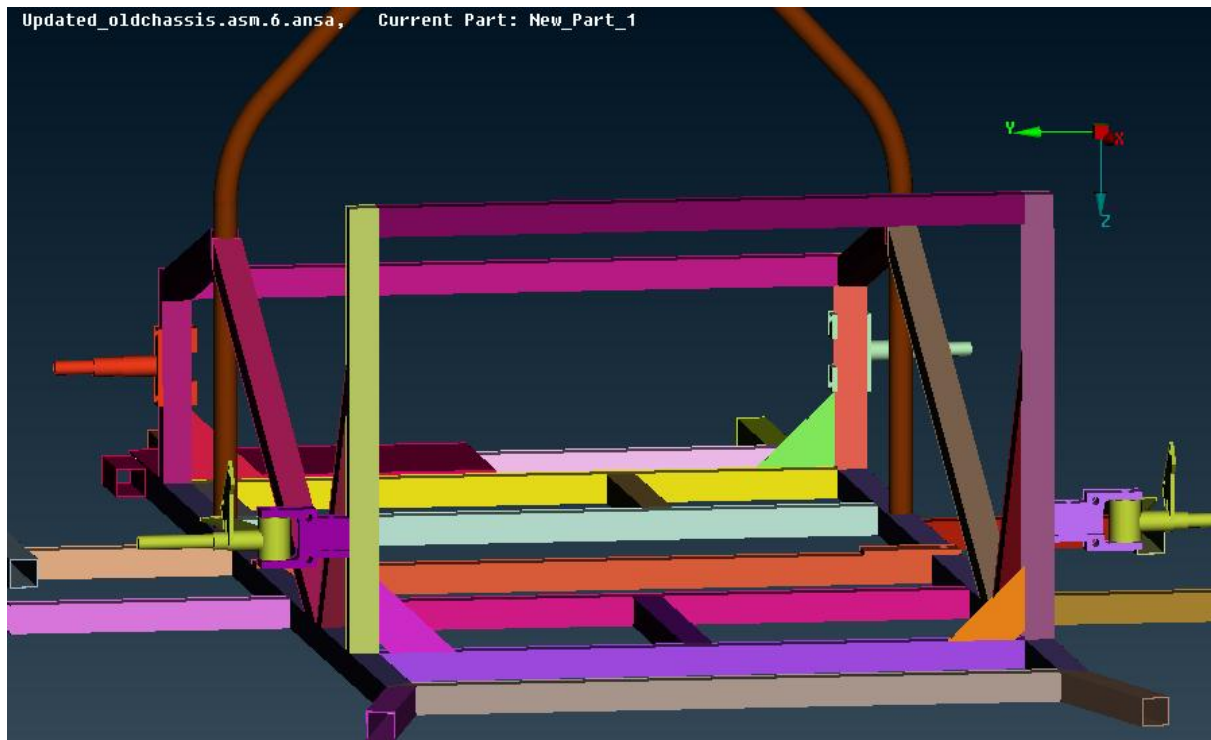


Figure 11-64 Aluminium Space Frame's Parts (View 2)

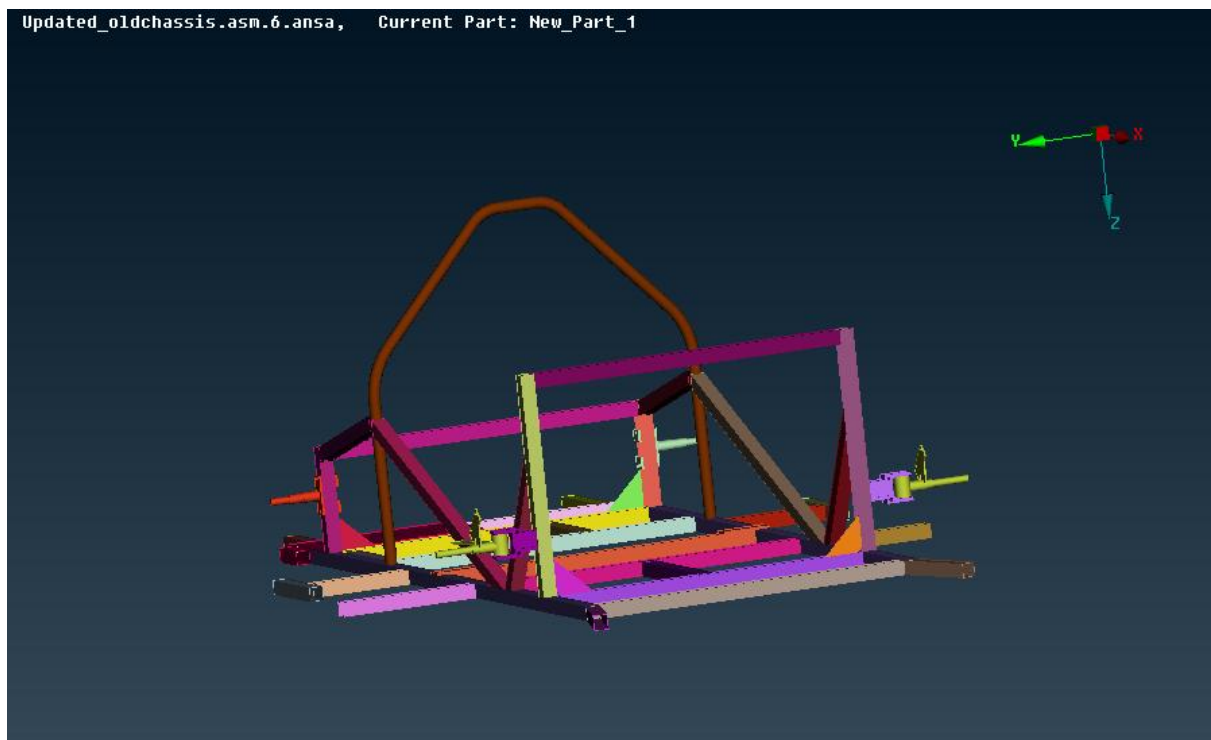


Figure 11-65 Aluminium Space Frame's Parts (View 3)

11.3.2.1 Clean geometry

By importing the file from Pro-engineer to ANSA, the ANSA software locates geometry problems. The next task is to fix them.

Geometry check

The next step is to perform a geometry check which will allow us to see if there are any more errors.

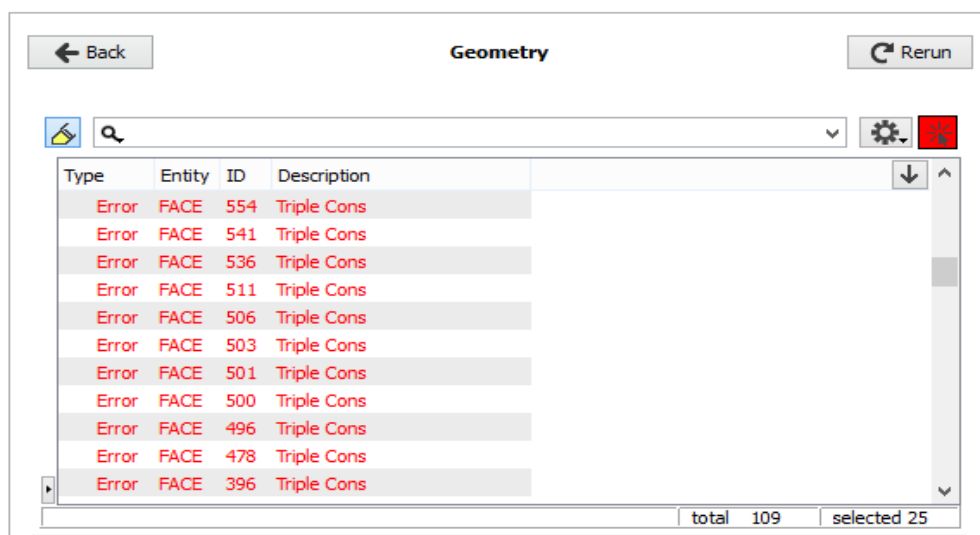


Figure 11-66 Geometry check

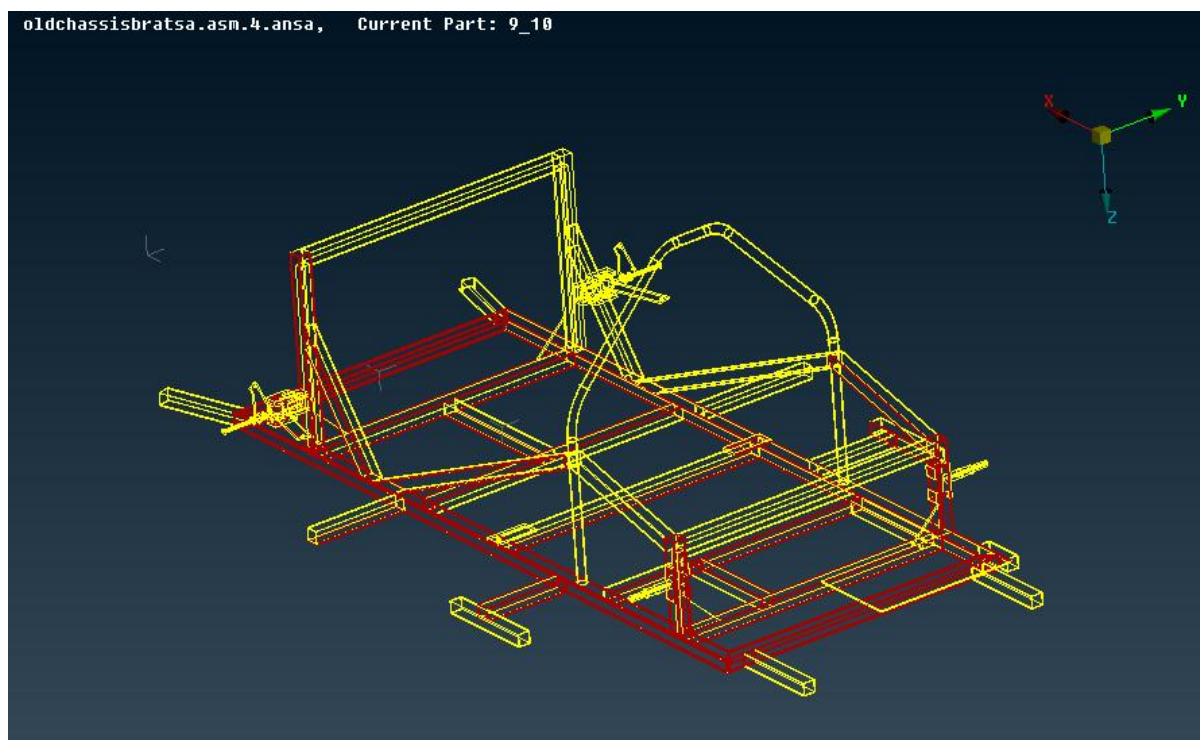


Figure 11-67 Geometry Check on the Aluminium Space Frame

Any triple cons errors (cyan in colour) can be observed below.

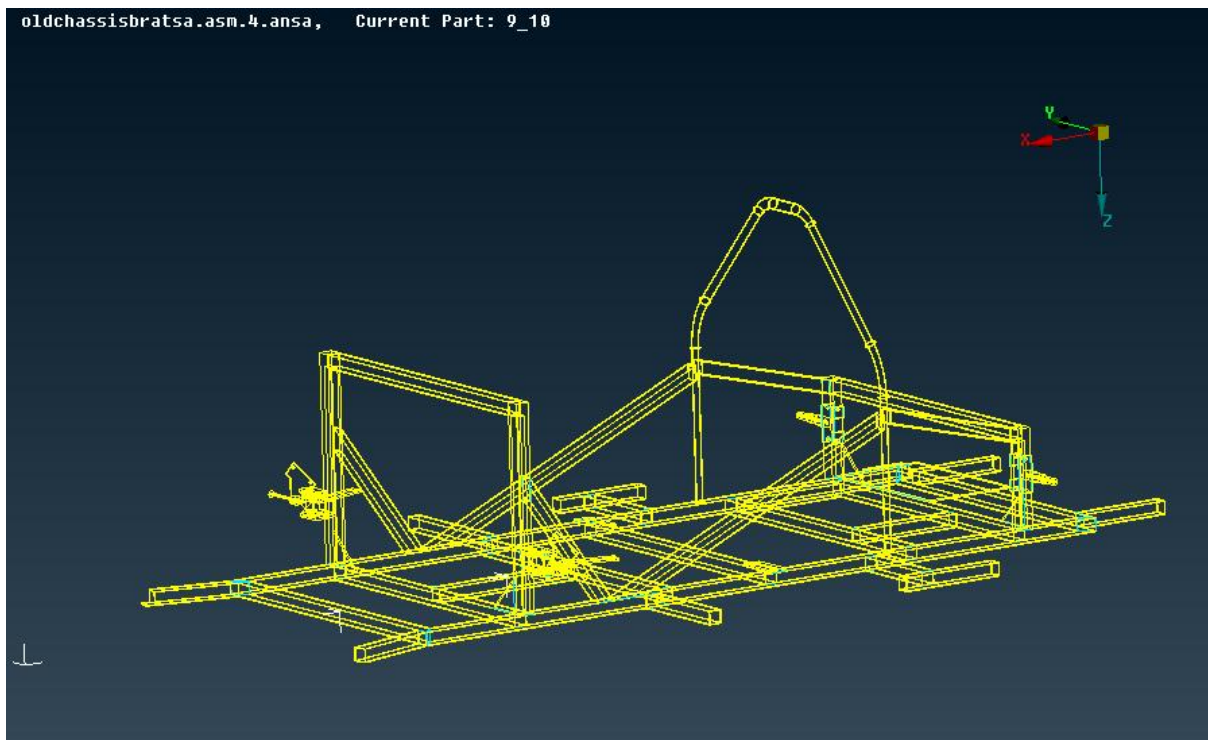


Figure 11-68 Triple Cons on the Aluminium Space Frame (View 1)

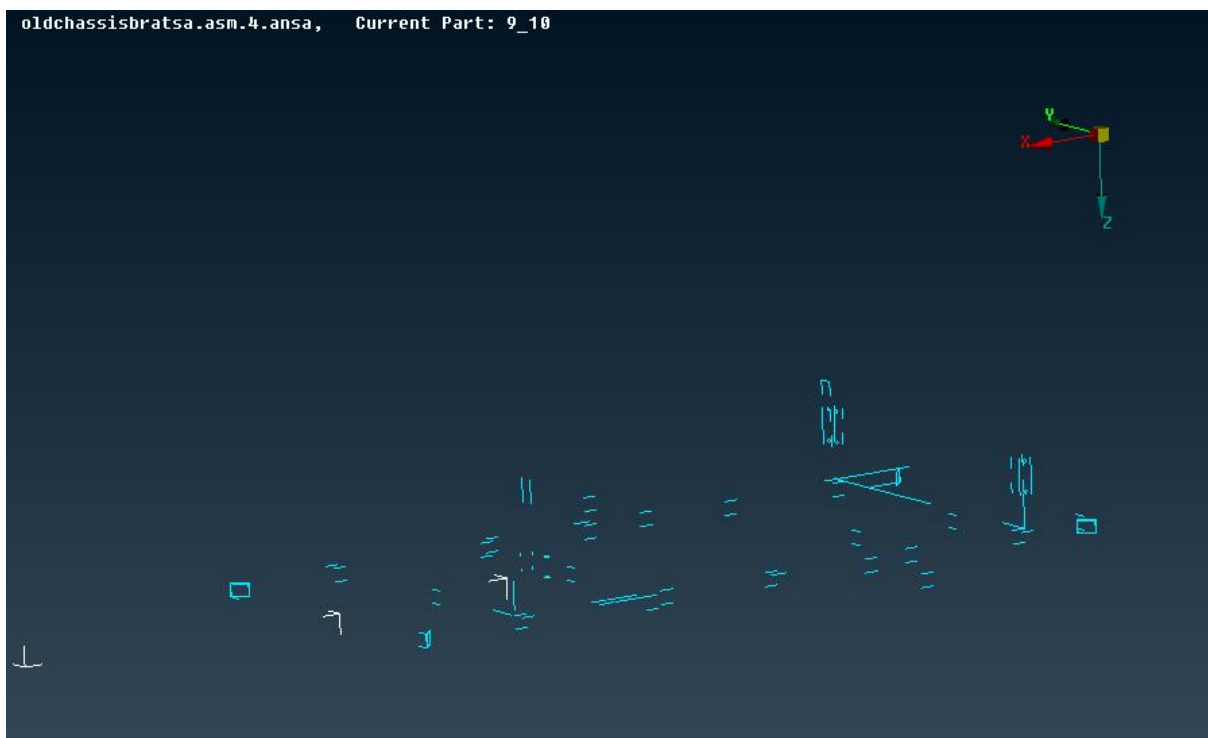


Figure 11-69 Triple Cons on the Aluminium Space Frame (View 2)

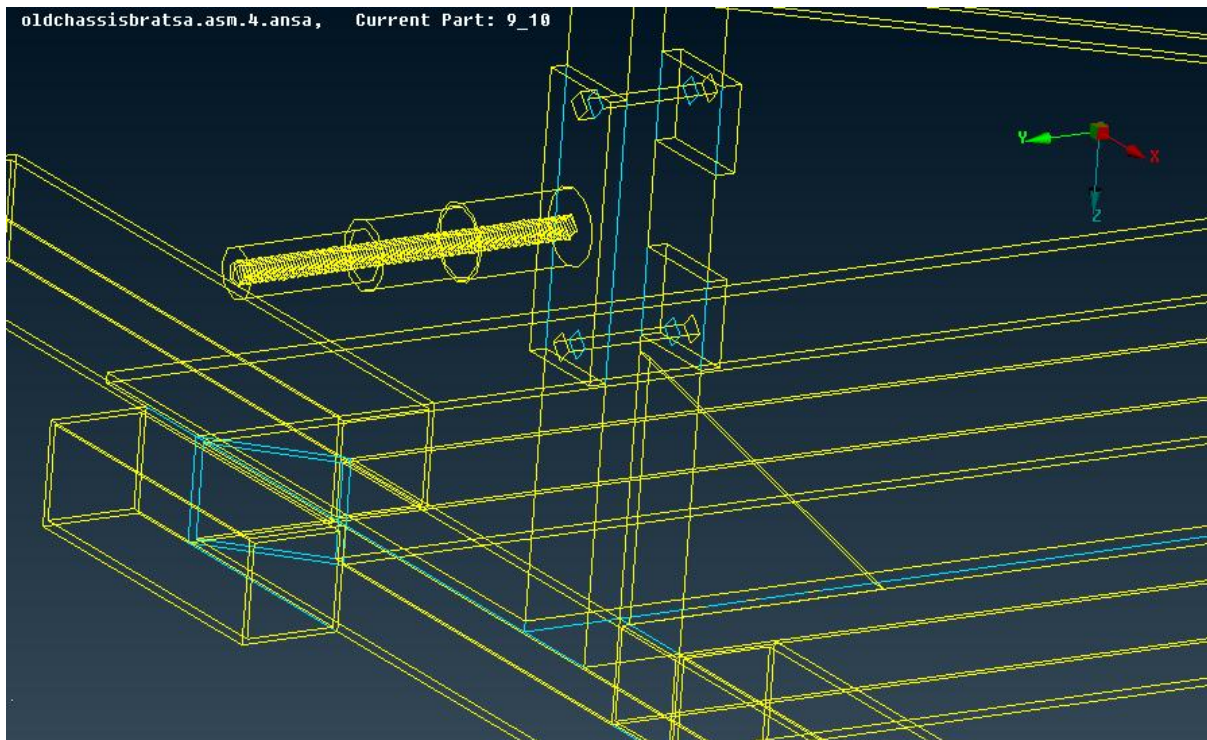


Figure 11-70 Triple Cons on the Aluminium Space Frame (View 3)

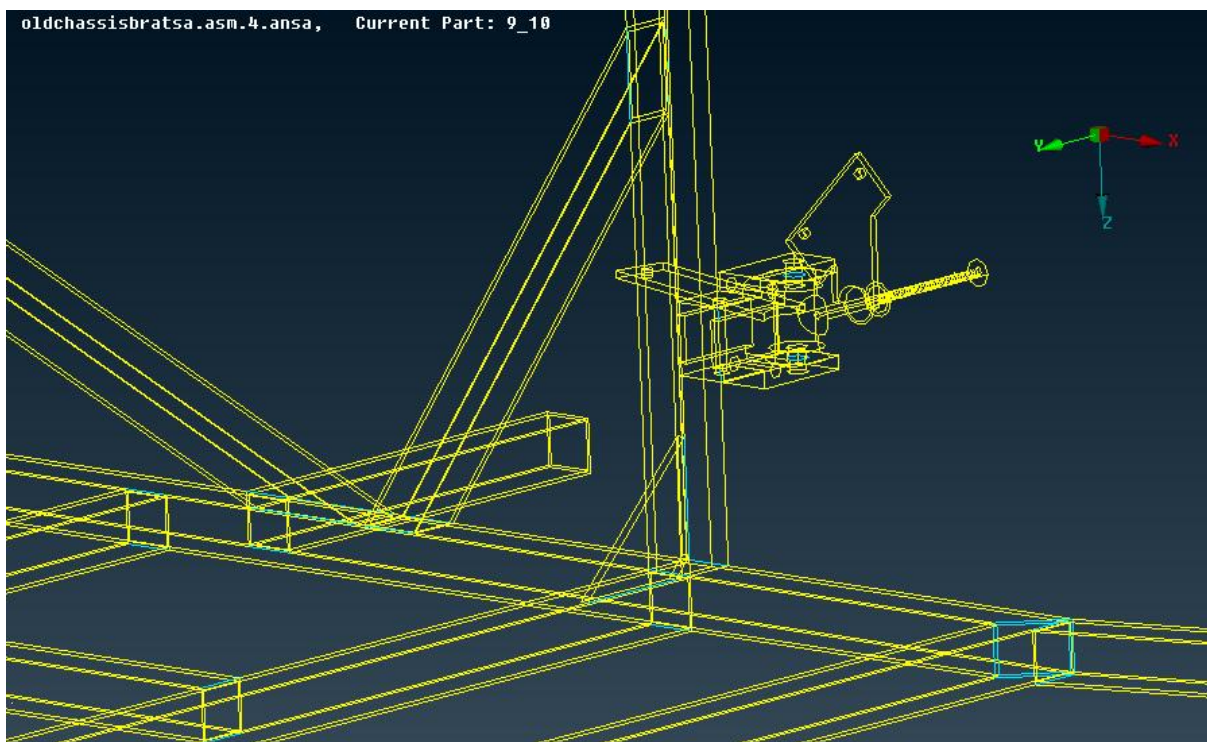


Figure 11-71 Triple Cons on the Aluminium Space Frame (View 4)

Penetration: Intersections check

Following this, the next step is to run a test in order to locate any possible intersections in our model.

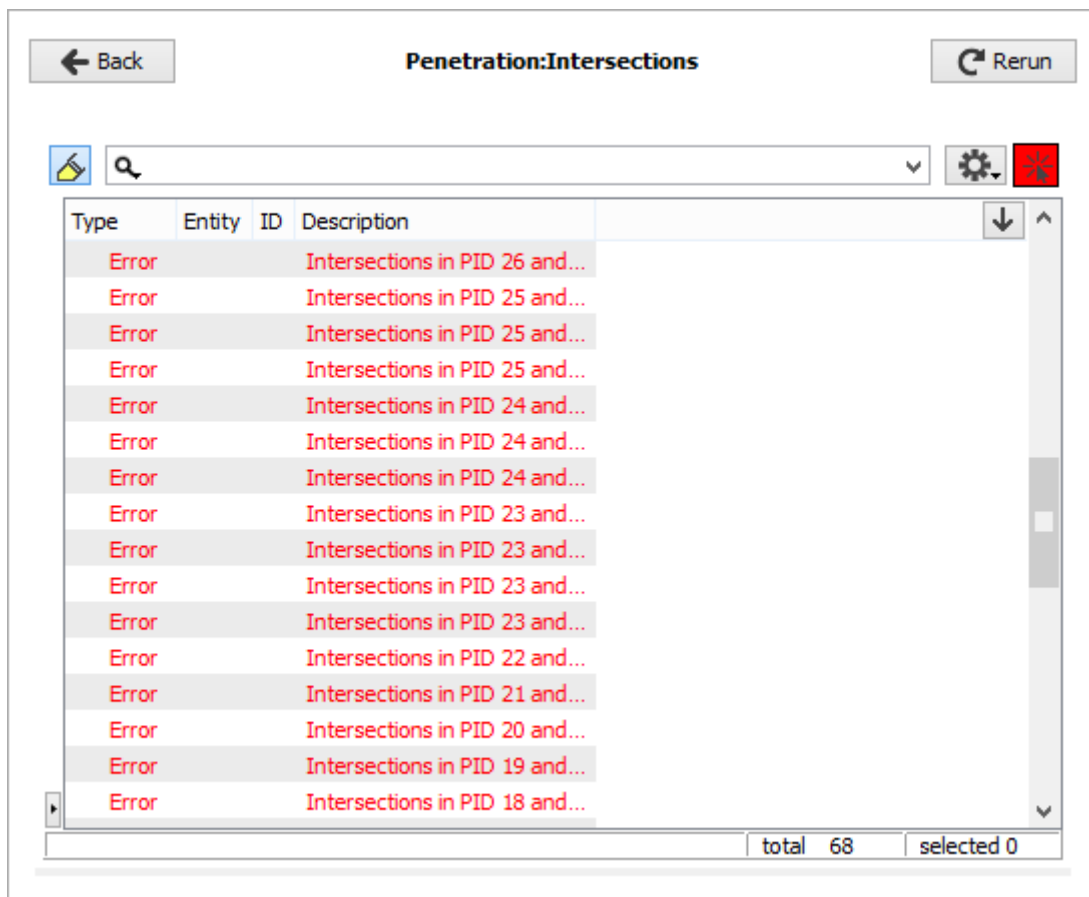


Figure 11-72 Penetration-Intersections check

There are some intersections (red in colour) which can be seen in the figure below (Figure 11-73).

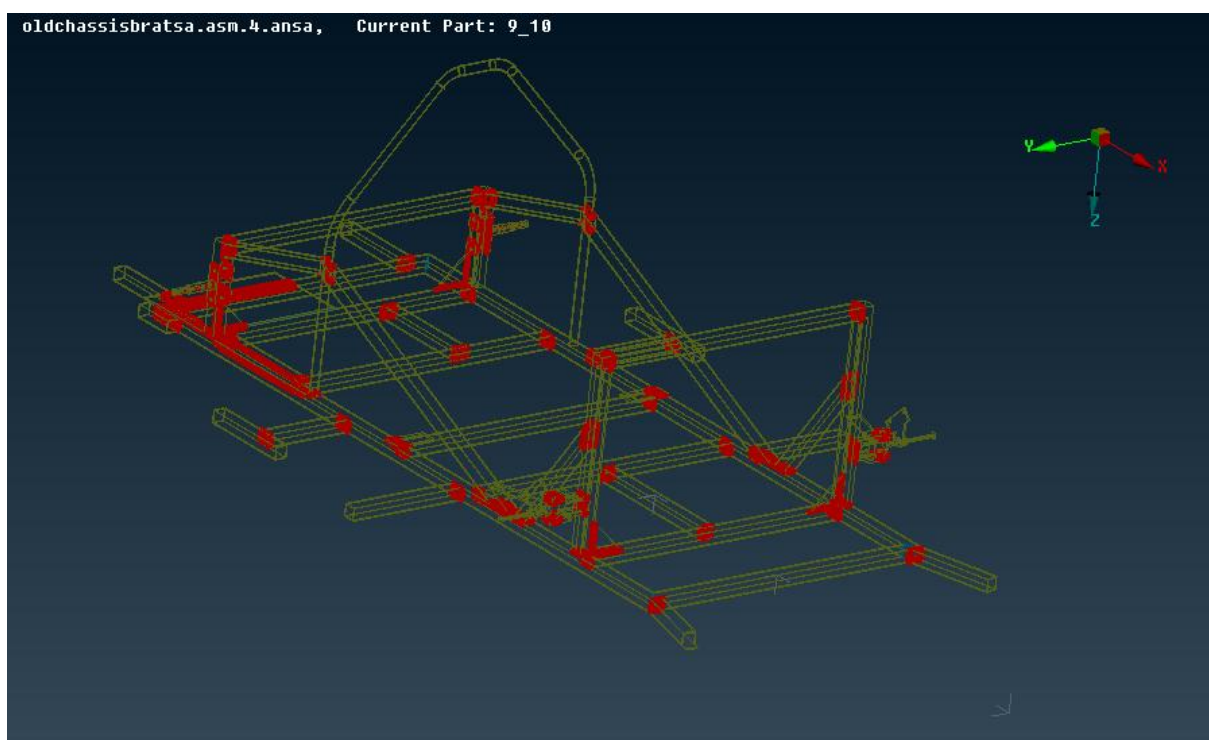


Figure 11-73 Intersections Check on the Aluminium Space Frame

Fix geometry and intersections

The geometry errors have been fixed and as a result there are no triple cons errors (cyan in colour) anymore. Furthermore, the intersections are fixed and this is observed by the absence of the red colour.

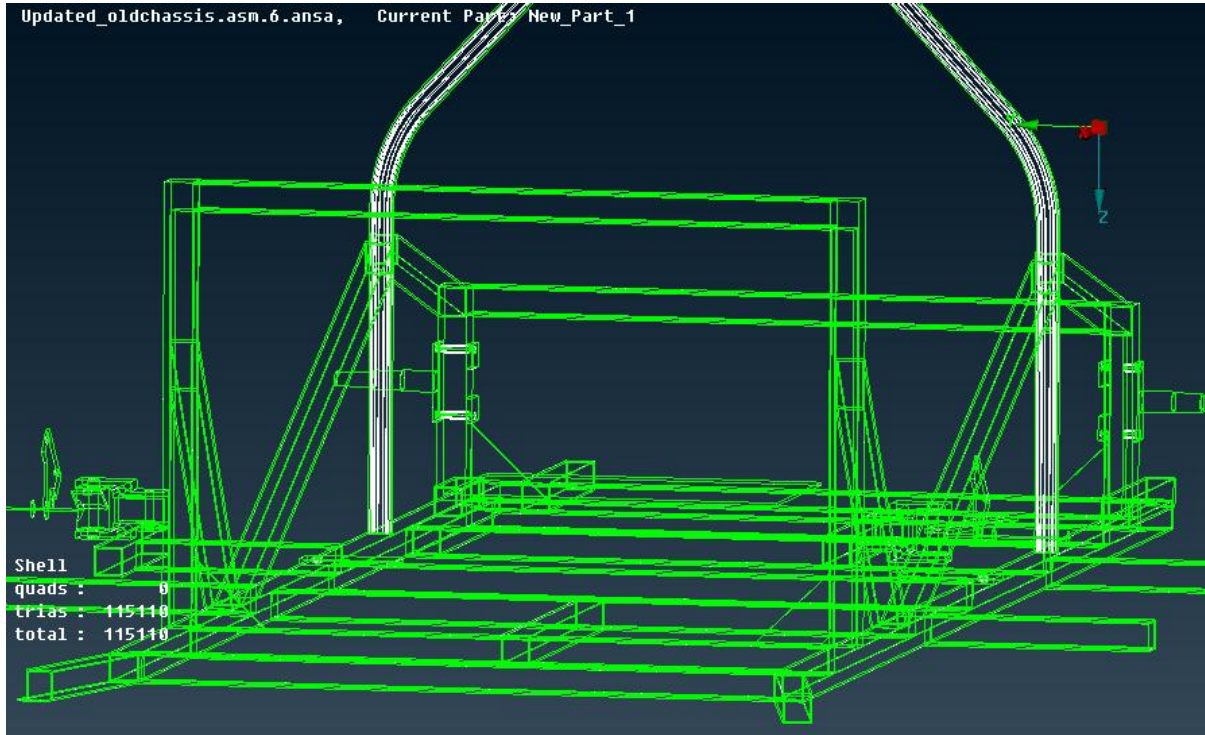


Figure 11-74 Geometry & Intersections on the Aluminium Space Frame fixed

11.3.2.2 Properties and materials definition

First, the chassis materials are defined and then presented in different colours.

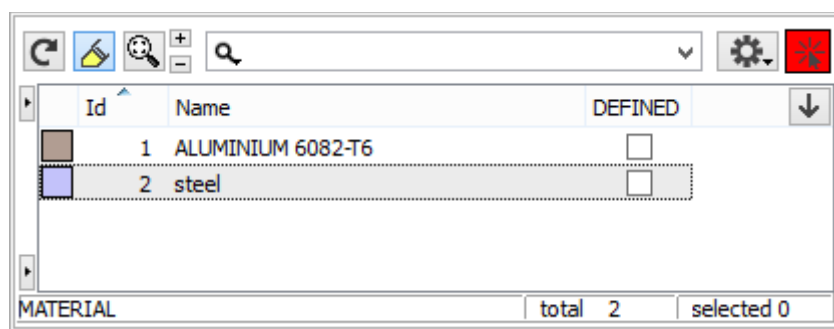


Figure 11-75 Materials definition

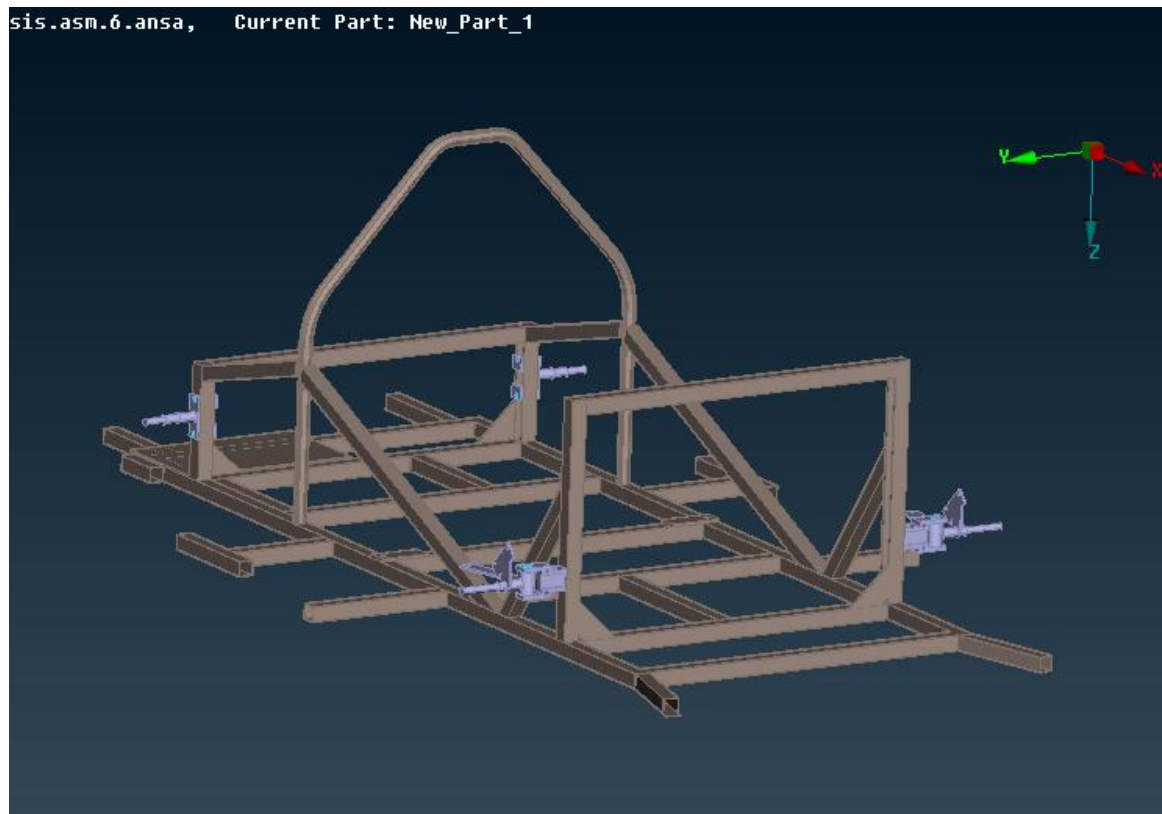


Figure 11-76 Materials Definition on the Aluminium Space Frame

Then, the aluminium characteristics are inserted into the following form. The same is done for the steel characteristics in a similar form.

Name:

FROZEN_ID: FROZEN_DELETE: DEFINED:

MATID:

EX	EY	EZ	PRXY
PRYZ	PRXZ	NUXY	NUZY
NUZX	GXY	GYZ	GXZ
ALPX	ALPY	ALPZ	REFT
MU	DAMP	DENS	KXX
KYX	KZZ	C	ENTH
HF	EMIS	QRATE	VISC
SONC	MURX	MURY	MURZ
MGXX	MGYX	MGZZ	RSVX
RSVY	RSVZ	PERX	PERY
PERZ	LSST		

OK ColorEdit Cancel

Figure 11-77 Properties definition

11.3.2.3 Meshing

Inside the software, in the field of Mesh Parameters, the maximum and the minimum dimension of the mesh is assigned as 10mm and 5mm respectively. This choice is derived from the need to include a great number of elements inside the mesh. It is also important to mention that the Meshing Scenario of ANSA is created in every single part separately. There are several images below which show the mesh that was created. Additionally, inside these images several characteristics of some areas of the chassis design are depicted in order to make the creation of the mesh more comprehensible. For the creation of the mesh, the command of Shell Mesh was used. With the Shell Mesh com-

mand, an initial mesh at the surfaces of the solid was able to be constructed. Then, by using the already created surface mesh as a base, the volume mesh was derived by the Mesh Volume command.

11.3.2.3.1 Shell meshing

In the beginning, we apply shell meshing to the model. The mesh's density is higher in the highlighted areas compared to the rest of the model.

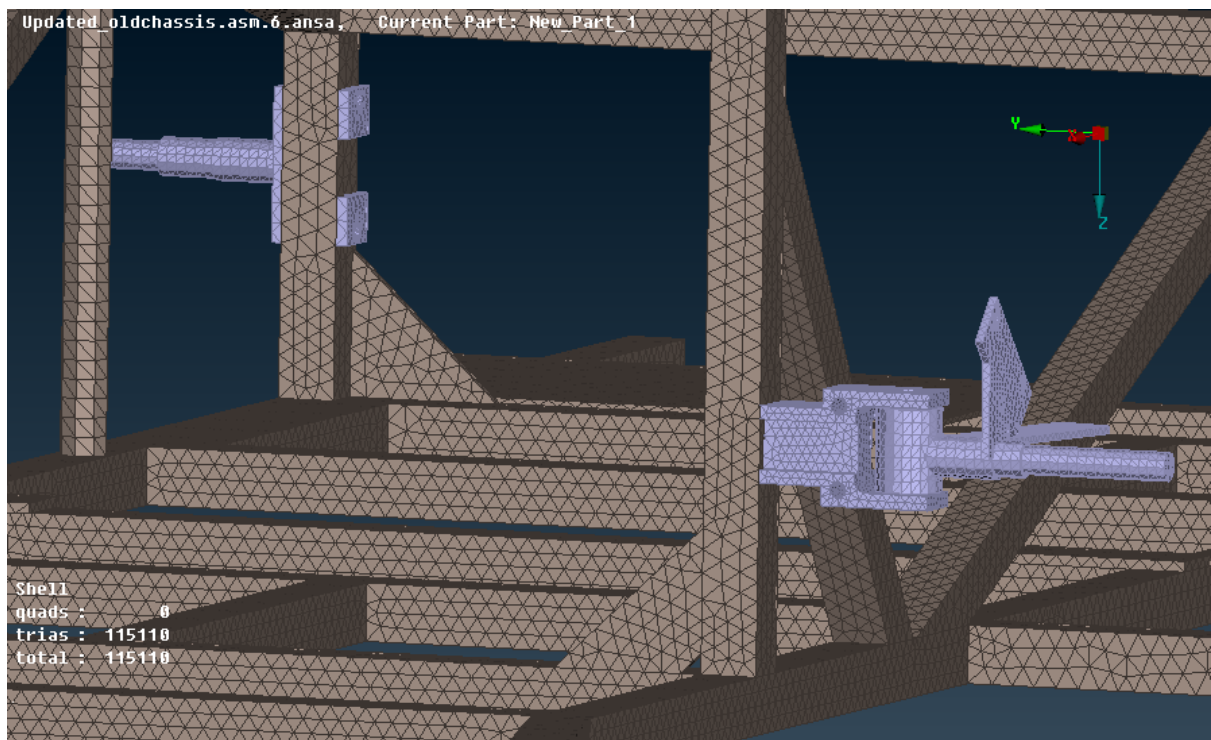


Figure 11-78 Shell Mesh on the Aluminium Space Frame (View 1)

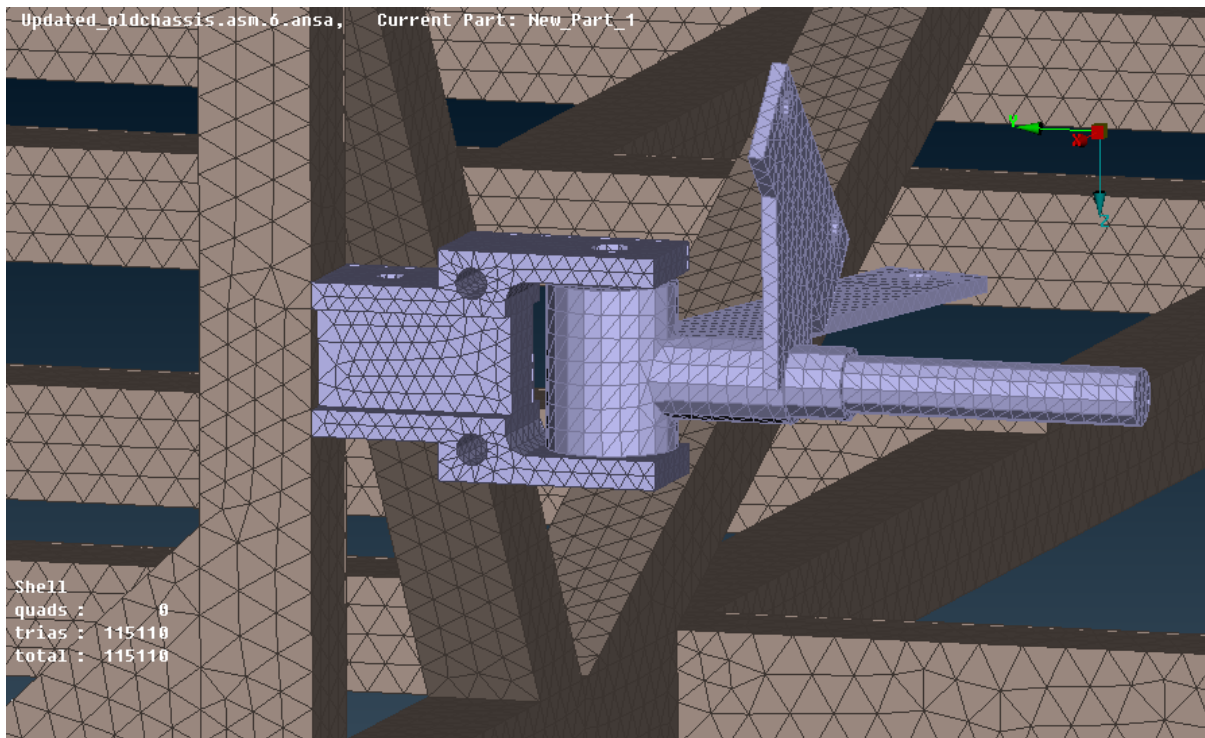


Figure 11-79 Shell Mesh on the Aluminium Space Frame (View 2)

11.3.2.3.2 Volume meshing

The next step is to perform volume meshing. In the following images we observe the volume mesh of our model and its density, as mentioned above.

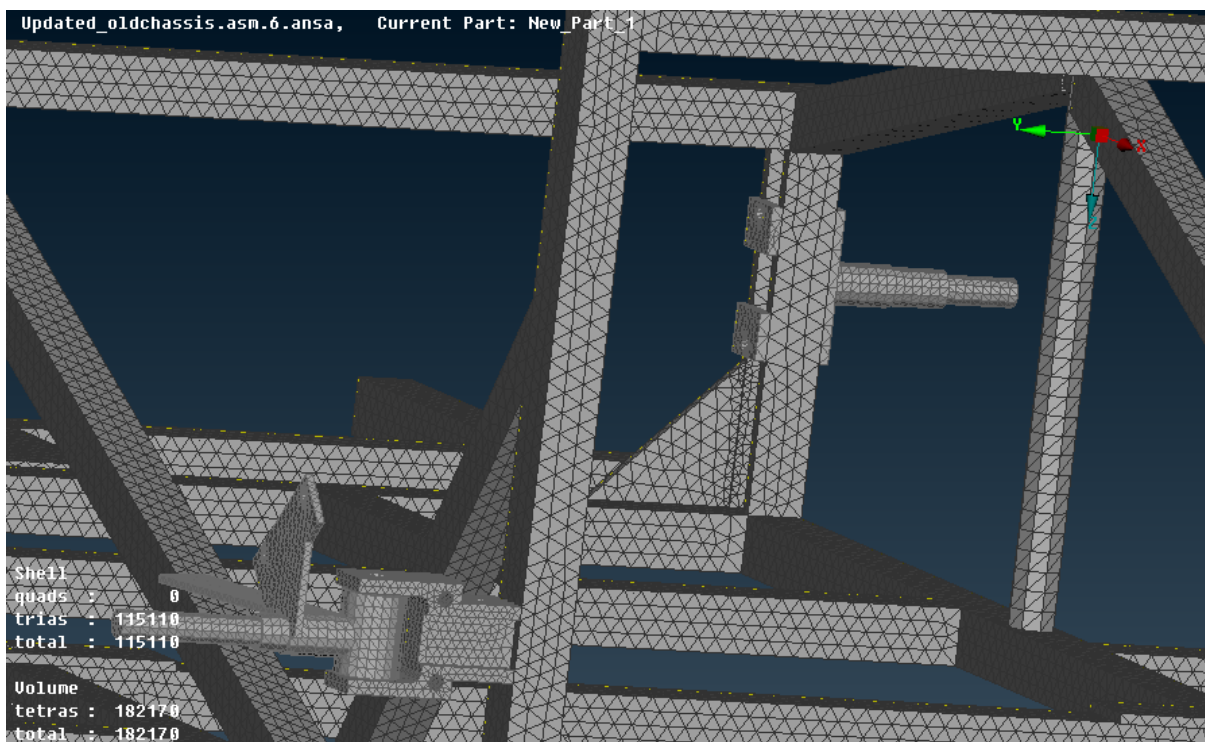


Figure 11-80 Volume Mesh on the Aluminium Space Frame (View 1)

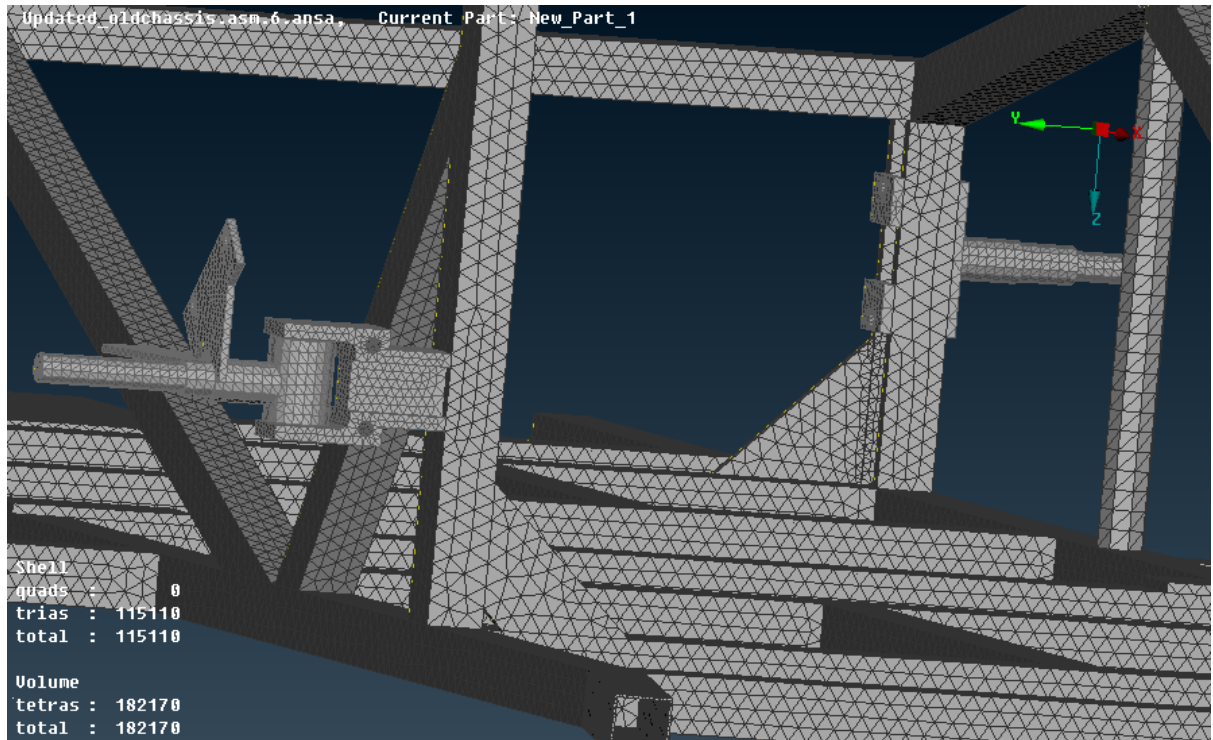


Figure 11-81 Volume Mesh on the Aluminium Space Frame (View 2)

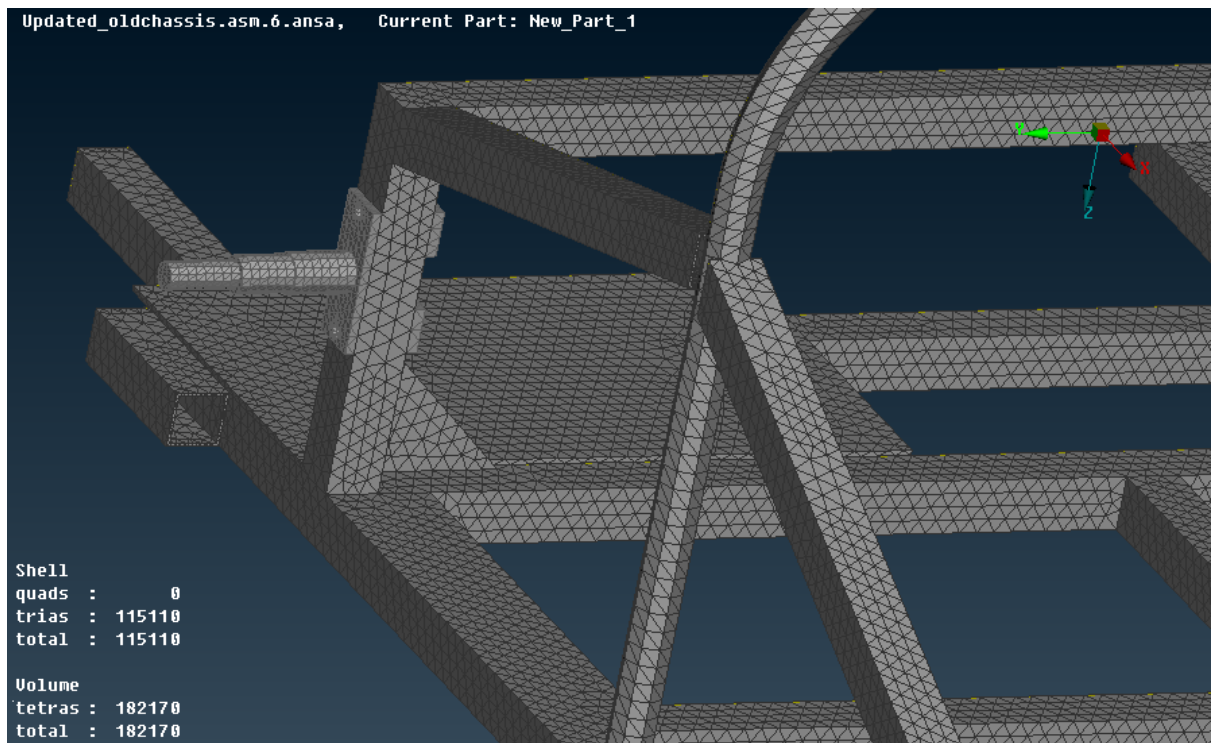


Figure 11-82 Volume Mesh on the Aluminium Space Frame (View 3)

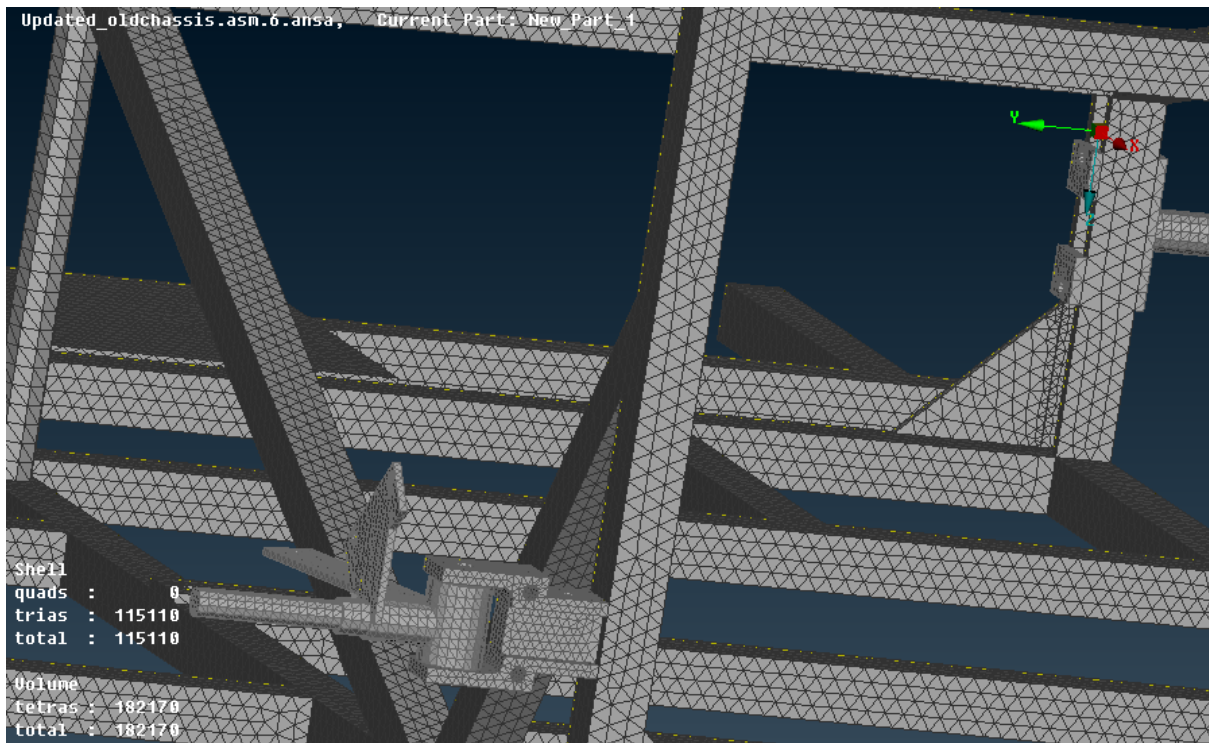


Figure 11-83 Volume Mesh on the Aluminium Space Frame (View 4)

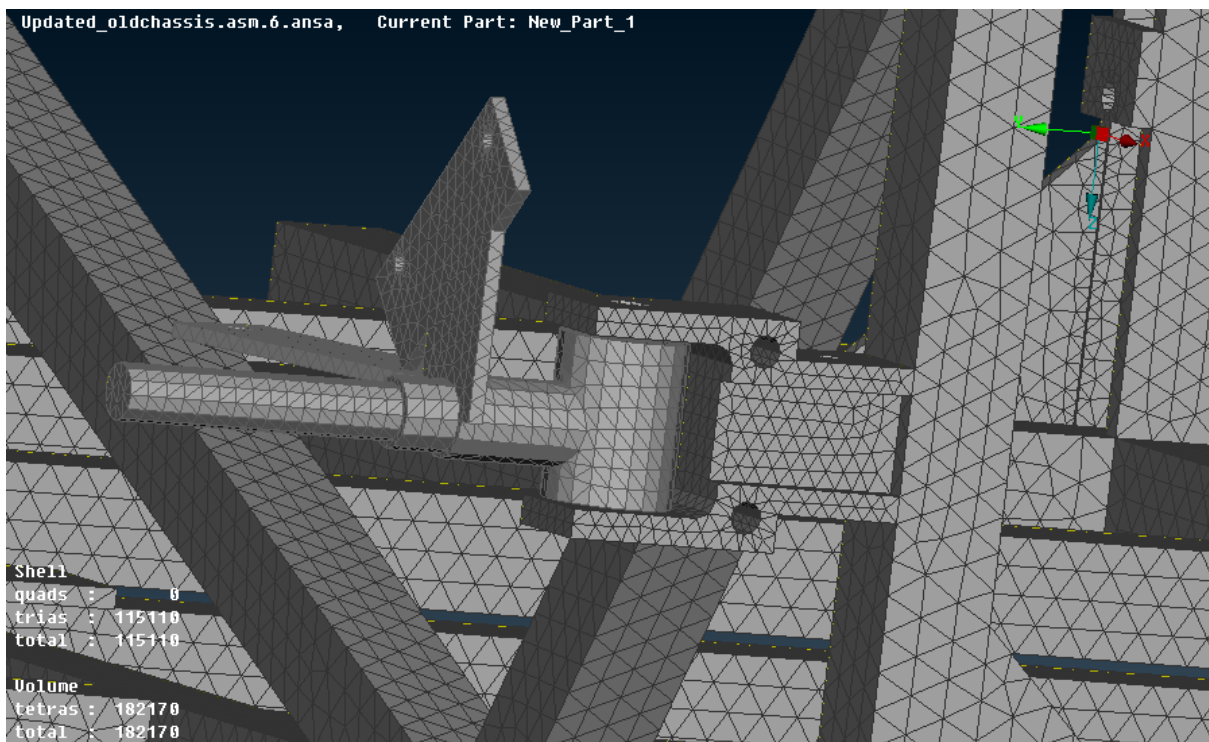


Figure 11-84 Volume Mesh on the Aluminium Space Frame (View 5)

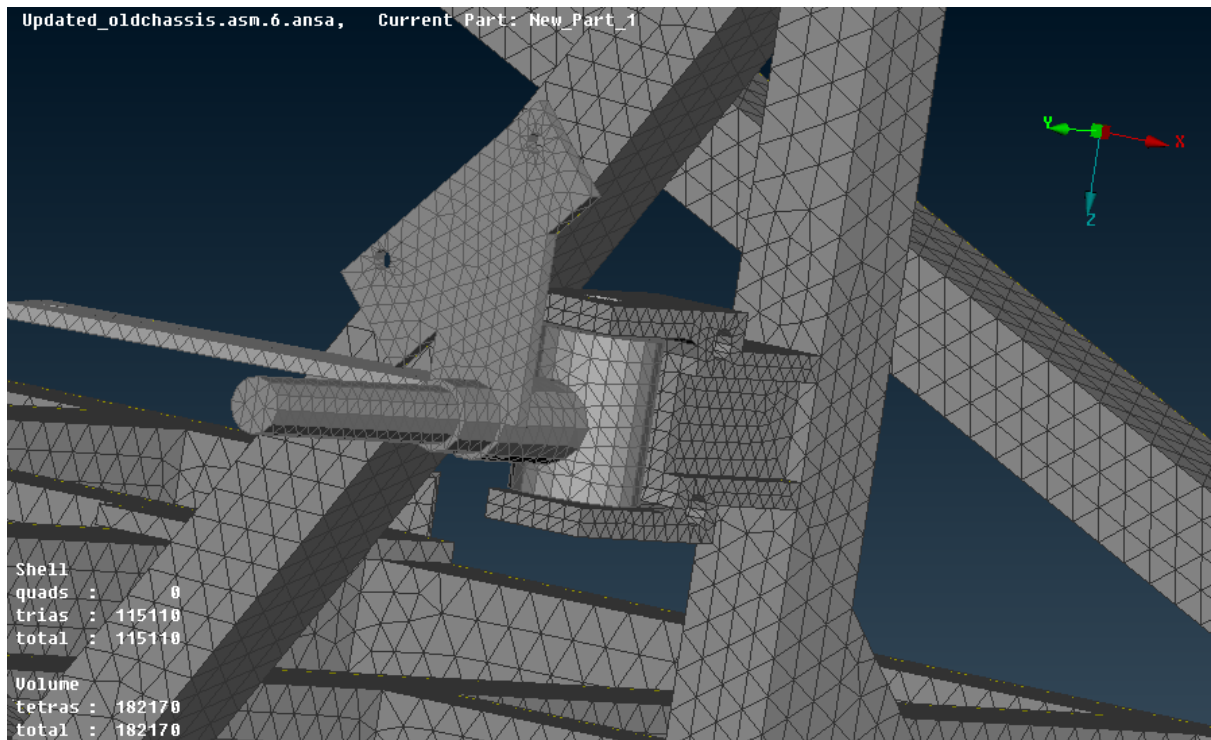


Figure 11-85 Volume Mesh on the Aluminium Space Frame (View 6)

11.3.2.3.3 Meshing check

A series of checks take place in order to ensure that our model is functional.

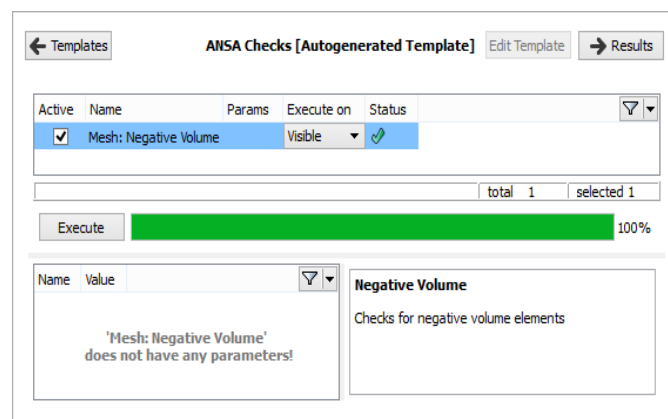


Figure 11-86 Negative volume check

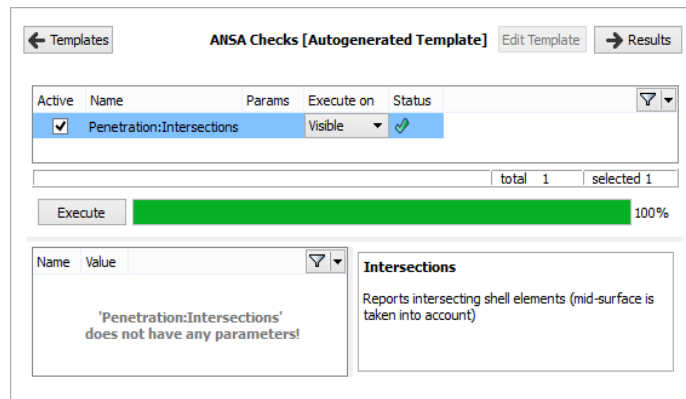


Figure 11-87 Penetrations-Intersections check

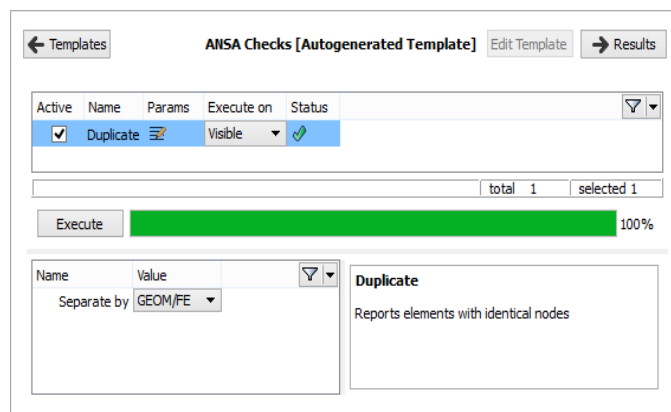


Figure 11-88 Duplicate elements check

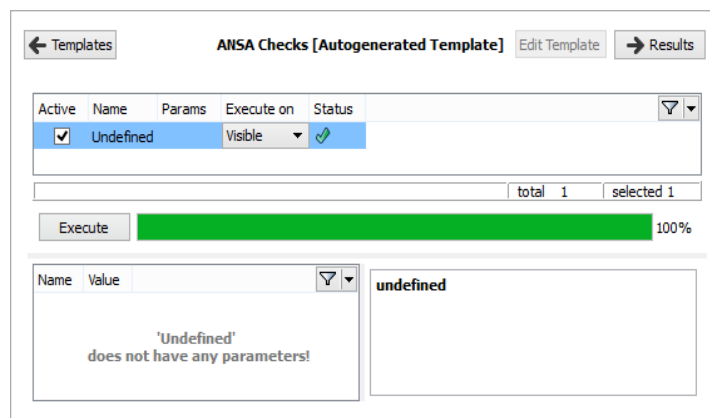


Figure 11-89 Undefined check

From the above figures, it can be seen that our model is error-free and ready for further processing.

11.3.2.4 Connections

The next step is to add the connections to our model. These connections consist of bolt connections and flanges.

11.3.2.4.1 Bolt connections

We place bolt connections, in the areas which have bolts.

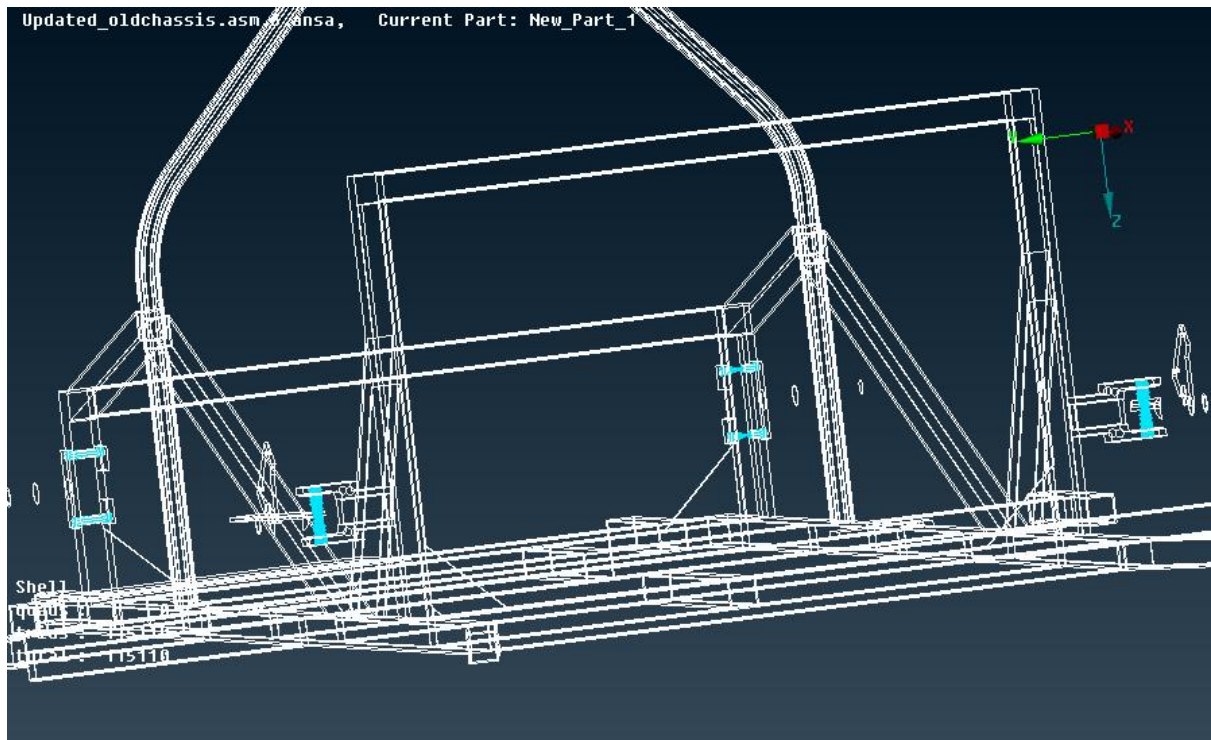


Figure 11-90 Bolt connections on the Aluminium Space Frame (View 1)

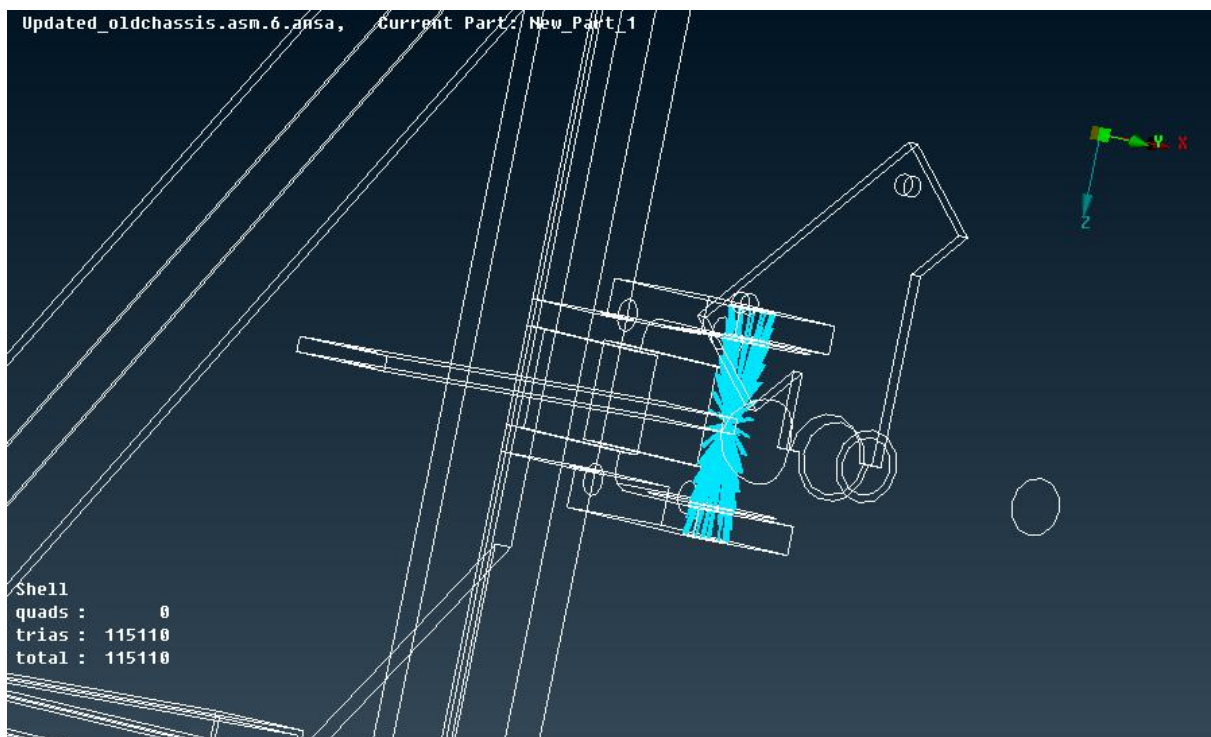


Figure 11-91 Bolt connections on the Aluminium Space Frame (View 2)

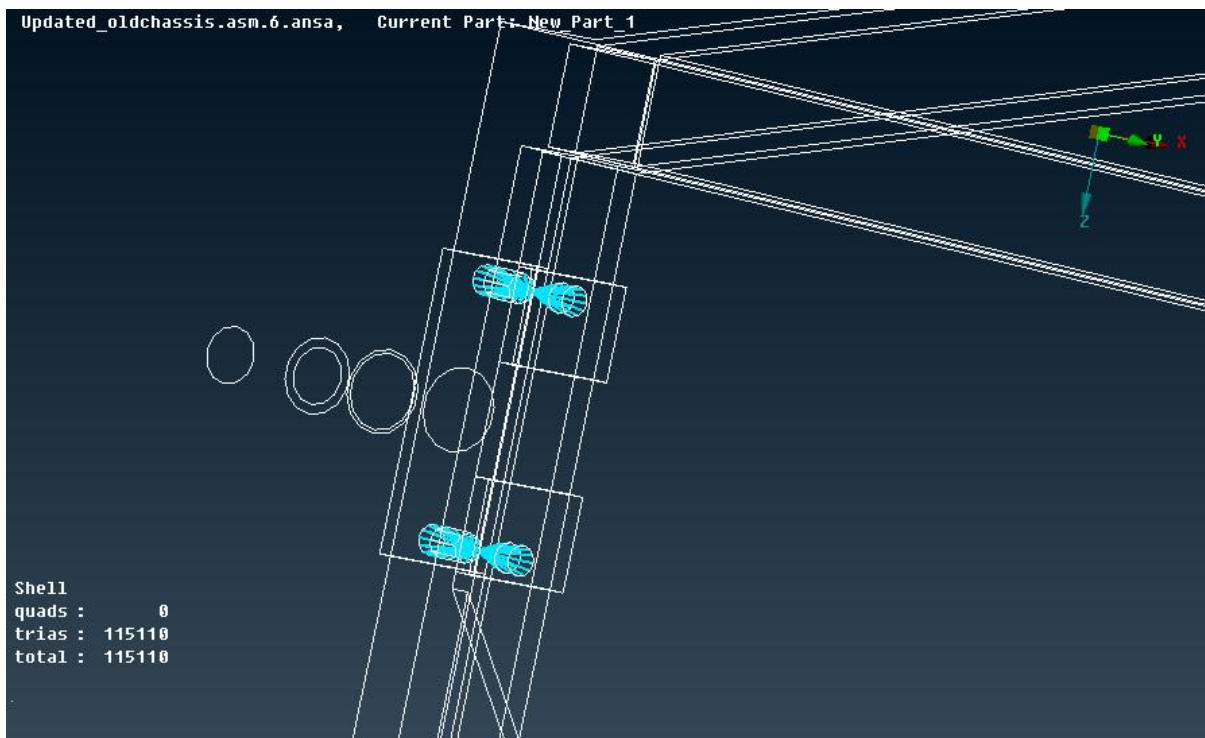


Figure 11-92 Bolt connections on the Aluminium Space Frame (View 3)

11.3.2.4.2 Contact flanges

In this stage, the contact flanges connections are placed.

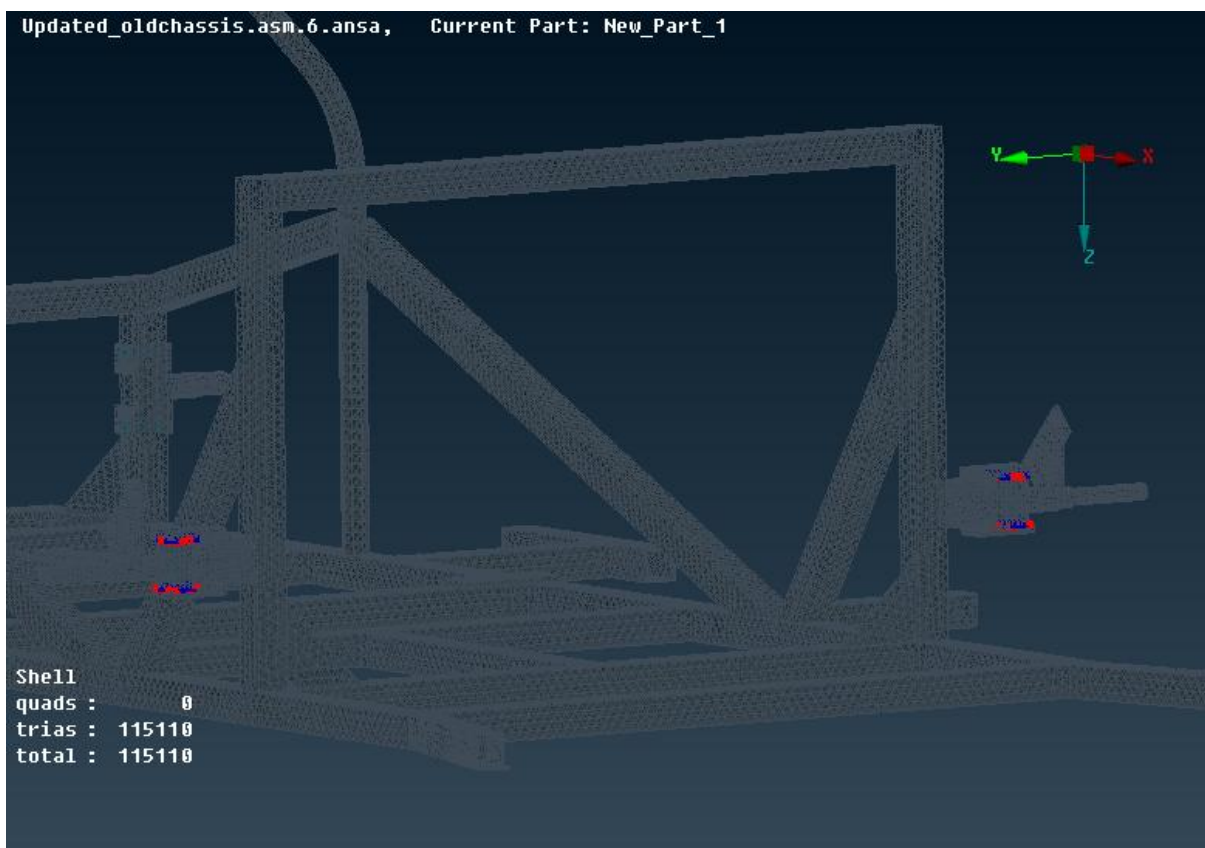


Figure 11-93 Contact Flanges on the Aluminium Space Frame (View 1)

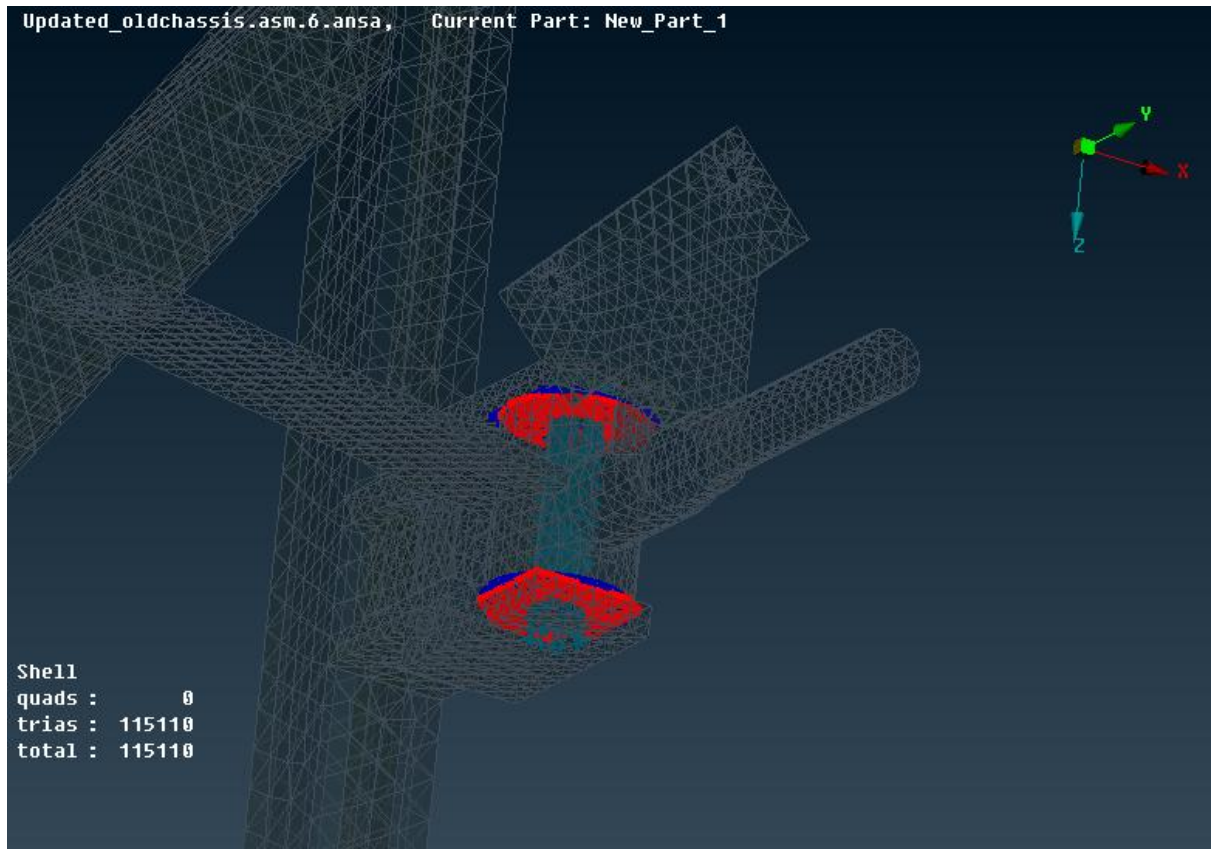


Figure 11-94 Contact Flanges on the Aluminium Space Frame (View 2)

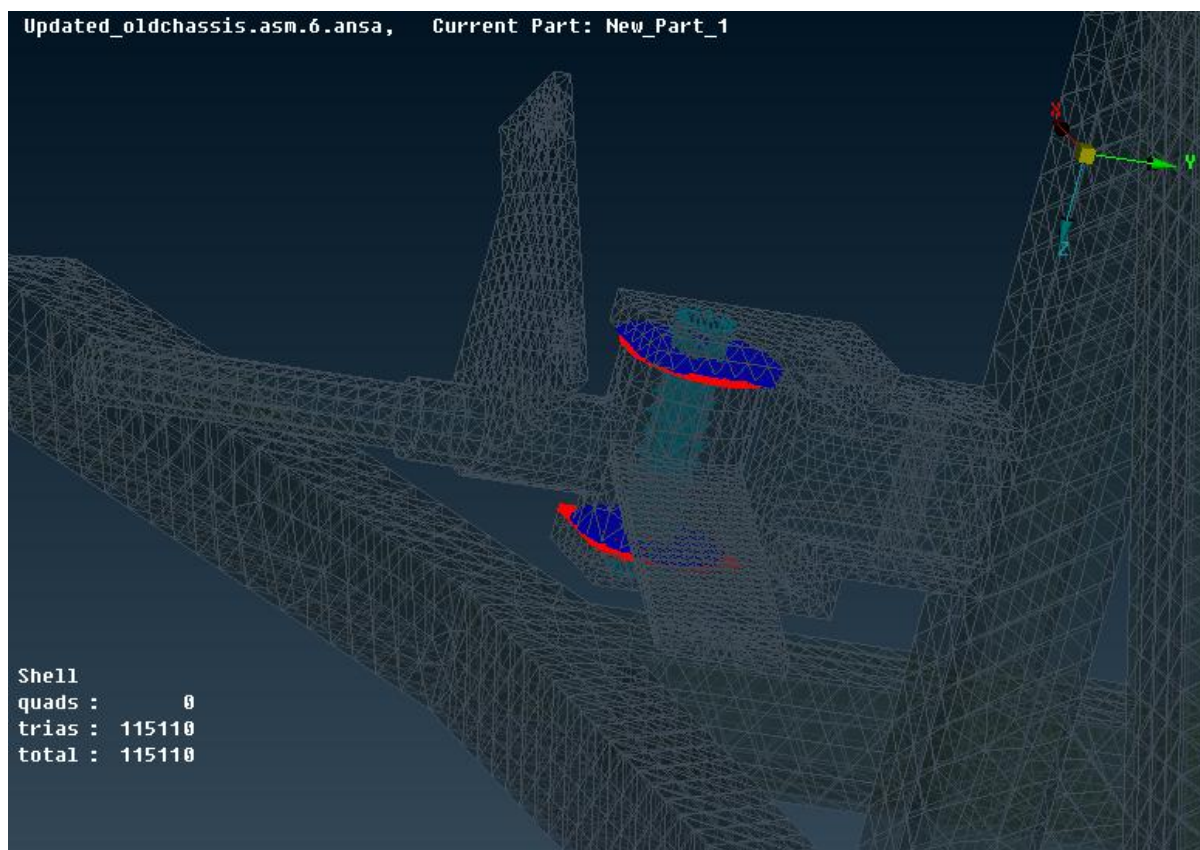


Figure 11-95 Contact Flanges on the Aluminium Space Frame (View 3)

11.3.2.5 Loadstep manager

In the loadstep manager, we define just one step which includes:

- a) the permanent static loads (that is, driver, fuel cell, battery light, steering system, electric motor loads) which always act on our chassis.
- b) the total dynamic loads on the front axles that act during the coexistence of braking and cornering.
- c) the loading constraints.

11.3.2.5.1 Loading constraints

The same loading constraints as the previous chassis are placed. The rearmost section of the chassis is constrained with all DOF's (degrees of freedom 123456).

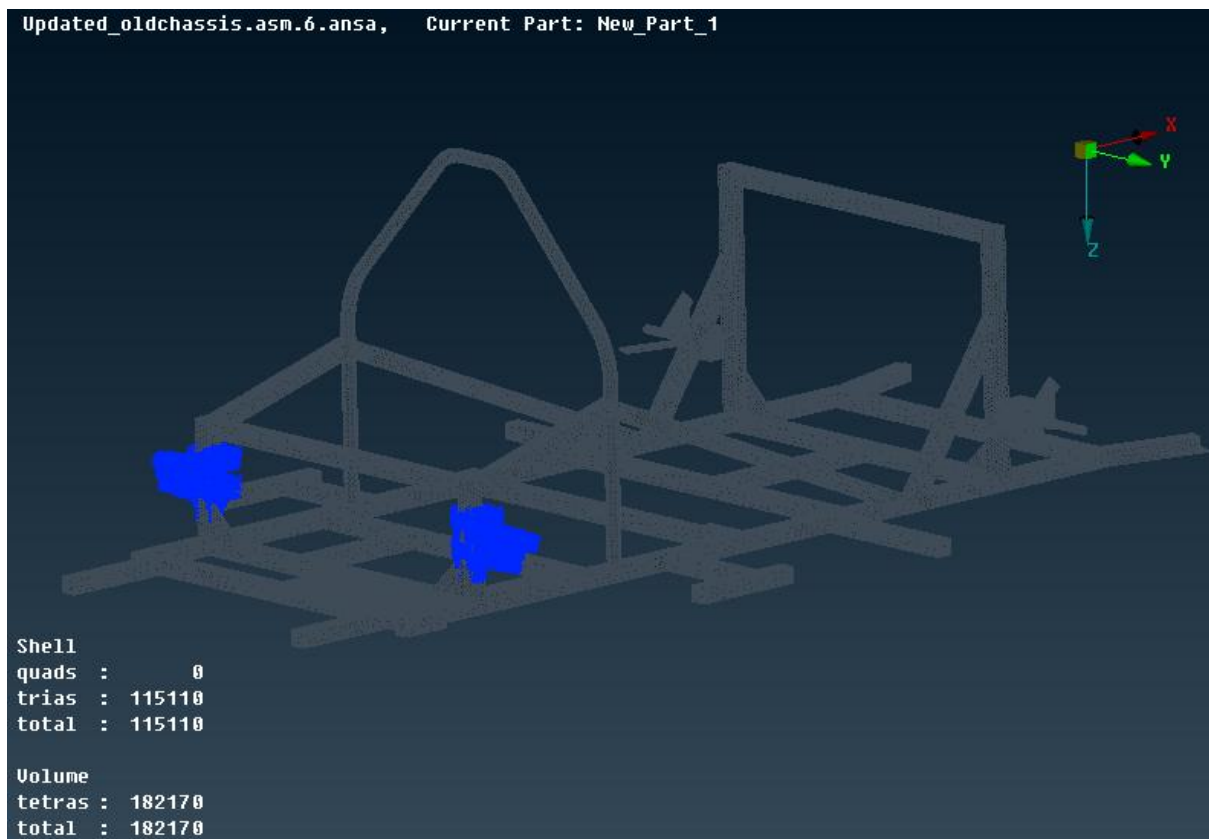


Figure 11-96 Loading Constraints on the Aluminium Space Frame (View 1)

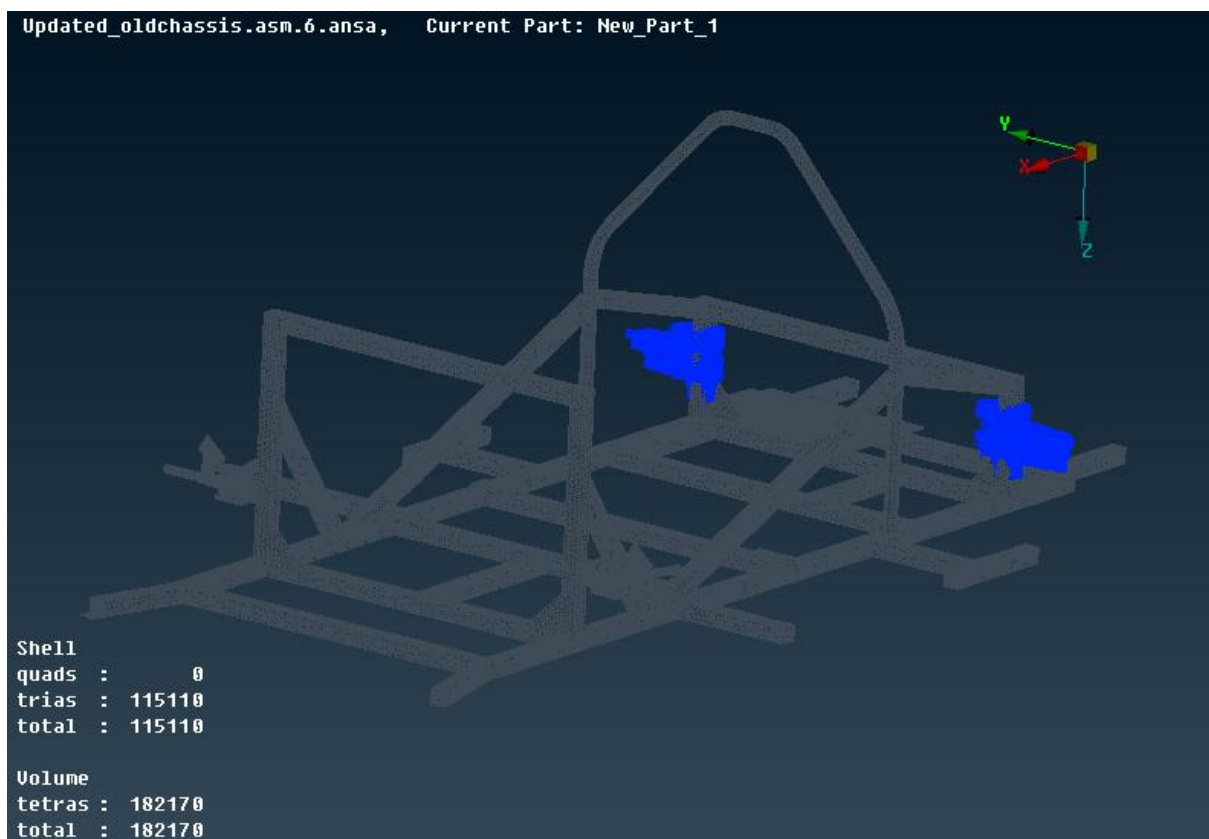


Figure 11-97 Loading Constraints on the Aluminium Space Frame (View 2)

11.3.2.5.2 Front axle loads

The longitudinal, the lateral and the vertical loads are applied, as well as the roll and the pitch moments on the front axles. These loads and moments have already been calculated in a previous chapter.

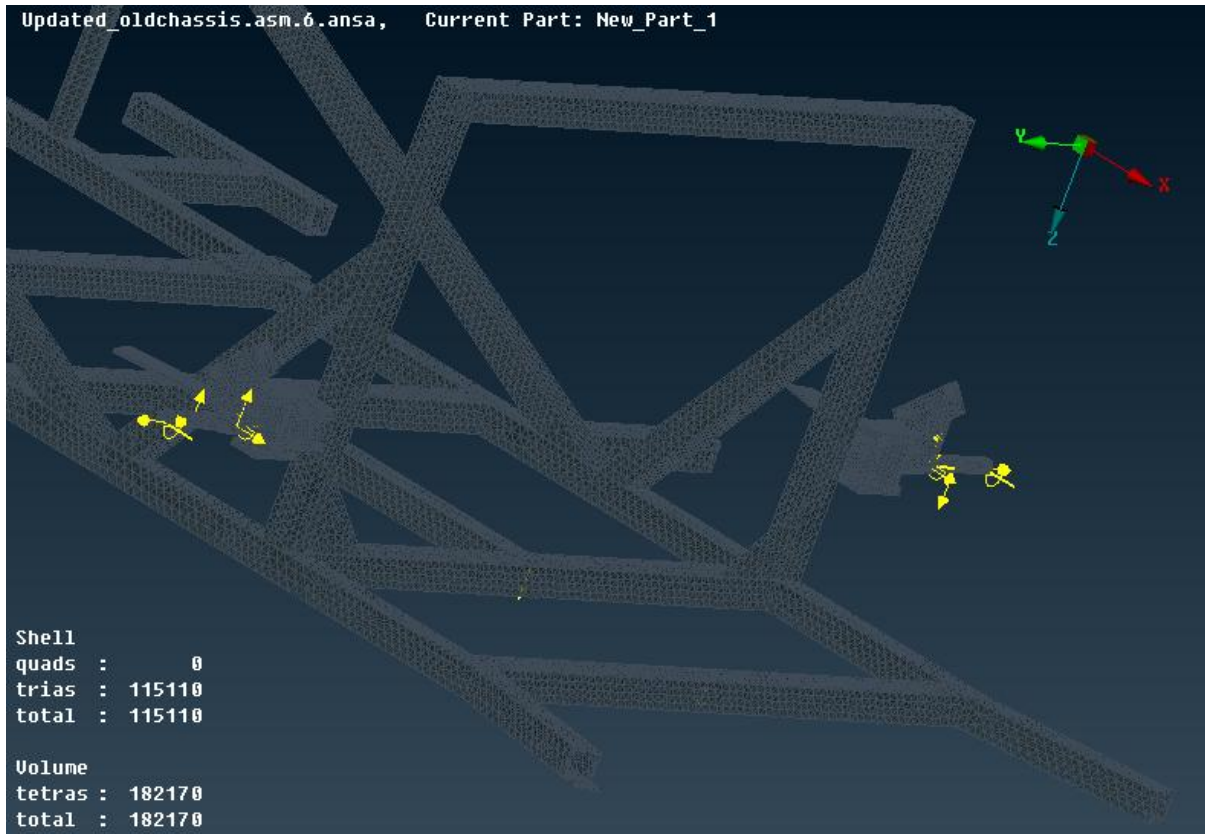


Figure 11-98 Front Axle Loads on the Aluminium Space Frame (View 1)

11.3.2.5.3 Permanent static loads

The permanent static loads (driver, fuel cell, battery light, steering system, electric motor loads) are applied on the space frame.

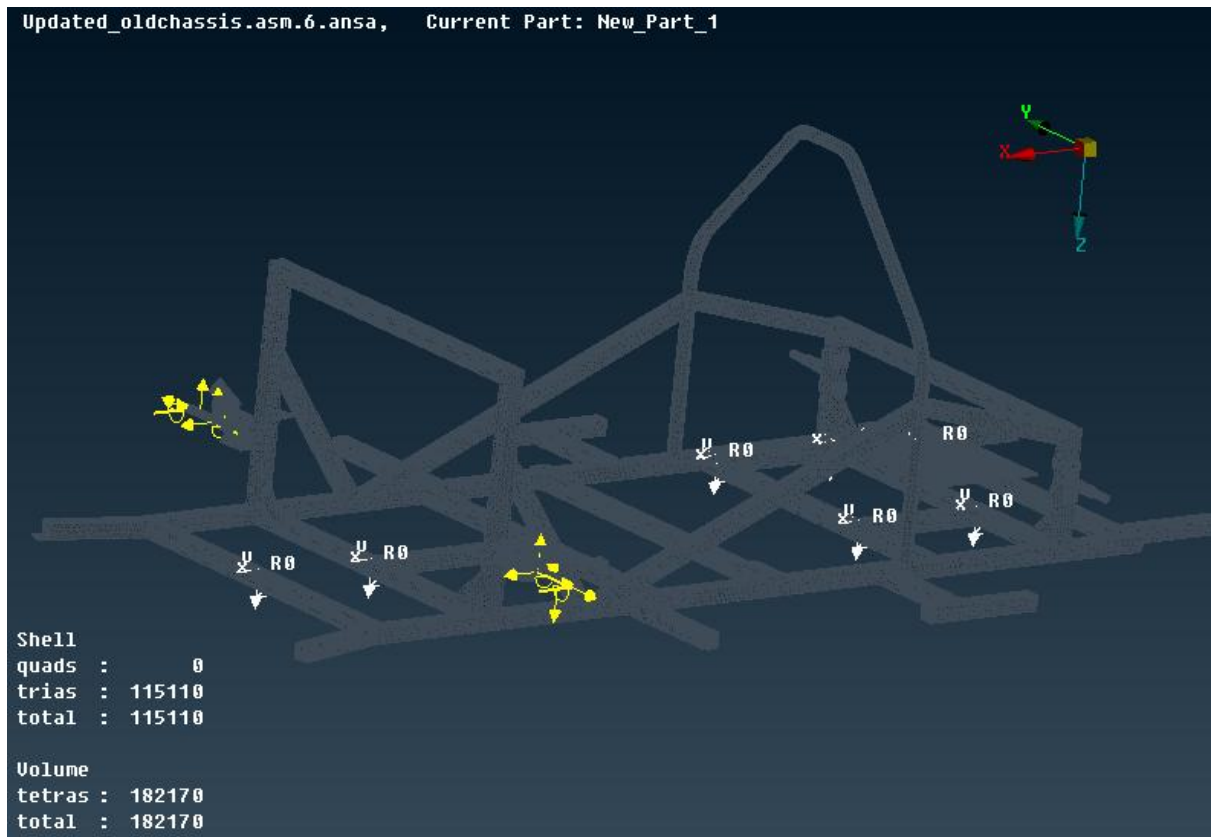


Figure 11-99 Permanent Static Loads on the Aluminium Space Frame (View 1)



Figure 11-100 Permanent Static Loads on the Aluminium Space Frame (View 2)

The pressure applied from the driver's body weight (from the table 11-2) is calculated, dividing the force applied by the driver, by the area that the driver's seat takes up on the chassis. We have four seat bases, so we have four equal pressures applied on the chassis:

Table 11-2 Pressure applied from the driver's body weight

DRIVER'S SEAT PRESSURE	
kg	75 kg
kg/4	18.75 kg
Force/4	183.9375 N
AREA	1621.5 mm ²
PRESSURE	0.113436633 Mpa

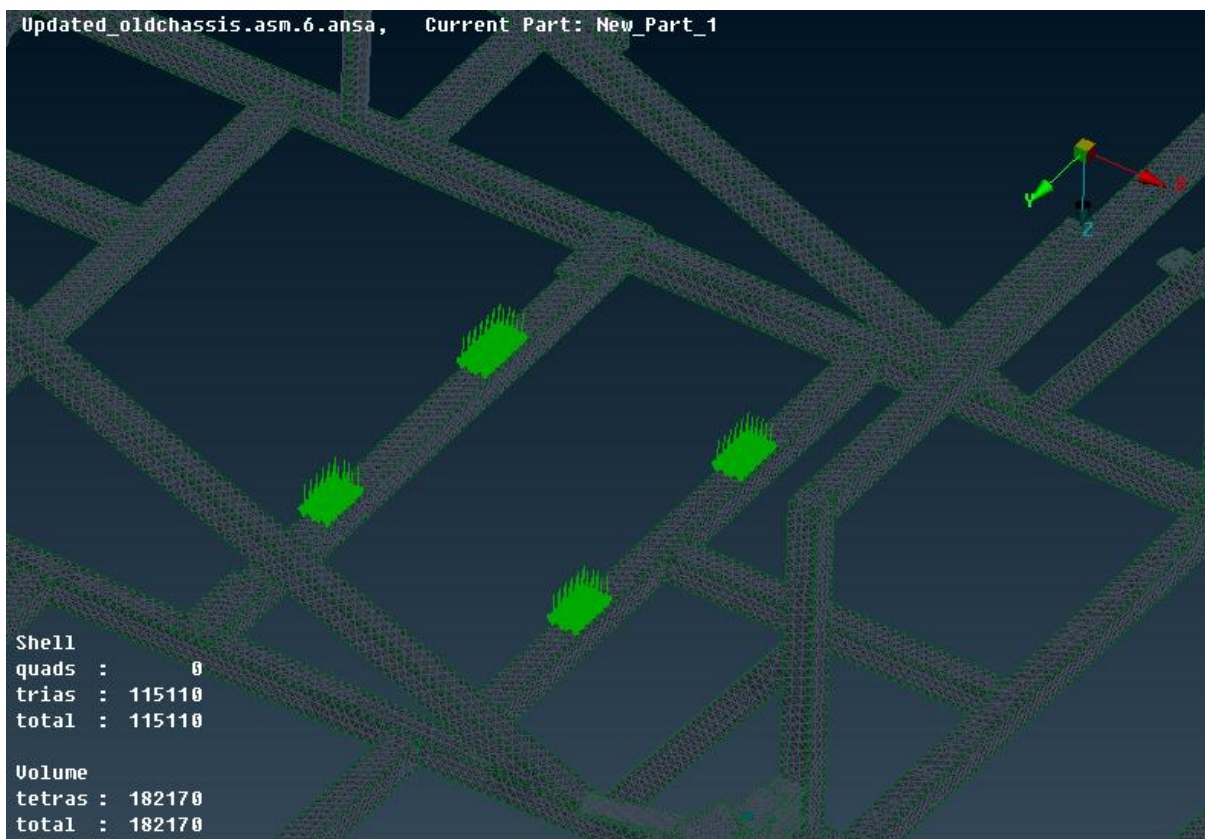


Figure 11-101 Driver's Pressure on the Aluminium Space Frame (View 1)

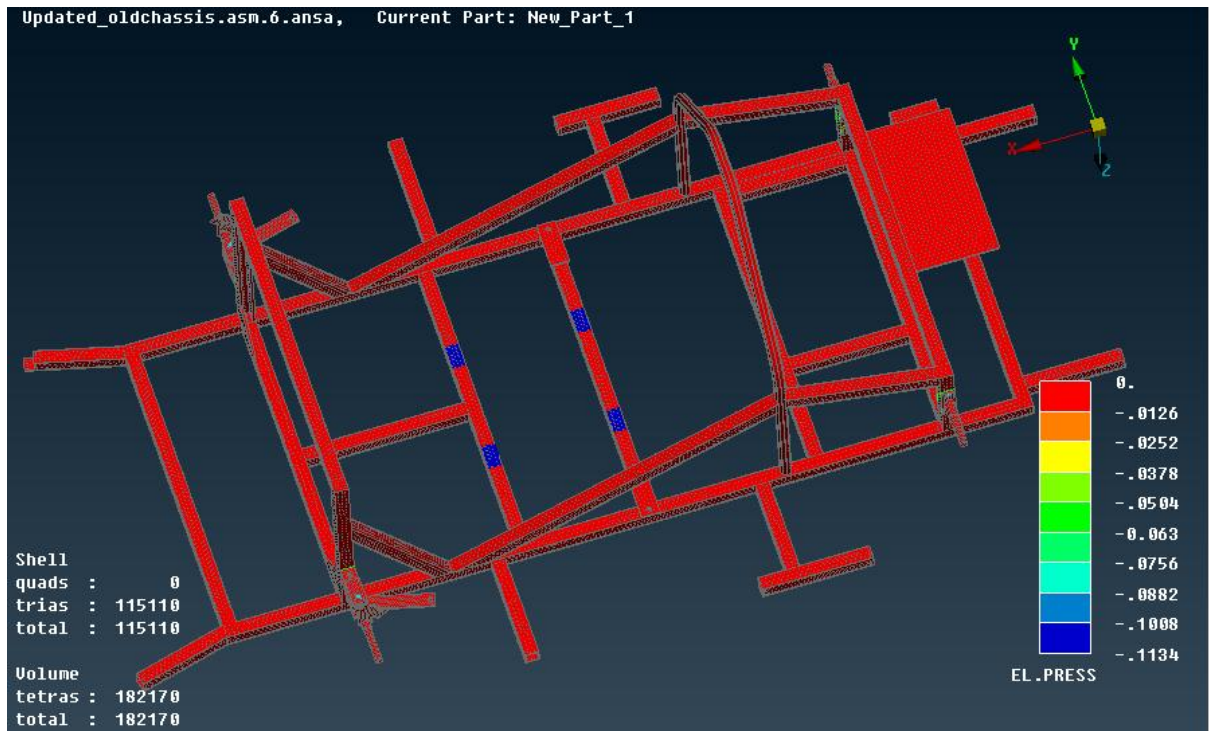


Figure 11-102 Driver's Pressure on the Aluminium Space Frame (View 2)

11.3.2.6 Gravity acceleration

In our analysis, we took into consideration the gravity acceleration (9.81m/s^2). We applied this acceleration on the z axis as one can see in the following images.

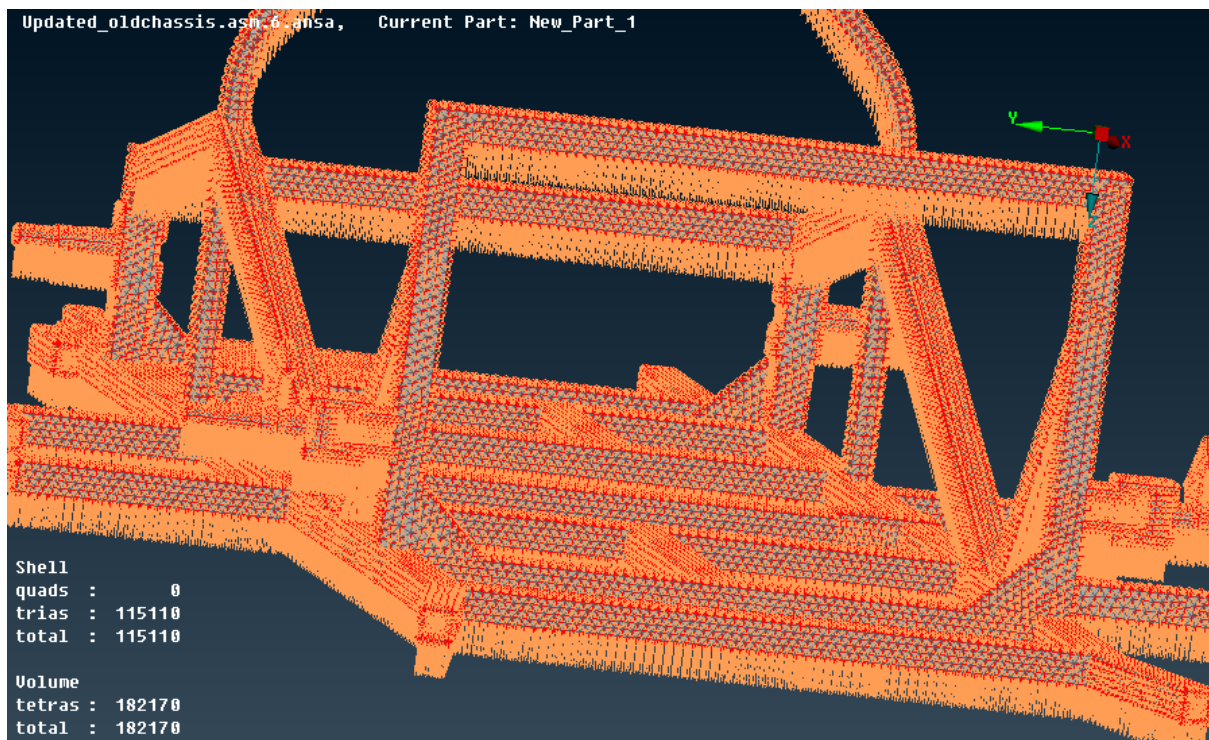


Figure 11-103 Gravity Acceleration on the Aluminium Space Frame (View 1)

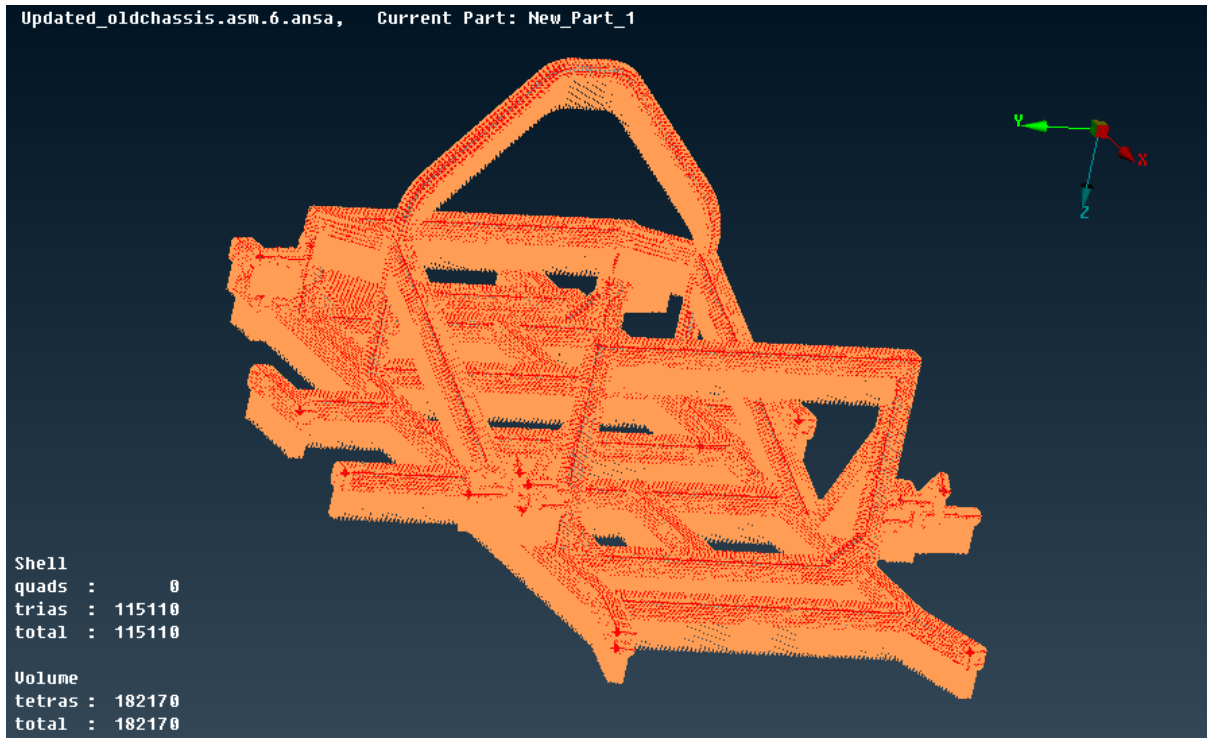


Figure 11-104 Gravity Acceleration on the Aluminium Space Frame (View 2)

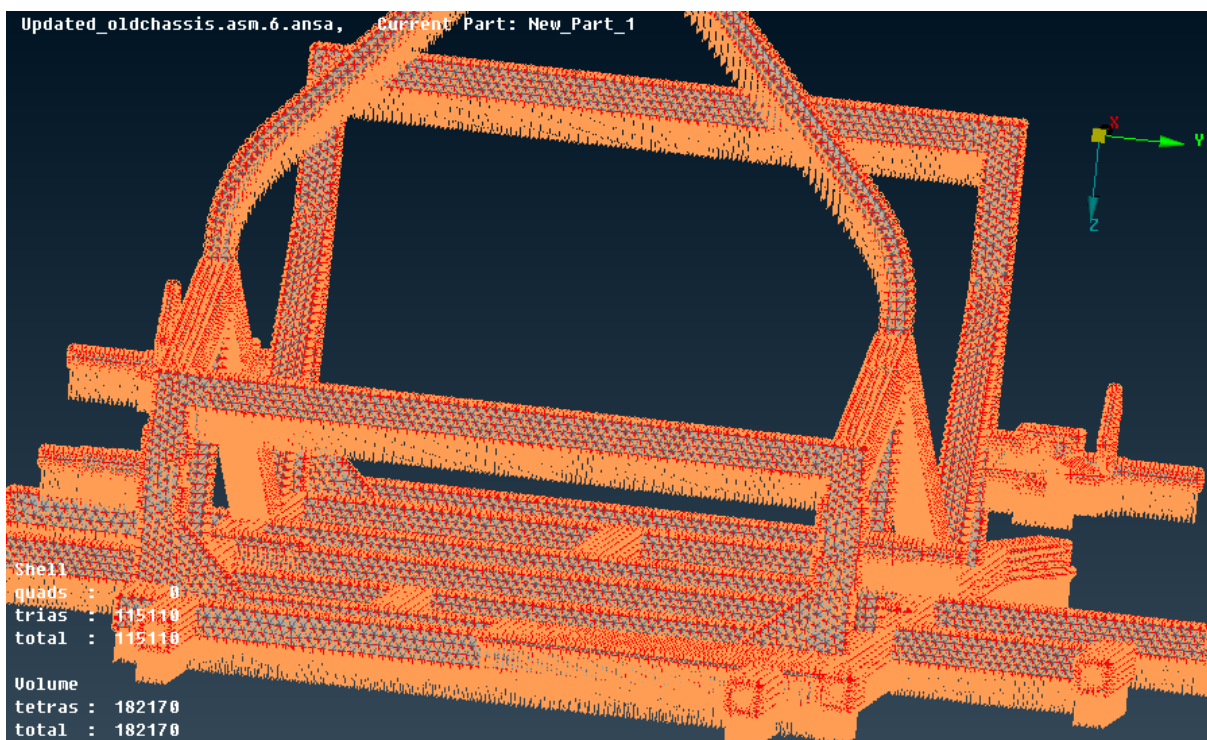


Figure 11-105 Gravity Acceleration on the Aluminium Space Frame (View 3)

12 FINAL DECISION

Each object that has a mass and moves with speed, has a particular energy, which is derived from the motor used. If the chassis is moved at a particular speed, energy can be calculated using the following formula:

$$E = \frac{1}{2} m v^2$$

- where m the mass and v the moving velocity.

The less mass the chassis has, the less energy is needed to move it.

Having designed and modeled the previous and the suggested chassis, the first phase of the work was completed. The criteria of comparison of the best design are the weight, the energy consumption, the durability, the ergonomics, the cost and the aesthetic acceptance of the chassis. Below is a comparative table (Table 12-1) with the previous and the proposed chassis.

Table 12-1 Chassis comparison

	Previous chassis	New chassis	Percentage change
Mass(kg)	10.85 kg 	5.38 kg 	50.41475 %
Energy consumption			
Ergonomics			
Aesthetic			

The new chassis and hence the new vehicle will be ultra light. It weights only 5.38kg and consequently less energy is consumed to move it, in relation to the previous one. This energy decrease, which we have obtained, is significantly high, if we take into account that the previous chassis of TUCER team was one of the lightest chassis of the competition.

Due to the positive results obtained so far, we propose that this research be continued, during the postgraduate studies, so as to simulate the suggested chassis, in order to prove that it conforms to the structural requirements. Undoubtedly, the cost of carbon-fiber composites is high. However, all the criteria should be analyzed carefully to achieve a good combination, which will make the project affordable for the research team.

13 MANUFACTURING PROCESS

13.1 Composite materials

Composite materials consist of two or more materials with different mechanical and chemical properties. The individual materials are easily distinguishable, when they are combined. The individual materials that make up composites are called constituents. Most composites have two constituent materials: a binder or matrix, and a reinforcement. The reinforcement is usually much stronger and stiffer than the matrix, and gives the composite its good properties. The reinforcement material in our case is carbon fiber.

The role of the matrix in a composite material:

- The matrix holds the fibers in an orderly pattern.
- Because the reinforcements are usually discontinuous, the matrix also helps to transfer load among the reinforcements.
- Protects the fiber from environmental conditions.
- Protects the fibers from mechanical degradation.

13.1.1 Composite resins (matrices)

Resins are of utmost importance within the composites markets as they bind the fibers together and help create the material's strength and stiffness characteristics. There are two types of resin systems: thermoset and thermoplastic. In a thermoset, the resin molecules are locked together in an irreversible way after a thermal cure; it is a one-way cure that cannot be undone. In a thermoplastic resin the chemical link which is bonding the molecules together can be broken again and again by increasing the temperature steadily which causes the matrix to go from solid to liquid. In the same way, when cooled down the thermoplastic matrix solidifies. We will now concentrate on the Thermoset resins that are playing a key role in the composite industry. These are Polyester, Vinyl Ester, Epoxy, Phenolic Resins and Cyanate Ester and Bismaleide. The polyesters and epoxies discussed here probably account for some 90% of all thermosetting resin systems used in structural composites. In summary the main advantages and disadvantages of each of these types are [66]:

13.1.1.1 Polyester resin

Polyester resins are one of the most common resin used in the composite industry. The success of Polyester is mainly based on the low cost that makes this it more attractive than some higher performing resins like epoxies (below). Polyester resins require a catalyst, which functions as an initiator of the chemical reaction, to solidify. The quantity of catalyst has an effect on the speed of the reaction and is responsible for the solidification. During the cure the polyester resins shrink significantly.

Advantages

Polyester resins have numerous advantages. The most well known benefit of polyester is the price; the resin is relatively cheap in comparison to other types of resin. Furthermore, polyester has the ability to accept a broad variety of fillers which makes them applicable to a wide range of projects. Another benefit of polyester is that once demolded,

the part can be sanded and finished resulting in an optically clear surface. Finally, Polyester is not impacted by UV radiation like other resins which is essential for applications exposed to the sun, for instance, surfboards.

Disadvantages

The most striking disadvantages are the mechanical properties which are not as good as, for example, epoxies. Furthermore, polyester resin has high styrene emission in open mould which is perceived as a disadvantage and that requires special precautions when processing. The high curing shrinkage is another major drawback. Moreover, the limited range of working times minimizes the usability for the polyester resin.

13.1.1.2 Epoxy resin

Although it is more expensive than other resin systems, the advantages outrun the disadvantages. Epoxy has much better physical and adhesion properties compared to polyester and/or vinyl ester. Based on its properties, this resin system is used in various industries including the aerospace, automotive and marine industries.

Advantages

The mechanical properties and its resistance to environmental degradation which makes the resin system especially attractive to the aircraft industry. Furthermore, epoxy is water resistant and therefore used heavily within the marine industry. The adhesive properties and the low shrinkage are further benefits of epoxies. Finally, epoxies cure easily and quickly making them beneficial for numerous projects.

Disadvantages

However, the epoxy systems also have some drawbacks that limit it to a certain degree. First of all the material itself is very expensive and the cost factor can determine the decision significantly. Moreover, the workers have to be skilled and know the exact mixing procedure and amounts to perform a satisfactory end result; the mixing is critical. Epoxies need a hardener that has to be mixed with the resin in order to start the curing process. The mixture of both components to get the required end result is critical; the correct ratio is needed to ensure optimal cross linking of the molecules during the cure. Skilled and experienced workers are more expensive and thus, influence the overall cost tremendously.

Regardless of the method of production that will be used it is worth noting the use of even two materials

13.1.2 Gel coat

Gel coat is a surface coating material made of unsaturated polyester resin as a main component to provide the protective and decorative surface to the products [67]. Gel coat enhances weatherability, water resistance, abrasion resistance and other physical and chemical properties, as well as the appearance of the finished products as required depending on the applications. The manufacture of carbon fiber parts typically requires a gelcoat layer to aid in the release of the parts from the mold. Standard resin does not

have the same ingredients as gel coat and has very little strength on its own. Gel coat is best applied by spray application with a pressure pot or catalyst injection system. Gel coat also can be applied with a standard paint gun with primer nozzle at 40-50 psi or Preval sprayer. Applied over the surface of the mold, when the surface is painted with wax and PVA.

13.1.3 PVA

PVA is in liquid form and is applied over the wax film on the surface of the mold. It forms a protective film that protects the wax against the resin was applied to the reinforcement. It also helps to avoid sticking of the product to the mold. In the end, PVA, becomes a thin plastic film which is usually removed with hot water. PVA is used in new molds. In old molds is undesirable because it leaves a rough surface which should be polished.

13.2 Composite molding processes

The carbon fiber reinforcements that was made in composites appearing as textiles inside the model (carbon textile). Many textile stages are infused with resin. After the polymerization of the resins, the final product is derived. Also, by taking into account the restrictions imposed from the desired properties of the construction, the available production processes and the desirable manufacturing cost, the final choice of the appropriate resin for the weaving of the carbon textile is made. There are two possible options for the choice of the resin namely polyester resin and epoxy resin. In industry exist many alternatives for the infusion of resin in fibers. The most common of them can be used for the (batch production of material) or “one-off” items are the following [68] [27]:

13.2.1 Hand lay-Up

Hand lay-up is the simplest and oldest open molding method of the composite fabrication processes. It is a low volume, labor intensive method suited especially for large components, such as boat hulls. Glass or other reinforcing mat or woven fabric or roving is positioned manually in the open mold, and resin is poured, brushed, or sprayed over and into the glass plies. Entrapped air is removed manually with squeegees or rollers to complete the laminates structure. Room temperature curing polyesters and epoxies are the most commonly used matrix resins. Curing is initiated by a catalyst in the resin system, which hardens the fiber reinforced resin composite without external heat. For a high quality part surface, a pigmented gel coat is first applied to the mold surface.

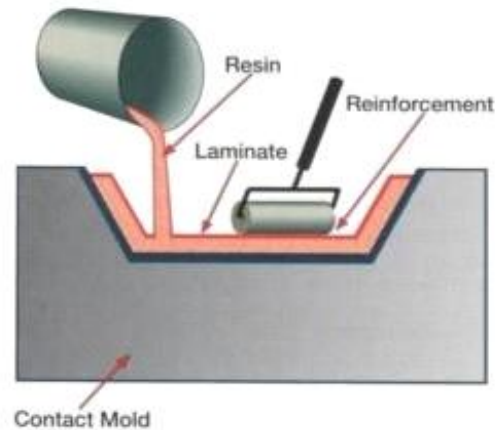


Figure 13-1 Hand Lay-Up

13.2.2 Vacuum bagging

Vacuum bag molding, a refinement of hand lay-up, uses a vacuum to eliminate entrapped air and excess resin. After the lay-up is fabricated on either a male or female mold from precut plies of glass mat or fabric and resin, a non-adhering film of polyvinyl alcohol or nylon is placed over the lay-up and sealed at the mold flange. A vacuum is drawn on the bag formed by the film while the composite is cured at room or elevated temperatures. Compared to hand lay-up, the vacuum method provides higher reinforcement concentrations, better adhesion between layers, and more control over resin/glass ratios. Advanced composite parts utilize this method with preimpregnated fabrics rather than wet lay-up materials and require oven or autoclave cures.

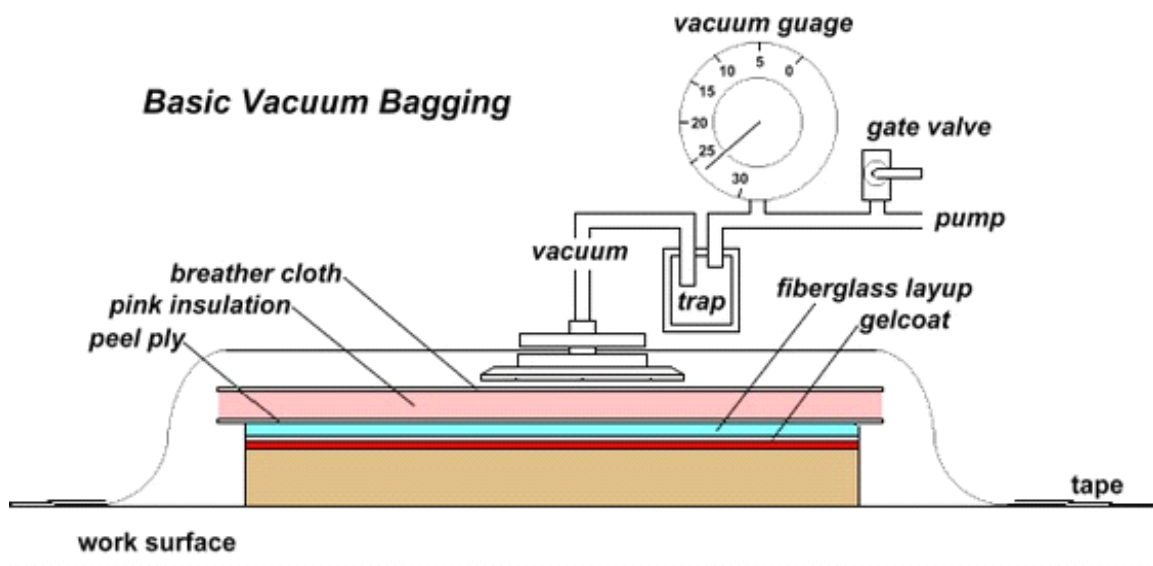


Figure 13-2 Vacuum Bagging

13.2.3 Vacuum assisted resin infusion (V.A.R.I)

Vacuum infusion, also called resin infusion, utilizes a vacuum bag to debulk or compact a parts complete laminate ply schedule of reinforcements and or core materials laid onto the mold. After debulking, the resin is allowed to be infused by the vacuum to completely wet out the reinforcements and eliminate all air voids in the laminate structure.

High quality composite parts made from a wide range of fiber and resin combinations can be utilized to infuse laminates up to six inches thick. Typical resins used are polyester, vinyl ester, and epoxy with many being UV cure initiated. This process can routinely produce large 2,000 sq. ft. parts such as boat hulls, bus bodies, and railcar panels. This processes added benefits include eliminating weaker secondary bonds and reduced VOC emissions vs. current open molding processes. Pigmented gel coats provide the parts surface finish and often a hand lay-up skin laminate may be fabricated to allow fabricators to walk on gel coated surface while loading the dry reinforcement laminate ply schedule and vacuum bag.

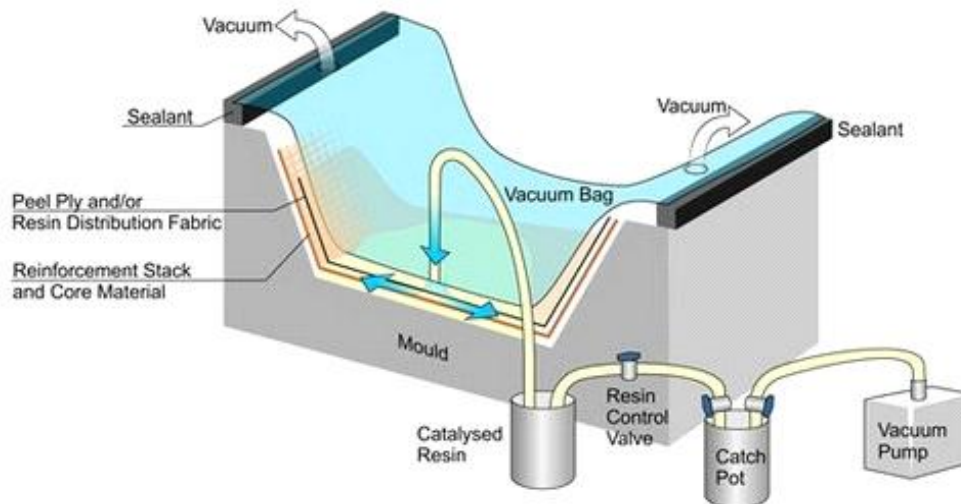


Figure 13-3 Vacuum Assisted Resin Infusion

13.3 Carbon fiber molding

Because we could not obtain a carbon fiber chassis without having a mold, it was important to start by thinking about how our mold would be made, how it would work and how we could get the best possible part from it. Its role is to give the desired shape in composites materials. After a product is designed, usually by an industrial designer or an engineer, molds are made by a mouldmaker (or toolmaker). It consists of two primary components, the upper and lower side and looks like a group of metal plates “sandwiched” together. They are made from metal, usually either steel or aluminium and their cost is very high.

To build a chassis requires the construction of the top and bottom of the mold, followed by the procedure of gluing the two pieces with a special glue. Despite the high cost, we selected the iron material to construct the mold, for strength but also because of the need for reproducibility of the process.

13.4 Developing parts to be molded

We should focus on how we can make sure that what comes out of the mold is what we need it to be. First of all, keeping the mold in mind while we design a part helps us to find ways to create high-quality parts cost-effectively. Draft angle is another characteristic that we need to think about when designing a part. It is a taper applied to the faces of the part that prevent them from being parallel to the motion of the mold opening. This keeps the part from being damaged due to the scraping as the part is ejected out of the mold [69]. If we don't include enough wall angle flaws may appear in the part, that are the result of the part sticking to the mold as the part is ejected. (See Figure 13-4)

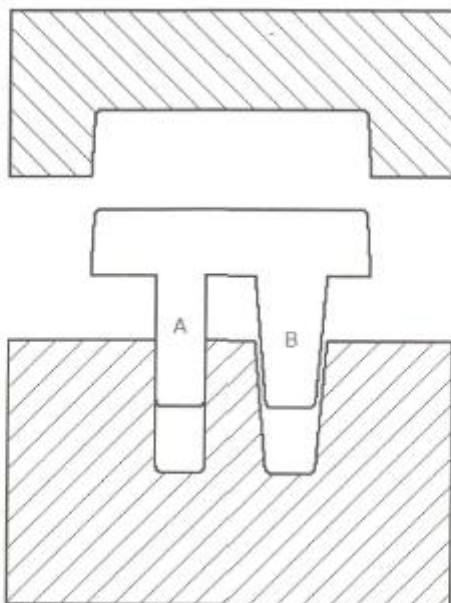


Figure 13-4 The undrafted rib (A) scrapes all the way out, while the drafted rib (B) pops out unblemished. [69]

The key to using the draft concept properly is knowing what angle the draft needs to be. Guidelines for draft angle exist which can be followed and applied. This angle is applied on each face. Furthermore, it is important to keep in mind that the part's corners should be rounded. The corners show high tendencies, which is undesirable. The rounds also help the mold to be easily removed.

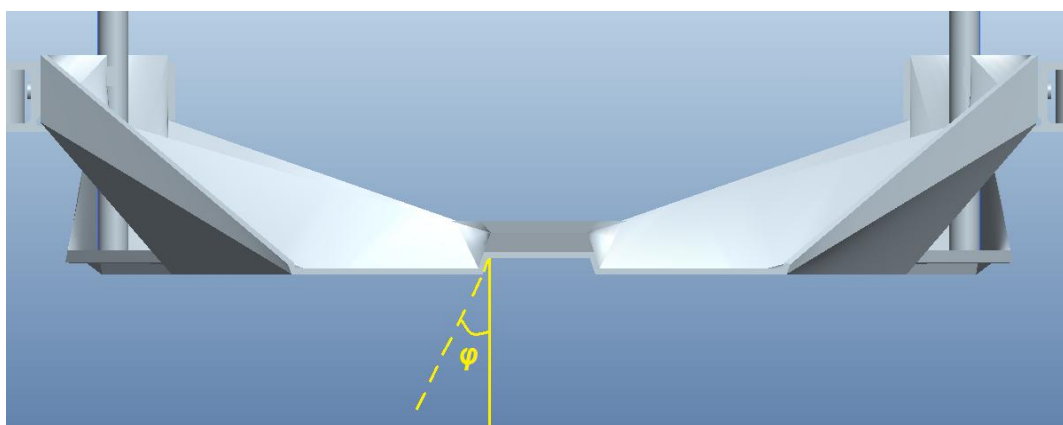


Figure 13-5 Draft angle (View 1)

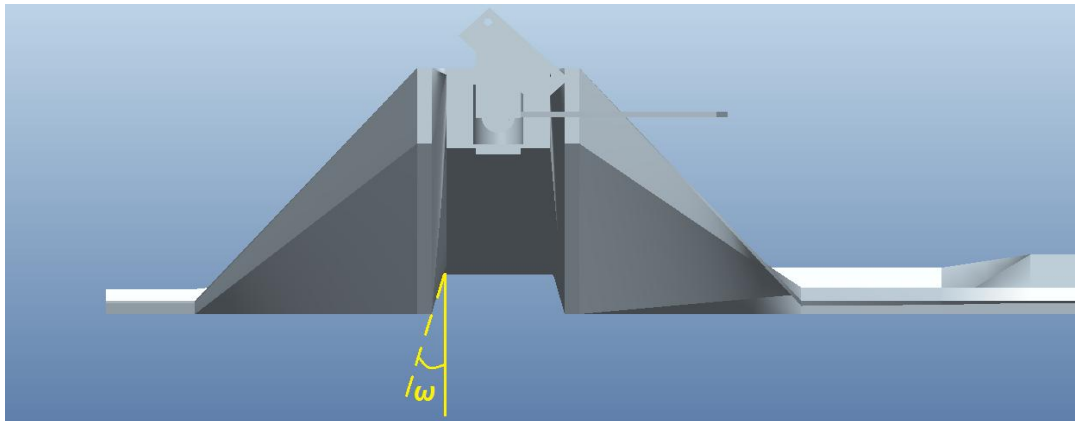


Figure 13-6 Draft angle (View 2)



Figure 13-7 Draft angle (View 3)

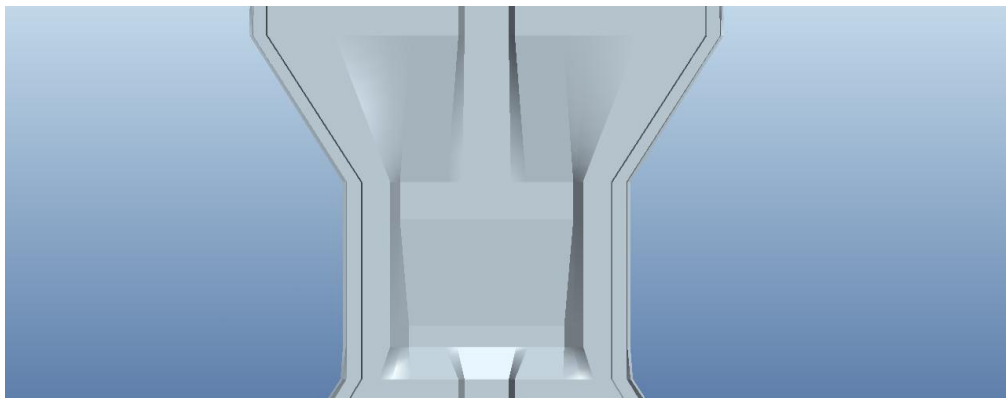


Figure 13-8 Draft angle (View 4)

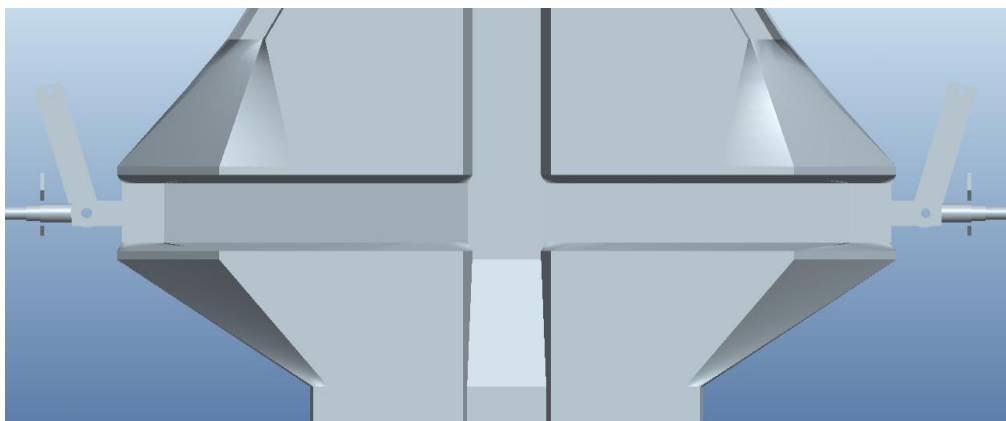


Figure 13-9 Draft angle (View 5)

14 FUTURE PROPOSALS

The study of the current project includes many opportunities for further development. Some proposals are:

- Simulation of the suggested chassis, in order to prove that it conforms to the structural requirements.
- Implementation of thermal analysis by using methodologies of finite elements.
- Design of additional parts which will cover the current chassis, appropriate for the implementation of aerodynamical analysis of these components. This analysis will be based on the properties and methodologies of Computational Fluid Dynamics (CFD), and their implementation will be possible by using appropriate CAE softwares.
- Case study of the possible design of the frontal and rear suspension system.
- Further study of the current chassis by implementing dynamical analysis and crash simulations using commercial softwares appropriate for these studies.
- Optimization of the placement of separate chassis components inside the model.

To conclude, by the completion of the current project, an important inference was made clear. The completion of a chassis design that is going to be incorporated inside a real commercial vehicle is a sophisticated project that needs the contribution of engineers of many different disciplines with extremely strict time limitations for its completion due to market pressures. A further analysis of this design is outside the primary scope of this thesis and was not strived due to severe limitations in appropriate tools for such endeavour



Figure 14-1 ER14 at the European Shell Eco Marathon 2014, in Rotterdam, the Netherlands. [70]



Figure 14-2 Training from Marc Gené, Driver of Formula1 Scuderia-Ferrari, with the Shell Eco Marathon Technology Manager and Student Liaison, Norman Koch, at the European Shell Eco Marathon 2013, in Rotterdam, the Netherlands. [70]



Figure 14-3 Shell Student Energy Challenge Award and People's Choice Award, at the European Shell Eco Marathon 2013, in Rotterdam, the Netherlands. [71]



Figure 14-4 Training by David Salters, Head of Engine Development for Scuderia-Ferrari, during our visit to the Ferrari factory in Maranello, Italy, May 2013. [71]

Citations and Bibliography

- [1] E. Shingley, C.R. Mischke, *Mechanical Engineering Design*, McGraw Hill Book Company, 1989.
- [2] Jason C. Brown, A. John Robertson, Stan T. Serpento, *Motor Vehicle Structures*, Butterworth-Heinemann, 2002.
- [3] Κατσαρός-Σεργίδτσας Θεόδωρος, *Σχεδιασμός και μελέτη αντοχής πλαισίου διθέσιου ηλεκτροκίνητου αυτοκινήτου σε περιβάλλον CAD/CAE*, Χανιά: Πολυτεχνείο Κρήτης, Τμήμα Παραγωγής & Διοίκησης, 2014.
- [4] "Formula1 Dictionary," [Online]. Available: <http://www.formula1-dictionary.net/>.
- [5] Πατσίκας Βασίλειος, *Μελέτη και σχεδίαση πλαισίου αυτοκινήτου με CAD και ανάλυση με την μέθοδο των πεπερασμένων στοιχείων*, Πολυτεχνείο Κρήτης, Τμήμα Μηχανικών Παραγωγής και Διοίκησης.
- [6] "Volkswagenag," [Online]. Available: <http://www.volkswagenag.com/>.
- [7] William B. Riley, Albert R. George, "Design, Analysis and Testing of a Formula SAE Car Chassis," in *Cornell University, SAE Technical Paper Series*.
- [8] Mark J. Moeller, Robert S. Thomas, Harish Maruvada, Nurani S. Chandra, Mark Zebrowski, "An Assesment of an FEA Body Model for Design Capability," Ford Motor Company, Michigan.
- [9] "Siemens," [Online]. Available: <http://www.plm.automation.siemens.com/>.
- [10] Μπιλάλης Ν., Μαραβελάκης Ε., in *Συστήματα CAM/CAD και τρισδιάστατη μοντελοποίηση*, 2009.
- [11] Ju Hyun, Ning Gu, Julie Jupp, Sue Sherratt, "Evaluating Creativity in Parametric Design Processes and Products: A Pilot Study," in *University of Newcastle, University of Technology Sydney, Springer, Australia*, 2012.
- [12] "Parametric Camp," [Online]. Available: <http://www.parametriccamp.com/>.
- [13] Pro Engineer User Guide, Parametric Technology Corporation(PTC).
- [14] "Shell Eco Marathon Official Rules," 2014. [Online]. Available: www.shellecomarathon.com.
- [15] Jannis D.G. van Kerkhoven, *Design of a Formula Student race car chassis*, Eindhoven: Technische Universiteit Eindhoven, Department Mechanical Engineering, Dynamics and

Control Technology Group, December 2008.

- [16] Society of Automotive Engineers (SAE), "Formula SAE Rules," 2008. [Online].
- [17] "Euroncap," [Online]. Available: <http://www.euroncap.com/>.
- [18] "Material Property Data," [Online]. Available: <http://www.matweb.com>.
- [19] D. Hull, T. W. Clyne, *An Introduction to Composite Materials*, Cambridge University.
- [20] "Protech Composites," [Online]. Available: <http://shop.protechcomposites.com/>.
- [21] J. Brydson, *Plastics Materials*, Oxford, UK: Butterworth-Heimann, 1999.
- [22] Branislav Dulaba, Frantisek Greskovic, "Simulation of Loading the Polymer/Carbon Fiber Composites and Prediction of Safety Factors," *International Journal of Engineering and Innovative Technology (IJEIT)*, vol. 2, no. 8, February 2013.
- [23] S. Peters, *Handbook of Composites, Second Edition*, Springer, 1998.
- [24] Αλέξανδρος Δ. Γκότσης, "Μη-Μεταλλικά υλικά ΙΙΙ Σύνθετα Υλικά," Εκδόσεις Πολυτεχνείου Κρήτης.
- [25] Αντώνης Ε. Αντωναγιαννάκης, Μελέτη της επίδρασης της ύφανσης των ινών στις μηχανικές ιδιότητες ινοπλισμένων σύνθετων υλικών-Υπολογισμός του μέτρου ελαστικότητας σε υφάσματα απλής πλέξης, Πολυτεχνείο Κρήτης, Γενικό Τμήμα.
- [26] Bryan Harris, *Engineering Composite Materials*, London: The Institute of Materials, 1999.
- [27] Πλουμάκης Ευάγγελος, Μελέτη και Κατασκευή του συστήματος Τροχού-Πλήμνης για χρήση σε πειραματικό όχημα χαμηλής κατανάλωσης, Χανιά: Πολυτεχνείο Κρήτης, Τμήμα Μηχανικών Παραγωγής και Διοίκησης, 2010.
- [28] Παππάς Αναστάσιος, *Σχεδίαση, μελέτη και κατασκευή συστήματος διεύθυνσης για το όχημα ER10*, Χανιά: Πολυτεχνείο Κρήτης-Τμήμα Μηχανικών Παραγωγής και Διοίκησης, 2010.
- [29] W.J.Wagtendonk, *Principles of Helicopter Flight*, Washington: Aviation Supplies & Academics Inc., 1996.
- [30] Σπανουδάκης Πολυχρόνης, Σχεδίαση νέου μή επανδρωμένου οχήματος κάθετης απογείωσης-προσγείωσης, Χανιά: Πολυτεχνείο Κρήτης, Τμήμα Μηχανικών Παραγωγής και Διοίκησης, 2003.
- [31] J. Seddon, *Basic Helicopter Aerodynamics*, Oxford: BSP Professional Books, 1990.
- [32] Raymond W. Prouty, *Helicopter Performance Stability and Control*, Florida: Krieger

Publishing Company, 1990.

- [33] James Hakewill, *Measuring Center of Gravity Height on a Formula Car*, 2007.
- [34] David Baraff, *Physically Based Modeling Rigid Body Simulation*, Pixar Animation Studios, 2001.
- [35] Thomas D. Gillespie, *Fundamentals of Vehicle Dynamics*, Society of Automotive Engineers (SAE).
- [36] Bonher Max, Gscheidle Rolf, Keil Wolfgang, Layer Siegfried, Saier Wolfgang, Schmidt Haro, Siegmayer Paul, Wimmer Alois, Zwickel Heinz, Μετάφραση Μελέτης Βούλγαρης, Παναγιώτα Ψαλλίδα, *Συστήματα Αυτοκινήτου 2*, Βιβλιοθήκη του μηχανικού αυτοκινήτων-οχημάτων.
- [37] Giancarlo Genta, Lorenzo Morello, *The automotive chassis, Volume 1: Components Design*, Mechanical Engineering Series, Springer, 2009.
- [38] Lorenzo Morello, Lorenzo Rosti Rossini, Guiseppe Pia, Andrea Tonoli, *The Automotive Body, Volume 1: Components Design*, Mechanical Engineering Series, Springer, 2011.
- [39] Lorenzo Morello, Lorenzo Rosti Rossini, Giuseppe Pia, Andrea Tonoli, *The Automotive Body, Volume 2: System Design*, Mechanical Engineering Series, Springer, 2011.
- [40] Giancarlo Genta, Lorenzo Morello, *The automotive chassis, Volume 2: System Design*, Mechanical Engineering Series, Springer, 2009.
- [41] John C. Stearns, *An Investigation of Stress and Displacement Distribution in a Aluminum Alloy Automobile Rim*, May 2000.
- [42] Jornsens Reimpell, Helmut Stoll, Jurgen W. Betzler, *The Automotive Chassis, Second Edition: Butterworth-Heinemann*, 2001.
- [43] Pierre Duysinx, *Introduction to Vehicle Dynamics*, University of Liege, LTAS Automotive Engineering, Academic Year 2011-2012.
- [44] [Online]. Available: http://www.hsu-hh.de/meywerk/index_r1GMIHdaeO43goQj.html.
- [45] Society of Automotive Engineers(SAE), *Vehicle Dynamics Terminology*.
- [46] Den Hartog, J.P., "Mechanics," New York NY, McGraw-Hill Book Company Inc., 1948, p. 174.
- [47] James Walker, "The Physics of Braking Systems," *scR motorsports*, 2005.
- [48] Paul S. Gritt, "An Introduction to Brake Systems," in *SAE Brake Colloquium, DaimlerChrysler Corporation*, October 6th 2002.

- [49] Mortimer, R.E., Segel, L., Dugoff, H., Campell, J.O., Jorgeson, C.M., Murphy, R.W., "Brake Force Requirement Study: Driver-Vehicle Braking Performance as a Function of Brake System Design Variables," The University of Michigan Highway Safety Research Institute, p. 22, April 1979.
- [50] Jack Limberg, "Introduction to Foundation Brake Design," in *SAE, E & J Enterprises, L.L.C., Bosch, St. Mary's College*.
- [51] Prof. Dr. George Rill, *Vehicle Dynamics-Lecture Notes*, Fachhochschule Regensburg University of Applied Sciences, October 2006.
- [52] Karl Popp, Werner Schiehlen, *Ground Vehicle Dynamics*, Stuttgart: Springer, 1993.
- [53] Tzanakis Athanasios, *Conceptual and aerodynamic design of an urban vehicle*, Chania: Technical University of Crete, Department of Production Engineering and Management, 2012.
- [54] Mehrdad Ehsani, Yimin Gao, Sebastien E. Gay, Ali Emadi, Muhammad H. Rashid, *Modern Electric, Hybrid Electric and Fuel Cell Vehicles*, Series Editor University of West Florida, CRC Press LLC, 2005.
- [55] "Shell Eco Marathon," [Online]. Available: <http://www.shell.com/global/environment-society/ecomarathon.html>.
- [56] Jan Bender, Kenny Erleben, Jeff Trinkle, Erwin Coumans, "Interactive Simulation of Rigid Body Dynamics in Computer Graphics," in *Graduate School CE, TU Darmstadt, Germany, Department of Computer Science, University of Copenhagen, Denmark, Department of Computer Science, Rensselaer Polytechnic Institute, Advanced Micro Devices, Inc., USA*.
- [57] Ευριπίδης Παπαμίχος, Νίκος Χ. Χαραλαμπίδης, *Αντοχή των υλικών*, Εκδόσεις Τζιόλα, 2006.
- [58] Beer, Johnson, *Στατική - Τεχνική Μηχανική*, Αθήνα: Fountas Engineering Books.
- [59] G. E. Dieter, *Engineering Design*, Singapore: McGraw Hill International Press, 2000.
- [60] *Ansys Mechanical User Guide*, Livermore Software Technology Corporation (LSTC).
- [61] *Ansa and meta User Guide*, BETA CAE Systems.
- [62] Michael Broad, Terry Gilbert, *Design, Development and Analysis of the NCSHFH.09 Chassis*, North Carolina State University, College of Mechanical and Aerospace Engineering, SAE International, 2009.
- [63] G. Stigliano, D. Mundo, S. Donders, T. Tamarozzi, "Advanced Vehicle Body Concept Modeling Approach Using Reduced Models of Beams and Joints," in *LMS International Belgium, University of Calabria, Department of Mechanical Engineering Italy, K.U.Leuven*,

- [64] Steven Tebby, Ebrahim Esmailzadeh, Ahmad Barari, Methods to Determine Torsion Stiffness in an Automotive Chassis, University of Ontario Institute of Technology, CAD Solutions LLC, 2011.
- [65] Thanneru Raghu, Krishna Prasad, Goutham Solasa, Nariganani SD Satyadeep, G.Suresh Babu, "Static Analysis and Optimization of Chassis and Suspension of an All-Terrain Vehicle," in *International Journal of Engineering and Advanced Technology (IJEAT)*, June 2013.
- [66] "Caterham Composites," [Online]. Available: <http://www.caterhamcomposites.com/>.
- [67] "Evercoat," [Online]. Available: <http://www.evercoat.com/>.
- [68] "Engineers Handbook," [Online]. Available: <http://www.engineershandbook.com/>.
- [69] Thom Tremblay, "Injection Moulding Part Design for Dummies Protomold Special Edition," *John Wiley & Sons, Inc*, 2012.
- [70] "TUCer (Technical University of Crete Eco Racing)," [Online]. Available: <http://www.tucer.tuc.gr/>.
- [71] "Shell," [Online]. Available: <http://www.shell.com/>.

